PART I. Sm-Nd AND Rb-Sr CHRONOLOGY OF CRUSTAL FORMATION

PART II. Ba, Nd AND Sm ISOTOPIC ANOMALIES IN THE ALLENDE METEORITE

Thesis by

Malcolm Thomas McCulloch

In Partial Fulfillment of the Requirements

for the Degree of

Doctor of Philosophy

California Institute of Technology

Pasadena, California

1980

(Submitted November 16, 1979)

This thesis is dedicated to Linda in appreciation of her unfailing support and patience.

ACKNOWLEDGEMENTS

I would like to thank Professor G.J. Wasserburg for his continuous interest, active encouragement and edifying criticism of this work. Dimitri Papanastassiou shared much of his experience in high precision mass spectrometry with me.

I am also indebted to Professor S.S. Goldich who shared with me much of his considerable knowledge of the geology of the Minnesota River Valley.

The work on the Samail Ophiolite was part of a cooperative study with Bob Gregory and Professor H.P. Taylor.

During the tenure of this study, I have benefited from numerous enlightening discussions with Bob Gregory, Stein Jacobsen and Jim Quick.

I thank Evelyn Brown for her assistance and friendliness and Joanne Clark for indispensible help in preparing this manuscript.

Many people contributed samples for this study and I would especially like to thank R.G. Coleman, J.R. de Laeter, S.S. Goldich, R.T. Gregory, R.W. Hurst, R.T. Pidgeon and S.R. Taylor.

The hospitality and friendliness of my colleagues has been greatly appreciated. This work has been supported by NASA grant NGL 05-002-188 and NSF grant PHY76-83685.

ABSTRACT

This thesis is divided into two parts. The first part has as its theme the chronology of crustal formation. The times at which new segments of crust were formed has been ascertained by using Sm-Nd and Rb-Sr isotopic systematics, together with plausible assumptions regarding the geochemical evolution of the crust and mantle. The general approach that has been used is to assume that the differentiation processes which produce magmatic rocks occur with a marked chemical fractionation of the Sm/Nd and Rb/Sr ratios relative to the source region. It is then the time of this chemical fractionation which has been dated. This approach is valid insofar as the dominant contribution to the crust comes from the emplacement of magmatic rocks derived from a "uniform" mantle reservoir.

Sm-Nd studies of early Archean complexes from the Minnesota River Valley, Labrador, and the Pilbara of Western Australia have shown that these rocks were derived at ~ 3.6 AE from a mantle with a time-average Sm/Nd ratio approximately equal to that in chondrites (CHUR). These results, together with a 3.6 AE Sm-Nd model age from a tonalitic gneiss in northern Michigan, confirm that this time period marks one of the earliest episodes of major continental crustal formation on the earth.

In contrast to the apparent uniformity of Sm/Nd in the mantle of the earth, many lunar magmatic rocks have initial $^{143}Nd/^{144}Nd$ ratios which indicate variability in the Sm/Nd ratios of their source reservoirs of up to 60%. These highly fractionated reservoirs must have formed within about 200 m.y. after the accretion of the moon. The Sm-Nd data

on highland breccias and KREEP samples indicate a low Sm/Nd ratio for these samples which was also plausibly established early in lunar history and is complementary to the early production of high Sm/Nd mare basalt source regions. The contrast between the lunar and terrestrial Nd isotopic data implies a grossly different early differentiation history for these two planets.

A study of the Nd, Sr, and O isotopic characteristics of the Samail Ophiolite is also presented. This complex represents oceanic crust that was obducted onto the Arabian continental margin during late Cretaceous times. Using the Sm-Nd method, internal isochrons were obtained from three gabbros establishing a Cretaceous crystallization age for the Samail Ophiolite. These results appear to be highly consistent in spite of extensive hydrothermal exchange which has altered the primary $^{87}Sr/^{86}Sr$ and $^{18}O/^{16}O$ ratios. Gabbros from Ibra give an age of 130±12 m.y., and a gabbro in the northern part of Oman gives an age of 100±20 m.y. These results show that the Sm-Nd technique can be used to determine crystallization ages and initial Nd ratios of relatively young, Mesozoic and Cenozoic mafic complexes.

In part two of this thesis, isotopic anomalies are reported for Ba, Nd, and Sm in two inclusions from the Allende meteorite. These inclusions are typical Ca-Al-rich objects associated with early condensates from the solar nebula but have distinctive O and Mg isotopic anomalies of the FUN type. Sample C1 shows ^{144}Sm enrichments and a depletion in ^{135}Ba of 2 parts in 10^4 and normal Nd. Sample EK1-4-1 shows large positive excesses in the unshielded isotopes ^{135}Ba and ^{137}Ba of 13.4 and 12.3 parts in 10^4, respectively. The Nd and Sm isotopic composition in EK1-4-1 is highly aberrant in at least five isotopes.

The Ba, Sm, and Nd anomalies in EK1-4-1 can be explained by a model of r-process addition. From the observations of ^{144}Sm isotopic anomalies in Cl, it is inferred that the p-process is decoupled from the r-process. All these anomalies are found to be uniform between coexisting mineral phases. These observations show the existence of substantial isotopic anomalies in refractory elements in the neighborhood of Xe and extend the range of elements showing isotopic effects to O, Ne, Si, Mg, Ca, Sr, Kr, Xe, Ba, Sm, and Nd. These observations, in conjunction with the presence of ^{107}Pd ($\tau_{1/2}$ = 6.5 x 10^6 yrs) and ^{26}Al ($\tau_{1/2}$ = 7 x 10^5 yrs), are interpreted as the result of a nearby supernova explosion which produced elements over a wide mass range and injected them into the early solar nebula shortly before condensation.

TABLE OF CONTENTS

PART I. Sm-Nd AND Rb-Sr CHRONOLOGY OF CRUSTAL FORMATION

CHAPTER 1. REVIEW

INTRODUCTION

The ability to determine the time of formation of new crustal segments is of fundamental importance in attempting to understand the growth and evolution of continental crust. New crust is considered to be the addition to the continents of material that has not previously been present in the crust but which is newly added during periods of continental growth and has its penultimate origin from the mantle as a result of differentiation processes. However, as a consequence of multiple generations of crustal formation, metamorphism, remelting and erosion, the actual time of formation of new continental crust is not always easy to ascertain. For example, it is often difficult to establish whether younger parts of continental crust as defined by relative geologic age or by isotopic age determinations, represent the addition of new material, or are simply the product of metamorphism of older pre-existing provinces or materials.

To determine the time of formation of crustal segments using the Sm-Nd technique, there are basically two different approaches. The first approach which is analogous to that commonly used in the Rb-Sr method, is to obtain an isochron by measuring $^{143}Nd/^{144}Nd$ and $^{147}Sm/^{144}Nd$ ratios from a suite of cogenetic minerals or whole rocks which have a range in $^{147}Sm/^{144}Nd$ ratios. Sm-Nd mineral isochrons have been obtained from a number of lunar igneous rocks (see, for example, Lugmair et al., 1976; Papanastassiou et al., 1977; and Nakamura et al., 1976) and more recently terrestrial igneous rocks (DePaolo and Wasserburg, 1976a,1979a;McCulloch et al.,1979a, and Jacobsen and Wasserburg, 1979). These rocks appear to be relatively pristine, having undergone at most a minor or low grade metamorphism

and the resultant isochrons have been interpreted as indicating the time of crystallization of the magmas. The internal isochron approach has the disadvantage that later metamorphism may cause re-equilibration between the mineral phases. At present there is almost no direct information available on the response of Sm-Nd in minerals to high grade metamorphic conditions.

Examples of terrestrial Sm-Nd whole rock isochrons have been given by Hamilton et al. (1977, 1978, 1979a,b). The main difficulty with this type of approach is in establishing that the whole rocks are a cogenetic system with the same initial $^{143}Nd/^{144}Nd$ ratio and crystallization age. Recent detailed studies of ophiolite complexes by McCulloch et al. (1979a) and Jacobsen and Wasserburg (1979) have shown that even within a suite of contemporaneous and closely related rocks there are small but significant variations in initial $^{143}Nd/^{144}Nd$ and $^{87}Sr/^{86}Sr$ ratios. This problem is further exacerbated in the Sm-Nd system where, due to the more limited range in $^{147}Sm/^{144}Nd$ ratios, it is often necessary to include minor or exotic lithologies to construct an "isochron." This problem will be discussed later with respect to the Minnesota River Valley rocks.

The second approach to finding the time of formation of crustal segments is to use model ages. In this approach it is assumed that the differentiation processes which produce magmatic rocks occur with a marked chemical fractionation of the Sm/Nd and Rb/Sr ratios relative to their mantle source reservoirs. It is then the time of this chemical fractionation which is dated. This approach is valid insofar as the dominant contribution to the crust comes from the emplacement

of magmatic rocks derived from a "uniform" mantle reservoir. This approach, particularly with respect to Sm-Nd model ages, has been shown (McCulloch and Wasserburg, 1978, 1979b; and Jacobsen and Wasserburg, 1978) to have considerable utility. Although this latter approach is subject to uncertainties in the model parameters, it has the advantage of providing age constraints from single samples. This is particularly useful in complex polymetamorphic terranes where it is not always possible to identify samples which have a range in $^{147}Sm/^{144}Nd$ ratios and are cogenetic. In the following sections we will outline the systematics involved in both approaches and describe the effects expected in systems disturbed by metamorphism and contamination.

Sm-Nd AND Rb-Sr ISOTOPIC SYSTEMATICS

1. Model Ages

The $^{143}Nd/^{144}Nd$ ratio measured today for a rock derived T years ago from a source with an initial $^{143}Nd/^{144}Nd$ ratio of I(T), is given by

$$\left(^{143}Nd/^{144}Nd\right)_m = I(T) + \left(^{147}Sm/^{144}Nd\right)_m \left(e^{\lambda T} - 1\right) \qquad (1\text{-}1)$$

where $\left(^{147}Sm/^{144}Nd\right)_m$ is the ratio measured in the rock today and the decay constant for ^{147}Sm is $\lambda = 6.54 \times 10^{-12}\ yr^{-1}$.

The Sm-Nd model age (T^{Nd}_{CHUR}) is the time in the past when the major REE fractionation in a rock occurs during its derivation from a mantle reservoir. The mantle reservoir (CHUR) used as a reference for the Sm-Nd system has a nominal chondritic ratio of $\left(^{147}Sm/^{144}Nd\right)_{CHUR} = 0.1936$ and a $^{143}Nd/^{144}Nd$ ratio today of $I_{CHUR}(0) = 0.511836$ (DePaolo and Wasserburg, 1976a). The evolution of $^{143}Nd/^{144}Nd$ in CHUR at any time in the past is given by:

$$I_{CHUR}(0) = I_{CHUR}(T) + \left(^{147}Sm/^{144}Nd\right)_{CHUR} \left(e^{\lambda T} - 1\right) \qquad (1\text{-}2)$$

A magma derived from CHUR at time T in the past has from equations (1-1) and (1-2), $I_{CHUR}(T) = I(T)$ and thus the Sm-Nd model age is given by:

$$T^{Nd}_{CHUR} = \frac{1}{\lambda} \ln\left(1 + \frac{I_{CHUR}(0) - \left(^{143}Nd/^{144}Nd\right)_m}{\left(^{147}Sm/^{144}Nd\right)_{CHUR} - \left(^{147}Sm/^{144}Nd\right)_m}\right) \qquad (1\text{-}3)$$

The validity of these model ages directly depends on the correctness of the assumption that magmas are derived from a source

Figure 1-1. Fractional deviations in parts in 10^4 of the initial $^{143}Nd/^{144}Nd$ ratio of Archean rocks, from the evolution to be found in a reservoir with a chondritic Sm/Nd ratio (CHUR). Data for Stillwater, Gt. Dyke, Louis Lake, Preissec Lacorne, Fiskenaesset, and Amitsoq, from DePaolo and Wasserburg (1976a,b; 1979b); Rhodesian Greenstones, Lewisian, Onverwacht, and Isua, from Hamilton et al. (1977, 1978, 1979a,b); and Duffer Dacite, Montevideo-Morton, and Uivak from this work. Within analytical uncertainty, most of the samples plot on the chondritic evolution line. The only exception is the Lewisian sample with $\varepsilon_{Nd} = +1.4 \pm 1.0$ and the Stillwater complex with $\varepsilon_{Nd} = -2.8 \pm 0.2$. The offset for the Lewisian gneiss is probably an artifact caused by an incorrect age assignment, and the negative ε_{Nd} value for the Stillwater complex may be due to contamination (see discussion). However, the coherence observed for most of the Archean ε_{Nd} values provides strong evidence for the derivation of both basaltic and sialic rocks from a CHUR source and supports the validity of the T^{Nd}_{CHUR} model ages.

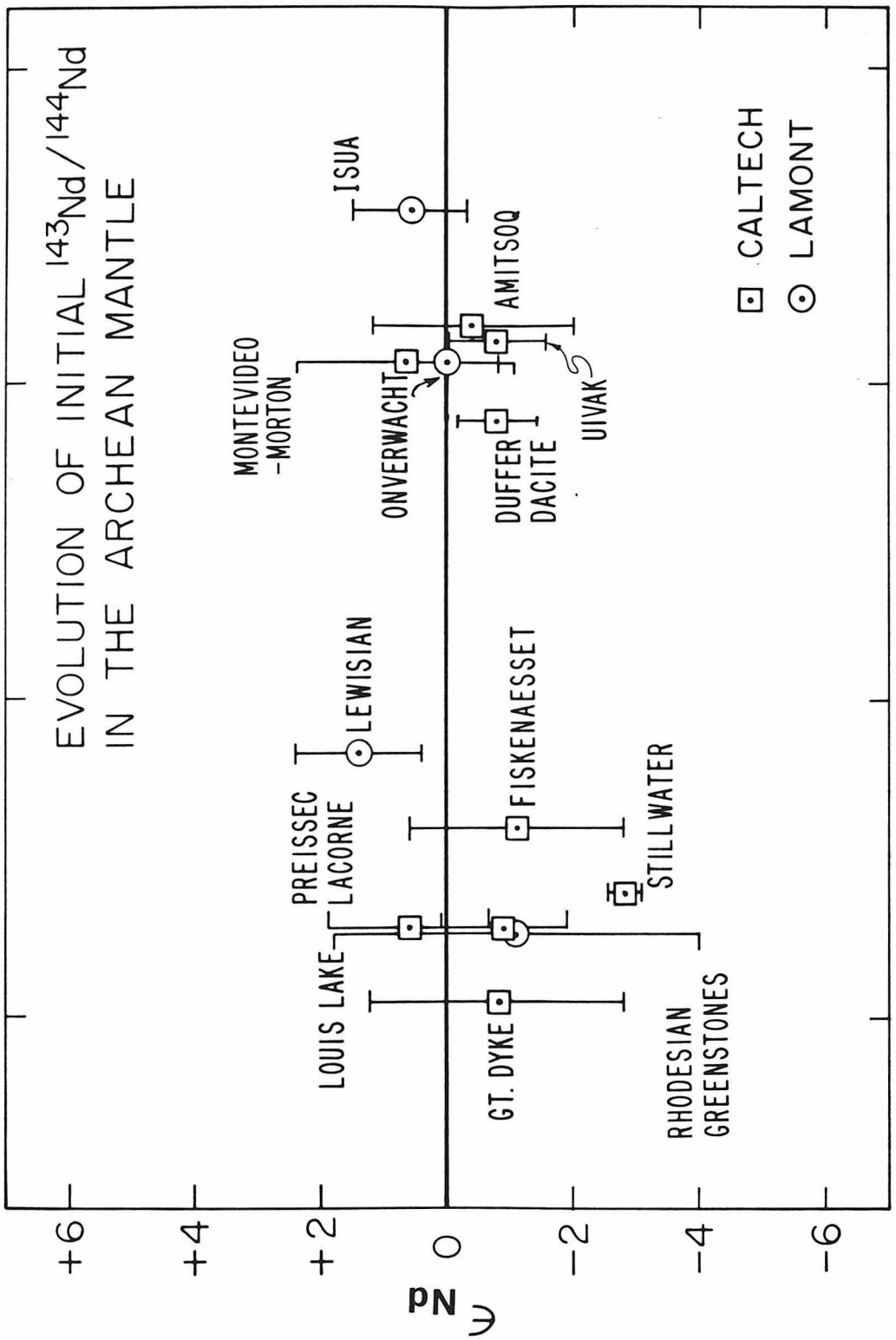
EVOLUTION OF INITIAL $^{143}Nd/^{144}Nd$
IN THE ARCHEAN MANTLE
ISUA
MONTEVIDEO
-MORTON
ONVERWACHT
AMITSOQ
DUFFER
DACITE
UIVAK
LEWISIAN
PREISSEC
LACORNE
LOUIS LAKE
FISKENAESSET
STILLWATER
GT. DYKE
RHODESIAN
GREENSTONES
CALTECH
LAMONT
+6
+4
+2
0
-2
-4
-6
ε_{Nd}
2.5
3.0
3.5
4.0
TIME AE

Fig. 1-1

reservoir with CHUR characteristics. In Fig. 1-1, the fractional deviations in parts in 10^4 of the initial $^{143}Nd/^{144}Nd$ ratio from the evolution in a CHUR reservoir are shown. These deviations are given by:

$$\varepsilon_{Nd} = \left[I(T)/I_{CHUR}(T) - 1 \right] 10^4 \qquad (1\text{-}4)$$

In this figure it can be seen that most of the Archean rocks which have been studied have an initial $^{143}Nd/^{144}Nd$ ratio which is identical within experimental error to that in a CHUR mantle. The exceptions are the Lewisian gneisses and the Stillwater complex. The Lewisian gneiss has $\varepsilon_{Nd} = +1.4 \pm 1.0$ for an age of 2.92 AE (Hamilton et al., 1979b). However, this age is derived from a Sm-Nd isochron which includes both quartzofeldspathic and basic whole rocks and is mainly controlled by the basic gneisses. A younger age of $\sim$ 2.8 AE would eliminate this apparent discrepancy in the ε_{Nd} value and would also be more consistent with the zircon ages from the quartzofeldspathic gneisses. The Stillwater complex has $\varepsilon_{Nd} = -2.8 \pm 0.2$ and an age of 2.701 ± 0.008 AE (DePaolo and Wasserburg, 1979b). The disparity from the CHUR evolution of this high precision point does raise the question of whether Nd isotopic heterogeneities are present in the Archean mantle. However, the authors have suggested that the lower ε_{Nd} value may be due to contamination with older country rock. This is plausible as the Stillwater complex has low measured concentrations of Nd ($\sim$ 1 ppm), low inferred Nd concentrations in the magma ($\sim$ 6 ppm), and is adjacent to older country rock of suitable composition for a contaminant.

The coherence observed for most of the Archean ε_{Nd} values provides strong evidence for the derivation of both basaltic and

silicic rocks from CHUR and supports the validity of the T^{Nd}_{CHUR} model ages. In addition, even if deviations of 1 part in 10^4 from CHUR exist in the Archean mantle for most tonalitic and granodioritic gneisses with highly fractionated Sm/Nd ratios, this would still only produce an error of $\sim$ 0.08 AE in the T^{Nd}_{CHUR} model ages.

In a manner analogous to that described for Sm-Nd, model ages can also be calculated using Rb-Sr isotopic systematics. For the Rb-Sr system, the reference mantle reservoir (UR) has a nominal value of $(^{87}Rb/^{86}Sr)_{UR} = 0.0827$ and $^{87}Sr/^{86}Sr$ ratio today of $I_{UR}(0) = 0.7045$. These reference mantle parameters for Rb-Sr are derived from the correlation of ε_{Nd} and ε_{Sr} observed in young mid-ocean ridge basalts and ocean islands (DePaolo and Wasserburg, 1976b; O'Nions et al., 1977). A magma derived from UR at time T has a Rb-Sr model age of

$$T^{Sr}_{UR} = \frac{1}{\lambda} \ell n \left(1 + \frac{I_{UR}(0) - (^{87}Sr/^{86}Sr)_m}{(^{87}Rb/^{86}Sr)_{UR} - (^{87}Rb/^{86}Sr)_m} \right) \qquad (1\text{-}5)$$

where $\lambda = 1.42 \times 10^{-11}$ yr.$^{-1}$ and m denotes the ratio measured in the rock today.

In Fig. 1-2 the systematics involved in calculating T^{Nd}_{CHUR} and T^{Sr}_{UR} model ages are illustrated. The evolution of $^{143}Nd/^{144}Nd$ in the mantle reservoir CHUR is shown in Fig. 1-2a. From 4.55 AE to the present day, the $^{143}Nd/^{144}Nd$ ratio in CHUR is assumed to have evolved from the Juvinas initial ratio of 0.505975 (Lugmair et al., 1976) to a value today of 0.511836. This is equivalent to a total variation in ε_{Nd} of 115 ε-units.

In Fig. 1-2b the evolution of $^{87}Sr/^{86}Sr$ is shown in the Sr

Figure 1-2. (a) $^{143}Nd/^{144}Nd$ versus time, illustrating the evolution of $^{143}Nd/^{144}Nd$ in the reference mantle reservoir CHUR and a sample derived from this reservoir at time T^{Nd}_{CHUR}. Typical continental crustal samples have $f^{Sm/Nd} < 0$ and therefore the evolution of $^{143}Nd/^{144}Nd$ in the continental crust is retarded relative to CHUR. The total evolution in $^{143}Nd/^{144}Nd$ during the earth's history is equivalent to 115 ε-units. The shaded area is for mid-ocean ridge basalts (MORB) which are derived from a reservoir which has been depleted in Nd relative to Sm ($f^{Sm/Nd} > 0$) for at least a billion years or more.

(b) $^{87}Sr/^{86}Sr$ versus time, illustrating the evolution of $^{87}Sr/^{86}Sr$ in the reference mantle reservoir UR and a sample derived from this reservoir at time T^{Sr}_{UR}. Typical continental crustal samples have $f^{Rb/Sr} > 0$ and therefore the evolution of $^{87}Sr/^{86}Sr$ in the continental crust is enhanced relative to UR. The evolution of $^{87}Sr/^{86}Sr$ in UR from 4.55 AE to the present day is equivalent to a change in ε_{Sr} of 78 ε-units. This is only $\sim$ 2/3 of the change in $^{143}Nd/^{144}Nd$ for the same period. The shaded area is for MORB which are derived from a long-time ($> 10^9$ yrs) depleted ($f^{Rb/Sr} < 0$) reservoir.

(c) $^{143}Nd/^{144}Nd$ versus time showing the effect of an additional Sm/Nd fractionation (at time T_{MET}) on the T^{Nd}_{CHUR} model age. In general, $T^{Nd}_{CHUR} > T_{MET}$ and therefore T^{Nd}_{CHUR} ages provide a strict upper limit for the time of the last fractionation event. T^{Nd}_{*} is the apparent Nd model for a multiple stage sample evolution.

(d) $^{87}Sr/^{86}Sr$ versus time showing the effect of an additional Rb/Sr fractionation (at time T_{MET}) on the T^{Sr}_{UR} model age.

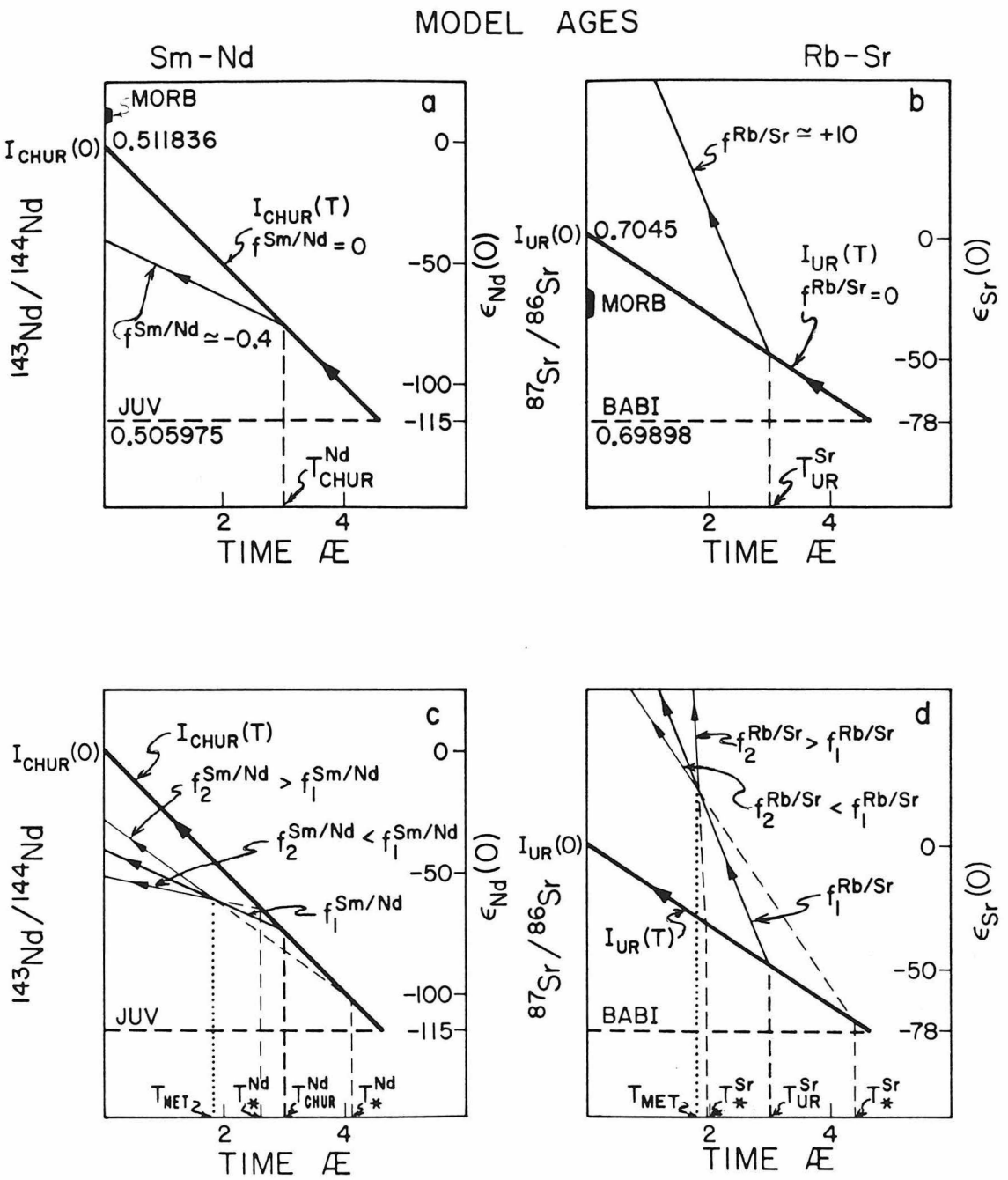
MODEL AGES
Sm-Nd
Rb-Sr
a
b
c
d
MORB
0.511836
$I_{CHUR}(0)$
$I_{CHUR}(T)$
$f^{Sm/Nd} = 0$
$f^{Sm/Nd} \simeq -0.4$
JUV
0.505975
T^{Nd}_{CHUR}
$^{143}Nd/^{144}Nd$
$\epsilon_{Nd}(0)$
0
-50
-100
-115
2
4
TIME Æ
$f^{Rb/Sr} \simeq +10$
$I_{UR}(0)$
0.7045
$I_{UR}(T)$
$f^{Rb/Sr} = 0$
BABI
0.69898
T^{Sr}_{UR}
$^{87}Sr/^{86}Sr$
$\epsilon_{Sr}(0)$
-50
-78
$f_2^{Sm/Nd} > f_1^{Sm/Nd}$
$f_2^{Sm/Nd} < f_1^{Sm/Nd}$
$f_1^{Sm/Nd}$
T_{MET}
T^{Nd}_*
$f_2^{Rb/Sr} > f_1^{Rb/Sr}$
$f_2^{Rb/Sr} < f_1^{Rb/Sr}$
$f_1^{Rb/Sr}$
T^{Sr}_*

Fig. 1-2

reference mantle reservoir UR. In this case the $^{87}Sr/^{86}Sr$ ratio in UR is assumed to have evolved from the value in BABI of 0.69898 (Papanastassiou and Wasserburg, 1969) to the present-day value of 0.7045. This is equivalent to a total variation in ε_{Sr} of 78 ε-units which is only $\sim$ 2/3 of the evolution of Nd in CHUR. The use of the $^{87}Sr/^{86}Sr$ initial value from Allende, 0.69877 (Gray et al., 1973) will in general cause only an insignificant change in the T_{UR}^{Sr} model ages.

The T_{CHUR}^{Nd} and T_{UR}^{Sr} model ages are given by the intersection of the sample evolution with the reference mantle evolution. For Sm-Nd, typical continental crustal rocks have $f^{Sm/Nd} < 0$ (Appendix 1) where $f^{Sm/Nd} = [(^{147}Sm/^{144}Nd)_m/(^{147}Sm/^{144}Nd)_{CHUR} - 1]$. For this reason, the evolution of $^{143}Nd/^{144}Nd$ in the crust is retarded relative to CHUR. For the Rb-Sr system, the opposite applies, as continental crustal rocks typically have $f^{Rb/Sr} \gg 0$ (Appendix 1) where $f^{Rb/Sr} = [(^{87}Rb/^{86}Sr)_m/(^{87}Rb/^{86}Sr)_{UR} - 1]$.

In Figs. 1-2c,d the effect of an additional fractionation event due to metamorphism at time T_{MET} is shown for $T_{MET} < T_{CHUR}^{Nd}$. If $f_1^{Sm/Nd}$ is the Sm/Nd ratio between times T_{CHUR}^{Nd} and T_{MET} and $f_2^{Sm/Nd}$ between T_{MET} and the present day, then for $f_2^{Sm/Nd} > f_1^{Sm/Nd}$ we have $T_{MET} < T_{CHUR}^{Nd} < T_*^{Nd}$ where T_*^{Nd} is the calculated or apparent time of derivation from CHUR. For $f_2^{Sm/Nd} < f_1^{Sm/Nd}$ we have $T_{MET} < T_*^{Nd} < T_{CHUR}^{Nd}$. Using the equivalent notation for Rb-Sr we have for

$$f_2^{Rb/Sr} > f_1^{Rb/Sr} \quad ; \quad T_{MET} < T_*^{Sr} < T_{UR}^{Sr}$$

and for $$f_2^{Rb/Sr} < f_1^{Rb/Sr} \quad ; \quad T_{MET} < T_{UR}^{Sr} < T_*^{Sr} .$$

From these systematics it is apparent that the T_{CHUR}^{Nd} and T_{UR}^{Sr} model

ages can still place constraints on the time and nature of the most recent fractionation event as well as the primary age. Actual examples of these systematics will be discussed later in this chapter and in chapter 2.

2. Closed Systems

The closed system evolution of two minerals (M1 and M2) and a whole rock (WR) is shown in Fig. 1-3a. If the minerals all have the same initial Nd isotopic composition but different Sm/Nd ratios, they will all initially lie on a horizontal straight line. T years following the condition of Nd isotopic homogeneity, all the mineral phases will lie on an isochron as shown in Fig. 1-3a. As long as the minerals or rocks remain closed systems for Nd and Sm, they evolve with a slope $d(^{143}Nd/^{144}Nd)/d(^{147}Sm/^{144}Nd) = -1$, (Lanphere et al., 1964) and therefore lie on an isochron given by equation 1-1. For comparison, Fig. 1-3b shows the growth of $^{143}Nd/^{144}Nd$, with time, in the same systems. It can be seen that the sample evolve from the initial composition I to the present-day $^{143}Nd/^{144}Nd$ ratio, with a slope proportional to $\lambda(^{147}Sm/^{144}Nd)$.

These systematics also apply to a series of cogenetic whole rocks which initially had the same Nd isotopic composition. In this case it is not necessary to assume that each individual mineral phase is closed, but only that the rock sampled, represents a closed system.

Figure 1-3. (a) Neodymium evolution diagram showing closed system evolution of $^{143}Nd/^{144}Nd$ and $^{147}Sm/^{144}Nd$ in mineral phases M1 and M2 and the whole rock WR. At the time of crystallization T all samples of a comagmatic suite of igneous rocks are assumed to have the same initial $^{143}Nd/^{144}Nd$ ratio I, but may have different $^{147}Sm/^{144}Nd$ ratios depending on the mineralogy. As long as the minerals or rocks remain closed systems for Nd and Sm, they evolve with a slope $d(^{143}Nd/^{144}Nd)/d(^{147}Sm/^{144}Nd = -1$, and therefore lie on an isochron given by equation (1-1).

(b) Neodymium growth curve for the systems in Fig. 1-3a, showing the evolution of $^{143}Nd/^{144}Nd$ with time from the initial composition I. The $^{143}Nd/^{144}Nd$ ratio of the minerals or rock of a comagmatic suite increase with time, as described by equation (1-1). The slopes of the evolution curves are equal to $\lambda(^{147}Sm/^{144}Nd)$. For a closed system, the evolution curves calculated from the measured $^{143}Nd/^{144}Nd$ and $^{147}Sm/^{144}Nd$ ratios converge to a point giving the age T and the initial $^{143}Nd/^{144}Nd$ ratio I.

(c) Neodymium evolution diagram showing the effects at time T_{MET}, of open system behavior in the mineral phases M1 and M2. The whole rock system WR is assumed to have remained closed. As in Fig. 1-3a, at time T, M1, M2, and WR are assumed to have the same initial Nd ratio I, and from T to T_{MET} the systems evolve in an identical manner to that shown for the closed systems. However, at time T_{MET} the $^{143}Nd/^{144}Nd$ ratio in systems M1 and M2 is re-equilibrated with the whole rock WR, to form a new

isochron with zero slope and $^{143}Nd/^{144}Nd = I_{MET}$. From T_{MET} to the present, M1, M2, and WR evolve to define an isochron of age T_{MET} and initial $^{143}Nd/^{144}Nd$ ratio I_{MET} .

(d) Neodymium growth curve for the systems in Fig. 1-3c showing isotopic homogenization of Nd in minerals M1 and M2 during metamorphism at time T_{MET} . In this diagram (and Fig. 1-3c) the $^{147}Sm/^{144}Nd$ ratios of M1 and M2 are assumed to have remained unchanged during metamorphism at T_{MET} . The difference in the present-day $^{143}Nd/^{144}Nd$ ratio between closed and open (at time T_{MET}) system behavior for M2 is given by $\delta M2$.

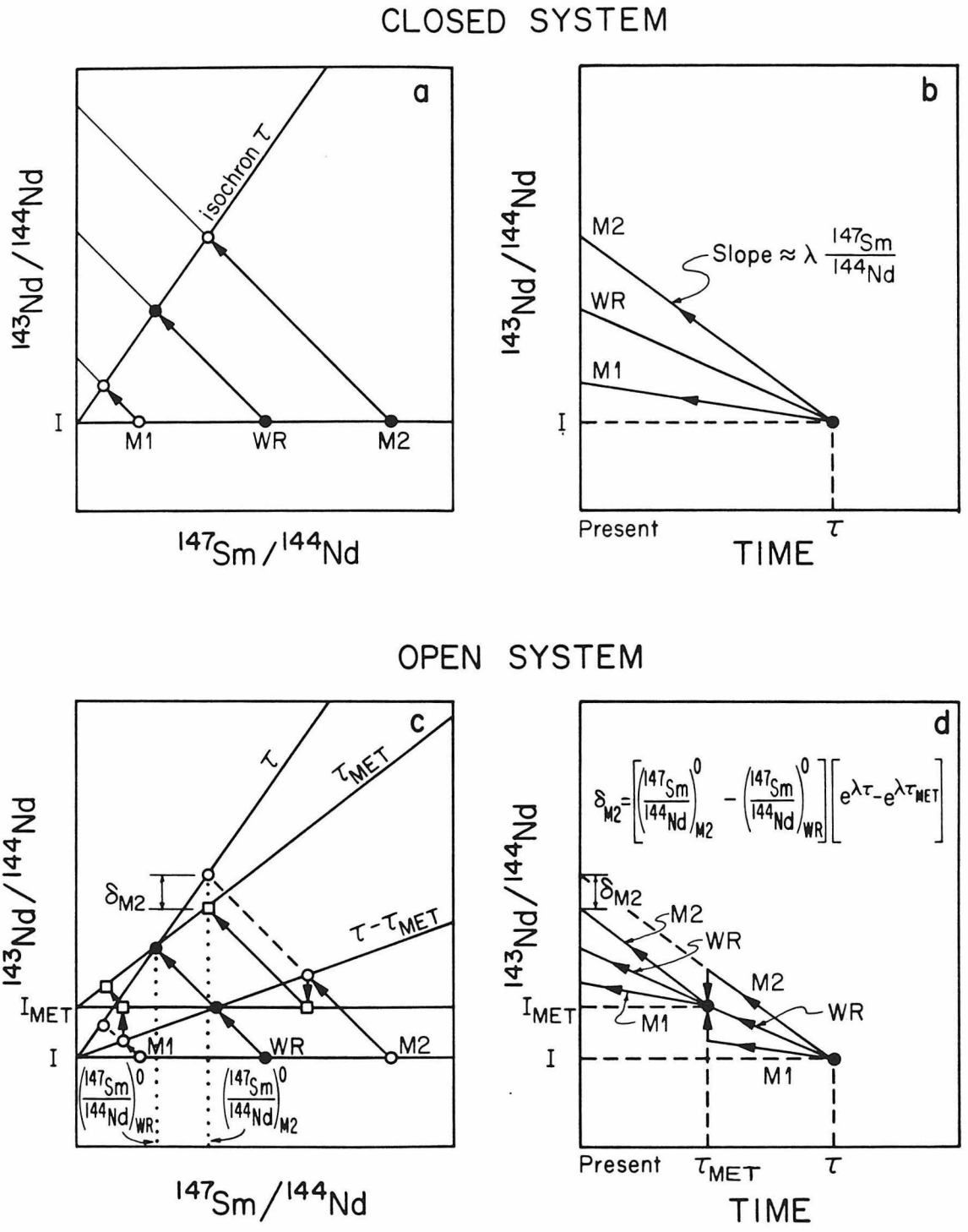
CLOSED SYSTEM
a
isochron τ
I
M1
WR
M2
$^{143}Nd/^{144}Nd$
$^{147}Sm/^{144}Nd$
b
M2
WR
M1
I
Slope ≈ λ $\frac{^{147}Sm}{^{144}Nd}$
Present
τ
TIME
OPEN SYSTEM
c
τ
τ_{MET}
δ_{M2}
$\tau-\tau_{MET}$
I_{MET}
I
M1
WR
M2
$\left(\frac{^{147}Sm}{^{144}Nd}\right)^0_{WR}$
$\left(\frac{^{147}Sm}{^{144}Nd}\right)^0_{M2}$
$^{143}Nd/^{144}Nd$
$^{147}Sm/^{144}Nd$
d
$\delta_{M2}=\left[\left(\frac{^{147}Sm}{^{144}Nd}\right)^0_{M2}-\left(\frac{^{147}Sm}{^{144}Nd}\right)^0_{WR}\right]\left[e^{\lambda\tau}-e^{\lambda\tau_{MET}}\right]$
δ_{M2}
M2
WR
M2
WR
I_{MET}
M1
I
M1
Present
τ_{MET}
τ
TIME

Fig. 1-3

3. Reset Internal Isochrons

These constructions are also particularly useful in studying more complex systems which at some time have been subject to redistribution of ^{143}Nd, Nd, or Sm. Fig. 1-3c is an isochron diagram showing the effects of internal isotopic re-equilibration on the mineral constituents (M1 and M2) of a whole rock (WR). At time T the whole rock and its minerals have the same initial $^{143}Nd/^{144}Nd$ ratio I, forming an isochron with a slope of zero. From T to T_{MET}, the whole rock and minerals evolve along trajectories, with a slope of -1. At time T_{MET} the $^{143}Nd/^{144}Nd$ ratios of the minerals are re-equilibrated with the whole rock during, for example, a short episode of metamorphism. In Fig. 1-3c it can be seen that the $^{143}Nd/^{144}Nd$ ratio of M1 is raised, while that of M2 is lowered to the same ratio as WR. For clarity, in Fig. 1-3c the $^{147}Sm/^{144}Nd$ ratios are assumed to have remained constant during metamorphism, but if new mineral phases are produced at time T_{MET}, then the $^{147}Sm/^{144}Nd$ ratios may change. At the end of the episode of metamorphism, the minerals form a new isochron with a slope of zero, but with a new initial $^{143}Nd/^{144}Nd$ ratio of I_{MET}. From T_{MET} to the present, the minerals evolve to define a metamorphic isochron of age T_{MET} and $^{143}Nd/^{144}Nd$ ratio, I_{MET}. The whole rock point WR is both on the metamorphic and primary isochron.

In Figs. 1-3c and 1-3d, the evolution of $^{143}Nd/^{144}Nd$ is shown for both open and closed systems. The difference between the open and closed systems is defined in this diagram as δ where

$$\delta = (^{143}Nd/^{144}Nd)_m^{closed} - (^{143}Nd/^{144}Nd)_m^{open} \qquad (1\text{-}6)$$

with $(^{143}Nd/^{144}Nd)_m^{closed}$ and $(^{143}Nd/^{144}Nd)_m^{open}$ being the ratios measured today in closed and open systems respectively. From equations (1-1) and (1-6) it can be shown that for the system M2,

$$\delta_{M2} = [(^{147}Sm/^{144}Nd)_{M2}^{0} - (^{147}Sm/^{144}Nd)_{WR}^{0}]\ [e^{\lambda T} - e^{\lambda T_{MET}}] \qquad (1\text{-}7)$$

Where $(^{147}Sm/^{144}Nd)_{M2}^{0}$ is the present-day ratio in the open system M2; $(^{147}Sm/^{144}Nd)_{WR}^{0}$ is the present-day ratio in the closed system WR, with which M2 was in isotopic equilibrium with at time T_{MET} ; and T is the primary age of the systems M2 and WR. Thus from equation (1-7), it can be seen that to produce large values of δ requires either a large difference in the $^{147}Sm/^{144}Nd$ ratios between open (M2) and closed (WR) systems, or a large difference between the primary and metamorphic ages. The importance of these parameters will be discussed later with respect to the Sm-Nd and Rb-Sr systematics in rocks from the Minnesota River Valley.

To distinguish a reset mineral or whole rock system from a "pristine" or undisturbed system of the same age, requires a comparison of the initial $^{143}Nd/^{144}Nd$ ratios in the two systems. Assuming that the "pristine" system is a direct mantle derivative, then this is approximately equivalent to comparing the differential evolution of $^{143}Nd/^{144}Nd$ in the mantle (CHUR) and crust. As typical crustal rocks have $f^{Sm/Nd} < 0$, the evolution of $^{143}Nd/^{144}Nd$ in the crust is retarded relative to the mantle evolution. The effect of

Figure 1-4. Neodymium evolution diagram (to scale) showing the effects of metamorphism at time T_{MET} = 2.6 AE on a whole rock WR and its mineral constituents M1 and M2. At time T = 3.6 AE, the whole rock and its comagmatic minerals are derived from a CHUR source and have a uniform $^{143}Nd/^{144}Nd$ ratio of I_{CHUR} (3.6 AE). From T, until T_{MET} , the minerals and whole-rock evolve as a closed system. At time T_{MET} , the $^{143}Nd/^{144}Nd$ ratios of the minerals M1 and M2 are re-equilibrated with the WR to form a new isochron of zero slope and $^{143}Nd/^{144}Nd$ ratio of I_{MET} (2.6 AE). From T_{MET} to the present day, the minerals and whole-rock again continue to evolve as a closed system to define an isochron of age T_{MET} = 2.6 AE and initial $^{143}Nd/^{144}Nd$ ratio of I_{MET} (2.6 AE). The isochron for a system derived from a CHUR source at 2.6 AE, and therefore having an initial $^{143}Nd/^{144}Nd$ ratio of I_{CHUR} (2.6 AE) is also shown. This isochron is parallel to the metamorphic isochron, but due to the more rapid evolution of $^{143}Nd/^{144}Nd$ in CHUR, compared to continental crust, I_{CHUR} (2.6 AE) > I_{MET} (2.6 AE). Therefore, metamorphic Sm-Nd isochrons are typically characterized by negative ε_{Nd} values.

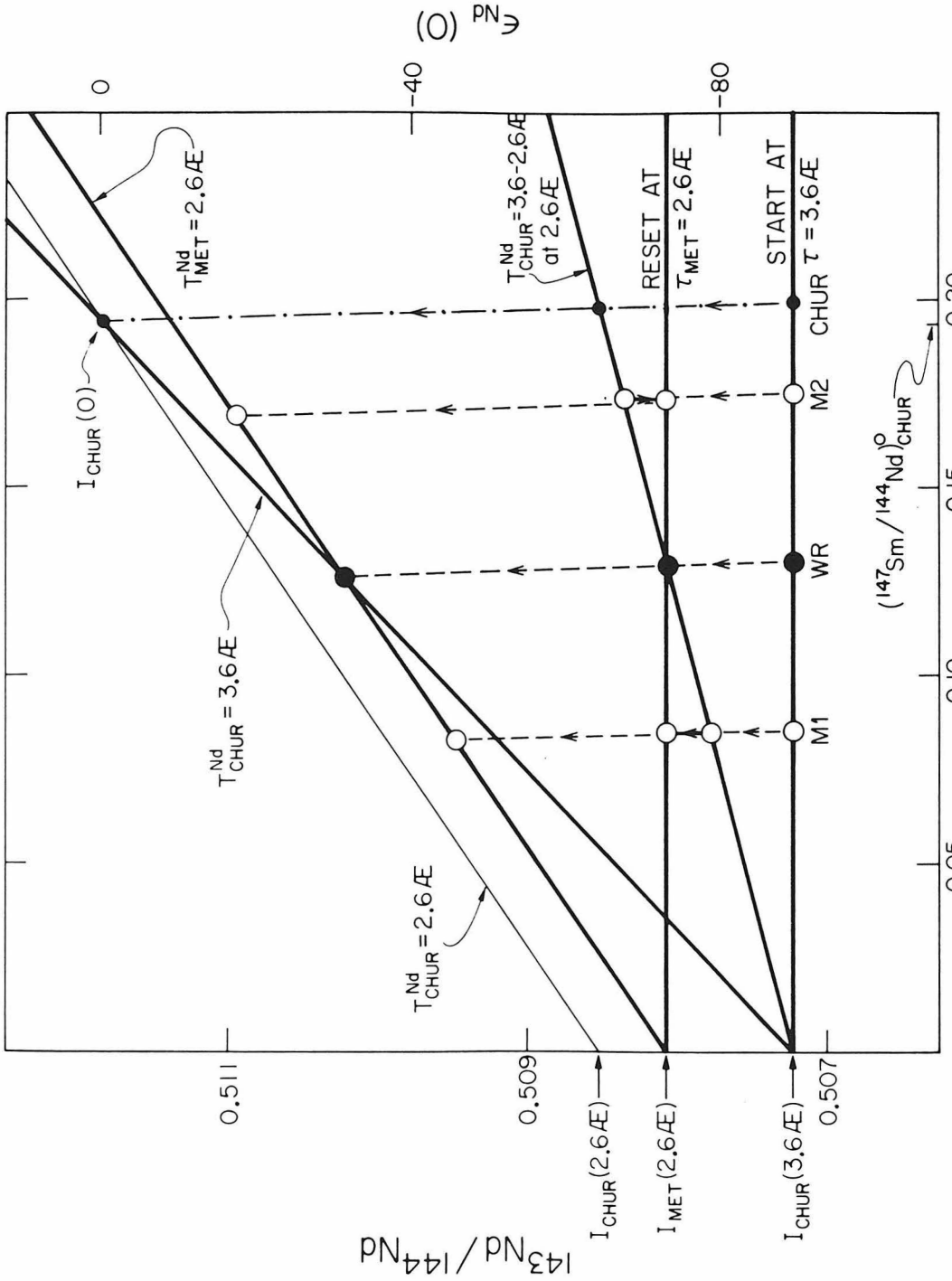
ε_{Nd} (0)
0
-40
-80
T^{Nd}_{MET} = 2.6Æ
T^{Nd}_{CHUR}=3.6-2.6Æ at 2.6Æ
RESET AT τ_{MET} = 2.6Æ
START AT CHUR τ = 3.6Æ
I_{CHUR} (0)
T^{Nd}_{CHUR} = 3.6Æ
T^{Nd}_{CHUR} = 2.6Æ
M2
M1
WR
$(^{147}Sm/^{144}Nd)^{0}_{CHUR}$
0.05
0.10
0.15
0.20
$^{147}Sm/^{144}Nd$
0.511
0.509
0.507
I_{CHUR}(2.6Æ)
I_{MET}(2.6Æ)
I_{CHUR}(3.6Æ)
$^{143}Nd/^{144}Nd$

Fig. 1-4

this differential crust-mantle $^{143}Nd/^{144}Nd$ evolution is shown in the evolution diagram of Fig. 1-4. This figure is the same as the open system example described in Fig. 1-3c, except that appropriate numerical values have been assigned to the parameters, with a primary age of $T = 3.6$ AE, a metamorphic age of $T_{MET} = 2.6$ AE, $f^{Sm/Nd} < 0$, and $I = I_{CHUR}$ (3.6 AE). Also shown in Fig. 1-4 is the evolution of $^{143}Nd/^{144}Nd$ in the reference mantle reservoir CHUR. Due to the retarded evolution (relative to CHUR) of Nd in the reset systems M1 and M2, we have

$$I_{MET}(2.6 \text{ AE}) < I_{CHUR}(2.6 \text{ AE}).$$

In general, for $f^{Sm/Nd} < 0$,

$$I_{MET}(T) < I_{CHUR}(T) \text{ for all times.}$$

For Rb-Sr, typical crustal rocks have $f^{Rb/Sr} \gg 0$ and therefore $I^{Sr}_{MET}(T) > I^{Sr}_{UR}(T)$ for all time. This contrast between the initial Nd and Sr ratios of reset systems has important implications which will be discussed further with respect to natural systems.

4. Open Systems: Contamination

The effects of contamination on the Rb-Sr system have been discussed in detail by Riley and Compston (1962) and Lanphere et al. (1964). Comparable effects are also present in the Sm-Nd system and have been discussed by DePaolo and Wasserburg,(1979b). An example is given in Fig. 1-5.

The most important distinction between the effects on contamination on the Sm-Nd and Rb-Sr systems is the nature of the

Figure 1-5. (a) Neodymium evolution diagram showing the effects of contamination. Sm contamination will cause the points to be shifted horizontally to the right. Sm and Nd contamination will displace a point from the true isochron along a chord to the contaminant of composition $(^{143}Nd/^{144}Nd)_{contam.}$ and $(^{147}Sm/^{144}Nd)_{contam.}$

(b) $^{143}Nd/^{144}Nd$ versus time showing the effects of contamination at time T_c. Contaminated samples will no longer converge to time T.

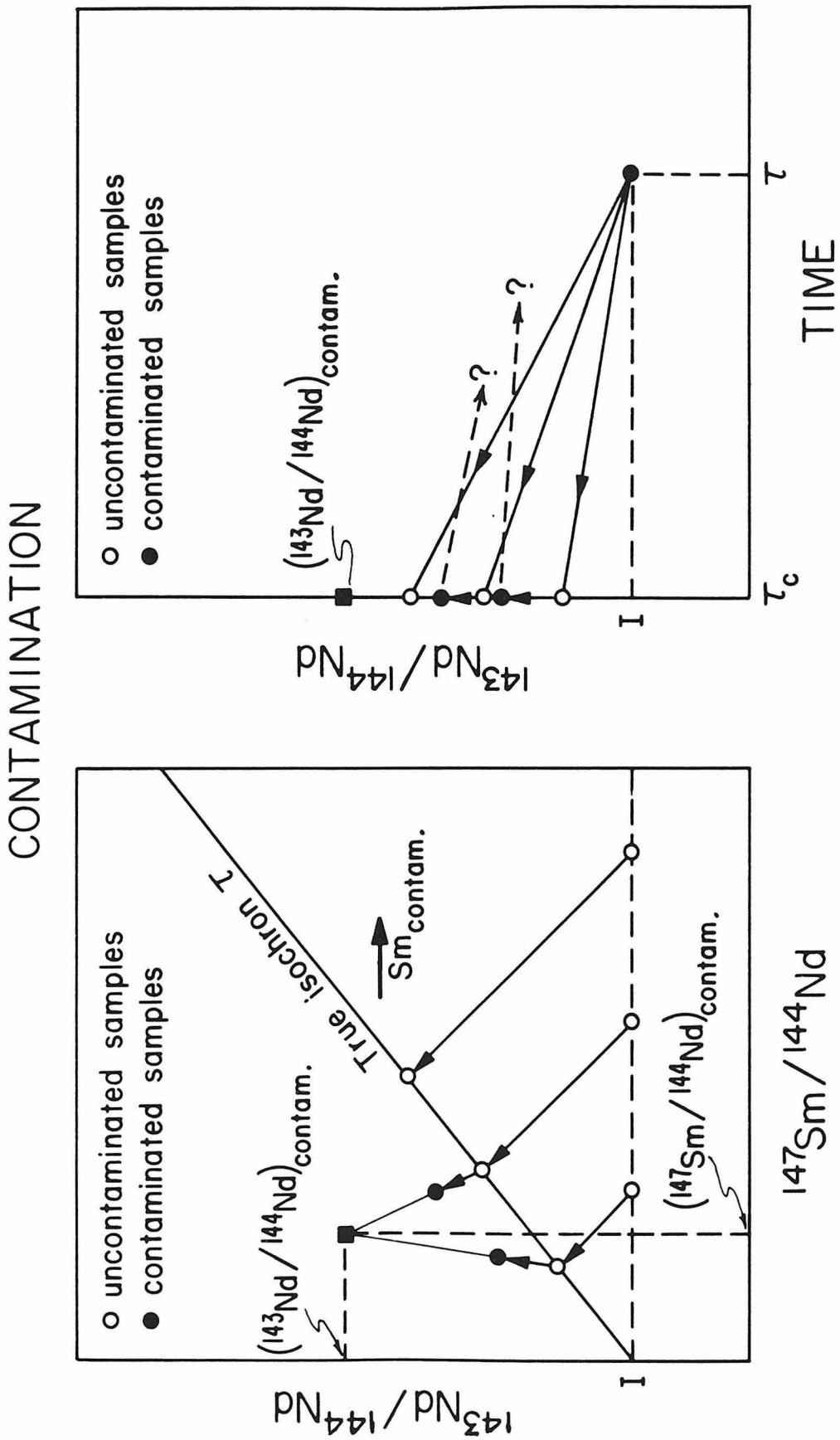
CONTAMINATION
o uncontaminated samples
● contaminated samples
$(^{143}Nd/^{144}Nd)_{contam.}$
True isochron τ
$Sm_{contam.}$
$(^{147}Sm/^{144}Nd)_{contam.}$
$^{143}Nd/^{144}Nd$
$^{147}Sm/^{144}Nd$
I
o uncontaminated samples
● contaminated samples
$(^{143}Nd/^{144}Nd)_{contam.}$
?
?
$^{143}Nd/^{144}Nd$
I
τ_c
τ
TIME

Fig. 1-5

contaminant. For example, contamination of a younger mantle derived melt by older upper continental crust generally produces positive ε_{Sr} values and negative ε_{Nd} values. This is due to the evolution of $^{87}Sr/^{86}Sr$ being enhanced in the upper continental crust, relative to the mantle, while the evolution of $^{143}Nd/^{144}Nd$ is retarded in the continental crust relative to the mantle.

EXAMPLES FROM NATURAL SYSTEMS

1. Samail ophiolite, Sultanate of Oman

As an example of a simple closed system evolution, Sm-Nd mineral isochrons from the Samail ophiolite are shown in Fig. 1-6. The upper array shown in Fig. 1-6 is defined by two gabbros K9 and G224-2 from the Ibra locality. The gabbro K9 is extremely fresh with only clinopyroxene exhibiting minor alteration to brown hornblende. The clinopyroxene from K9 has a significantly higher Sm/Nd and $^{143}Nd/^{144}Nd$ ratio than the coexisting plagioclase; together they indicate a crystallization age of 128±20 m.y. with an initial $^{143}Nd/^{144}Nd$ ratio of $\varepsilon_{Nd} = 7.7\pm0.3$. The other gabbro (G224-2) is from the upper part of the same gabbro unit as K9. This gabbro contains uralite as a late-stage replacement of both pyroxene and primary hornblende. The uralite has the highest $^{147}Sm/^{144}Nd$ and $^{143}Nd/^{144}Nd$ ratios for this rock, and together with the plagioclase gives an age of 150±40 m.y. and an initial $^{143}Nd/^{144}Nd$ ratio of $\varepsilon_{Nd} = 7.8\pm0.4$. The larger uncertainty in the age for this gabbro compared to K9 is due to the smaller difference in the $^{147}Sm/^{144}Nd$ ratios for the plagioclase and uralite. Both gabbros have the same age and initial ratio within analytical uncertainty, and the Sm-Nd systematics do not appear to be disturbed by the presence of hydrous alteration products such as uralite. The combined data are shown in Fig. 1-6 and give a crystallization age of 130±12 m.y. and $\varepsilon_{Nd} = 7.8\pm0.2$.

The lower array shown in Fig. 1-6 is defined by the gabbros

Figure 1-6. Sm-Nd evolution diagram showing the data for whole rocks and coexisting pyroxene-plagioclase and uralite-plagioclase pairs for gabbros from the Samail ophiolite at Ibra, Wadi Fizh, and Rustaq. The gabbros from Ibra give an age of 130±12 m.y. and ε_{Nd} = 7.8±0.2. The gabbro from north of the Samail gap gives an age of 100±20 m.y. and ε_{Nd} = 7.6±0.2. These isochrons are examples of simple closed system Sm-Nd evolution. The ages are considered to be the times of formation of the oceanic crust that was formed in the Hawasina ocean basin and is now preserved as the Samail ophiolite. The distinctive positive ε_{Nd} values of oceanic crust may be used to recognize dismembered ophiolite complexes.

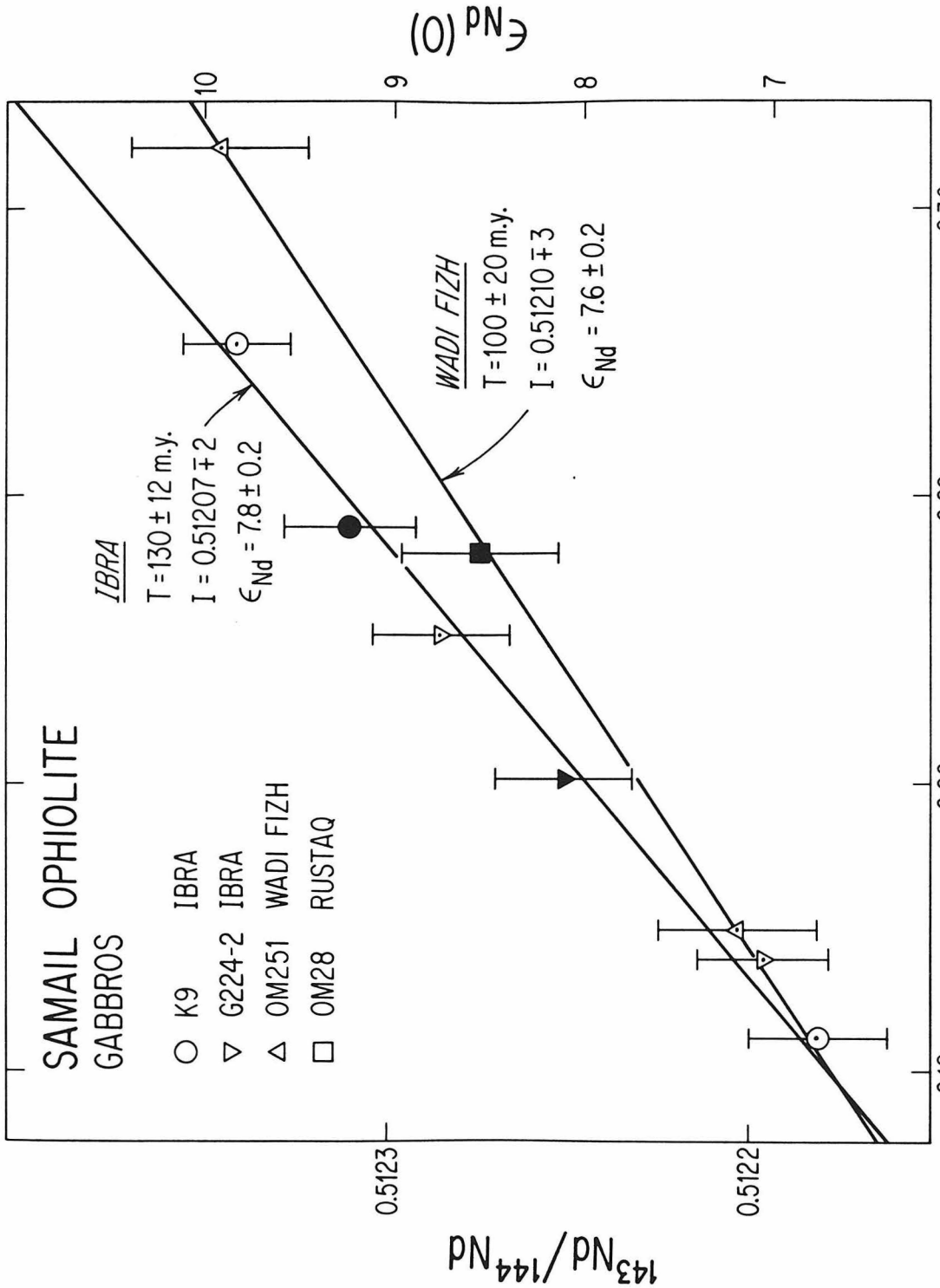
SAMAIL OPHIOLITE
GABBROS
○ K9 IBRA
▽ G224-2 IBRA
△ OM251 WADI FIZH
□ OM28 RUSTAQ
IBRA
T = 130 ± 12 m.y.
I = 0.51207 ∓ 2
ϵ_{Nd} = 7.8 ± 0.2
WADI FIZH
T = 100 ± 20 m.y.
I = 0.51210 ∓ 3
ϵ_{Nd} = 7.6 ± 0.2
$^{143}Nd/^{144}Nd$
$^{147}Sm/^{144}Nd$
$\epsilon_{Nd}(0)$
0.5123
0.5122
0.12
0.20
0.28
0.36
10
9
8
7

Fig. 1-6

OM251 and OM28. These two gabbros were collected from Wadi Fizh and Rustaq, which are located north of the Samail gap . The clinopyroxene and plagioclase from OM251 give an age of 100±20 m.y. and an ε_{Nd} = 7.6±0.3. Although the isochron ages from Ibra and Wadi Fizh overlap within analytical uncertainty, the Sm-Nd results suggest that there may be an age difference of approximately 30 m.y. between these two areas. More precise measurements will be required for this to be established definitively, but the present results clearly indicate that these rocks crystallized in the time interval from 100 m.y. to 130 m.y. These results show that the Sm-Nd technique can also be used to determine crystallization ages of relatively young Mesozoic and Cenozoic mafic complexes.

In contrast to the regular Sm-Nd systematics, the Rb-Sr data from the same samples of the Samail ophiolite give highly discordant results. In Fig. 1-7, a 130 m.y. reference isochron is shown. This isochron is a near horizontal line, and shows that the change in $^{87}Sr/^{86}Sr$ from ^{87}Rb decay is negligible in these samples. The large deviations from the reference isochron and the isotopic relationships between coexisting mineral phases indicate open system behavior due to partial exchange with a source of high $^{87}Sr/^{86}Sr$. These systematics are similar to those illustrated for Nd in the contamination diagram of Fig. 1-5.

Figure 1-7. Rb-Sr evolution diagram showing whole rock and mineral data from the Samail ophiolite. The near horizontal line is a 130 m.y. isochron. The large discrepancy of the data from the reference isochron is an example of open system behavior and is attributed to contamination by seawater with high $^{87}Sr/^{86}Sr$ (see Appendixes 3 and 4).

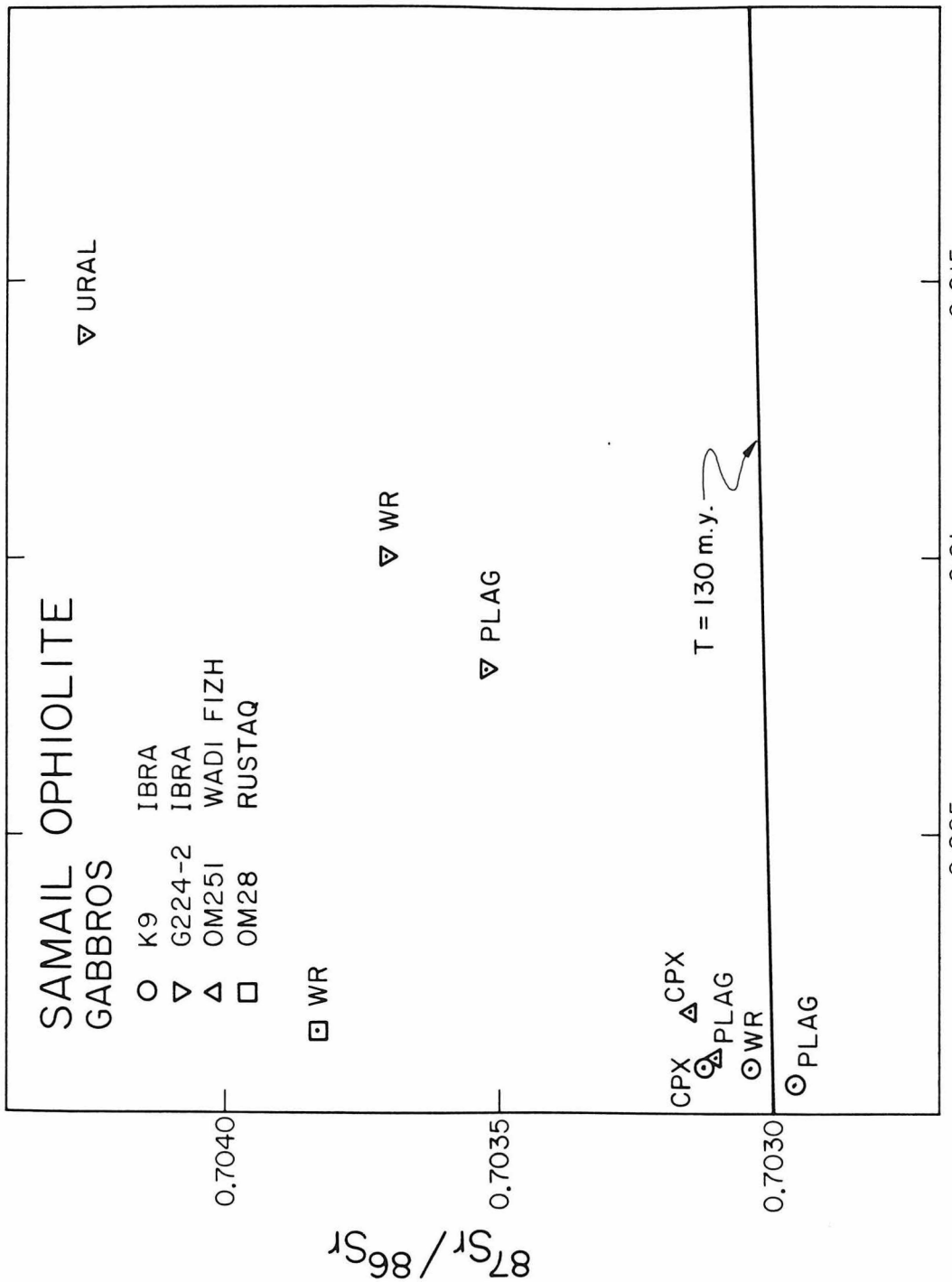
SAMAIL OPHIOLITE
GABBROS
K9 IBRA
G224-2 IBRA
OM251 WADI FIZH
OM28 RUSTAQ
URAL
WR
PLAG
T = 130 m.y.
CPX
PLAG
WR
PLAG
CPX
0.7040
0.7035
0.7030
0.005
0.01
0.015
87Sr/86Sr
87Rb/86Sr

Fig. 1-7

2. Early Archean gneisses from the Minnesota River Valley

The purpose of this study is to use the Sm-Nd isotopic system to better constrain the time and nature of formation of the gneisses of the Minnesota River Valley and to test the effect of metamorphism on Sm-Nd whole rock and mineral systems. The gneisses of the Minnesota River Valley are among the oldest rocks on the earth, but the time of formation of these rocks is not yet well constrained because of their polymetamorphic history and intimate association with younger igneous rocks.

The first radiometric age measurements from the Minnesota River Valley were K-Ar and Rb-Sr age measurements on feldspars and biotites (Goldich, et al., 1956; and Goldich and Hedge, 1962) which suggested two events at 2.5 AE and 1.8 AE. However, the first definitive evidence for the antiquity of this complex was provided by U-Pb zircon ages by Catanzaro (1963). These gave a minimum age of 3.25 AE and suggested a maximum age of up to 3.50 AE (using decay constants recommended by the International Subcommission on Geochronology, Steiger and Jager, 1977). More comprehensive U-Pb zircon studies by Goldich et al. (1970), Farhat (1975), Michard-Vitrac et al. (1977), and Goldich and Wooden (1979) have given similar minimum ages in the range of from 3.15 AE to 3.30 AE, but have revealed a more complex discordance pattern for the zircons. For this reason there is disagreement on the U-Pb zircon age with the results ranging from 3.23 AE (Farhat, 1975; and Michard-Vitrac et al., 1977) to 3.60 AE (Goldich et al., 1970; and Goldich and Wooden, 1979). A similar situation also exists for the Rb-Sr studies by Goldich et al. (1970), Goldich and Hedge (1974), Farhat (1975), Goldich and Wooden (1979), and Goldich et al. (1979). These studies have generally shown discordant systematics and have been interpreted as indicating

ages of from 3.60 AE to 3.72 AE (Goldich et al., 1979; and Goldich and Hedge, 1974) to as young as 3.10 AE - 3.30 AE (Farhat and Wetherill, 1975). In this study it is hoped that by using an independent isotopic system that is relatively inert to metamorphic processes some of the ambiguities in the time of formation of the Minnesota River Valley gneisses may be resolved.

a. T^{Nd}_{CHUR} and T^{Sr}_{UR} model ages

In Fig. 1-8, the Sm-Nd and Rb-Sr model ages of the Montevideo and Morton gneisses are compared. The diagonal line in this figure represents the special case of $T^{Nd}_{CHUR} = T^{Sr}_{UR}$. Rocks which lie on this line presumably have relatively simple Sr-Nd and Rb-Sr isotopic systematics which have been undisturbed since crustal formation and are consistent with derivation from the model source reservoirs (CHUR, UR).

The Sm-Nd and Rb-Sr results for the Morton and Montevideo gneisses are tabulated in Tables 1-1 and 1-2. The geology and sample descriptions are presented in Appendix 5. The most striking feature of these rocks, particularly the tonalitic gneisses, is the strongly fractionated Sm/Nd ratios (i.e., LREE enriched) and extremely primitive measured $^{143}Nd/^{144}Nd$ ratios. For example, the tonalitic gneiss 339 has a measured ratio of $^{143}Nd/^{144}Nd = 0.508880 \pm 22$ which is the lowest yet reported for a whole rock and corresponds to an $\varepsilon_{Nd}(0) = -57.7$. For comparison, a sample which has been Sm free during the earth's history would today have $\varepsilon_{Nd}(0) = -115$. Thus even without correction for ^{147}Sm decay, the primitive $^{143}Nd/^{144}Nd$ ratios in these gneisses shows unequivocally that this is an ancient complex.

In the Montevideo gneiss four felsic samples (608, 605, 606, 609) and one mafic sample (GC-9) appear to follow these simple

Figure 1-8. T^{Nd}_{CHUR} versus T^{Sr}_{UR} model ages. The diagonal line represents the special case of $T^{Nd}_{CHUR} = T^{Sr}_{UR}$. Rocks which lie on this line presumably have relatively simple Sm-Nd and Rb-Sr isotopic systematic which are consistent with derivation from the model source reservoirs CHUR and UR. The felsic Montevideo gneiss samples with $T^{Nd}_{CHUR} \simeq T^{Sr}_{UR}$ form a coherent group having T^{Nd}_{CHUR} and T^{Sr}_{UR} ages ranging from 3.56 AE to 3.72 AE, indicating that this is the time of formation of this crustal segment. The interlayered mafic gneiss GC-9 is also part of this category with T^{Nd}_{CHUR} = 3.54 AE and T^{Sr}_{UR} = 3.57 AE. The other group of Montevideo gneiss samples which lie on the $T^{Nd}_{CHUR} = T^{Sr}_{UR}$ line are the adamellite 431 and the massive mafic gneisses 817 and 845.

The Montevideo gneiss samples which have $T^{Nd}_{CHUR} < T^{Sr}_{UR}$ are 607, 54GN, and GC-2. These also have lower T^{Nd}_{CHUR} ages (3.41 AE to 3.53 AE) than the concordant felsic gneisses. This suggests that in these rocks both the Rb-Sr system and to a lesser extent the Sm-Nd system has been disturbed.

Most of the Morton gneiss samples (apart from 659 and clay (LOC 5) have a narrow range in T^{Nd}_{CHUR} age of from 3.50 AE to 3.62 AE, but a wider range in T^{Sr}_{UR} ages. In general the Morton gneiss has $T^{Nd}_{CHUR} > T^{Sr}_{UR}$.

It is noted that mixtures of two rock which lie on the $T^{Nd}_{CHUR} = T^{Sr}_{UR}$ line, will <u>not</u> in general lie on this line (see appendix 1).

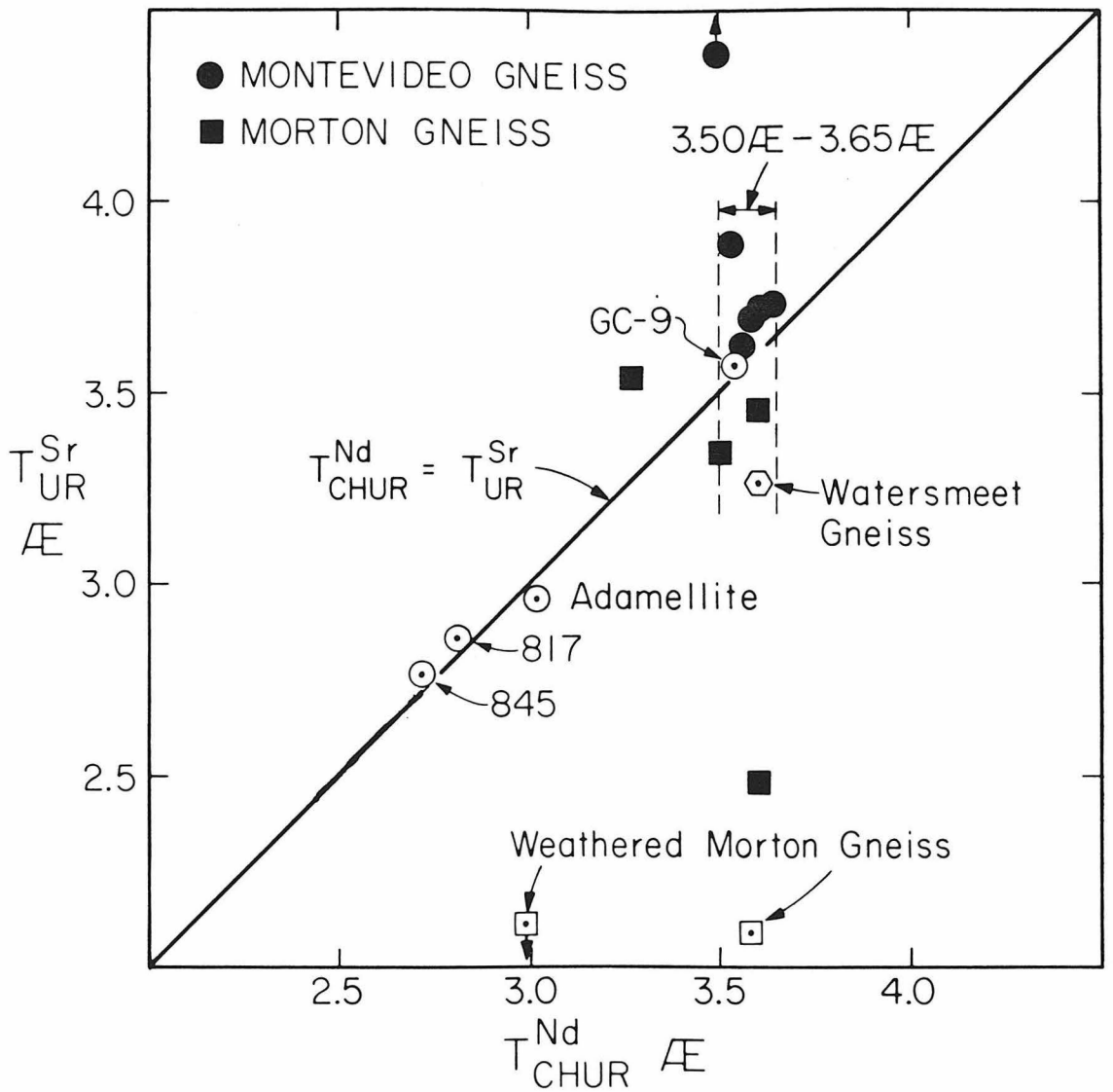
MONTEVIDEO GNEISS
MORTON GNEISS
3.50Æ - 3.65Æ
GC-9
$T^{Nd}_{CHUR} = T^{Sr}_{UR}$
Watersmeet Gneiss
Adamellite
817
845
Weathered Morton Gneiss
T^{Sr}_{UR} Æ
T^{Nd}_{CHUR} Æ
4.0
3.5
3.0
2.5
2.5
3.0
3.5
4.0

Fig. 1-8

systematics having Sm-Nd and Rb-Sr model ages that are approximately identical and in the range of from 3.56 AE to 3.72 AE (Table 1-2). The close concordance of these model ages for this group of samples provides strong evidence for a 3.6 AE age of formation for these rocks.

The Montevideo gneiss samples which do not lie on the $T^{Nd}_{CHUR} = T^{Sr}_{UR}$ line are GC-2, 607, and 54GN. These have high T^{Sr}_{UR} model ages of 6.89 AE, 4.66 AE, and 3.88 AE and T^{Nd}_{CHUR} ages of 3.41 AE, 3.49 AE, and 3.53 AE, respectively. It therefore seems plausible that the discordant ages are due to disturbance of both the Rb-Sr and to a lesser extent the Sm-Nd whole rock systems. This would require both gain of ^{87}Sr and ^{143}Nd or loss of Rb and Sm. This type of effect may be expected if, for example, during, or prior to, segregation of minerals into mafic and felsic layers, they were isotopically re-equilibrated. This would produce felsic layers with unsupported radiogenic ^{87}Sr and ^{143}Nd and mafic layers with excess Rb and Sm.

The other group of Montevideo gneiss samples which lie on the $T^{Nd}_{CHUR} = T^{Sr}_{UR}$ line have distinctly younger model ages. These are the adamellite 431 and the massive mafic gneisses 817 and 845. The younger model ages of $T^{Nd}_{CHUR} = 3.02 \pm 0.05$ AE and $T^{Sr}_{UR} = 2.96 \pm 0.02$ AE for the adamellite 431 is consistent with the field relationships which indicate that the adamellite is a younger neosome component of the Montevideo gneiss. The close agreement of these model ages also indicates that the adamellite is a younger mantle derived component and not a remelted or derivative phase of the older granodiorite-tonalite gneiss complex. The younger T^{Nd}_{CHUR} and T^{Sr}_{UR} ages of

2.72 AE to 2.84 AE which were obtained for the mafic gneisses 817 and 845 from the Memorial Park body (see Appendix 5) indicate that this body is a younger component of the Montevideo gneiss. However, the interlayered mafic gneiss GC-9 (Green Company) has a T^{Nd}_{CHUR} age of 3.54±0.04 AE and a T^{Sr}_{UR} age of 3.57±0.02 AE, which indicates that there are also mafic rocks of essentially the same age as the older felsic Montevideo gneiss.

Most of the Morton gneiss samples (apart from 659 and the residual clay from LOC 5) have a narrow range in T^{Nd}_{CHUR} ages (3.50 AE to 3.62 AE), but a wide range in T^{Sr}_{UR} ages (2.13 AE to 3.54 AE) with $T^{Nd}_{CHUR} > T^{Sr}_{UR}$. For some of these samples, such as the residual clays from the weathered Morton gneiss, the low and more deviant T^{Sr}_{UR} ages are clearly due to loss of Sr relative to Rb during weathering. For the fresh Morton gneiss samples such as 673 and S-1, the lower T^{Sr}_{UR} ages are probably due to their low $^{87}Rb/^{86}Sr$ ratios which makes the T^{Sr}_{UR} ages extremely sensitive to the model parameters.

b. Whole rock data from the Montevideo and Morton gneisses

Most of the samples of the Montevideo gneiss had previously been analyzed for Rb-Sr by Goldich and Hedge (1974) and Goldich et al. (1970). These samples have $\varepsilon_{Nd}(0)$ values ranging from -33.0 to -52.5, reflecting a relatively restricted range in Sm/Nd ratios despite a factor of x5 variation in concentrations. Due to this limited range in Sm/Nd ratios, the samples do not define an isochron. Therefore, for comparison, a T^{Nd}_{CHUR} reference isochron of age 3.6 AE is shown in Fig. 1-9. It can be seen in this figure that most of the samples are within experimental

Figure 1-9. Sm-Nd evolution diagram showing the whole rock data from the Montevideo and Morton gneisses. The filled symbols are the samples of the Montevideo and Morton gneisses which define a whole rock isochron of age 3.54 ± 0.11 (2σ) and $\varepsilon_{Nd} = +0.7 \pm 1.7$. The criterion of $T^{Nd}_{CHUR} \simeq T^{Sr}_{UR}$ (for samples with $f^{Rb/Sr} > 1$) was used to distinguish concordant and discordant samples. The ε_{Nd} value of the Montevideo-Morton gneiss complex is consistent with derivation from a CHUR mantle.

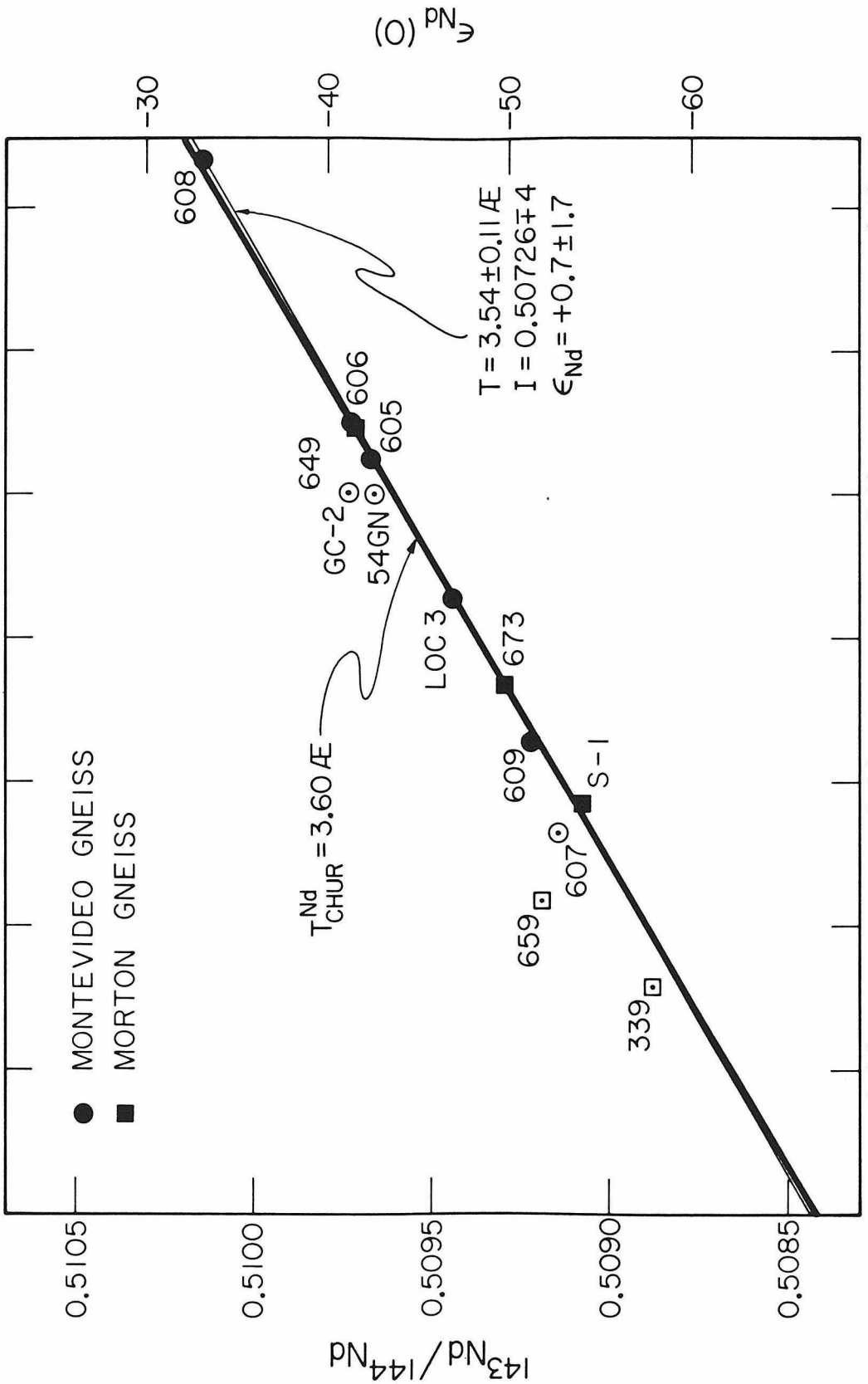
MONTEVIDEO GNEISS
MORTON GNEISS
608
606
605
649
GC-2
54GN
LOC 3
673
609
S-1
607
659
339
T = 3.54±0.11 Æ
I = 0.50726±4
ϵ_{Nd} = +0.7±1.7
T^{Nd}_{CHUR} = 3.60 Æ
ϵ_{Nd} (0)
-30
-40
-50
-60
$^{143}Nd/^{144}Nd$
0.5105
0.5100
0.5095
0.5090
0.5085
$^{147}Sm/^{144}Nd$
0.06
0.08
0.10
0.12

Fig. 1-9

uncertainty of this reference isochron with T^{Nd}_{CHUR} model ages of from 3.54 AE to 3.62 AE. Samples GC-2, 607, and 54GN are displaced above the 3.6 AE reference isochron and have T^{Nd}_{CHUR} model ages of from 3.41 AE to 3.53 AE.

The Morton gneiss consists predominantly of tonalites with generally somewhat more fractionated Sm/Nd ratios and, as already mentioned, the most primitive $\varepsilon_{Nd}(0)$ values ranging from -41.4 to -57.7. As shown in Fig. 1-9 the tonalites from Morton gneiss also have a restricted range in Sm/Nd ratios and also do not define a whole-rock isochron with adequate precision. However, as for the Montevideo gneiss, most of the Morton gneiss samples are within analytical uncertainty of the 3.6 AE T^{Nd}_{CHUR} reference isochron. The exceptions are 339 and 659, which lie above the reference isochron and have T^{Nd}_{CHUR} model ages of 3.50±0.04 AE and 3.27±0.06 AE, respectively. Included in the suite of samples which are within analytical uncertainty of the 3.6 AE reference isochron is a residual clay sample from LOC 3. This analysis had been reported previously by McCulloch and Wasserburg (1978) together with an analysis of another clay sample from LOC 5 which gave a somewhat younger model age of 2.90 AE.

To construct a whole rock Sm-Nd isochron with a sufficient range in the Sm/Nd ratios, it is necessary to combine the data from both the Montevideo and Morton gneisses. This is not unreasonable, as the terranes are juxtaposed, have a similar range in T^{Nd}_{CHUR} model ages, and have overlapping chemical characteristics (Goldich et al., 1979). In addition, it is also necessary to exclude from the whole

rock isochron calculation samples in which the Sm-Nd system has been disturbed and those samples which represent younger generations of gneisses, or mixtures of old and young gneisses. From the geological relationships, it is apparent that the adamellite 431 is a younger phase. This may also be the case for the sample 659 which was collected approximately 40 km S.W. from Morton. The mafic and felsic components of the Montevideo gneiss can also be considered separately. However, due to the complex geological setting, the field relationships alone do not allow disturbed, contaminated, or concordant younger components within the older felsic gneiss to be distinguished. This is in contrast to West Greenland where the Ameralik dykes have been used to distinguish the older Amitsoq gneiss from the younger Nuk gneiss (McGregor, 1973) and in Labrador where the Saglek dykes have been used to distinguish the Uivak I gneiss from the Uivak II gneiss (Hurst et al., 1975).

Due to the lack of comparable field relationships in the Minnesota River Valley, we will use instead the combined T^{Nd}_{CHUR} and T^{Sr}_{UR} model ages as a sample selection criterion to calculate Sm-Nd and Rb-Sr whole rock isochrons. Using the criterion of $T^{Nd}_{CHUR} \simeq T^{Sr}_{UR}$ (for samples with $f^{Rb/Sr} > 1$), the Montevideo gneiss samples 607, 54GN, and GC-2, and the Morton gneiss samples 339 and 659 are excluded from the whole rock isochron calculation.

With this criterion the combined Sm-Nd data for the Montevideo and Morton gneisses (solid symbols Fig. 1-9) give an age of 3.54±0.11 AE (2σ) with an initial $^{143}Nd/^{144}Nd$ ratio of 0.50726∓8 (2σ). This corresponds to ε_{Nd} (3.54 AE) = 0.7±1.7 or to a

Figure 1-10. Rb-Sr evolution diagram showing the whole rock data for the Montevideo and Morton gneisses (data from Goldich and Hedge, 1974; Goldich and Wooden, 1979; Goldich et al., 1979; and this work). The solid symbols show the samples with $T^{Nd}_{CHUR} \simeq T^{Sr}_{UR}$ (for $f^{Rb/Sr} > 1$). These samples define an age of 3.53±0.15 AE (2σ) and an initial ratio of $^{87}Sr/^{86}Sr = 0.7018 \mp 13$ corresponding to $\varepsilon_{Sr} = 22 \pm 18$. The initial $^{87}Sr/^{86}Sr$ ratio is approximately consistent with derivation of the Montevideo-Morton gneiss complex from a UR mantle. However, due to the relatively large uncertainty in the initial $^{87}Sr/^{86}Sr$ ratio, an additional short period (< 0.1 AE) of crustal evolution with $f^{Rb/Sr} > f^{Rb/Sr}_{UR}$ cannot be excluded.

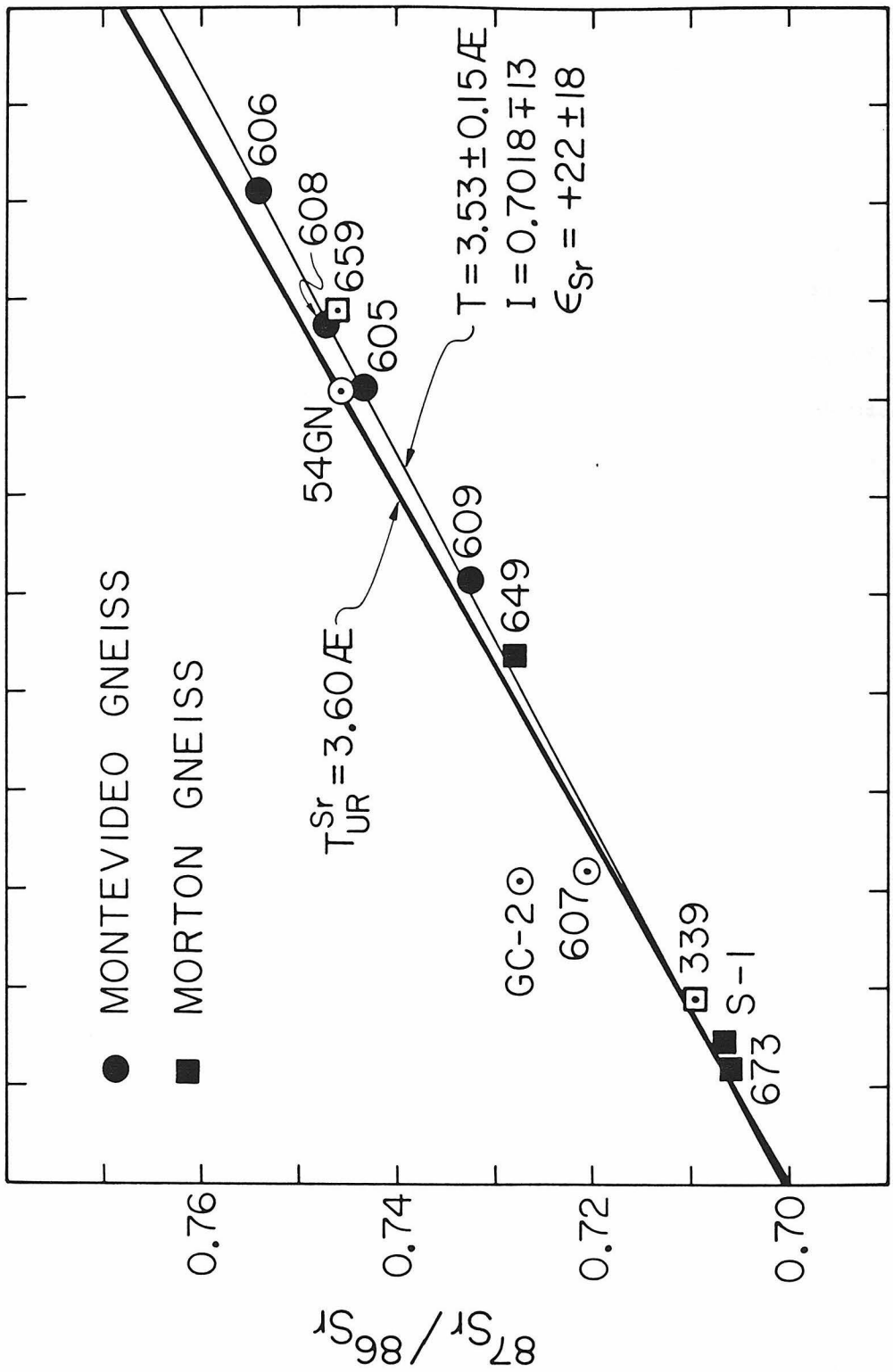
MONTEVIDEO GNEISS
MORTON GNEISS
606
608
659
605
54GN
609
649
GC-20
607
339
S-1
673
T_{UR}^{Sr} = 3.60 AE
T = 3.53 ± 0.15 AE
I = 0.7018 ∓ 13
ϵ_{Sr} = +22 ± 18
$^{87}Sr/^{86}Sr$
$^{87}Rb/^{86}Sr$
0.70
0.72
0.74
0.76
0.2
0.4
0.6
0.8
1.0

Fig. 1-10

time average ratio in the source reservoir from 4.55 AE to 3.55 AE of $^{147}Sm/^{144}Nd = 0.19\pm0.01$. This datum point is also shown in Fig. 1-1. The Rb-Sr data for the Montevideo and Morton gneisses is shown in Fig. 1-10. Using the same criterion of $T^{Nd}_{CHUR} \simeq T^{Sr}_{UR}$ (for $f^{Rb/Sr} > 1$), the same samples give an age of 3.53±0.15 AE (2σ) and an initial $^{87}Sr/^{86}Sr$ ratio of 0.7018∓13 (2σ). This corresponds to $\varepsilon_{Sr}(3.53AE) = +22\pm18$. The excellent agreement between the Sm-Nd and Rb-Sr whole rock isochron ages of 3.54±0.11 AE and 3.53±0.15 AE, respectively, supports the validity of the combined Sm-Nd and Rb-Sr approach described here. For comparison, the Rb-Sr results from Goldich et al. (1979) give an age of 3.62±0.07 AE with an initial ratio of $^{87}Sr/^{86}Sr = 0.7011\pm14$. This relatively low initial $^{87}Sr/^{86}Sr$ ratio is also consistent with a mantle source reservoir having a time average $^{87}Rb/^{86}Sr$ ratio of 0.15±0.10. Therefore both the initial $^{143}Nd/^{144}Nd$ and $^{87}Sr/^{86}Sr$ ratios indicate derivation from a mantle source, rather than reworking or remelting of a substantially older (i.e., ≫ 3.6 AE) crust.

c. Mineral data from the Morton gneiss

To obtain a better understanding of the response of the Sm-Nd system to high grade metamorphic conditions, mineral phases were separated and analyzed from the tonalitic Morton gneiss S-1. This sample contains plagioclase, K-spar, quartz, biotite, and trace amounts of hornblende, sphene, apatite, and zircon. The gneiss consists of coarse-grained, light gray, irregular 1-2 cm quartzo-feldspathic layers and dark gray, thinner discontinuous biotite layers.

In Tables 1-1 and 1-2 and Fig. 1-11 the results of the analysis of the whole rock and mineral separates of plagioclase, hornblende, and apatite are shown. The apatite has the highest Sm/Nd and $^{143}Nd/^{144}Nd$ ratios. Together, the apatite, hornblende, and whole rock define a

Figure 1-11. Sm-Nd evolution diagram showing the mineral and whole rock data from the Morton gneiss S-1. The apatite, hornblende, and whole rock define a linear array corresponding to an age of 3.22 AE and $\varepsilon_{Nd} = -6.0$. This line is clearly offset from the primary $T^{Nd}_{CHUR} = 3.60$ AE reference isochron. The initial $^{143}Nd/^{144}Nd$ ratio of $\varepsilon_{Nd} = -6.0$ and the linear relationship suggests re-equilibration of $^{143}Nd/^{144}Nd$ in the apatite and hornblende with the whole rock at 3.22 AE. The discordant plagioclase point indicates disturbance of this phase at a time < 3.2 AE together with an as yet unidentified complementary phase or phases.

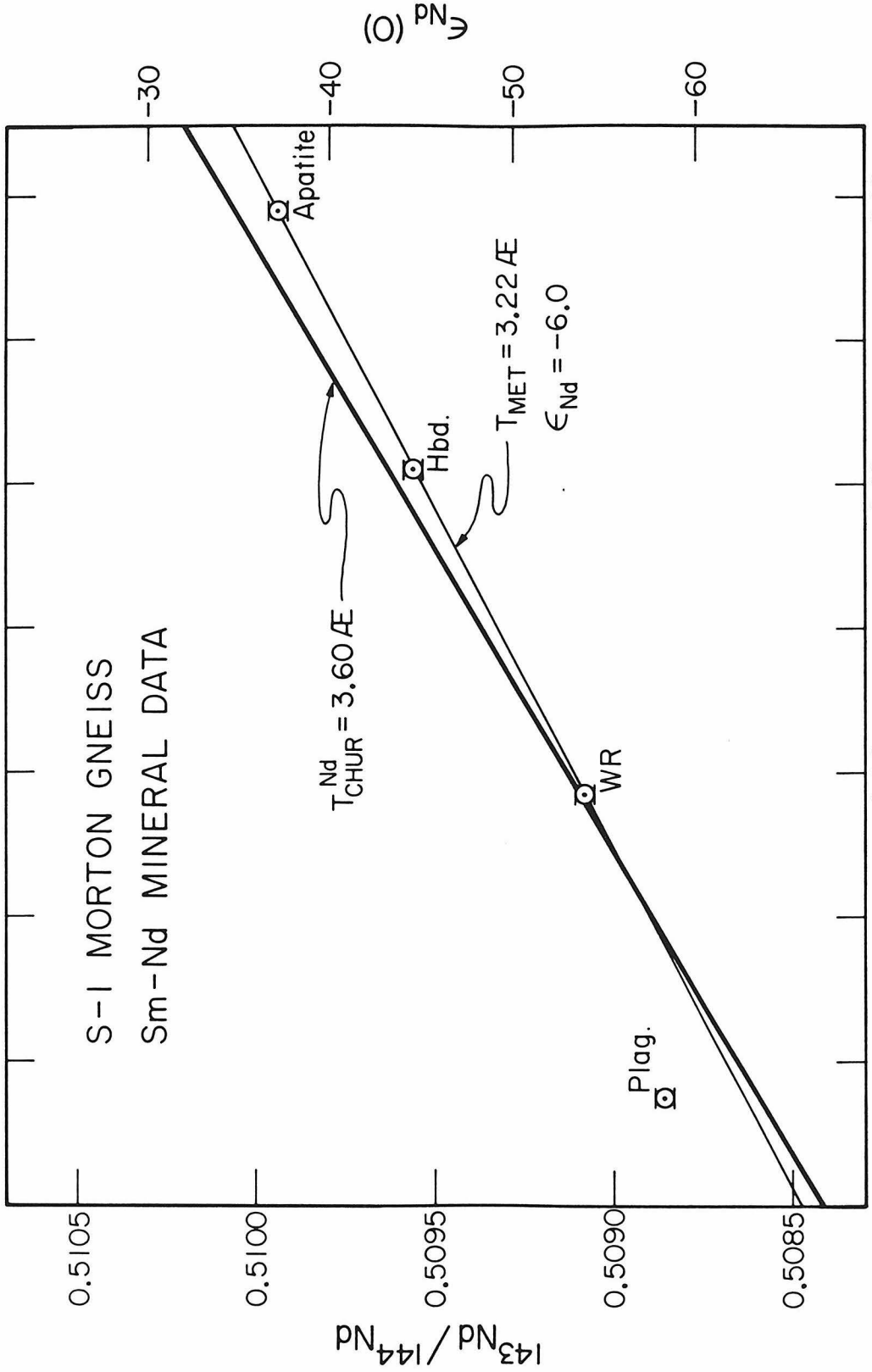
S-I MORTON GNEISS
Sm-Nd MINERAL DATA
Apatite
Hbd.
WR
Plag.
T_{CHUR}^{Nd} = 3.60 Æ
T_{MET} = 3.22 Æ
ϵ_{Nd} = -6.0
$^{143}Nd/^{144}Nd$
$^{147}Sm/^{144}Nd$
ϵ_{Nd} (0)
0.5105
0.5100
0.5095
0.5090
0.5085
0.06
0.08
0.10
0.12
-30
-40
-50
-60

Fig. 1-11

linear array which is clearly offset from the primary T^{Nd}_{CHUR} = 3.6 AE reference whole rock isochron. The linear array defined by these minerals corresponds to an age of 3.22 AE and an initial ratio of ε_{Nd} = -6.0. From the previous discussion of the Sm-Nd isotopic systematics in metamorphic systems, it is plausible that the rotated apatite, hornblende, and whole rock linear array is due to re-equilibration of $^{143}Nd/^{144}Nd$ in the apatite and hornblende, with the whole rock, at 3.22 AE. The initial $^{143}Nd/^{144}Nd$ ratio of ε_{Nd} = -6.0 is consistent with this interpretation. The 3.22 AE "event" is $\sim$ 0.4 AE younger than the inferred primary age of the tonalitic gneiss of $\sim$ 3.6 AE. The plagioclase mineral separate from S-1 is highly fractionated with $f^{Sm/Nd}$ = -0.705 and contains extremely primitive $^{143}Nd/^{144}Nd$, with $\varepsilon_{Nd}(0)$ = -58.2. The plagioclase does not lie on either the primary T^{Nd}_{CHUR} = 3.6 AE reference isochron, or the apatite, hornblende, whole rock array. Its position suggests disturbance < 3.2 AE ago. The phase required by mass balance to be complementary to the plagioclase has not yet been identified.

The results of Rb-Sr analyses of plagioclase, hornblende, apatite, and the whole rock are shown in Fig. 1-12. The hornblende is by far the most radiogenic point and together with whole rock, apatite, and plagioclase defines an approximately linear array corresponding to an age of 2.51 AE and ε_{Sr} = -0.6. For comparison, the primary reference isochron of T^{Sr}_{UR} = 3.60 AE is also shown. The Rb-Sr data suggest that $^{87}Sr/^{86}Sr$ in the hornblende, apatite, and plagioclase was re-equilibrated with the whole rock at $\sim$ 2.5 AE. The low initial $^{87}Sr/^{86}Sr$ ratio in the reset isochron requires the whole rock to have a low $^{87}Rb/^{86}Sr$ ratio of $f^{Rb/Sr} \approx f^{Rb/Sr}_{UR}$ from 3.6 AE to 2.5 AE. The low measured value of $f^{Rb/Sr}$ = 0.753 (Table 1-2) suggests that this may be plausible. In the inset of

Figure 1-12. Rb-Sr evolution diagram showing the mineral and whole rock data from the Morton gneiss S-1. The hornblende, apatite, plagioclase and whole rock define an approximately linear array corresponding to an age of 2.51 AE and $\varepsilon_{Sr} = -0.6$. The 2.51 AE array is almost completely controlled by the high $^{87}Rb/^{86}Sr$ ratio in the hornblende and is clearly offset from the primary $T_{UR}^{Sr} = 3.60$ AE reference isochron. The low initial $^{87}Sr/^{86}Sr$ ratio at 2.51 AE of $\varepsilon_{Sr} = -0.6$ indicates that from 3.6 AE to 2.5 AE, the whole rock had $f^{Rb/Sr} \approx f_{UR}^{Rb/Sr}$. Thus, the Rb-Sr data provide no evidence of the crustal history of this sample prior to 2.5 AE.

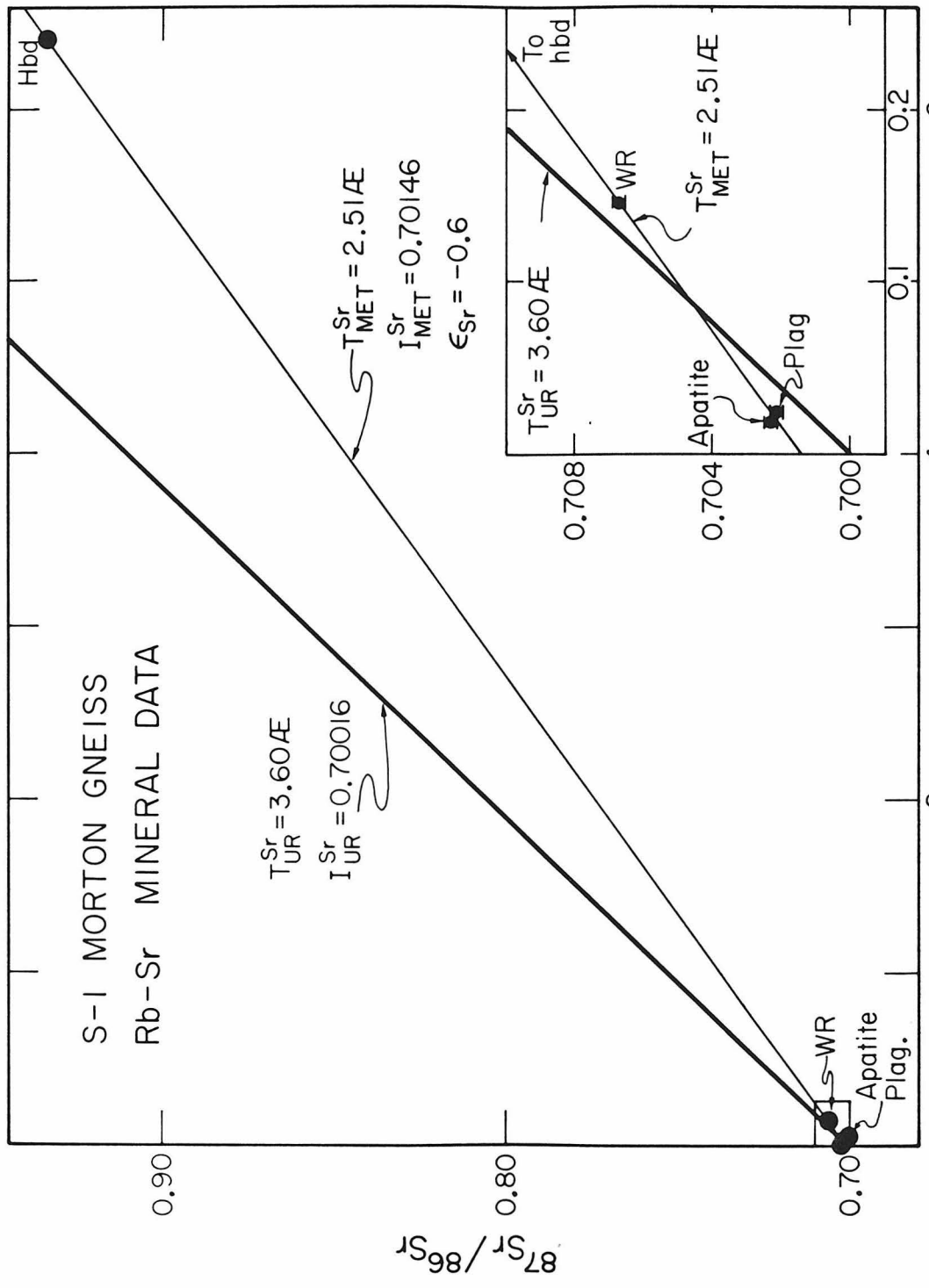
S-I MORTON GNEISS
Rb-Sr MINERAL DATA
Hbd
WR
Apatite
Plag.
T^{Sr}_{UR} = 3.60 Æ
I^{Sr}_{UR} = 0.70016
T^{Sr}_{MET} = 2.51 Æ
I^{Sr}_{MET} = 0.70146
ϵ_{Sr} = -0.6
To hbd
T^{Sr}_{UR} = 3.60 Æ
T^{Sr}_{MET} = 2.51 Æ
0.90
0.80
0.70
0.708
0.704
0.700
0.1
0.2
2
4
6
$^{87}Sr/^{86}Sr$
$^{87}Rb/^{86}Sr$

Fig. 1-12

Fig. 1-12, it can be seen that the Rb-Sr systematics for the apatite and plagioclase are slightly, but clearly, distinct from the 2.51 AE line defined by the hornblende and whole rock. This also suggests a more complex pattern of disturbance, as indicated by the Sm-Nd data for the plagioclase.

From the more extensive Rb-Sr and U-Th-Pb geochronological studies reported by Goldich and Wooden (1979), it is clear that the shearing and high grade metamorphism associated with the formation of the tonalitic gneisses occurred at or prior to $\sim$ 3.0 AE. This is based on emplacement ages for the pegmatitic granite and adamellite-1 of 3.04 AE, and the disturbed Rb-Sr systematics recorded in the amphibolite (Goldich and Wooden, 1979). The 3.2 AE event recorded by Sm-Nd in the apatite and hornblende of S-1 may be due to the emplacement or high grade metamorphism of the gneissic complex. This event presumably also reset the Rb-Sr mineral system and may have disturbed the U-Th-Pb systematics in the zircons.

The younger 2.5 AE event which is still recorded by the Rb-Sr mineral systems is probably due to the emplacement of aplite dikes which are post-kinematic, clearly crosscut the Morton gneiss, and have a Rb-Sr age of 2.59±0.04 AE (Goldich and Wooden, 1979). This younger event presumably almost completely removed the record of the 3.2 AE event from the Rb-Sr mineral system, but left the Sm-Nd mineral system (apart from plagioclase ?) essentially undisturbed. Further work on other mineral phases is being undertaken to substantiate this hypothesis.

From the Sm and Nd concentration data listed in Table 1-1, it

is also apparent that the minor phase apatite, which has a modal abundance of < 1% but a Nd concentration of 419 ppm, makes up a substantial part of the Nd budget in the whole rock (Nd = 15.9 ppm). In contrast, the Nd concentration in the major phases plagioclase and quartz (~ 80% modal abundance) is almost insignificant (Nd = 2.1 ppm). The important role in the whole rock, Sm, Nd budget of the minor phase apatite may account for some of the discordant Sm-Nd whole rock samples. These may be due to inadequate whole rock sampling. The Rb,Sr mineral concentration data indicates that the major phase plagioclase contains most of the Sr in the whole rock budget. This suggests that although the Rb-Sr mineral system is more easily disturbed than the Sm-Nd system, representative whole rock sampling may be less of a problem for Rb-Sr.

IMPLICATIONS FOR THE FORMATION OF EARLY ARCHEAN CONTINENTAL CRUST

The presence of ~3.6 AE gneisses in the Minnesota River Valley has regional importance as rocks of similar age have now been recognized (see Fig. 1-13) in the upper peninsula of Michigan (Peterman et al., 1979; McCulloch and Wasserburg, 1979b; Labrador (Hurst et al., 1975; Barton, 1975), and western Greenland (Moorbath et al., 1972; Baadsgaard, 1973). The possibility, therefore, exists that the gneisses in the Minnesota River Valley represent remnants of a 3.6 AE proto-continent that extended at least as far as western Greenland. The widespread occurrence of rocks of age 3.5 AE - 3.6 AE is also clearly illustrated in Table 1-3 and the histogram of T^{Nd}_{CHUR} model ages (Fig. 1-14). This histogram also shows the period of major crustal formation at 2.6 AE to 2.7 AE. No attempt has been made to make this histogram representative of the volumetric or areal distribution of these rocks. These data together with the well established crustal formation events at ~1.8 AE (Hudsonian regime) and ~1.1-0.9 AE (Grenville regime), suggest intervals of ~0.9 AE between major crustal formation events. Similar compilations for example, of K-Ar ages, have been made by a number of workers (see for example Dearnley, 1965), indicating the presence of "magic numbers". However as pointed out by Wasserburg (1961) many of these apparent hiatuses are probably due to resetting of the radiometric chronometers. The T^{Nd}_{CHUR} model ages presumably do not suffer from these deficiencies and thus the 0.9 AE period may be a more fundamental evolutionary constant of the earth.

There are basically two types of hypotheses that have been

Figure 1-13. Localities (stippled areas and dots) in Minnesota, northern Michigan, Labrador and western Greenland where ages of approximately 3.6 AE or greater, have been determined. Compiled from Baadsgaard (1973, 1976), Barton (1975), Catanzaro (1963), Goldich et al. (1970, 1979), Goldich and Hedge (1974), Hurst et al. (1975), McCulloch et al. (1979b), Moorbath et al. (1972), Peterman et al. (1979), and this work.

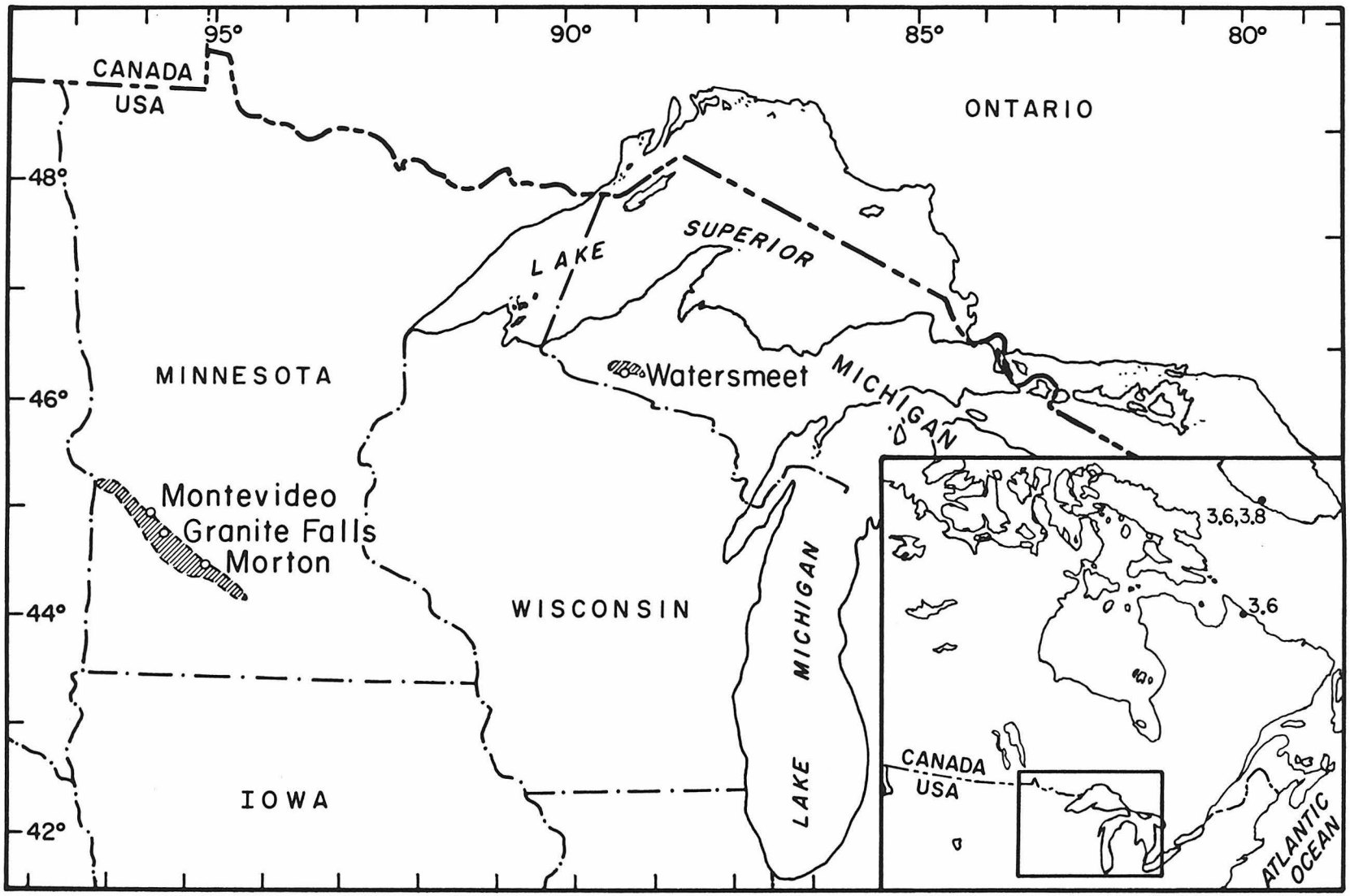
95°
90°
85°
80°
CANADA
USA
ONTARIO
48°
LAKE
SUPERIOR
MINNESOTA
Watersmeet
MICHIGAN
46°
Montevideo
Granite Falls
Morton
WISCONSIN
LAKE MICHIGAN
44°
3.6,3.8
3.6
CANADA
USA
IOWA
42°
ATLANTIC
OCEAN

Fig. 1-13

Figure 1-14. Histogram of Archean T^{Nd}_{CHUR} model ages (the smallest vertical division represents one locality). There is a strong bimodal distribution, reflecting periods of major continental crustal formation at 2.6 AE-2.8 AE and 3.5 AE-3.6 AE. No attempt has been made to weigh the data according to areal or geographical distribution.

Sources: Louis Lake, Preissec Lacorne, Gt. Dyke, Stillwater, Fiskenaesset, and Amitsoq (DePaolo and Wasserburg, 1976a,b); Rhodesian greenstones, Lewisian, Onverwacht and Isua (Hamilton et al., 1977, 1978, 1979a,b); Montevideo, Morton, Duffer Dacite, and Uivak (this work); Canadian Shield composites, KH44 (Black Flag Beds, Coolgardie W.A.), and Figtree Shale (McCulloch and Wasserburg, 1978); Watersmeet (McCulloch and Wasserburg, 1979b); and Lofoten-Vesteralen gneisses (Jacobsen and Wasserburg, 1978).

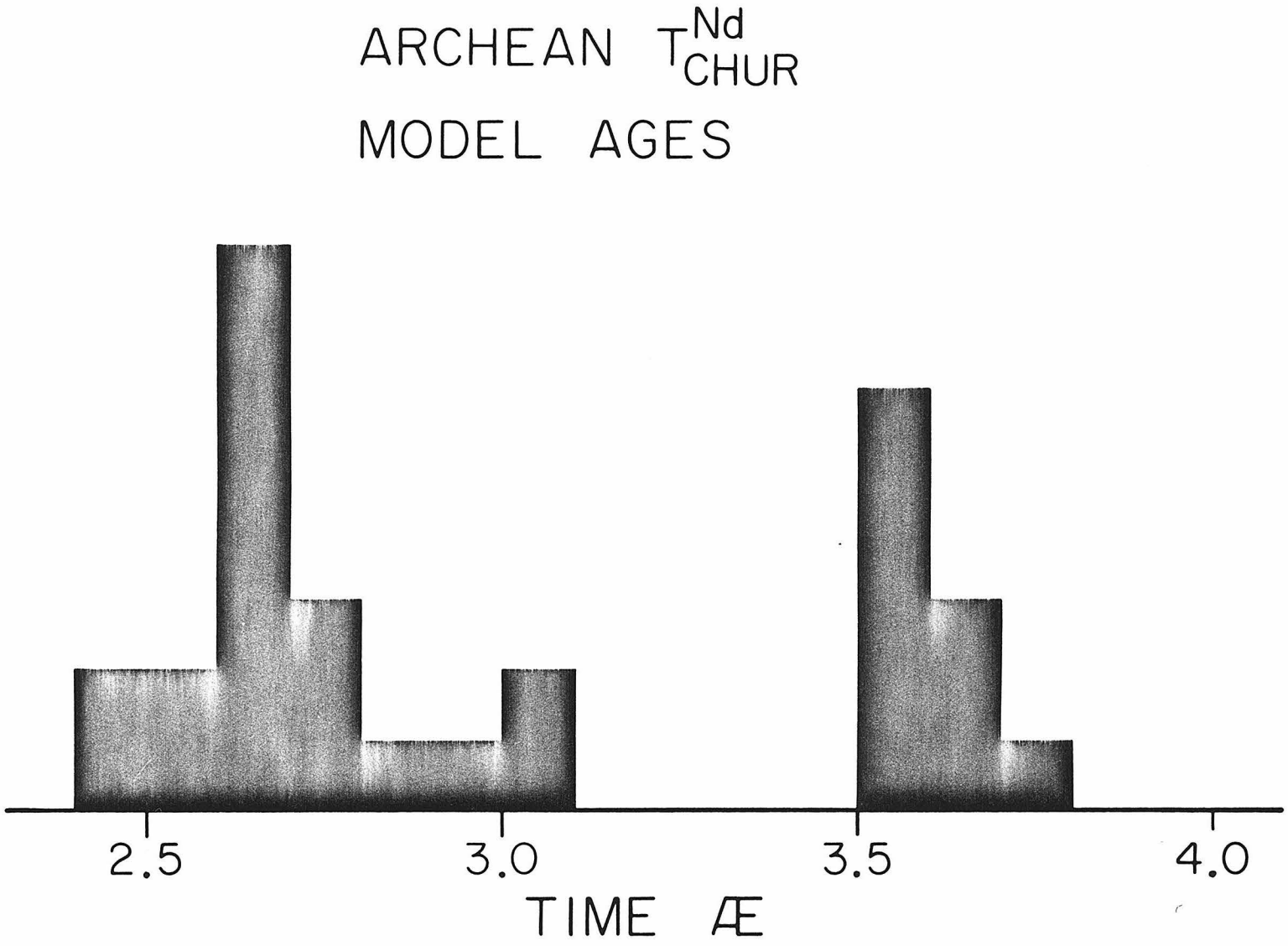

Fig. 1-14

proposed to explain the origin of Archean continental (sialic) crust: 1) They are derived by partial melting and anatexis of pre-existing sialic crust or 2) They are derived by partial melting of the mantle or basaltic crust.

The present available Rb-Sr isotopic data clearly exclude the derivation of most of the Archean gneiss complexes from substantially older (>0.1 AE) high Rb/Sr ($_{f}Rb/Sr \geq 10$) sources. However due to the relatively large uncertainties in the initial $^{87}Sr/^{86}Sr$ ratios (see Fig. 1-15) an origin from an older (>0.4 AE) low Rb/Sr crustal source (e.g. granulite facies lower crust) is still permissible. Bridgwater and Collerson (1976) and Collerson and Fryer (1978) have suggested that the Labrador Uivak gneisses were derived from a substantially older (>0.4 AE) lower crustal granulite facies source with a low Rb/Sr ratio. Although this generally satisfies the requirement for a primitive $^{87}Sr/^{86}Sr$ source reservoir, it has been shown by Green et al. (1969) and McCulloch and Wasserburg (1978) that the REE patterns in granulites are uneffected by metamorphism and similar to upper crustal patterns with LREE enrichments (i.e. low Sm/Nd ratios). Therefore remelting of older lower crustal sources would produce magmas with $\varepsilon_{Nd} \ll 0$ or time average $^{147}Sm/^{144}Nd$ ratios in the source significantly lower than in CHUR. This is contrary to the observations (see Fig. 1-1).

Although the isotopic data exclude the derivation of these gneisses from a crustal source which is significantly older than 3.6 AE, it is still possible, within the age uncertainties (~0.10 AE), to have a multiple-stage derivation. An origin of this type is in fact suggested by the trace element data. In particular, the highly fractionated Sm/Nd ratios (LREE enrichments) are exceedingly difficult to produce

Figure 1-15. Fractional deviations in parts in 10^4 of the initial $^{87}Sr/^{86}Sr$ ratio of Archean rocks, from the evolution in the reference mantle reservoir UR. The evolution in UR is calculated assuming an initial $^{87}Sr/^{86}Sr$ ratio of 0.69898 at 4.55 AE (Papanastassiou and Wasserburg, 1969) and present-day values of $^{87}Sr/^{86}Sr = 0.7045$ and $^{87}Rb/^{86}Sr = 0.0827$ (DePaolo and Wasserburg, 1976b). Compiled from Davies et al. (1970), Hart and Brooks (1977), Jahn and Shih (1974), Hurst et al. (1975), Moorbath and Pankhurst (1976), Moorbath et al. (1972) and this work. The high precision initial $^{87}Sr/^{86}Sr$ ratios of ultramafics in the Abitibi and Onverwacht greenstone belts are in excellent agreement with derivation from a mantle with UR characteristics. The Montevideo-Morton, Uivak and Amitsoq gneisses have somewhat high initial $^{87}Sr/^{86}Sr$ ratios ($\varepsilon_{Sr} = +14$ to $+22$) but within their relatively large uncertainties are approximately consistent with derivation from a UR mantle. Due to the relatively large uncertainties in these initial $^{87}Sr/^{86}Sr$ ratios, an additional stage of evolution, with for example $f^{Rb/Sr} \approx 10$ (typical upper crustal value) for a period of from 0.05 AE to 0.1 AE cannot be excluded.

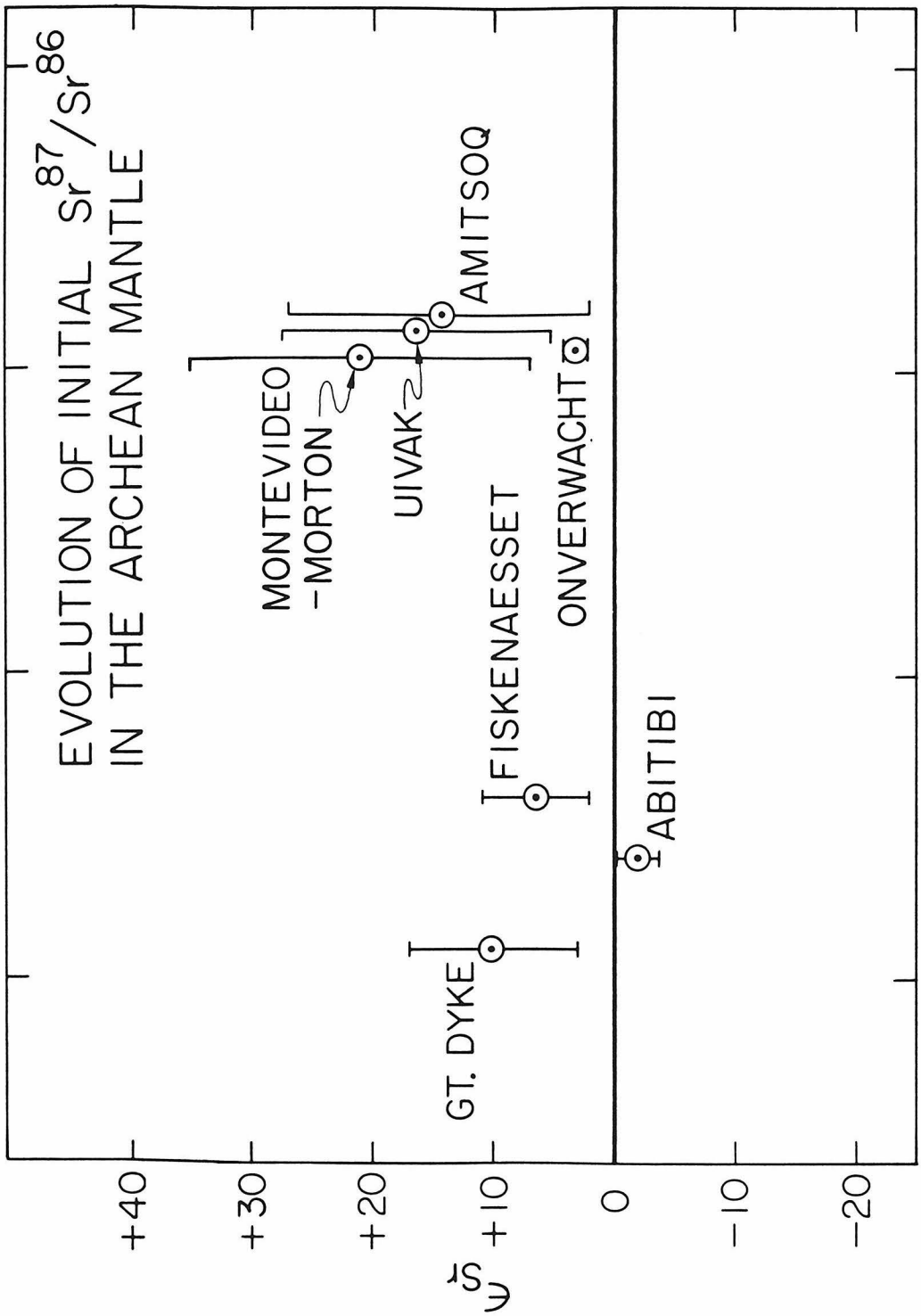
EVOLUTION OF INITIAL Sr^{87}/Sr^{86}
IN THE ARCHEAN MANTLE
MONTEVIDEO
-MORTON
UIVAK
AMITSOQ
ONVERWACHT
FISKENAESSET
ABITIBI
GT. DYKE
+40
+30
+20
+10
0
-10
-20
ε_{Sr}
2.5
3.0
3.5
4.0
TIME Æ

Fig. 1-15

by directly melting of a chondritic Sm/Nd source such as a garnet peridotite or quartz-eclogite (Green and Ringwood, 1968; Barker and Arth, 1976). This can be illustrated using equation (11) of Shaw (1970) for equilibrium modal melting, which gives

$$\frac{C^L}{Co} = \frac{1}{Do + F\ (1-Do)} \qquad (1\text{-}8)$$

where F is the fraction of melting, Co the initial trace element concentration of the solid, C^L the trace element concentration of the liquid and Do the bulk distribution coefficient. The maximum fractionation between liquid and solid is obtained when F approaches zero and equation (1-8) reduces to

$$\frac{C^L}{Co} = \frac{1}{Do} \quad .$$

For the optimum case of partial melting of a quartz-eclogite source, the mineral/liquid partition coefficients (Shimizu, 1974) and Schnetzler and Philpotts, 1970) and modal abundances gives Do^{Sm} ~0.22 and Do^{Nd} ~0.11 and from equation (1-9)

$$\frac{(Sm/Nd)^L}{(Sm/Nd)_o} = 0.5.$$

Therefore for partial melting of a chondritic Sm/Nd source the most fractionated (i.e. lowest Sm/Nd ratio) melt would be expected to have $^{147}Sm/^{144}Nd \geq 0.10$. However from Table 1-1 it can be seen that many of the gneisses have significantly lower $^{147}Sm/^{144}Nd$ ratios. A plausible scenario which could account for these strongly LREE enrichments would be firstly the formation of a sequence of moderately LREE enriched basalts and basaltic andesites which are comparable to modern day island arcs. This sequence could then, within ~0.1 AE, be partially melted, producing more fractionated magmas with strong LREE enrichments. This type of scenario could also account for the common occurrence of

basic or mafic amphibolitic xenoliths on the gneisses. Alternate models could include partial melting of short-lived graywackes (Arth and Hanson, 1975) or a combination of partial melting and fractional crystallization of an eclogite type component.

Table 1-1. Nd and Sr isotopic data from the Minnesota River Valley

Sample	Nd(ppm)	Sr(ppm)	$^{87}Rb/^{86}Sr$[a]	$^{147}Sm/^{144}Nd$[b]	$^{87}Sr/^{86}Sr$[c]	$^{143}Nd/^{144}Nd$[d]
Morton Gneiss						
339[e]	12.1	588	0.191	0.0658	0.7097	0.508880±22[f]
649[e]	51.4	362	0.537	0.1046	0.7279	0.509715±19
659[e]	19.6	283	0.888	0.0717	0.7459	0.509196±34
673[e]	16.8	1448	0.123	0.0869	0.7059	0.509297±24
Clay 3	51.3	38.1	8.375	0.0926	0.9545±3	0.509445±18
Clay 5	102.3	35.1	5.910	0.0955	0.85224±8	0.509946±14
S-1 WR	15.9	913	0.145	0.0786	0.70673±8	0.509080±19
Apatite	419.2	527	0.019	0.1188	0.70231±5	0.509936±27
Hbd.	115.4	106	6.409	0.1011	0.93428±10	0.509563±25
Plag.	2.12	1019	0.024	0.0572	0.70219±2	0.508859±25
Montevideo Gneiss						
605[e]	18.8	288	0.808	0.1023	0.7434	0.509673±34
606[e]	18.8	257	1.009	0.1048	0.7544	0.509726±25
607[e]	29.3	388	0.318	0.0770	0.7206	0.509148±19
608[e]	18.0	308	0.873	0.1234	0.7474	0.510146±18
609[e]	6.66	339	0.613	0.0827	0.7324	0.509222±23
54GN[e]	17.9	270	0.807	0.1004	0.7455	0.509662±25
GC-2	30.6	469	0.308	0.1003	0.72766±10	0.509735±35
431 Adm.[e]	11.3	170	2.388	0.1037	0.8033	0.510040±28
Mafic Gneiss						
817[e]	24.6	324	0.495	0.1064	0.7211	0.510199±28
845	34.7	474	0.230	0.1243	0.71040±3	0.510593±43
GC-9 WR	32.4	315	0.686	0.0964	0.73587±4	0.509559±25
Plag.	4.34	198	0.607	0.0841	0.73495±6	0.509360±28
Sacred Heart Granite						
SH-1	54.2	379	1.182	0.0673	0.74101±6	0.509452±21

[a]Uncertainty ±0.4%. [b]Uncertainty ±0.1%. [c]Normalized to $^{86}Sr/^{88}Sr = 0.1194$. [d]Normalized to $^{146}Nd/^{142}Nd = 0.636151$. [e]Rb-Sr data from Goldich and Hedge (1974) and Goldich et al. (1970). [f]Errors are 2σ mean.

Table 1-2. Evolutionary parameters for Nd and Sr

Sample	$f^{Rb/Sr}$	$\varepsilon_{Sr}(0)$	$f^{Sm/Nd}$	$\varepsilon_{Nd}(0)$	$T^{Sr}_{UR\ AE}$	$T^{Nd}_{CHUR\ AE}$
Morton Gneiss						
339	1.31	73.8	-0.660	-57.7	3.30±0.13[a]	3.50±0.03[b]
649	5.49	332	-0.460	-41.4	3.54±0.03	3.60±0.03
659	9.73	588	-0.630	-51.6	3.53±0.02	3.27±0.05
673	0.487	19.9	-0.551	-49.6	2.41±0.34	3.60±0.04
Clay LOC 3	100.3	3548	-0.522	-46.7	2.09±0.02	3.58±0.03
Clay LOC 5	70.4	2097	-0.506	-36.9	1.76±0.02	2.90±0.03
S-1 WR	0.753	31.6	-0.594	-53.8	2.48±0.11	3.62±0.03
Apatite	-0.770	-31.1	-0.386	-37.0	2.38±0.10	3.82±0.05
Hbd.	76.5	3262	-0.477	-46.7	2.51±0.01	3.91±0.04
Plag.	-0.710	-32.8	-0.705	-58.2	2.72±0.03	3.30±0.03
Montevideo Gneiss						
605	8.77	552	-0.472	-42.3	3.68±0.02	3.58±0.06
606	11.20	708	-0.459	-41.2	3.70±0.02	3.59±0.04
607	2.85	228	-0.602	-52.5	4.66±0.03	3.49±0.03
608	9.56	609	-0.363	-33.0	3.72±0.02	3.64±0.04
609	6.41	396	-0.573	-51.1	3.61±0.02	3.56±0.03
54GN	8.76	582	-0.481	-42.5	3.88±0.02	3.53±0.04
GC-2	2.72	329	-0.482	-41.0	6.89±0.03	3.41±0.06
431 Adm.	27.9	1402	-0.464	-35.1	2.96±0.02	3.02±0.05
Mafic Gneisses						
817	4.99	236	-0.450	-32.0	2.78±0.02	2.84±0.05
845	1.78	83.7	-0.358	-24.3	2.77±0.03	2.72±0.09
GC-9 WR	7.29	445	-0.502	-44.8	3.57±0.02	3.54±0.04
Plag.	6.34	432	-0.566	-48.4	3.98±0.02	3.42±0.04
Sacred Heart Granite						
SH-1	13.3	518	-0.652	-46.6	2.30±0.02	2.86±0.03

[a] $\lambda^{87}Rb = 1.42 \times 10^{-11}\ yr^{-1}$. [b] $\lambda^{147}Sm = 6.54 \times 10^{-12}\ yr^{-1}$.

Table 1-3. Sm-Nd evolutionary parameters and model ages for early Archean complexes

Sample	Nd (ppm)	$f^{Sm/Nd}$	$\varepsilon_{Nd}(0)$	$T^{Nd}_{CHUR\ AE}$
Morton Gneiss				
S-1	15.9	-0.594	-53.8±0.4	3.62±0.03
Montevideo Gneiss				
606	18.8	-0.459	-41.2±0.5	3.59±0.04
Watersmeet Gneiss[a]	41.0	-0.612	-55.0±0.5	3.60±0.04
Uivak Gneiss	45.8	-0.522	-47.6±0.3	3.64±0.03
Amitsoq Gneiss[b]	75.0	-0.390	-35.4±0.6	3.62±0.09
Duffer Dacite	18.6	-0.458	-40.3±0.3	3.52±0.03
Figtree Shale[c]	10.8	-0.317	-28.0±0.4	3.53±0.06

a. McCulloch and Wasserburg, 1979b.

b. DePaolo and Wasserburg, 1976a.

c. McCulloch and Wasserburg, 1978.

REFERENCES

Arth, J. G., and G. N. Hanson, Geochemistry and origin of the early Precambrian crust of northeastern Minnesota, Geochim. Cosmochim. Acta, 39, 325-362, 1975.

Baadsgaard, H., U-Th-Pb dates on zircons from the early Precambrian Amitsoq Gneisses, Godthaab district, west Greenland, Earth Planet. Sci. Lett., 19, 22-28, 1973.

Baadsgaard, H., Further U-Pb dates on zircons from the early Precambrian rocks of the Godthaabsfjord area, west Greenland, Earth Planet. Sci. Lett., 33, 261-267, 1976.

Barker, F., and J. G. Arth, Generation of trondhjemitic-tonalitic liquids and Archean bimodal trondhjemite-basalt suites, Geology, 4, 596-600, 1976.

Barton, J. M., Rb-Sr isotopic characteristics and chemistry of the 3.6 b.y. Hebron Gneiss, Labrador, Earth Planet. Sci. Lett., 27, 427-435, 1975.

Bridgwater, D., and K. D. Collerson, On the origin of early Archean gneisses, Contrib. Mineral. Petrol., 62, 171-178, 1978.

Catanzaro, E. J., Zircon ages in southwestern Minnesota, J. Geophys. Res., 68, 2045-2048, 1963.

Collerson, K. D., and B. J. Fryer, The role of fluids in the formation and subsequent development of early continental crust, Contrib. Mineral. Petrol., 67, 151-167, 1978.

Davies, R. D., H. L. Allsopp, A. J. Erlank, and W. I. Manton, Sr-isotopic studies on various layered mafic intrusions in southern Africa, Geol. Soc. South Africa, Spec. Pub., 1, 576-593, 1970.

Dearnley, R., Orogenic fold-belts and continental drift, Nature, 206, 1083-1087.

DePaolo, D. J., and G. J. Wasserburg, Nd isotopic variations and petrogenetic models, Geophys. Res. Lett., 3, 249-253, 1976a.

DePaolo, D. J., and G. J. Wasserburg, Inferences about magma sources and mantle structure from variations of $^{143}Nd/^{144}Nd$, Geophys. Res. Lett., 3, 743-747, 1976b.

DePaolo, D. J., and G. J. Wasserburg, Sm-Nd age of the Stillwater complex and the mantle evolution curve for neodymium, Geochim. Cosmochim. Acta, 43, 999-1008, 1979a.

DePaolo, D. J., and G. J. Wasserburg, Petrogenetic mixing models and Nd-Sr isotopic patterns, Geochim. Cosmochim. Acta, 43, 615-627, 1979b.

Farhat, J. S., and G. W. Wetherill, Interpretation of apparent ages in Minnesota, Nature, 257, 721-722, 1975.

Farhat, J. S., Geochemical and geochronological investigation of the early Archean of the Minnesota River Valley, and the effect of metamorphism on Rb-Sr whole rock isochrons, Ph.D. Thesis, University of California, Los Angeles, Calif., 1975.

Goldich, S. S., A.O.C. Nier, H. Baadsgaard, and J. H. Hoffman, $^{40}K/^{40}Ar$ dating of the Precambrian rocks of Minnesota (abs.), Geol. Soc. America Bull., 67, 1698-1699, 1956.

Goldich, S. S., and C. E. Hedge, Dating of the Precambrian of the Minnesota River Valley, Minnesota (abs.), J. Geophys. Res., 67, 3561-3562, 1962.

Goldich, S. S., C. E. Hedge, and T. W. Stern, Age of the Morton and Montevideo gneisses and related rocks, southwestern Minnesota, Geol. Soc. America Bull., 81, 3671-3695, 1970.

Goldich, S. S., and C. E. Hedge, 3,800-Myr granitic gneiss in southwestern Minnesota, Nature, 252, 467-468, 1974.

Goldich, S. S., C. E. Hedge, T. W. Stern, J. L. Wooden, J. B. Bodkin, and R. M. North, Archean rocks of the Granite Falls area, southwestern Minnesota, In press, Geol. Soc. America Memoirs, 1979.

Goldich, S. S., and J. L. Wooden, Origin of the Morton Gneiss, southwestern Minnesota, Part III, Geochronology, In press, Geol. Soc. America Memoirs, 1979.

Gray, C. M., D. A. Papanastassiou, and G. J. Wasserburg, The identification of early condensates from the solar nebula, Icarus, 20, 213-239, 1973.

Green, T. H., and A. E. Ringwood, Genesis of the calc-alkaline igneous rock suite, Contr. Mineral. Petrol., 18, 105-162, 1968.

Green, T. H., A. O. Brunfelt, and K. S. Heier, Rare-earth element distribution in anorthosites and associated high grade metamorphic rocks, Lofoten-Vesteraalen, Norway, Earth Planet. Sci. Lett., 7, 93-98, 1969.

Hamilton, P. J., R. K. O'Nions, and N. M. Evensen, Sm-Nd dating of Archean basic and ultrabasic volcanics, Earth Planet. Sci. Lett., 36, 263-268, 1977.

Hamilton, P. J., R. K. O'Nions, N. M. Evensen, D. Bridgwater, and J. H. Allaart, Sm-Nd isotopic investigations of Isua supracrustals and implications for mantle evolution, Nature, 272, 41-43, 1978.

Hamilton, P. J., N. M. Evensen, R. K. O'Nions, H. S. Smith, and A. J. Erlank, Sm-Nd dating of Onverwacht Group volcanics, southern Africa, Nature, 279, 298-300, 1979a.

Hamilton, P. J., N. M. Evensen, R. K. O'Nions, and J. Tarney, Sm-Nd systematics of Lewisian gneisses: implications for the origin of granulites, Nature, 277, 25-28, 1979b.

Hart, S. R., and C. Brooks, The geochemistry and evolution of early Precambrian mantle, Contrib. Mineral. Petrol., 61, 109-128, 1977.

Hurst, R. W., D. Bridgwater, K. D. Collerson, and G. W. Wetherill, 3600 m.y. Rb-Sr ages from very early Archean gneisses from Saglek Bay, Labrador, Earth Planet. Sci. Lett., 27, 393-403, 1975.

Hurst, R. W., Sr evolution in the West Greenland-Labrador craton: a model for early Rb depletion in the mantle, Geochim. Cosmochim. Acta, 42, 39-44, 1978.

Jacobsen, S. B., and G. J. Wasserburg, Interpretation of Nd, Sr and Pb isotope data from Archean migmatites in Lofoten-Vesteralen, Norway, Earth Planet. Sci. Lett., 41, 245-253, 1978.

Jacobsen, S. B., and G. J. Wasserburg, Nd and Sr isotopic study of the Bay of Islands Ophiolite complex and the evolution of the source of mid-ocean ridge basalts, In press, J. Geophys. Res., 1979.

Jahn, B., and C. Shih, On the age of the Archean rocks from the Vermilion district, northeastern Minnesota, Geochim. Cosmochim. Acta, 38, 873-885, 1974.

Lanphere, M. A., G. J. Wasserburg, A. L. Albee, and G. R. Tilton, Redistribution of strontium and rubidium isotopes during metamorphism, World Beater complex, Panamint Range, California, in Isotopic and Cosmic Chemistry (editors H. Craig, S. L. Miller and G. J. Wasserburg), North Holland, 269-320, 1964.

Lugmair, G. W., K. Marti, J. P. Kurtz, and N. B. Scheinin, History and genesis of lunar troctolite 76535 or: How old is old? Proc. Lunar Sci. Conf. 7th, 2009-2032, 1976.

Michard-Vitrac, A., J. Lancelot, C. J. Allegre, and S. Moorbath, U-Pb ages on single zircons from the early Precambrian rocks of west Greenland and the Minnesota River Valley, Earth Planet. Sci. Lett., 35, 449-453, 1977.

McCulloch, M.T. and G.J. Wasserburg, Sm-Nd and Rb-Sr chronology of continental crust formation, Science, 200, 1003-1011, 1978.

McCulloch, M. T., R. T. Gregory, G. J. Wasserburg, and H. P. Taylor, A neodymium, strontium and oxygen isotopic study of the Cretaceous Samail Ophiolite and implications for the petrogenesis and seawater-hydrothermal alteration of oceanic crust, In press, Earth Planet. Sci. Lett., 1979a.

McCulloch, M. T., and G. J. Wasserburg, Sm-Nd model ages from an early Archean tonalitic gneiss, northern Michigan, In press, Geol. Soc. America Memoirs, 1979b.

McGregor, V. R., The early Precambrian gneisses of the Godthaab district, West Greenland, Phil. Trans. R. Soc. (London), A 273, 343-358, 1973.

Moorbath, S., R. K. O'Nions, R. J. Pankhurst, N. H. Gale, and V. R. McGregor, Further rubidium-strontium age determinations on the very early Precambrian rocks of the Godthaab District, West

Greenland, Nature, 240, 78-82, 1972.

Moorbath, S., and R. J. Pankhurst, Further rubidium-strontium age and isotopic evidence for the nature of late Archaean plutonic event in West Greenland, Nature, 262, 124-126, 1976.

Nakamura, N., M. Tatsumoto, P. D. Nunes, D. M. Unruh, A. P. Schwab, and T. R. Wildeman, 4.4 b.y.-old clast in boulder 7, Apollo 17: A comprehensive chronological study by U-Pb, Rb-Sr and Sm-Nd methods, Proc. Lunar Sci. Conf. 7th, 2309-2333, 1976.

O'Nions, R. K., P. J. Hamilton, and N. M. Evensen, Variations in $^{143}Nd/^{144}Nd$ and $^{87}Sr/^{86}Sr$ ratios in oceanic basalts, Earth Planet. Sci. Lett., 34, 13-22, 1977.

Papanastassiou, D. A., and G. J. Wasserburg, Initial strontium isotopic abundances and the resolution of small time differences in the formation of planetary objects, Earth Planet. Sci. Lett., 5, 361-376, 1969.

Papanastassiou, D. A., D. J. DePaolo, and G. J. Wasserburg, Rb-Sr and Sm-Nd chronology and genealogy of mare basalts from the Sea of Tranquility, Proc. Lunar Sci. Conf. 8th, 1639-1672, 1977.

Peterman, Z. E., R. E. Zartman, and P. K. Sims, Tonalitic gneiss of early Archean age from northern Michigan, In press, Geol. Soc. America Memoirs, 1979.

Riley, G. H., and W. Compston, Theoretical and technical aspects of Rb-Sr geochronology, Geochim. Cosmochim. Acta, 26, 1255-1281, 1962.

Schnetzler, C. C., and J. A. Philpotts, Partition coefficients of

rare-earth elements between igneous matrix material and rock-forming phenocrysts. -II., Geochim. Cosmochim. Acta., 34, 331-340, 1970.

Shaw, D. M., Trace element fractionation during anatexis, Geochim. Cosmochim. Acta, 34, 237-243, 1970.

Shimizu, N., An experimental study of the partitioning of K, Rb, Cs, Sr and Ba between clinopyroxene and liquid at high pressures, Geochim. Cosmochim. Acta, 38, 1789-1798, 1974.

Steiger, R. H., and E. Jager, Subcommission on Geochronology: Convention and use of decay constants in geo- and cosmochronology, Earth Planet. Sci. Lett., 37, 359-362, 1977.

Stern, T. W., S. S. Goldich, and M. F. Newell, Effects of weathering on the U-Pb ages of zircons from the Morton gneiss, Minnesota, Earth Planet. Sci. Lett., 1, 369-371, 1966.

Wasserburg, G. J., Crustal evolution and the Precambrian time scale, Ann. N. Y. Acad. Sci., 91, 583-594, 1961.

CHAPTER 2. MODEL AGES AND CONTRAINTS FROM THE LUNAR HIGHLANDS

INTRODUCTION

The lunar highlands are one of the oldest features in the solar system and contain a record of the first 0.5 AE of planetary differentiation. This record of differentiation, from $\sim$ 4.5 AE to $\sim$ 4.0 AE, is unique, as rocks of equivalent age do not appear to have been preserved on the earth. Unfortunately, the interpretation of the lunar highland record is difficult, as it has been largely overprinted by meteoritic impacts.

In this study we will use the Sm-Nd isotopic system in an attempt to obtain further constraints on the evolution of the lunar highlands. Studies of terrestrial rocks (McCulloch and Wasserburg, 1978; Jacobsen and Wasserburg, 1978) have shown that the Sm-Nd isotopic system is relatively inert during metamorphic processes. Therefore, by using the Sm-Nd system it may still be possible to trace the history of early lunar differentiation despite the effects of impact metamorphism.

To obtain Sm-Nd (or Rb-Sr) ages that are pertinent to early lunar evolution, there are two different methodological approaches available. The direct approach is to obtain an isochron using the variations in the Sm/Nd and $^{143}Nd/^{144}Nd$ ratios from genetically related specimens as opposed to the approach of using model ages which give age constraints rather than definitive ages for individual

samples. As most of the highlands has been intensely brecciated by meteorite impacts, it has so far been possible to obtain only two internal Sm-Nd isochrons. These are the troctolite 76535 which gives an age of 4.26±0.06 AE (Lugmair et al., 1976) which is distinctly younger than the Rb-Sr age of 4.54±0.07 (Papanastassiou and Wasserburg, 1976), and the norite breccia 77215 which gives a Sm-Nd age of 4.37±0.07 AE and Rb-Sr age of 4.35±0.04 AE (Nakamura et al., 1976). In addition, Rb-Sr isochrons have given ages of 4.48±0.1 AE for the dunite 72417 (Papanastassiou and Wasserburg, 1975) and although not as well constrained, an age of ~ 4.45 AE for the polymict breccia 12013 (Lunatic Asylum, 1970). Thus apart from the norite breccia 77215 and the discordant Sm-Nd age from the troctolite 76535, these data indicate a major differentiation event at ~ 4.50 AE.

Information on the early differentiation of the moon has also been obtained from the U-Th-Pb isotopic system. This system has recorded a rather well defined event in the interval 4.44 AE to 4.49 AE from a broad variety of highland lithologies (Tera and Wasserburg, 1974; Oberli et al., 1978). Although slightly younger than the Rb-Sr ages, this event or events also probably represents the time of major differentiation of the moon into core, mantle, and crust.

The U-Th-Pb system has also recorded younger events at 3.8 AE to 4.0 AE. These younger events have been attributed to a "terminal lunar cataclysm" characterized by major impact melting and redistribution of lunar crustal rocks on a semi-global scale. Secondary isochrons of ~ 4.0 AE obtained from 12013 and the dunite

(72417) matrix also show that the small scale isotopic systems have been modified by the lunar cataclysm. This has been substantiated by numerous Rb-Sr mineral isochrons and ^{39}Ar-^{40}Ar ages from highland rocks (see compilation of Nyquist, 1977, and Turner, 1977) giving ages from 3.8 AE to 4.1 AE. The pre-cataclystic ^{39}Ar-^{40}Ar record has also with few exceptions (see for example Oberli et al., 1979) been largely obliterated from most of the lunar highlands.

In contrast to these results, Rb-Sr T_{BABI} model ages from a wide variety of highland lithologies have given intermediate ages in the range of $\sim$ 4.1 AE to $\sim$ 4.4 AE. It is not a priori apparent that these intermediate ages are due to partial resetting as a consequence of the terminal cataclysm. The results instead suggest that the highland crust was formed continuously, rather than during a single event at $\sim$ 4.5 AE as indicated by U-Th-Pb and Rb-Sr isochrons.

In an attempt to resolve this apparent conflict we examined the Sm-Nd isotopic systematics in a suite of highland breccias for which T_{BABI} and U-Th-Pb ages had been obtained. The highland breccias that were analyzed are major and direct representatives of the early lunar crust but cannot a priori be shown to be genetically related. It is, therefore, necessary to evaluate the Sm-Nd data using constraints from model ages. The validity and applicability of these model ages will depend on the external boundary conditions and the systematics involved in calculating the ages. We will now examine the systematics and the assumptions involved in the boundary conditions.

MODEL AGES

There are two types of model ages that we will consider. They require different assumptions and depending on the fractionation history and evolution of the sample can give different information. The first type of model age is the T_{JUV} model age which is analogous to the T_{BABI} model age of the Rb-Sr system (Wasserburg and Papanastassiou, 1976). This model age requires the assumption of a unique and well-defined initial value of $^{143}Nd/^{144}Nd$. In the case of the moon, it requires that the moon formed with the same initial $^{143}Nd/^{144}Nd$ ratio as that determined for the Juvinas meteorite by Lugmair and Marti (1977). This assumption cannot be directly tested on the moon as the initial $^{143}Nd/^{144}Nd$ ratio has not been determined on a lunar sample of age 4.56 AE. Based on the initial $^{143}Nd/^{144}Nd$ ratios in the $\sim$ 3.38 AE green glass 15426 and the troctolite 76535 which are consistent with a "chondritic" Sm-Nd evolution (i.e., chondritic as represented by Juvinas) Lugmair and Marti (1978) have concluded that "the lunar initial $^{143}Nd/^{144}Nd$ is consistent with the chondritic Sm-Nd data." However, as will be discussed later, the assumptions of Lugmair and Marti (1978) are untenable as other samples such as the norite breccia 77215 and most of the mare basalts have initial $^{143}Nd/^{144}Nd$ values which are highly deviant from a chondritic Sm-Nd evolution. However, indirect evidence which may support the contention that the moon has the same initial $^{143}Nd/^{144}Nd$ and age as Juvinas, is that within analytical uncertainty this is a characteristic other meteorites such as Angra dos Reis (Lugmair and

Figure 2-1. Schematic diagram showing the evolution of $^{143}Nd/^{144}Nd$ in the lunar highlands. The T_{JUV} model ages correspond to the intersection of the sample evolution with Juvinas initial (I_{JUV}). T_{JUV} model ages are given by the intersection of the sample evolution with Juvinas initial (I_{JUV}). T^{Nd}_{CHUR} model ages are given by the intersection of the sample evolution with chondritic evolution.

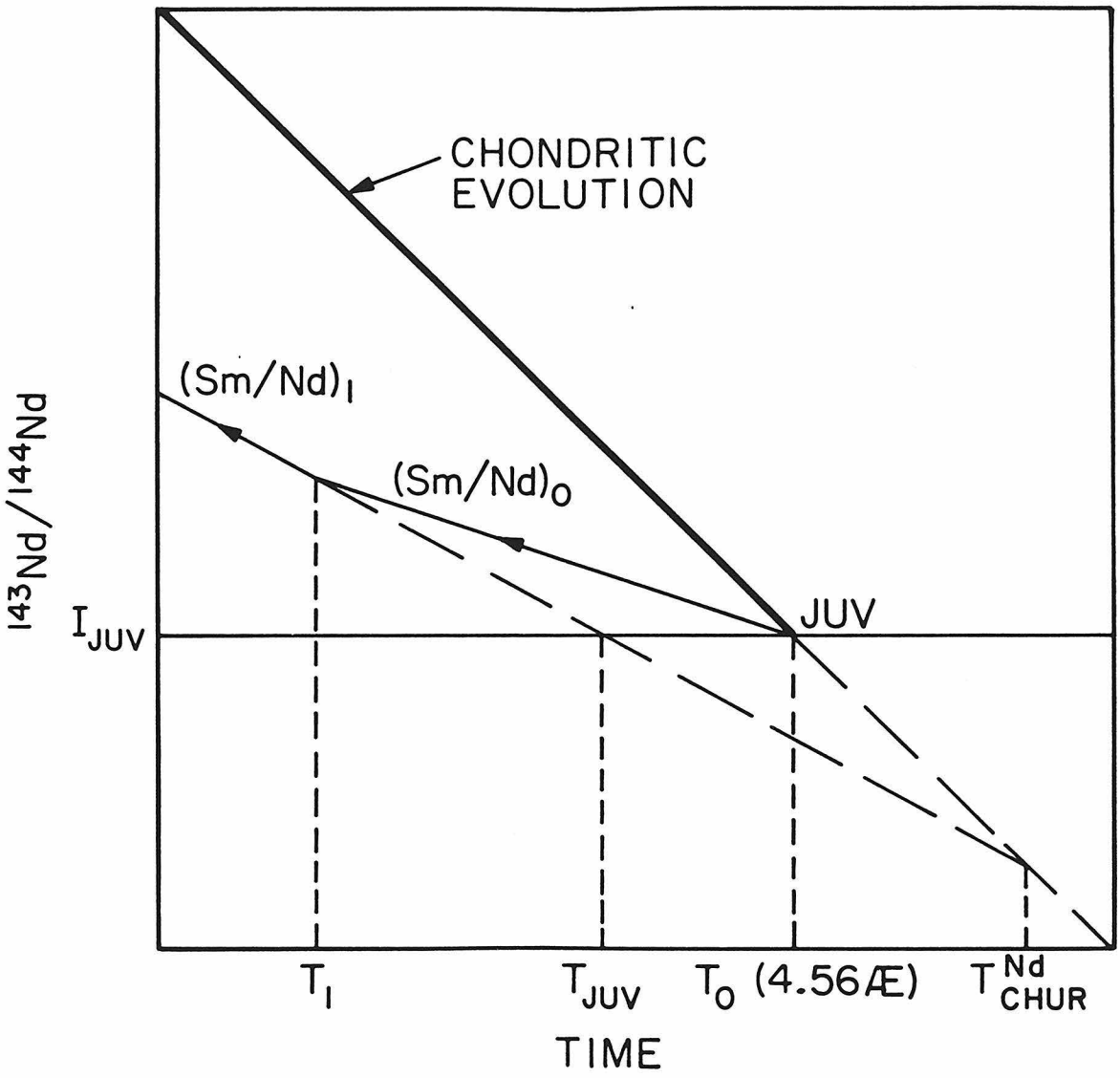
CHONDRITIC
EVOLUTION
(Sm/Nd)$_1$
(Sm/Nd)$_0$
JUV
$^{143}Nd/^{144}Nd$
I_{JUV}
T_1
T_{JUV}
T_0 (4.56Æ)
T^{Nd}_{CHUR}
TIME

Fig. 2-1

Marti, 1977) and Pasamonte (Unruh et al., 1977). For lack of a better estimate but being cognizant of the uncertainties, in this study we will continue to assume that the moon initially had chondritic Sm/Nd and $^{143}Nd/^{144}Nd$ ratios as defined by the Juvinas meteorite.

Using these assumptions, the T_{JUV} age then gives the time required for a sample to evolve to its present $^{143}Nd/^{144}Nd$ value with its measured $^{147}Sm/^{144}Nd$, from the initial $^{143}Nd/^{144}Nd$ in Juvinas. An example is shown in Figure 2-1 for a sample that has had a two-stage evolution, with a ratio $(Sm/Nd)_0$ between T_0 (the time of formation of the moon) and $(Sm/Nd)_1$ between T_1 and the present. Then, the model age T_{JUV} is given by

$$T_{JUV} = \frac{1}{\lambda} \ln \left(1 + \frac{(^{143}Nd/^{144}Nd)_m - I_{JUV}}{(^{147}Sm/^{144}Nd)_1} \right) \qquad (2\text{-}1)$$

where $(^{143}Nd/^{144}Nd)m$ is the ratio measured in the sample, I_{JUV} is the initial $^{143}Nd/^{144}Nd$ in Juvinas (Lugmair and Marti, 1977) and is equivalent to 0.505975, and $(^{147}Sm/^{144}Nd)_1$ is the ratio measured in the sample.

To a good approximation it can be shown that

$$T_{JUV} = T_1 + \frac{(Sm/Nd)_0}{(Sm/Nd)_1} (T_0 - T_1) \qquad (2\text{-}2)$$

As these samples have only small fractionations of Sm/Nd (Table 2-1) the ratio $(Sm/Nd)_0/(Sm/Nd)_1 \sim 1.1$ and therefore $T_{JUV} \sim T_0$ and thus for these samples the T_{JUV} ages are relatively insensitive to T_1 the

time of Sm/Nd fractionation. For Rb/Sr the opposite is true, as the samples have relatively high Rb/Sr ratios (Table 2-2) in a low Rb/Sr environment (Papanastassiou and Wasserburg, 1976). Thus the T_{BABI} model ages are sensitive to the time of Rb/Sr fractionation.

The second type of model age is the T^{Nd}_{CHUR} or T_{ICE} age of Lugmair and Marti (1977), and is the time in the past at which the $^{143}Nd/^{144}Nd$ in the sample coincides with the $^{143}Nd/^{144}Nd$ in a chondritic reservoir. If the sample was fractionated during derivation from a magma reservoir which had a chondritic Sm-Nd evaluation, then the T^{Nd}_{CHUR} age would represent the time of this fractionation. This time is given by

$$T^{Nd}_{CHUR} = \frac{1}{\lambda} \ln \left(1 + \frac{(^{143}Nd/^{144}Nd)_m - (^{143}Nd/^{144}Nd)_{CHUR}}{(^{147}Sm/^{144}Nd)_1 - (^{147}Sm/^{144}Nd)_{CHUR}} \right) \quad (2\text{-}3)$$

where CHUR is the CHondritic Uniform Reservoir (DePaolo and Wasserburg, 1976a)with $(^{143}Nd/^{144}Nd)_{CHUR} = 0.511836$ and $(^{147}Sm/^{144}Nd)_{CHUR} = 0.1936$. It is apparent from this equation that for precise determination of T^{Nd}_{CHUR} ages, a relatively large fractionation of the sample Sm/Nd ratio from the chondritic ratio is required.

Because of the considerable utility of the T^{Nd}_{CHUR} model ages on the earth (McCulloch and Wasserburg, 1978) we will now consider in detail their applicability to the moon. The major assumption required for the validity of T^{Nd}_{CHUR} model ages, is that the sample was derived from a magma reservoir which has had a chondritic Sm/Nd ratio. An example of a reservoir with these characteristics is the

Figure 2-2. Fractional deviations in parts in 10^4 of the initial $^{143}Nd/^{144}Nd$ ratio from the evolution to be found in a reservoir with a chondritic Sm/Nd ratio. Open symbols are Archean terrestrial data from DePaolo and Wasserburg (1976a, 1976b), Hamilton et al. (1977, 1978, 1979, 1979a, 1979b), and McCulloch et al. (1979). Solid symbols are lunar data which display a large dispersion from the chondritic growth curve. The large positive ε_{Nd} values of the Apollo 12 and Apollo 17 maria basalts are consistent with an early differentiation of the moon at approximately 4.5 AE. The lower lines illustrate the evolution of the lunar highland and KREEP samples as determined by this study and Lugmair and Carlson (1978). The T^{Nd}_{CHUR} ages are given by the intersection of these lines with CHUR and for these samples is very sensitive to the model parameters. The offset of the U.C.S.D. data correspond to a variation in $^{143}Nd/^{144}Nd$ of approximately 1.5 parts in 10^4 and is presumably caused by an interlaboratory bias. Note that only two lunar samples lie within error of the $\varepsilon_{Nd} = 0$ line in contrast to the Archean terrestrial rocks.

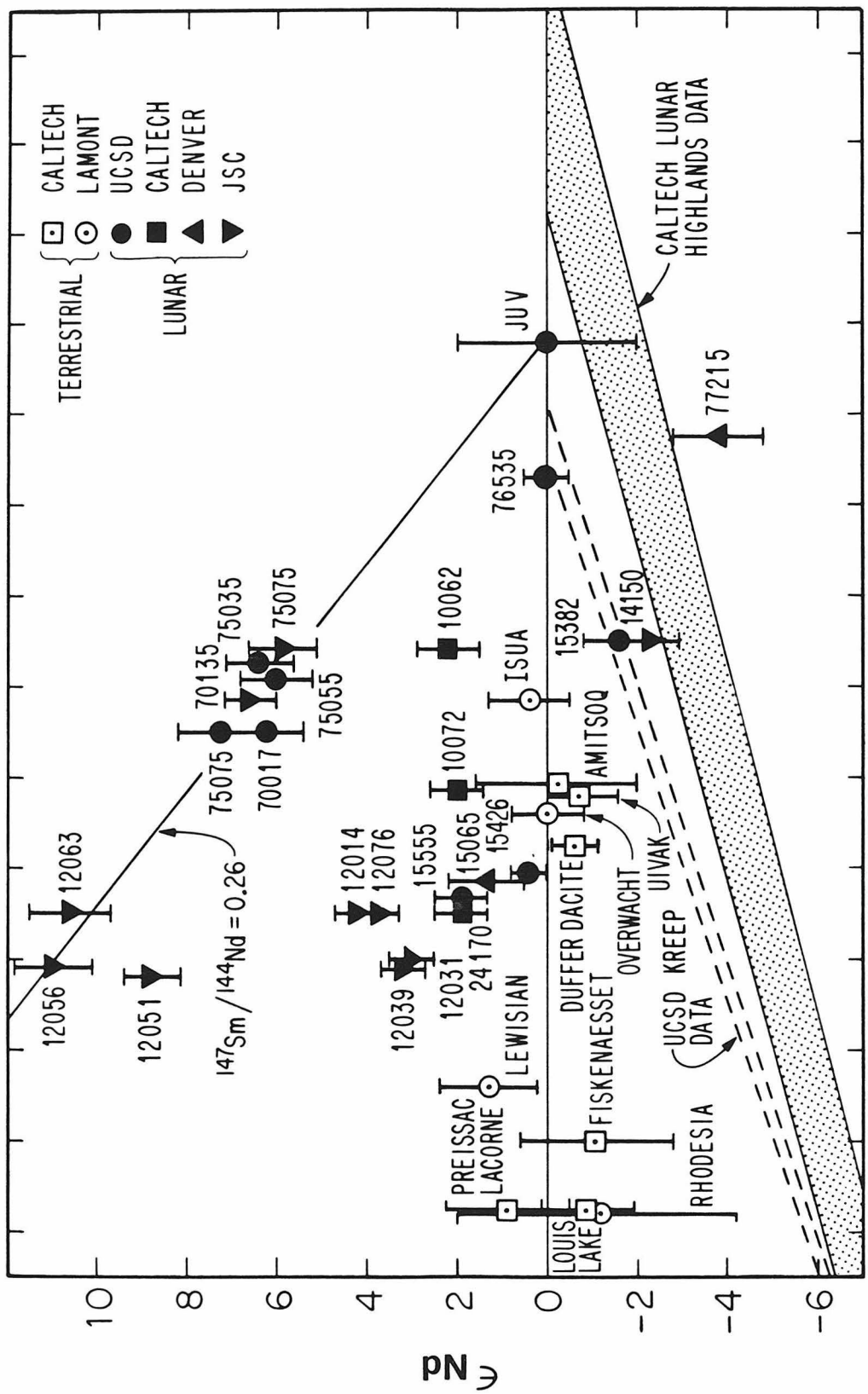
TERRESTRIAL
CALTECH
LAMONT
UCSD
LUNAR
CALTECH
DENVER
JSC
CALTECH LUNAR HIGHLANDS DATA
$^{147}Sm/^{144}Nd = 0.26$
12056
12063
12051
75075
70135
75035
75075
70017
75055
12014
12076
15555
15065
15426
10072
10062
12039
12031
24170
ISUA
JUV
76535
15382
14150
AMITSOQ
77215
DUFFER DACITE
OVERWACHT
UIVAK
KREEP
UCSD DATA
PREISSAC
LACORNE
LEWISIAN
FISKENAESSET
RHODESIA
LOUIS LAKE
ϵ_{Nd}
TIME Æ
10
8
6
4
2
0
-2
-4
-6
2.6
3.0
3.4
3.8
4.2
4.6
5.0

Fig. 2-2

terrestrial reservoirs whose evolution is shown in Figure 2-2. The figure shows the fractional deviations in parts in 10^4 of the initial $^{143}Nd/^{144}Nd$ ratio of Archean terrestrial samples from the evolution to be found in a reservoir with a chondritic Sm/Nd ratio. It can be seen that within the experimental uncertainties, the terrestrial source reservoirs are remarkably consistent with a chondritic Sm/Nd evolution (DePaolo and Wasserburg, 1976a,b). In contrast to this uniformity, the fractional deviations of lunar initial $^{143}Nd/^{144}Nd$ ratios which are also shown in Figure 2-2 produce a highly disparate array indicating source reservoirs with variable Sm/Nd ratios. This distinction between the lunar and terrestrial Nd isotopic evolution has been discussed by Papanastassiou et al. (1977) and must reflect a fundamental difference in planetary evolution. In any case it is apparent that there is no evidence for lunar source regions with only chondritic Sm/Nd ratios as in the earth. The only lunar samples which meet this requirement are the troctolite 76535 and the green glass 15426 (Lugmair and Marti, 1978). However, initial $^{143}Nd/^{144}Nd$ values from other samples (Figure 2-2) indicate different evolutions for the moon. For example, the norite breccia 77215 indicates either a source reservoir with a low Sm/Nd or a lower ($\sim$ 4 parts in 10^4) initial $^{143}Nd/^{144}Nd$ value for the moon. Thus, the T^{Nd}_{CHUR} ages for the moon, in contrast to the earth, cannot be interpreted as giving the time of magma derivation from a source reservoir.

SAMPLE DESCRIPTIONS

The samples analyzed comprise seven highland breccias from the Apollo 14, 16 and 17 missions, representing a broad variety of lithologies and metamorphic textures. Due to the heterogeneity of most of these rocks, the chunks selected are not representative of the total breccia. All samples reported here consist of interior, uncrusted chunks obtained from larger fragments by careful removal of exterior surface by means of stainless steel chisels.

14311 and 14321

These rocks are classified as crystalline matrix breccias belonging to the Fra Mauro group. In Warner's (1972) classification scheme, 14321 is the least annealed breccia (class 4) and 14311 is in an intermediate position (class 5). 14311 and 14321 have typical KREEP rare earth patterns and very high KREEPUTh concentrations (Hubbard et al., 1974; Wänke et al., 1972). Lindstrom et al. (1972) show that KREEPUTh concentration in 14321 is higher in some microbreccia clasts than in the surrounding last-stage matrix, suggesting the presence or introduction of KREEP material in an early stage of brecciation.

Breccia 66075

Parallel to the isotopic work, the petrology of 66075 was examined by Quick et al. (1977). These authors describe the rock as a coherent light-matrix breccia comprised of lithic ANT-suite clasts, impact-generated melt rocks, mineral fragments of plagioclase and subordinate amounts of pyroxene and olivine. No mare basalt components were found. Trace amounts of K-rich glass clasts,

however, were recognized, representing an exotic component that could have a profound effect on the U-Th-Pb, Rb-Sr and Sm-Nd systems of this rock.

Breccias 73235 and 73275

Both breccias are coherent, displaying annealed fabrics. Approximately 95% of 73275 is a fine-grained breccia comprising ~ 80% plagioclase. Its clast population is dominated by plagioclase generally lacking shock features, low Ca-pyroxene and olivine.

The breccia 73235 has a fine-grained matrix which reflects the mineralogical composition of its clast population, consisting of noritic microbreccias, anorthositic and troctolitic fragments as well as mono-mineralic fragments of a similar (coarser-grained) ANT-suite provenance. Two samples were studied from 73235. A homogeneous chunk (73235,50B) consisting predominantly of matrix material and a plagioclase-rich white clast (73235,50W). The REE-pattern of 73235 is KREEP-like, with abundances distinctly low compared to KREEPUTh-rich Apollo 14 breccias (Philpotts et al., 1974).

79215

The rock has been studied in detail by Bickel et al. (1976), who describe it as a granulitic gabbroic anorthosite, averaging ~81% plagioclase, 4.1% high-Ca pyroxene and 9.2% olivine. This nearly monomict breccia is thought to have been derived by relatively deep-seated annealing of a crushed plagioclase-olivine cumulate. The rock is distinct from other ANT-suite derived rocks by its high ratio of high-Ca pyroxene to total pyroxene and high apatite content (~0.8%). Some of the specimens

analyzed by Blanchard (1977) have positive heavy REE slopes in contrast to HREE depleted KREEP, whereas all specimens show a distinct positive Eu anomaly. Warner et al. (1977) link the breccia to a suite of granulitic early impactites with low to negligible KREEP components.

76055

This sample is a recrystallized noritic breccia and has been described by Albee et al. (1973). It contains two distinct lithologies consisting of a vesicular non-poikilitic portion containing fragments of plagioclase olivine and high-Ca pyroxene in a meta-clastic matrix and a non-vesicular, poikilitic portion containing plagioclase and olivine clasts set in a fine-grained poikilitic meta-clastic matrix. 76055 has high KREEPUTh concentrations and has a typical KREEP rare earth pattern (Hubbard et al., 1974).

RESULTS

1. Sm-Nd. The Sm-Nd analytical data and model ages are given in Table 2-1. The samples have Sm/Nd ratios lower by only 10 to 14 percent from the chondritic ratio, and have an extremely limited range in Sm/Nd ratios. In contrast, the Sm and Nd concentrations vary by almost a factor of 50 from the REE rich KREEP rock 14311 (227.5 ppm Nd) to the white anorthositic clast in the breccia 73235,50W (4.79 ppm Nd). There is no correlation between the Sm/Nd ratio and Sm and Nd concentrations in these samples.

The T_{JUV} model ages listed in Table 2-1 range from 4.46 AE for 76055 to 4.52 AE for 73235,50B. These model ages are still distinctly lower than the Juvinas age of 4.56 AE and imply at least a two stage evolution history from 4.56 AE . However, because of the small Sm/Nd fractionation the T_{JUV} ages do not provide any resolution of this fractionation history (see equation 2-2).

The second type of model age which has been discussed is the T^{Nd}_{CHUR} ages. They are shown in Table 2-1 and Figure 2-2 and range from 4.82 AE to 5.40 AE . These ages are significantly greater than the age of the moon indicating either a more complex evolution (as shown for example in Figure 2-1) or incorrect model parameters. Due to the near parallel relationship between the sample evolution line and the chondritic evolution the T^{Nd}_{CHUR} ages are particularly sensitive to the model parameters. For example, a shift in $^{143}Nd/^{144}Nd$ in CHUR of only -1.5 parts in 10^4 would reduce the T^{Nd}_{CHUR} ages by $\sim$0.5 AE which is equivalent to the complete time scale of possible lunar highland formation (4.0-4.5 AE). Considering the dispersion in lunar initial $^{143}Nd/^{144}Nd$ ratios as shown in Figure 2-2,

Table 2-1. Sm-Nd analytical data and model ages for the lunar highlands

Sample	Sm 10^{-8}	^{144}Nd mole/g	$\frac{^{147}Sm}{^{144}Nd}$	$\frac{^{143}Nd}{^{144}Nd}$	T^{JUV} AE	T^{Nd}_{CHUR} AE
73235,50B	6.9809	6.1820	0.1693	0.511057±17	4.52±0.02	4.82±0.13
73235,50W	0.8752	0.7903	0.1661	0.510931±21	4.50±0.02	4.95±0.13
73275	9.5346	8.3462	0.1713	0.511092±19	4.50±0.02	5.02±0.15
79215	0.9388	0.8087	0.1740	0.511159±20	4.49±0.02	5.19±0.18
76055	6.6485	5.7905	0.1721	0.511063±27	4.46±0.03	5.40±0.21
66075	3.6679	3.2306	0.1702	0.511073±23	4.51±0.02	4.91±0.19
14311	42.122	37.515	0.1683	0.511004±24	4.50±0.02	4.95±0.18
14321	28.641	25.500	0.1684	0.511008±27	4.50±0.03	4.94±0.18

Decay constant $\lambda(^{147}Sm) = 0.00654\ AE^{-1}$

a shift of this amount (or greater) cannot be discounted. An offset of this magnitude is also required to explain the discrepancy between the KREEP model ages of Lugmair and Carlson (1978) and those reported here. Thus, although the analytical data are of a high quality, the sensitivity of the T^{Nd}_{CHUR} ages to the model parameters do not enable the T^{Nd}_{CHUR} ages to provide a useful chronology of the formation of the lunar highlands.

Despite this limitation, the Sm-Nd system does provide some resolution of the variations in either the formation age or initial $^{143}Nd/^{144}Nd$ ratios between the highland samples. This is evident in Figure 4-3 which shows the initial $^{143}Nd/^{144}Nd$ ratio for these rocks as a function of $^{147}Sm/^{144}Nd$ at 3.9 AE. The data points therefore represent whole rock data as would be measured in the laboratory at 3.9 AE. Figure 2-3 therefore has the advantage of amplifying the sample evolution from $\sim$ 4.5 AE to 3.9 AE. An age of 3.9 AE was chosen as other isotopic systems have shown that at approximately this time many of the samples were recrystallized during the "lunar cataclysm" but have since remained undisturbed. If the samples were undisturbed at 3.9 AE and all derived contemporaneously from a magma reservoir with the same initial $^{143}Nd/^{144}Nd$ ratio then they will produce a linear array with the slope corresponding to the time of formation (i.e., Sm/Nd fractionation). However, if the Sm-Nd system in these samples was completely reset at 3.9 AE, then they would form a horizontal array. The data do not produce a linear array and with the exception of 76055, all the data points form a tight cluster with deviations (parts in 10^4)

Figure 2-3. Sm-Nd evolution diagram for lunar highlands with $^{143}Nd/^{144}Nd$ and $^{147}Sm/^{144}Nd$ ratios corrected to 3.9 AE assuming a single stage evolution since this time. The data points therefore represent whole rock data as would be measured in a laboratory 3.9 AE ago. The data do not define an isochron and provide evidence for significant variations in the initial $^{143}Nd/^{144}Nd$ ratio between the samples of at least 1 part in 10^4.

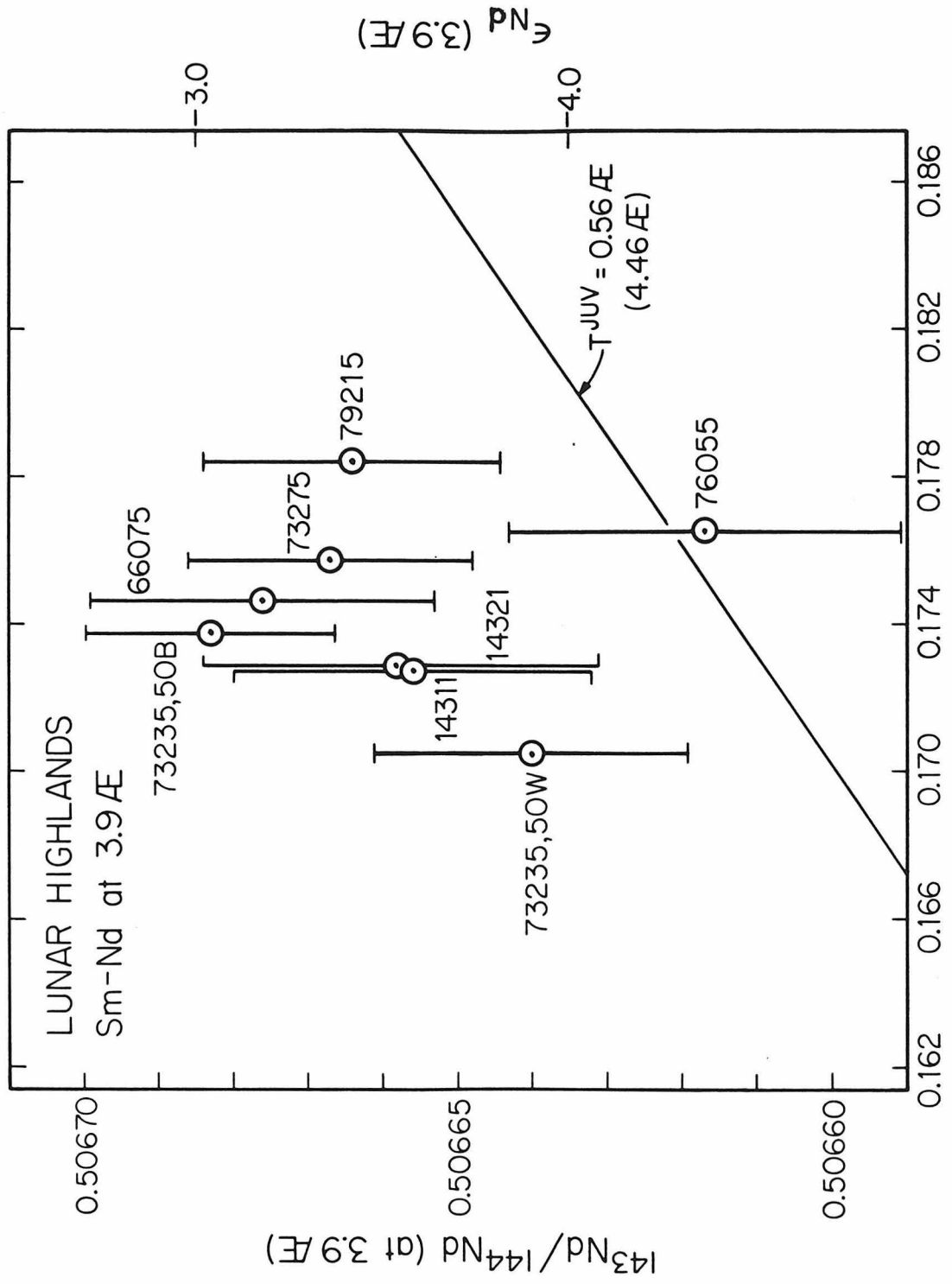
LUNAR HIGHLANDS
Sm-Nd at 3.9 Æ
73235,50B
66075
73275
79215
14321
14311
73235,50W
76055
T^JUV = 0.56 Æ
(4.46 Æ)
0.50670
0.50665
0.50660
143Nd/144Nd (at 3.9 Æ)
0.162
0.166
0.170
0.174
0.178
0.182
0.186
147Sm/144Nd (at 3.9 Æ)
-3.0
-4.0
εNd (3.9 Æ)

Fig. 2-3

of the initial $^{143}Nd/^{144}Nd$ from the chondritic ratio at 3.9 AE of approximately ε_{Nd} (3.9 AE) = -3. However, 76055 has ε_{Nd} (3.9 AE) = -3.8 which is significantly different from the other points, indicating a distinct source reservoir with initial $^{143}Nd/^{144}Nd$ lower than that in the other samples by approximately 1 part in 10^4. Smaller variations in the initial $^{143}Nd/^{144}Nd$ may also be present between the other samples. It is also apparent in Figure 2-3 that due to the limited dispersion of the $^{147}Sm/^{144}Nd$ and variable initial $^{143}Nd/^{144}Nd$ ratios that these points do not define a useful whole rock isochron.

2. Rb-Sr. The Rb-Sr analytical data and T_{BABI} model ages are given in Table 2-2. The samples have an extremely wide variation in Rb concentrations of from 0.984 ppm (73235,50W) to 17.9 ppm (14321) and a more limited range in Sr of from 132 ppm to 229 ppm. In contrast to the restricted range for $^{147}Sm/^{144}Nd$ ratios, the $^{87}Rb/^{86}Sr$ ratios have a wide variation of from 0.02159 to 0.2754.

The T_{BABI} ages (which are equivalent to the Sm-Nd T_{JUV} ages) are listed in Table 2-2 and range from 4.16 AE (66075) to 4.39 AE (76055). As many of the samples have large enrichments in Rb/Sr compared to the low Rb/Sr source reservoirs, T_{BABI} ages can provide useful constraints on the time of the last Rb/Sr fractionation. The range in T_{BABI} ages could therefore indicate magmatism from $\sim$ 4.4 AE to as late as $\sim$ 4.2 AE or could reflect a multiple stage evolution between $\sim$ 4.5 AE and the time of recrystallization of these rocks at $\sim$ 3.9 AE. To amplify the evolution prior to recrystallization at $\sim$ 3.9 AE, in Figure 2-4, we show the $^{87}Sr/^{86}Sr$ and $^{87}Rb/^{86}Sr$ ratios corrected to

Table 2-2. Rb-Sr analytical data and model ages for the lunar highlands

Sample	Rb 10^{-8}	^{88}Sr mole/g	$\frac{^{87}Rb}{^{86}Sr}$	$\frac{^{87}Sr}{^{86}Sr}$	T^{BABI} AE
73235,50B	6.639	136.2	0.1137	0.70606±5	4.27±0.03
73235,50W	1.151	124.4	0.0216	0.70030±5	4.18±0.16
73275	10.66	155.6	0.1598	0.70870±5	4.16±0.02
76055	6.090	151.1	0.0940	0.70503±6	4.39±0.04
66075	2.635	174.5	0.0352	0.70112±5	4.16±0.10
14311	18.64	216.3	0.2010	0.71192±6	4.39±0.02
14321	20.94	177.5	0.2752	0.71620±9	4.27±0.02

Decay constant $\lambda(^{87}Rb) = 0.0142\ AE^{-1}$

Figure 2-4. Rb-Sr evolution diagram for lunar highlands with $^{87}Sr/^{86}Sr$ and $^{87}Rb/^{86}Sr$ ratios corrected to 3.9 AE assuming a single stage evolution since this time. The data points therefore represent whole rock data as would be measured in a laboratory at 3.9 AE. The Rb-Sr data do not define a whole rock isochron and for a BABI initial ratio give ages from 0.2 AE (4.1 AE) to 0.5 AE (4.4 AE). Three Apollo 17 samples form a near horizontal array suggesting Rb (or Sr) redistribution at 3.9 AE.

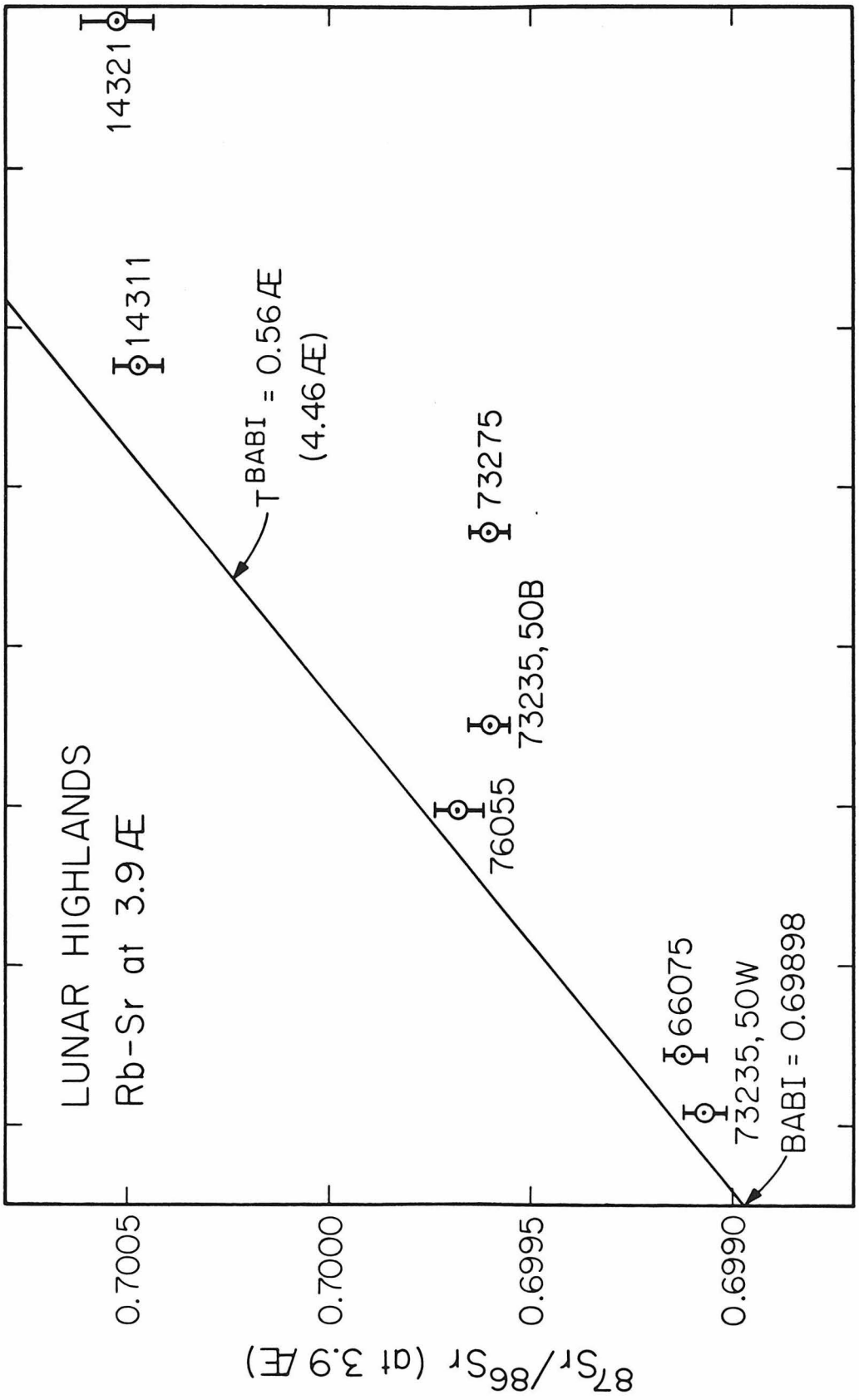
LUNAR HIGHLANDS
Rb-Sr at 3.9 AE
T^{BABI} = 0.56 AE
(4.46 AE)
BABI = 0.69898
14321
14311
73275
73235,50B
76055
66075
73235,50W
0.7005
0.7000
0.6995
0.6990
.02
.06
0.10
0.14
0.18
0.22
0.26
$^{87}Sr/^{86}Sr$ (at 3.9 AE)
$^{87}Rb/^{86}Sr$ (at 3.9 AE)

Fig. 2-4

Figure 2-5. Sm-Sr evolution diagram for lunar highlands with $^{87}Sr/^{86}Sr$ and $^{147}Sm/^{86}Sr$ ratios corrected to 3.9 AE. If the dispersion in the Rb-Sr data (Figure 2-4) is only due to redistribution of the more volatile Rb at 3.9 AE, then $^{87}Sr/^{86}Sr$ versus the refractory $^{147}Sm/^{86}Sr$ ratio should eliminate this scatter. Although the scatter is reduced somewhat, the data do not produce a linear array indicating either variable Sm/Rb or initial $^{87}Sr/^{86}Sr$ ratios at 3.9 AE. A reference line is shown which corresponds to T_{BABI} = 4.46 AE for $^{147}Sm/^{87}Rb$ = 1.0.

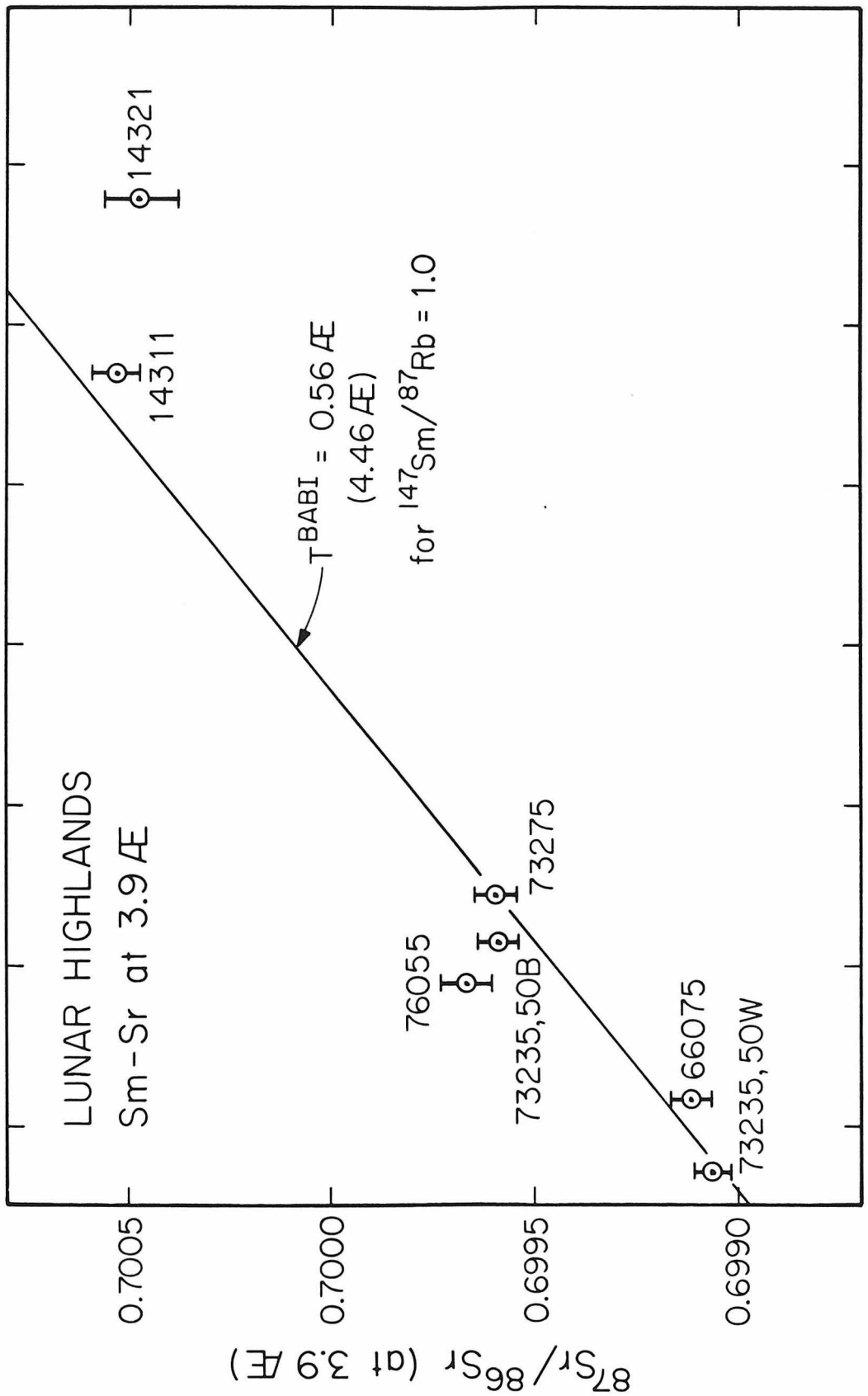
LUNAR HIGHLANDS
Sm-Sr at 3.9 AE
T^{BABI} = 0.56 AE
(4.46 AE)
for $^{147}Sm/^{87}Rb$ = 1.0
14321
14311
76055
73235,50B
73275
66075
73235,50W
0.7005
0.7000
0.6995
0.6990
.02
.06
0.10
0.14
0.18
0.22
0.26
$^{87}Sr/^{86}Sr$ (at 3.9 AE)
$^{147}Sm/^{86}Sr$ (at 3.9 AE)

Fig. 2-5

3.9 AE in a manner analogous to that described for Sm-Nd (Figure 4-3). Redistribution of Rb/Sr at 3.9 AE, presumably due to the effects of impact metamorphism, appears to be evident in at least three samples, 76055, 73235,50B, and 73275. They form an approximate horizontal array. Similar effects may also be present for the Apollo 14 samples 14311 and 14321. Assuming that this disturbance of the Rb-Sr system is only due to redistribution of Rb at 3.9 AE, then as described by Palme (1977) a plot of $^{87}Sr/^{86}Sr$ versus $^{147}Sm/^{86}Sr$ should produce a linear array. This is shown in Figure 2-5 and it can be seen that the scatter is somewhat reduced. However, some dispersion is still present indicating either variable Sm/Rb or initial $^{87}Sr/^{86}Sr$ ratios prior to 3.9 AE.

3. U-Th-Pb. The U-Th-Pb results and their interpretation have already been discussed in detail by Oberli et al. (1979), and therefore only the conclusions relevant to the interpretation of the Sm-Nd and Rb-Sr results will be presented here. In Figure 2-6, the data are shown on a U-Pb evolution diagram (Tera and Wasserburg, 1972) with coordinates ($^{238}U/^{206}Pb$, $^{207}Pb/^{206}Pb$). The data form an approximately linear array with a lower-intersection with the concordia at 3.86±0.05 AE and an upper-intersection at 4.46±0.03 AE. For $^{238}U/^{206}Pb = 0$, the initial radiogenic $^{207}Pb/^{206}Pb = 1.475±0.004$.

In the U-Pb evolution diagram, a mixture of two components lie on a straight-line segment between two end members. In terms of a simple two stage evolution, the two end members are (1) the initial radiogenic Pb produced in the interval 4.46 AE-3.86 AE which corresponds

Figure 2-6. U-Pb evolution diagram after Tera and Wasserburg (1972) showing radiogenic Pb data (corrected for PAT) of Oberli et al. (1978) for terra samples from Apollo 14, 16, and 17. The numbers in parentheses next to the sample number is the measured $\mu \equiv {}^{238}U/{}^{204}Pb$ and U concentration for that sample. The line intersecting the concordia at 4.46 AE and 3.86 AE in a reference isochron which is a best-fit line to the data array and has an initial radiogenic ${}^{207}Pb/{}^{206}Pb$ ratio of 1.475. The upper intersection is interpreted as the time of formation of the lunar highlands and the lower intersection as the time of impact metamorphism (Oberli et al., 1978).

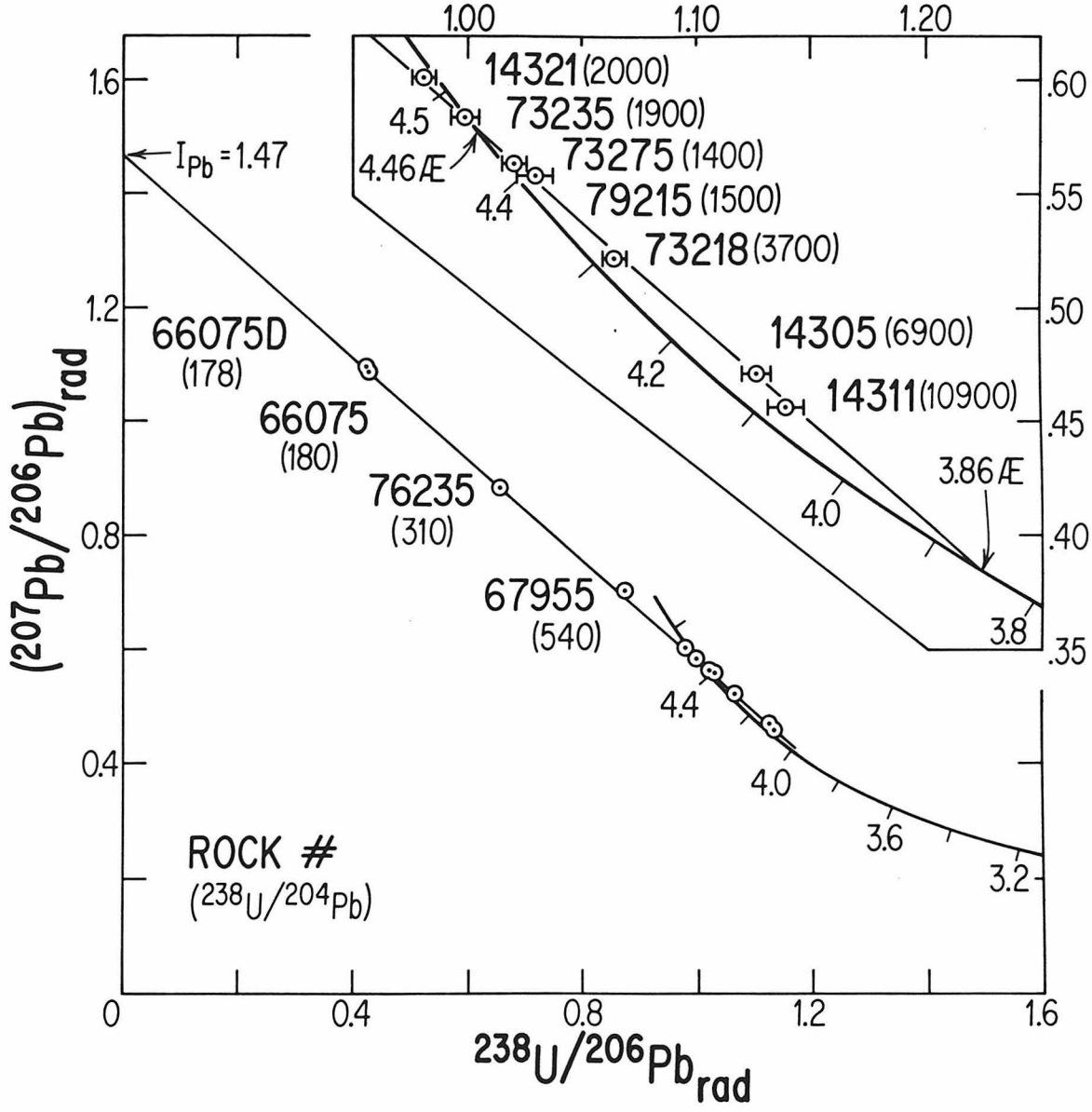
1.00
1.10
1.20
14321 (2000)
73235 (1900)
73275 (1400)
79215 (1500)
73218 (3700)
14305 (6900)
14311 (10900)
4.5
4.46 Æ
4.4
4.2
4.0
3.86 Æ
3.8
I_{Pb} = 1.47
66075D
(178)
66075
(180)
76235
(310)
67955
(540)
4.4
4.0
3.6
3.2
ROCK #
($^{238}U/^{204}Pb$)
1.6
1.2
0.8
0.4
0
.60
.55
.50
.45
.40
.35
$(^{207}Pb/^{206}Pb)_{rad}$
$^{238}U/^{206}Pb_{rad}$

Fig. 2-6

to the intersection of the data array with the y-axis and 2) the lower intersection of the data array with the concordia (3.86 AE) and corresponds to the Pb produced only by *in situ* decay since 3.86 AE.

The upper intersection of the data array with the concordia (4.46 AE) does not have a unique interpretation (Tera and Wasserburg, 1974). It may represent 1) The time of formation and instantaneous differentiation of the moon at 4.46 AE with U-Pb fractionation resulting in high μ values of surface materials. 2) 4.46 AE represents the age of the crust while the moon itself accreted earlier, say at 4.55 AE. 3) The upper intersection at 4.46 AE has no specific time meaning, but is the consequence of a spectrum of initial Pb values resulting from continuous crustal formation from $\sim$4.55 AE to $\sim$4.0 AE, being averaged and homogenized by the terminal cataclysm at $\sim$3.86 AE.

However the most plausible interpretation of the upper intersection (Oberli *et al.*, 1978) is with the crust forming at 4.46 AE and the moon itself accreting earlier ($\sim$4.55 AE). This constraint will now be used to interpret the Sm-Nd and Rb-Sr data and to further characterise the processes which could have formed the crust at 4.46 AE.

DISCUSSION

1. A multi-stage evolution model.

For these samples, it is apparent that the most powerful constraint on the time of lunar crust formation is provided by the 4.46 AE upper intersection age of the U-Pb system. Although the interpretation of the upper intersection is somewhat model dependent, the 4.46 AE age probably represents the time of differentiation of the lunar crust and mantle (Oberli et al., 1978). We will now consider the implications of forming the lunar crust in a single event at 4.46 AE.

As first pointed out by Tera and Wasserburg (1972), a crustal formation age of 4.46 AE is "significantly younger than the age of the solar system." Therefore, in interpreting the results, three stages of evolution must be considered. These are from: 1) the time of accretion of the moon at ∿4.55 AE to the time of crustal formation at 4.46 AE; 2) 4.46 AE to the lunar cataclysm at 3.86 AE; and 3) 3.86 AE to the present. For U-Pb, a three stage evolution model gives, for example, a measured $^{206}Pb/^{204}Pb$ of:

$$\left(\frac{^{206}Pb}{^{204}Pb}\right)_m = \left(\frac{^{206}Pb}{^{204}Pb}\right)_{PAT} + \mu_o\left(e^{\lambda_{238}T_0} - e^{\lambda_{238}t_1}\right) \quad (2\text{-}4)$$

$$+ \mu_1\left(e^{\lambda_{238}t_1} - e^{\lambda_{238}t_2}\right) + \mu_2\left(e^{\lambda_{238}t_2} - 1\right)$$

where T_0 = 4.55 AE, t_1 = 4.46 AE and t_2 = 3.86 AE, $(^{206}Pb/^{204}Pb)_m$ and $\mu_2 = {}^{238}U/^{204}Pb$ are measured ratios and $(^{206}Pb/^{204}Pb)_{PAT}$ = 9.307 (Tatsumoto et al., 1973). The unknowns in this equation are thus μ_o and μ_1 which are the $^{238}U/^{204}Pb$ ratios from 4.55 AE to 4.46 AE and from 4.46 AE

Table 2-3. Three-stage evolution of $^{238}U/^{204}Pb$ (μ)

Sample	μ_o 4.55 AE - 4.46 AE	μ_1 4.46 AE - 3.86 AE	μ_2 3.86 AE - Present (meas)
73235,50B	$\leqslant$ 200	1910	1899
73275	$\leqslant$ 200	1240	1410
79215	$\leqslant$ 200	1250	1515
76055	$\leqslant$ 200	1570	12840
66075	$\leqslant$ 200	1490	179
14311	$\leqslant$ 200	3540	10950
14321	$\leqslant$ 200	2260	2036

to 3.86 AE respectively. An independent constraint can be placed on μ_o, if it is assumed that the mantle reservoirs from which the lunar crust and maria basalts were derived had a uniform value of μ. If this is the case, then the very primitive measured $^{206}Pb/^{204}Pb$ and $^{207}Pb/^{204}Pb$ ratios in the orange glass balls from 74220 (Tera and Wasserburg, 1975) imply that μ_o <<200. Using this constraint, μ_1 can now be evaluated for each sample with equation 2-4. The results are tabulated in Table 2-3. It can be seen that $\mu_o << \mu_1$, indicating an increase in μ at 4.46 AE of about a factor of 6 to 20. Thus, the calculated value of μ_1 is relatively insensitive to μ_o for μ_o <200. Depending on whether the samples either gained or lost Pb during the terminal cataclysm, then $\mu_1 < \mu_2$ or $\mu_1 > \mu_2$ respectively.

The $^{232}Th/^{238}U$ fractionation history can also be ascertained in an analogous manner from the Th-Pb systematics. For this system, the measured $^{208}Pb/^{206}Pb$ ratios are given by

$$\left(\frac{^{208}Pb}{^{204}Pb}\right)_m = \left(\frac{^{208}Pb}{^{204}Pb}\right)_{PAT} + \left(\frac{^{232}Th}{^{204}Pb}\right)_o \left(e^{\lambda_{232}T_0} - e^{\lambda_{232}t_1}\right) \qquad (2\text{-}5)$$

$$+ \left(\frac{^{232}Th}{^{204}Pb}\right)_1 \left(e^{\lambda_{232}t_1} - e^{\lambda_{232}t_2}\right) + \left(\frac{^{232}Th}{^{204}Pb}\right)_2 \left(e^{\lambda_{232}t_2} - 1\right)$$

The $(^{232}Th/^{204}Pb)_1$ ratios are evaluated in a similar manner as described for the μ_1 ratios except that it is assumed that $(^{232}Th/^{204}Pb)_0 = 0$. Thus, $(^{232}Th/^{238}U)_1 = (^{232}Th/^{204}Pb)_1/\mu_1$ (see Table 2-4). It is apparent that in contrast to the μ values the $(^{232}Th/^{238}U)$ ratios are relatively constant reflecting the geochemical coherence of these two elements.

Table 2-4. Three-stage evolution of $^{232}Th/^{238}U$

Sample	$\left(\frac{^{232}Th}{^{238}U}\right)_o$	$\left(\frac{^{232}Th}{^{238}U}\right)_1$	$\left(\frac{^{232}Th}{^{238}U}\right)_2$
	4.55 AE - 4.46 AE	4.46 AE - 3.86 AE	3.86 AE - Present (meas)
73235,50B	-	3.73	3.85
73275	-	3.70	4.05
79215	-	3.57	2.62
76055	-	-	-
66075	-	3.83	3.96
14311	-	-	-
14321	-	2.78	3.96

For Rb-Sr, a three stage evolution gives

$$\left(\frac{^{87}Sr}{^{86}Sr}\right)_m = \left(\frac{^{87}Sr}{^{86}Sr}\right)_{BABI} + \left(\frac{^{87}Rb}{^{86}Sr}\right)_o \left(e^{\lambda_{87}T_0} - e^{\lambda_{87}t_1}\right) \qquad (2\text{-}6)$$

$$+ \left(\frac{^{87}Rb}{^{86}Sr}\right)_1 \left(e^{\lambda_{87}t_1} - e^{\lambda_{87}t_2}\right) + \left(\frac{^{87}Rb}{^{86}Sr}\right)_2 \left(e^{\lambda_{87}t_2} - 1\right)$$

where $(^{87}Sr/^{86}Sr)_m$ and $(^{87}Rb/^{86}Sr)_2$ are the measured ratios and $(^{87}Rb/^{86}Sr)_o$ and $(^{87}Rb/^{86}Sr)_1$ are the ratios from 4.55 AE to 4.46 AE and 4.46 AE to 3.86 AE respectively. In a manner analogous to that described for μ_o, an independent constraint can also be ascertained for $(^{87}Rb/^{86}Sr)_o$ from the very primitive measured $^{87}Sr/^{86}Sr$ of 0.69896±3 for the breccia 60025. This is essentially identical to BABI (0.69898) and implies $(^{87}Rb/^{86}Sr)_o \leqslant 0.02$ for an initial $^{87}Sr/^{86}Sr$ of BABI. With this value of $(^{87}Rb/^{86}Sr)_o$ and using equation 2-6, $(^{87}Rb/^{86}Sr)_1$ ratios have been calculated and are tabulated in Table 2-7. It can be seen that $(^{87}Rb/^{86}Sr)_o \ll (^{87}Rb/^{86}Sr)_1 < (^{87}Rb/^{86}Sr)_2$. Thus at 4.46 AE an increase in $^{87}Rb/^{86}Sr$ of about a factor of 4 to 10 is required, which is similar to that estimated for μ. However, in contrast to the U-Th-Pb system, at the terminal cataclysm, the $^{87}Rb/^{86}Sr$ ratios are only increased. This indicates that volatile loss or gain of Rb cannot be a dominant process and suggests that magmatic fractionation of Rb/Sr occurred at~3.86 AE.

For Sm-Nd, a similar approach could be used, but in this case the limited Sm/Nd fractionations from the chondritic ratio make the multi-stage model extremely sensitive to the initial $^{143}Nd/^{144}Nd$ ratio.

Table 2-5. Three-stage evolution of $^{87}Rb/^{86}Sr$

Sample	$\left(\frac{^{87}Rb}{^{86}Sr}\right)_o$ 4.55 AE - 4.46 AE	$\left(\frac{^{87}Rb}{^{86}Sr}\right)_1$ 4.46 AE - 3.86 AE	$\left(\frac{^{87}Rb}{^{86}Sr}\right)_2$ 3.86 AE - Present (meas)
73235,50B	$\leqslant 0.02$	0.072	0.1137
73235,50W	$\leqslant 0.02$	0.009	0.0216
73275	$\leqslant 0.02$	0.077	0.1598
79215	-	-	-
76055	$\leqslant 0.02$	0.081	0.0940
66075	$\leqslant 0.02$	0.015	0.0352
14311	$\leqslant 0.02$	0.176	0.2010
14321	$\leqslant 0.02$	0.187	0.2752

As the initial ratio of the moon is not at present sufficiently well contained, for simplicity we will assume that the Sm/Nd fractionation from the chondritic ratio only occurred at 4.46 AE (see Table 2-8). Evidence for the formation of magma reservoirs and concomitant fractionation of the REE early in the moon's history is also provided by the initial $^{143}Nd/^{144}Nd$ ratios of the Apollo 12 and Apollo 17 mare basalts (Lugmair et al., 1976; Nyquist et al., 1979). These basalts have large positive ε_{Nd} values (Figure 2-2) indicating derivation from source reservoirs enriched in Sm/Nd relative to the chondritic ratio. If these reservoirs formed at 4.56 AE with the Juvinas initial $^{143}Nd/^{144}Nd$ then to produce the observed ε_{Nd} value, they require $^{147}Sm/^{144}Nd = 0.26$ compared to the chondritic value of $^{147}Sm/^{144}Nd = 0.1936$. This is a relatively high Sm/Nd value and is approximately the same as that estimated for modern mid-ocean ridge basalt source reservoirs (McCulloch et al., 1979). However, for the formation of these maria basalt reservoirs at a substantially younger time, say at 4.20 AE, then an implausibly high value of $^{147}Sm/^{144}Nd = 0.34$ would be required.

2. Implications.

The implications of a multi-stage evolution are summarized in Table 2-9 where the fractionation factors are listed. In this table, for Rb/Sr for example

$$F_1(4.46\ AE) = \frac{(^{87}Rb/^{86}Sr)_1}{(^{87}Rb/^{86}Sr)_o}$$

Table 2-6. Three-stage evolution of $^{147}Sm/^{144}Nd$

Sample	$(^{147}Sm/^{144}Nd)_o$ 4.55 AE - 4.46 AE	$(^{147}Sm/^{144}Nd)_1$ 4.46 AE - 3.86 AE	$(^{147}Sm/^{144}Nd)_2$ 3.86 AE - Present (meas)
73235,50B	0.1936	0.1693	0.1693
73235,50W	0.1936	0.1661	0.1661
73275	0.1936	0.1713	0.1713
79215	0.1936	0.1740	0.1740
76055	0.1936	0.1721	0.1721
66075	0.1936	0.1702	0.1702
14311	0.1936	0.1683	0.1683
14321	0.1936	0.1684	0.1684

and

$$F_2(3.86\ AE) = \frac{(^{87}Rb/^{86}Sr)_2}{(^{87}Rb/^{86}Sr)_1}$$

From Table 2-7 the main features which must be accounted for at 4.46 AE are (1) the increase in μ by a factor of 10 to 20.

(2) the increase in Rb/Sr by a factor of 3 to 10.

and (3) the approximate 10 to 14 percent lowering of the Sm/Nd ratios relative to the chondritic ratio.

At 3.86 AE the fractionations which must be accounted for are

(1) the increase in Rb/Sr of up to a factor of 2.

(2) the increase and decrease in μ.

and (3) the approximately constant Th/U ratios.

In an attempt to account for these features we will now consider two types of processes. These are enrichments produced by magmatic processes involving either partial melting or fractional crystallization and fractionation resulting from depletion of volatiles as might be expected, for example, by derivation of the moon from the earth's mantle.

3. Magmatic processes.

For elements to be fractionated during magmatic processes requires differential partitioning of the element between solid and liquid. In Table 2-8 the solid/liquid partition coefficients are listed for the mineral phases which are likely to be important constituents of the lunar crust and source regions. From this table of partition

Table 2-7. Fractionation factors at 4.46 AE (F_1) and 3.86 AE (F_2)

Sample	$^{87}Rb/^{86}Sr$		$^{147}Sm/^{144}Nd$		$^{238}U/^{204}Pb$		$^{232}Th/^{238}U$	
	F_1	F_2	F_1	F_2	F_1	F_2	F_1	F_2
73235,50B	≥ 3.6	1.57	0.87	1.0	≥ 9.5	0.99	-	1.03
73235,50W	-	2.35	0.86	1.0	-	-	-	-
73275	≥ 3.9	2.07	0.88	1.0	≥ 6.2	1.14	-	1.09
79215	-	-	0.90	1.0	≥ 6.3	1.21	-	0.73
76055	≥ 4.1	1.16	0.89	1.0	≥ 7.8	8.18	-	-
66075	-	2.33	0.88	1.0	≥ 7.4	0.12	-	1.03
14311	≥ 8.8	1.14	0.87	1.0	≥17.7	3.10	-	-
14321	≥ 9.4	1.47	0.87	1.0	≥11.3	0.90	-	1.42

where for example $F_1(4.46\ AE) = \frac{(^{87}Rb/^{86}Sr)_1}{(^{87}Rb/^{86}Sr)_o}$

and $F_2(3.86\ AE) = \frac{(^{87}Rb/^{86}Sr)_2}{(^{87}Rb/^{86}Sr)_1}$

Table 2-8. Solid/liquid partition coefficients

Element	opx	cpx	plag	olivine
Rb	0.01	0.01	0.033	0.008
Sr	0.02	0.1	1.5	0.009
Sm	0.024	0.26	0.029	0.011
Nd	0.016	0.17	0.037	0.01
U	0.0005	0.01	0.01	0.0001
Th	0.0005	0.02	0.01	0.0001
Pb	< 0.1	0.5	1.0	< 0.1

Sources: Philpotts and Schnetzler (1970), Schnetzler and Philpotts (1970), Hart and Brooks (1974), Shimizu (1974), Beswick and Carmichael (1978).

coefficients it can be seen that the only minerals which are likely to be important in fractionating Rb from Sr and Pb from U are plagioclase and to a lesser extent clinopyroxene. For fractionating Sm and Nd, clinopyroxene is the most important phase. However, for U and Th the partition coefficients are similar and $\ll 1$ and thus these two elements are unlikely to be fractionated by magmatic processes which is consistent with the data (Table 2-7).

We will now consider the plausibility of fractional crystallization and/or partial melting as mechanisms for producing the fractionations tabulated in Table 2-7. First, at 3.86 AE, it can be seen from Table 2-7 that Rb/Sr is enriched by a factor of ~ 2. For a simple Rayleigh fractionation process the concentration of a trace element in the melt (X^{melt}) relative to the initial melt concentration (X^o) is given by

$$\frac{X^{melt}}{X^o} = f^{K_D - 1} \tag{2-7}$$

where f is the fraction of melt remaining and K_D is the partition coefficient. Thus for Rb/Sr,

$$\frac{(Rb/Sr)^{melt}}{(Rb/Sr)^o} = f^{K_D^{Rb} - K_D^{Sr}} \tag{2-8}$$

So, for a factor of 2 enrichment of Rb/Sr in the melt requires crystallization of $\sim 40\%$ ($f = 0.6$) plagioclase.

Alternatively, partial melting of a plagioclase rich source material could also produce the required enrichments in Rb/Sr. For modal melting

$$\frac{(Rb/Sr)^{melt}}{(Rb/Sr)^{solid}} = \frac{D^{Sr} + f(1-D^{Sr})}{D^{Rb} + f(1-D^{Rb})} \qquad (2\text{-}9)$$

where D^{Rb} and D^{Sr} are the whole rock partition coefficients and f is the fraction of melt. For source material consisting of say 20% cpx, 10% opx, 20% ol, and 50% plag, $D^{Rb} = 0.02$ and $D^{Sr} = 0.8$. So for a factor of 2 enrichment in Rb/Sr, approximately 40% partial melting ($f = 0.4$) is required. Larger enrichments would, of course, be produced by smaller degrees of partial melting. Therefore, redistribution and dilution of a more enriched component (KREEP?) by meteorite impacts may be a feasible variation of this process. Of these two processes, the latter appears to be the most reasonable mechanism for producing the Rb/Sr enrichment. This mixing between a young (3.86 AE) high Rb/Sr KREEP component with an older (4.46 AE) anorthositic component would also account for many of the intermediate T_{BABI} model ages.

For crystallization of $\sim$ 40% plagioclase, or $\sim$ 40% partial melting, the U/Pb ratio would be increased by only a factor of 1.6 and 1.8 respectively. However, Table 2-7 indicates that both enrichments and depletions of U/Pb of up to a factor of 10 are present, which indicates that volatile transfer of Pb has dominated this system at 3.86 AE. However, for Sm/Nd and Th/U, 40% crystallization or partial melting would produce negligible ($< 2\%$) changes in these ratios.

At 4.46 AE significantly larger enrichments, by at least factors of 10 to 20, in Rb/Sr and U/Pb ratios are required (see F_1 values from

Table(2-7). For the Rb/Sr and U/Pb enrichments to be produced by fractional crystallization of plagioclase, equation 2-8 indicates crystallization of at least 80% to 95% of the melt. This is an inordinately large amount of crystallization and apart from the difficulty of separating the lighter plagioclase from the melt, it would also require that the terra samples represent only a small fraction (< 5%) of the initial source. Producing the enrichments by partial melting encounters similar difficulties. For example, from equation 2-9, to produce the enrichments of Rb/Sr and U/Pb requires less than 6% to 2% partial melting. Thus in addition to requiring that terra rocks be only a small fraction of the source material, there are also difficulties in extracting the small amounts of melt. In summary then, magmatic processes or a combination of these processes could account for approximately a factor of 2 enrichment of Rb/Sr at 3.86 AE, but they have severe difficulties in accounting for the larger, factor of 10 to 20, enrichments in Rb/Sr and U/Pb indicated by the isotopic systematics at 4.46 AE.

4. Depletion of Volatiles.

An alternate process which could conceivably account for the massive enrichments in the Rb/Sr and U/Pb ratios is volatile loss of Rb and Pb at 4.46 AE. In the hypothesis of Ringwood (1977) and Ringwood and Kesson (1977), where the moon is derived from the earth's mantle, loss of volatiles is an important process, and is used to account for the drastic depletion of many volatile elements in the moon compared to

the earth's mantle. In Table 2-9, the parent/daughter ratios derived from isotopic systematics are tabulated for the highlands source regions and compared to the depleted and undepleted terrestrial mantle and to C1 chondrites. The first order feature is that the highland source reservoirs and the terrestrial mantle are depleted in Rb/Sr by a factor of 10 to 30 and enriched in U/Pb by a factor of at least 50, compared to the primordial solar composition given by C1 chondrites. This feature has been pointed out by a number of workers (for example, Larimer, 1973) and is part of a more general depletion of volatiles in the moon and earth compared to the primordial abundances. This probably reflects the environment in which the earth and the moon accreted.

However, the comparison which is relevant in this work is that between the highland source regions and the terrestrial mantle. The ratios should, of course, be comparable if they have a common origin as proposed by Ringwood and Kesson (1977). However, in contrast to Ringwood and Kesson (1977) we recognize two types of terrestrial mantle, a depleted mantle and an undepleted mantle. The depleted mantle is the source of mid-ocean ridge tholeiites and it has been shown (Gast, 1968; DePaolo and Wasserburg, 1976a) to have been depleted in the incompatible elements for at least a billion years or more. There is no evidence for the presence of an analogous depleted mantle in the Archean (see Figure 2-2) and thus moon-earth models based on MOR tholeiites (Ringwood and Kesson, 1977) are not strictly valid.

The undepleted terrestrial mantle is today represented by

Table 2-9. Parent/daughter ratios of radioactive decay systems for the moon, earth, and C1 chondrites

	$^{87}Rb/^{86}Sr$	$^{147}Sm/^{144}Nd$	$^{238}U/^{204}Pb$
C1 Chondrites	0.65	0.19	0.25
Lunar Highlands			
Source Reservoir	< 0.02	0.19	< 200
Terrestrial Mantle			
undepleted	0.084	0.19	9
depleted	0.04	0.24	7

continental basalts (DePaolo and Wasserburg, 1976a) and is probably what should be used in comparing the earth's mantle with the moon. However, from Table 2-9 it can be seen that the main difficulty in deriving the moon from an undepleted earth mantle is the $^{87}Rb/^{86}Sr$ ratio of 0.084 in the earth (DePaolo and Wasserburg, 1976a) compared to < 0.02 estimated for the early lunar source reservoirs. As has already been pointed out, the estimation of $^{87}Rb/^{86}Sr$ in the moon from 4.55 AE to 4.46 AE is highly dependent on the assumed initial $^{87}Sr/^{86}Sr$ ratio. For a lunar initial ratio lower than BABI, for example, the same as that in the Allende meteorite ($^{87}Sr/^{86}Sr = 0.69877$; Gray et al., 1973), the $^{87}Rb/^{86}Sr$ of the early moon is then ≤ 0.15. This is now compatible with that estimated for the undepleted terrestrial mantle and therefore the isotopic data are consistent with a cogenetic origin of the moon and the earth.

CONCLUSIONS

The most powerful constraint for the time of formation of the lunar highland crust is provided by the U-Pb system. This gives an upper intersection with the concordia at 4.46 AE and a lower intersection at 3.86 AE. The 4.46 AE age probably represents the time of differentiation of the lunar crust and mantle. During this process, U was enriched in the highland crust relative to Pb, by at least a factor of 10. The lower intersection age of 3.86 AE represents the time of redistribution of U and Pb (with both increase and decrease in the U/Pb ratios) due to massive impact metamorphism.

The Rb-Sr T_{BABI} model ages range from 4.18 AE to 4.39 AE and are markedly younger than the U-Pb upper intersection age. Many of the samples (e.g., KREEP sample 14311 and 14321) have relatively high $^{87}Rb/^{86}Sr$ ratios compared to their mantle sources, and therefore the T_{BABI} ages are relatively insensitive to the model parameters. For the T_{BABI} ages to be compatible with the U-Pb data, a factor of approximately two increase in $^{87}Rb/^{86}Sr$ is required at 3.86 AE. This suggests that significant melting and fractionation of Rb/Sr occurred prior to or during the impact metamorphism.

Due to the relatively small fractionation of Sm and Nd relative to the chondritic ratio, the T^{Nd}_{CHUR} model ages are not particularly sensitive to the time of differentiation. In addition these model ages are highly dependent on the model parameters. These considerations indicate that internal Sm-Nd mineral isochrons which identify truly ancient relic samples may provide more definitive constraints on the early evolution of the highlands.

REFERENCES

Albee, A. L., D. S. Burnett, A. A. Chodos, E. L. Haines, J. C. Huneke, D. A. Papanastassiou, F. A. Podesek, G. Price Russ III, and G. J. Wasserburg (Lunatic Asylum), Mineralogic and Isotopic Investigations of Lunar Rock 12013, Earth Planet Sci. Lett., 9, 137-163, 1970.

Albee, A. L., A. J. Gancarz, and A. A. Chodos, Metamorphism of Apollo 16 and 17 and Lunar 20 metaclastic rocks at about 3.9 AE: Samples 61156, 64423, 14-2, 65015, 67483, 15-2, 76055, 22006, and 22007, Proc. Lunar Sci. Conf. 4th, 569-595, 1973.

Beswick, A. E., and I. S. E. Carmichael, Constraints on mantle source compositions imposed by phosphorus and rare-earth elements, Contrib. Mineral. Petrol., 67, 317-330, 1978.

Bickel, C. E., J. L. Warner, and W. C. Phinney, Petrology of 79215: Brecciation of a lunar cumulate, Proc. Lunar Sci. Conf. 7th, 1793-1819, 1976.

Blanchard, D. P., Chemistry of ANT-suite and felsite clasts from consortium breccia 73215 and of gabbroic anorthosite 79215, Proc. Lunar Sci. Conf. 8th, 2507-2524, 1977.

DePaolo, D. J., and G. J. Wasserburg, Nd isotopic variations and petrogenetic models, Geophys. Res. Lett., 3, 249-253, 1976a.

DePaolo, D. J., and G. J. Wasserburg, Inferences about magma sources and mantle structure from variations of $^{143}Nd/^{144}Nd$, Geophys. Res. Lett., 3, 743-747, 1976b.

Gast, P. W., Trace element fractionation and the origin of tholeiitic and alkaline magma types, Geochim. Cosmochim. Acta, 32, 1057-1086, 1968.

Gray, C. M., D. A. Papanastassiou, and G. J. Wasserburg, The identification of early condensates from the solar nebula, Icarus, 20, 213-239, 1973.

Hamilton, P. J., R. K. O'Nions, and N. M. Evensen, Sm-Nd dating of Archean basic and ultrabasic volcanics, Earth Planet. Sci. Lett., 36, 263-268, 1977.

Hamilton, P. J., R. K. O'Nions, N. M. Evensen, D. Bridgwater, and J. H. Allaart, Sm-Nd isotopic investigations of Isua supracrustals and implications for mantle evolution, Nature, 272, 41-43, 1978.

Hamilton, P. J., N. M. Evensen, R. K. O'Nions, H. S. Smith, and A. J. Erlank, Sm-Nd dating of Onverwacht Group volcanics, southern Africa, Nature, 279, 298-300, 1979a.

Hamilton, P. J., N. M. Evensen, R. K. O'Nions, and J. Tarney, Sm-Nd systematics of Lewisian gneisses: implications for the origin of granulites, Nature, 277, 25-28, 1979b.

Hart, S. R. and C. Brooks, Clinopyroxene matrix partitioning of K, Rb, Cs, Sr and Ba, Geochim. Cosmochim. Acta, 38, 1799-1803, 1974.

Hubbard, N. J., M. Rhodes, H. Wiesmann, C. Y. Shih, and B. M. Bansal, The chemical definition and interpretation of rock types returned from the non-mare regions of the moon, Proc. Lunar Sci. Conf. 5th, 1227-1246, 1974.

Jacobsen, S. B., and G. J. Wasserburg, Interpretation of Nd, Sr, and Pb isotope data from Archean migmatites in Lofoten-Vesterålen, Norway, Earth Planet. Sci. Lett., 41, 245-253, 1978.

Larimer, J. W., Chemistry of the solar nebular, Space Science Reviews, 15, 103-119, 1973.

Lindstrom, M. M., A. R. Duncan, J. S. Fruchter, S. M. McKay, J. W. Stoeser, G. G. Goles, and D. J. Lindstrom, Compositional characteristics of some Apollo 14 clastic materials, Proc. Lunar Sci. Conf. 3rd, 1201-1214, 1972.

Lugmair, G. W., K. Marti, J. P. Kurtz, and N. B. Scheinin, History and genesis of lunar troctolite 76535 or: How old is old? Proc. Lunar Sci. Conf. 7th, 2009-2032, 1976.

Lugmair, G. W., and K. Marti, Sm-Nd-Pu timepieces in the Angra Dos Reis Meteorite, Earth Planet Sci. Lett., 35, 273-284, 1977.

Lugmair, G. W. and K. Marti, Lunar initial $^{143}Nd/^{144}Nd$: Differential evolution of the lunar crust and mantle, Earth Planet. Sci. Lett., 39, 349-357, 1978.

Lugmair, G. W., and R. W. Carlson, The Sm-Nd history of KREEP, Proc. Lunar Sci. Conf. 9th, 689-704, 1978.

McCulloch, M. T., and G. J. Wasserburg, Sm-Nd and Rb-Sr chronology of continental crust formation, Science, 200, 1003-1011, 1978.

McCulloch, M. T., G. J. Wasserburg, and S. S. Goldich, Sm-Nd systematics in the early Archean gneisses of the Minnesota River valley, In preparation.

McCulloch, M. T., R. T. Gregory, G. J. Wasserburg, and H. P. Taylor, Sm-Nd, Rb-Sr, and $^{18}O/^{16}O$ isotopic systematics in an oceanic crustal section: evidence from the Samail Ophiolite, submitted to J. Geophys. Res., 1979.

Nakamura, N., M. Tatsumoto, P. D. Nunes, D. M. Unruh, A. P. Schwab, and T. R. Wildeman, 4.4 b.y.-old clast in boulder 7, Apollo 17: A comprehensive chronological study by U-Pb, Rb-Sr and Sm-Nd methods, Proc. Lunar Sci. Conf. 7th, 2309-2333, 1976.

Nyquist, L. E., Lunar Rb-Sr chronology, Phys. Chem. Earth, 10, 103-142, 1977.

Nyquist, L., C. Shih, J. Wooden, B. Bansal, and H. Wiesmann, The Sr and Nd isotopic record of Apollo 12 basalts, Abstract in Lunar Science X, 931-933, 1979.

Oberli, F., M. T. McCulloch, F. Tera, D. A. Papanastassiou, and G. J. Wasserburg, Early lunar differentiation constraints from U-Th-Pb, Sm-Nd, and Rb-Sr model ages, Abstract in Lunar Science IX, 832-834, 1978.

Oberli, F., J. C. Huneke, and G. J. Wasserburg, U-Pb and K-Ar systematics of cataclysm and precataclysm lunar impactites, Abstract in Lunar Science X, 940-942, 1979.

Palme, H., On the age of KREEP, Geochim. Cosmochim. Acta, 41, 1791-1801, 1977.

Papanastassiou, D. A., and G. J. Wasserburg, Rb-Sr study of a lunar dunite and evidence for early lunar differentiates, Proc. Lunar Sci. Conf. 6th, 1467-1489, 1975.

Papanastassiou, D. A., and G. J. Wasserburg, Rb-Sr age of troctolite 76535, Proc. Lunar Sci. Conf. 7th, 2035-2054, 1976.

Papanastassiou, D. A., D. J. DePaolo, and G. J. Wasserburg, Rb-Sr and Sm-Nd chronology and genealogy of mare basalts from the Sea of Tranquility, Proc. Lunar Sci. Conf. 8th, 1639-1672, 1977.

Philpotts, J. A., and C. C. Schnetzler, Phenocryst-matrix partition coefficients for K, Rb, Sr and Ba, with application to anorthosite and basalt genesis, Geochim. Cosmochim. Acta, 34, 307-322, 1970.

Philpotts, J. A., S. Schuhmann, C. W. Kouns, R. K. L. Lum, and S. Winzer, Origins of Apollo 17 rocks and soils, Proc. Lunar Sci. Conf. 5th, 471-504, 1974.

Quick, J. E., B. S. Brock, and A. L. Albee, Petrology of Apollo 16 breccia 66075, Proc. Lunar Sci. Conf. 9th, 921-940, 1978.

Ringwood, A. E., Basaltic magmatism and the bulk composition of the moon. I. Major and heat producing elements, The Moon, 16, 389-423, 1977.

Ringwood, A. E. and S. E. Kesson, Composition and origin of the moon, Proc. Lunar Sci. Conf. 8th, 371-398, 1977.

Schnetzler, C. C., and J. A. Philpotts, Partition coefficients of rare-earth elements between igneous matrix material and rock-forming phenocrysts. II., Geochim. Cosmochim. Acta, 34, 331-340, 1970.

Shimizu, N., An experimental study of the partitioning of K, Rb, Cs, Sr and Ba between clinopyroxene and liquid at high pressures, Geochim. Cosmochim. Acta, 38, 1789-1798, 1974.

Tatsumoto, M., R. J. Knight, and C. J. Allegre, Time differences in the formation of meteorites as determined from the ratio of lead 207 to lead 206, Science, 180, 1279-1283, 1973.

Tera, F., and G. J. Wasserburg, U-Th-Pb systematics in lunar highland samples from Luna 20 and Apollo 16 missions, Earth Planet. Sci. Lett., 17, 36-51, 1972.

Tera, F., and G. J. Wasserburg, U-Th-Pb systematics on lunar rocks and inferences about lunar evolution and the age of the moon, Proc. Lunar Sci. Conf. 5th, 1571-1600, 1974.

Tera, F., and G. J. Wasserburg, Precise isotopic analysis of lead in picomole and subpicomole quantities, Anal. Chem., 47, 2214-2220, 1975.

Turner, G., Potassium-argon chronology of the moon, Phys. Chem. Earth, 10, 145-195, 1977.

Unruh, D. M., N. Nakamura, and M. Tatsumoto, History of the Pasamonte achondrite: relative susceptibility of the Sm-Nd, Rb-Sr, and U-Pb systems to metamorphic events, Earth Planet Sci. Lett., 37, 1-12, 1977.

Wänke, H., H. Baddenhausen, A. Balacescu, F. Teschke, B. Spettel, G. Dreibus, H. Palme, K. Quijano-Rico, F. Wlotzka, and F. Begeman, Multielement analyses of lunar samples and some implications of the results, Proc. Lunar Sci. Conf. 3rd, 1251-1268, 1972.

Warner, J. L., Metamorphism of Apollo 14 breccias, Proc. Lunar Sci. Conf. 3rd, 623-644, 1972.

Warner, J. L., C. E. Bickel, W. C. Phinney, and C. H. Simonds, Feldspathic, granulitic impactites that pre-date the final lunar bombardment, Abstract in Lunar Science VIII, 979-981, 1977.

Wasserburg, G. J., and D. A. Papanastassiou, Model ages, Nature, 259, 159-160, 1976.

APPENDIX 1

Sm-Nd and Rb-Sr Chronology of Continental Crust Formation

Times of addition to continents of chemically fractionated mantle-derived materials are determined.

M. T. McCulloch and G. J. Wasserburg

One of the most obvious features of the outermost part of the earth is the difference between continents and ocean basins. This topographical duality is a reflection of major differences in the structure and the chemistry of the outer parts of the earth and of the dynamic interaction between the interior layers, the outer crustal layers, and the hydrosphere often biased and distorted, of the growth and evolution of the continents. They indicate that the continents have grown by addition of new material from underlying mantle sources, accretion of island arc volcanic systems to the continental margins, and interaction with ocean basins. In this article we present some data that may aid in identifying the times at which

Summary. Samarium-neodymium and rubidium-strontium isotopic systematics, together with plausible assumptions regarding the geochemical evolution of continental crust material, have been used to ascertain the times at which segments of continental crust were formed. Analyses of composites from the Canadian Shield representing portions of the Superior, Slave, and Churchill structural provinces indicate that these provinces were all formed within the period 2.5 to 2.7 aeons. It has been possible to determine the mean age of sediment provenances, as studies of sedimentary rocks suggest that the samarium-neodymium isotopic system is not substantially disturbed during sedimentation or diagenesis.

of the earth. The crust that occupies the ocean basins is only ~ 6 kilometers thick, is relatively uniform in chemical composition, and consists of very young materials less than ~ 0.2 aeon old [1 aeon (AE) = 10^9 years]. This young age reflects rapid recycling, which has almost completely destroyed all record of older oceanic crust within the present ocean basins. In contrast, continental crust is about 35 km thick, has a variable and distinctive chemical composition, and consists of materials ranging in age from 0 to 3.8 AE. These constituents of diverse age preserve a record, although new materials were derived from the earth's mantle and added to the continental crust.

The ability to determine the time of formation of new crustal segments is of fundamental importance in attempting to understand the growth and evolution of continental crust. We consider "new crust" to be material that has not previously been present in the crust but is newly added during periods of continental growth and has its origin in the mantle. The decay of long-lived radioactive isotopes to stable daughter products has been used to obtain ages for a

variety of rocks. However, because there have been multiple generations of crustal formation, metamorphism, remelting, and erosion, these ages may not be related to the actual times of formation of new crust. For example, it is often difficult to establish whether younger parts of continental crust (as defined by relative geologic age or by isotopic age determinations) represent the addition of new material, or are simply the product of metamorphism or remelting of preexisting crustal provinces or materials. This is particularly important in attempting to estimate the rate of development of continental crust through time. Hurley and co-workers (*1*), using whole rock Rb-Sr together with K-Ar age determinations, found crustal ages that indicated accelerated generation of crustal material from ~3.8 AE to the present. However, other workers, using U-Pb values in beach and river sands (*2*) and initial $^{87}Sr/^{86}Sr$ values in rocks of well-established age to identify remelted crust (*3*), concluded that major rock-forming events have been approximately episodic, with only relatively short periods of accelerated crustal growth.

In this article we will show that, by using the recently developed Sm-Nd isotopic technique together with Rb-Sr systematics and plausible assumptions regarding the geochemical evolution of crustal material from mantle sources, the times of formation of new crust can be obtained from both igneous rocks and metamorphic and sedimentary derivatives. In particular, we will show that by using Sm-Nd isotopic systematics, the times of formation of new continental crust can be obtained from a more diverse range of materials, including sedimentary and metamorphic rocks that have complex histories including erosion, deposition, and chemical alteration. To obtain formation ages of large segments of continental crust, we studied sediments that were probably derived from widespread source areas and composites consisting of a large number of igneous and metamorphic rock samples from the Canadian Shield (*4*, *5*). This approach should yield further insight into questions related to the episodic or uniform growth of continental crust through time. In addition, it may be possible to identify source areas (provenances) of sedimentary rocks because the sediments retain information about the time of formation of the crustal segments that were their sources.

The general approach we used is to assume that each time new material is added to the continental crust, the dominant contribution comes from the emplacement of magmatic rocks derived from a mantle reservoir, and that the differentiation processes that produce the magmatic rocks occur with a marked chemical fractionation of the daughter and parent elements relative to the source region. It is these times of chemical fractionation that are dated; the values obtained are, of course, model-dependent.

The mantle reservoir that is taken to be the source of the new crust is assumed to have evolved through geologic time with the characteristic Sm/Nd ratio identified by DePaolo and Wasserburg (*6*, *7*). These workers used the evolution of Nd through geologic time and the correlation of Nd and Sr isotopic variations in geologically young samples to identify the characteristics of the mantle reservoir. The arguments presented here are directly dependent on the validity of the mantle reservoir characteristics that they outlined. Such a simplified model will be subject to revision insofar as the Nd and Sr isotopic correlation is imprecise or not fully understood, and the mantle sources are chemically and isotopically complex regions.

Sm-Nd and Rb-Sr Systematics

Although the Rb-Sr method has been in use for some time [for example, see (*8*)], application of the Sm-Nd method has only recently been made possible by the development of high-precision mass spectrometric techniques and chemical separation procedures (*9*). Lugmair *et al.* (*10*) first applied the Sm-Nd method to meteoritic and lunar samples, and DePaolo and Wasserburg (*6*, *7*), O'Nions and co-workers (*11*), and Richard *et al.* (*12*) subsequently studied terrestrial samples.

Both Sm and Nd are rare earth elements (REE), and ^{147}Sm decays to ^{143}Nd with a half-life of 1.06×10^{11} years. The $^{143}Nd/^{144}Nd$ ratio measured today for a rock derived T years ago from a source with an initial $^{143}Nd/^{144}Nd$ ratio I_S is given by

$$\left(\frac{^{143}Nd}{^{144}Nd}\right)_M = I_S + \left(\frac{^{147}Sm}{^{144}Nd}\right)_M (e^{\lambda T} - 1) \qquad (1)$$

where M denotes the ratio measured in the rock today and λ the ^{147}Sm decay constant.

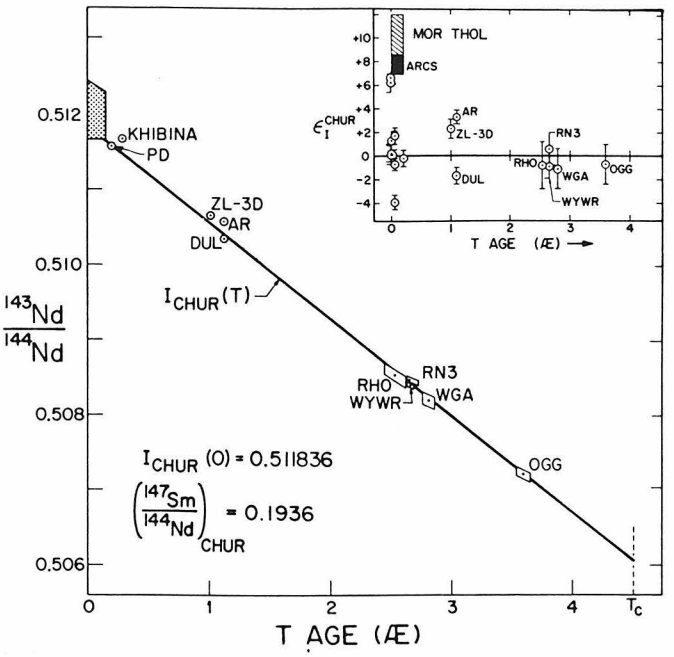

Fig. 1. Evolution of initial $^{143}Nd/^{144}Nd$ in sources of crustal rocks, determined for a suite of rock samples of known ages [from De Paolo and Wasserburg (*6*, *7*)]. (Inset) Fractional deviation in parts in 10^4 of the initial $^{143}Nd/^{144}Nd$ ratio from the evolution to be found in a reservoir with a chondritic Sm/Nd ratio. The shaded area is for midocean ridge tholeiites and island arc volcanics. The initial $^{143}Nd/^{144}Nd$ ratio from the 2.64 ± 0.14 AE greenstone belt in Rhodesia (*11*) is coincident with the point WYWR (grandiorite from Wind River Mountains, Wyoming).

Variations in I_S in terrestrial samples through geologic time were first studied by DePaolo and Wasserburg (*6*, *7*), who showed that to a reasonable approximation the evolution of $^{143}Nd/^{144}Nd$ in the source of continental rocks implies a uniform ratio essentially equal to that found in chondrites. Figure 1 shows the initial $^{143}Nd/^{144}Nd$ values for a variety of igneous rock types as a function of age. The fractional deviations in parts in 10^4 of I_S from $^{143}Nd/^{144}Nd$ in a reservoir with a chondritic Sm/Nd ratio $I_{CHUR}(T)$ are shown in the inset of Fig. 1. The maximum deviation is less than 3 parts in 10^4 and is at present recognized only in continental rocks younger than 1 AE. It is thus plausible to assume that the mantle reservoir which is the source of crustal rocks has an Sm/Nd ratio very close to the relative abundance found in a chondritic uniform reservoir (CHUR). The value of $^{143}Nd/^{144}Nd$ in CHUR today is defined as $I_{CHUR}(0)$ and is given by

$$I_{CHUR}(0) = I_{CHUR}(T) + \left(\frac{^{147}Sm}{^{144}Nd}\right)_{CHUR}(e^{\lambda T} - 1) \quad (2)$$

where $I_{CHUR}(0) = 0.511836$ and $I_{CHUR}(T)$ is $^{143}Nd/^{144}Nd$ in CHUR at any time T in the past and $(^{147}Sm/^{144}Nd)_{CHUR} = 0.1936$ is that in CHUR (*10*). A magma derived from the CHUR reservoir T years ago would have $I_S = I_{CHUR}(T)$. Then from Eqs. 1 and 2, assuming that a rock remains a closed system from the time of differentiation until today, the time of fractionation and concurrent derivation from the CHUR reservoir is given by

$$T^{Nd}_{CHUR} = \frac{1}{\lambda} \ln\left[1 + \frac{\epsilon_{Nd}(0)\, I_{CHUR}(0) \times 10^{-4}}{f_{Sm/Nd}(^{147}Sm/^{144}Nd)_{CHUR}}\right] \quad (3)$$

where

$$f_{Sm/Nd} = \left[\frac{(Sm/Nd)_M}{(Sm/Nd)_{CHUR}} - 1\right] \quad (4)$$

and

$$\epsilon_{Nd}(0) = \left[\frac{(^{143}Nd/^{144}Nd)_M}{I_{CHUR}(0)} - 1\right] \times 10^4 \quad (5)$$

It is apparent from Eq. 3 that T^{Nd}_{CHUR} is indeterminate for $f_{Sm/Nd} = 0$. For precise determination of T^{Nd}_{CHUR} ages, a relatively large fractionation of Sm/Nd from the chondritic ratio at the time of derivation from CHUR is required, along with a value of $\epsilon_{Nd}(0)$ distinct from zero. An example is shown schematically in Fig. 2 for a rock with an enrichment factor $f_{Sm/Nd} = -1$ [that is, $(Sm/Nd)_M = 0$] and with the ratio of $^{143}Nd/^{144}Nd$ measured today (R_A) unchanged since the derivation from CHUR $T^{Nd}_{CHUR}(A)$ years ago. In this example for a closed system (no addition of Sm or Nd), remelting and metamorphic and sedimentary processes are assumed not to change $(^{143}Nd/^{144}Nd)_M$ or Sm/Nd, and thus the T^{Nd}_{CHUR} age would be unaffected by these processes. A more

general example is shown with $f_{Sm/Nd} < 0$ and the $(^{143}Nd/^{144}Nd)_M$ as measured today (R_B) somewhat evolved since derivation from CHUR. Again, for a closed system, later metamorphic and sedimentary events shown schematically as T_{MET} and T_{SED}, respectively, are assumed not to change the T^{Nd}_{CHUR} age.

The classic REE distribution studies by Haskin *et al.* (*13*), Taylor (*14*), Ronov *et al.* (*15*), and Shaw *et al.* (*16*) have shown that for most crustal rocks $f_{Sm/Nd} < 0$. This can be seen in Table 1, where estimates of $f_{Sm/Nd}$ range from -0.26 to -0.46. Regardless of the particular model invoked for the formation of continental crust, the observation that in a wide variety of crustal rocks Sm/Nd is markedly fractionated with respect to the source (CHUR) value implies that this is an important characteristic of continental crust. Insofar as the CHUR reservoir is the source of new crustal materials, and if the major fractionation of Sm/Nd occurs when rocks are derived from this reservoir, the time of formation of new crustal segments is given by T^{Nd}_{CHUR}. To find T^{Nd}_{CHUR} ages of the sources of metamorphic and sedimentary rocks also requires the assumption that no change in Sm/Nd and $^{143}Nd/^{144}Nd$ occurred during the secondary processes that formed these rocks. The validity of this approach is suggested by REE distribution studies which indicate that Sm/Nd does not change with increasing metamorphic grade (*17*) and that many sedimentary rocks preserve the average Sm/Nd of their source (*13, 14*). However, the validity can be fully established only by the self-consistency of the T^{Nd}_{CHUR} ages.

The samples we studied are composites of igneous and metamorphic rocks from the Canadian Shield, shales, graywackes, loess deposits, a schist, and a deep-sea sediment. These samples do not represent a single source, but almost certainly a mixture of a variety of sources. Although the isotopic systematics as outlined were for a single source, they are also applicable to a mixture of a number of sources. For example, it can be shown that a mixture of two rocks, A and B, with different T^{Nd}_{CHUR} ages $T^{Nd}_{CHUR}(A)$ and $T^{Nd}_{CHUR}(B)$ and enrichment factors $f_{Sm/Nd}(A)$ and $f_{Sm/Nd}(B)$, as in Fig. 2, would give a mean age

$$\langle T^{Nd}_{CHUR}(A + B)\rangle = \frac{T^{Nd}_{CHUR}(A)Nd_A f_{Sm/Nd}(A)}{Nd_A f_{Sm/Nd}(A) + Nd_B f_{Sm/Nd}(B)} + \frac{T^{Nd}_{CHUR}(B)Nd_B f_{Sm/Nd}(B)}{Nd_B f_{Sm/Nd}(B) + Nd_A f_{Sm/Nd}(A)} \quad (6)$$

Here Nd_A is the Nd contribution from rock A and Nd_B is the Nd contribution from rock B. From this equation it can be seen that $\langle T^{Nd}_{CHUR}(A + B)\rangle$ is simply the average of $T^{Nd}_{CHUR}(A)$ and $T^{Nd}_{CHUR}(B)$, weighted by the Nd concentrations and enrichment factors of the rocks. So, in general, the average $\langle T^{Nd}_{CHUR}\rangle$ is greater than the minimum T^{Nd}_{CHUR} and less than the maximum T^{Nd}_{CHUR} in any mixture.

From the correlation between Nd and Sr isotopic abundances in young igneous rocks, discovered by DePaolo and Wasserburg (*7*) and O'Nions and co-workers (*11*), it appears possible to estimate a characteristic Rb/Sr value of a standard unfractionated reservoir (UR) that is the source region of continental rocks. In a manner analogous to that discussed for Sm and Nd, Rb-Sr model ages can also be calculated, assuming that simple rules apply to Rb-Sr isotopic systematics. For this system

$$T^{Sr}_{UR} = \frac{1}{\lambda} \ln\left[1 + \frac{\epsilon_{Sr}(0)I_{UR}(0) \times 10^{-4}}{f_{Rb/Sr}(^{87}Sr/^{86}Sr)_{UR}}\right] \quad (7)$$

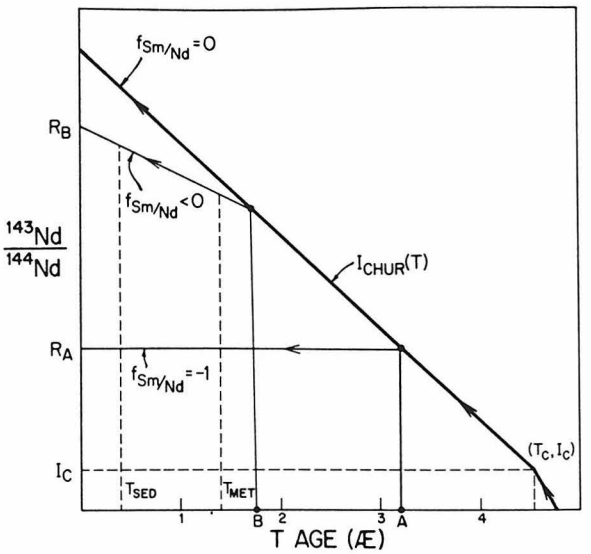

Fig. 2. Schematic representation of the evolution of $^{143}Nd/^{144}Nd$ on the earth since it condensed at time T_c. Assuming it to have a chondritic Sm/Nd, the growth rate of $^{143}Nd/^{144}Nd$ in a reservoir or a rock is proportional to Sm/Nd. Examples are shown of the evolution of $^{143}Nd/^{144}Nd$ with the Sm/Nd fractionated from CHUR. A rock derived from CHUR at time T(B) and enriched in Sm/Nd by a factor $f_{Sm/Nd}$ will evolve subsequent to T(B) along the secondary trajectory to the $^{143}Nd/^{144}Nd$ ratio today, R_B.

where $I_{UR} = 0.7045$ is the $^{87}Sr/^{86}Sr$ ratio, $(^{87}Rb/^{86}Sr)_{UR} = 0.084$, and $\lambda = 1.39 \times 10^{-11}$ year^{-1} in the source of continental rocks today (*7, 11*). Similarly

$$\epsilon_{Sr}(0) = \left[\frac{(^{87}Sr/^{86}Sr)_M}{I_{UR}(0)} - 1\right] \times 10^4 \quad (8)$$

and

$$f_{Rb/Sr} = \left[\frac{(Rb/Sr)_M}{(Rb/Sr)_{UR}} - 1\right] \quad (9)$$

A relationship analogous to Eq. 6 for the mean Rb-Sr age of a mixture may also be derived. We have also carried out Rb-Sr studies on the samples for which Sm-Nd results are reported here. The major difference between the Rb-Sr system and the Sm-Nd system is that for most continental crustal rocks $f_{Rb/Sr} >> 0$. This is also shown in Table 1, where estimates of the continental crustal $f_{Rb/Sr}$ range from +10.3 to +11.3. In addition, the response of Rb and Sr to metamorphic and sedimentary processes is markedly different from that of Sm and Nd. In metamorphic processes redistribution of Rb and Sr between minerals has been well documented (*18, 19*). Rubidium-strontium isochrons have also been obtained from some sedimentary rocks (*20–22*), which suggests that large enrichments of Rb relative to Sr and reequilibration of $^{87}Sr/^{86}Sr$ have occurred, presumably during or subsequent to deposition of these rocks.

Experimental Results

Detailed descriptions of the experimental procedures are given by Papanastassiou and Wasserburg (*23*) for Rb and Sr and by Papanastassiou *et al.* (*24*) for Sm and Nd. Errors given for $^{143}Nd/^{144}Nd$ and $^{87}Sr/^{86}Sr$ are 2 σ_{mean} (two standard deviations of the mean) of about 200 ratios for Nd and 100 ratios for Sr. The Nd, Sm, Rb, and Sr concentrations were obtained by isotope dilution techniques. The errors in Rb/Sr and Sm/Nd are less than 1 percent and include an assessment of errors from gravimetry and measurement of isotopic ratios. The 2 σ_{mean} errors given for the T^{Nd}_{CHUR} and T^{Sr}_{UR} ages only allow for analytical errors and do not include uncertainties in the parameters used for the mantle sources. Table 3 summarizes the $\epsilon_{Nd}(0)$, $f_{Sm/Nd}$, $\epsilon_{Rb/Sr}(0)$, and $f_{Rb/Sr}$ values used to calculate T^{Nd}_{CHUR} and T^{Sr}_{UR} ages. With only a few exceptions, the $f_{Sm/Nd}$ values in Table 3 are

Table 1. Estimates of upper crustal Sm/Nd and Rb/Sr enrichment factors. The enrichment factors $f_{Sm/Nd}$ and $f_{Rb/Sr}$ are defined in Eqs. 4 and 9, respectively.

Composite	$f_{Sm/Nd}$	$f_{Rb/Sr}$	Reference
Canadian Shield	−0.46	+11.3	Shaw *et al.* (*5*, *16*)
Upper crust	−0.45	+10.1	Taylor (*40*)
Continental crust	−0.26		Ronov *et al.* (*15*)
North American shales	−0.46	+30.1	Haskin *et al.* (*57*); this article
Chondrites	0.0	+8.3	Haskin *et al.* (*13*); Urey (*64*)
Model mantle reservoir	0.0	0.0	

Table 2. Lithologies of Canadian Shield composites.

Composite	Lithologic type	Reference
New Quebec* and Fort Enterprise	Banded gneisses, migmatites, and granitic gneisses	(*4*)
Fort Enterprise	High-level granite and quartz monzonite	(*4*)
North Quebec, Saskatchewan, Baffin Island, and Quebec	Quartzofeldspathic rocks including granite, granitic gneiss, pegmatite, rhyolite, arkose, sandstone	(*5*)

*Area 12.

relatively constant. Hence, variations in the calculated T^{Nd}_{CHUR} age are mainly dependent on $\epsilon_{Nd}(0)$. For this reason, where appropriate, discussion of either $\epsilon_{Nd}(0)$ values or the calculated T^{Nd}_{CHUR} ages will be emphasized.

Canadian Shield Composites

The Canadian Shield is one of the better-studied Precambrian areas, and the results of these studies have been important in formulating theories of continental growth and evolution. Based on geologic evidence, derived primarily from field mapping and integrated with isotopic dating, a number of structural provinces have been recognized in the Canadian Shield. From areas within different provinces, we measured $\epsilon_{Nd}(0)$, $f_{Sm/Nd}$, $\epsilon_{Sr}(0)$, and $f_{Rb/Sr}$ values and calculated T^{Nd}_{CHUR} and T^{Sr}_{UR} ages. In an attempt to determine the average age of relatively large areas of continental crust without a prohibitive number of analyses, we analyzed composite samples. These composites, in some cases consisting of several thousand samples, were originally used by Eade and Fahrig (*4*) and Shaw *et al.* (*5*, *16*) to estimate the average chemical composition of the upper continental crust of the Canadian Shield. The generalized provinces and the areas represented by the composites analyzed are shown in Fig. 3. From the composites prepared by Shaw *et al.* (*5*) we analyzed the "quartzofeldspathic" lithologic type (Table 2), which constitutes approximately 70 percent of the area sampled. Two different lithologies from the composites of Eade and Fahrig (*4*) were studied. These are the gneisses and the granite-quartz monzonites. As described in Table 2, the different lithologies of Eade and Fahrig (*4*) are comparable to those of Shaw *et al.* (*5*) and also constitute a significant portion of the sample area.

From Fig. 3 it can be seen that the New Quebec and a large portion of the

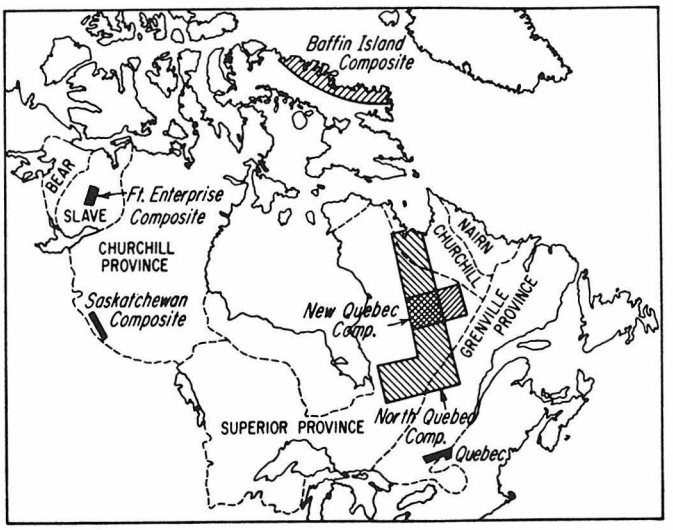

Fig. 3. Location of the areas sampled by the Canadian Shield composites and the tectonic provinces of the Canadian Shield.

North Quebec composites are in the Superior Province. This province contains some of the older rocks in the Canadian Shield, where a major granodiorite-forming event has been recognized at ~2.5 to 2.7 AE (*25*). For New Quebec $\epsilon_{Nd}(0) = -29.4 \pm 0.4$ with a T^{Nd}_{CHUR} age of 2.66 ± 0.06 AE. The T^{Sr}_{UR} age is 2.73 ± 0.03 AE and is in excellent agreement. The North Quebec composite, which includes a small proportion of younger material from the Grenville Province, gives $\epsilon_{Nd}(0) = -28.9 \pm 0.3$, a T^{Nd}_{CHUR} age of 2.50 ± 0.05 AE, and a T^{Sr}_{UR} age of 2.52 ± 0.03 AE. The striking agreement between the T^{Nd}_{CHUR} and T^{Sr}_{UR} ages for New Quebec and North Quebec composites is also fully consistent with previously determined radiometric ages (*25*) and confirms that the Superior Province consists predominantly of new crust that was first formed 2.5 to 2.7 AE ago.

The Fort Enterprise composites are in the Slave Province of northern Canada (Fig. 3). This province has some K-Ar (*26*) and Rb-Sr (*27*) dates of the same age (2.5 to 2.7 AE) as those found in the Superior Province, and the provinces are generally thought to be of similar age. For the gneissic composite the T^{Nd}_{CHUR} age is 2.62 ± 0.05 AE and the T^{Sr}_{UR} age is 2.58 ± 0.03 AE. From the same area, the granite–quartz monzonite composite gives a T^{Nd}_{CHUR} age of 2.49 ± 0.04 AE and a T^{Sr}_{UR} age of 2.56 ± 0.03 AE. The T^{Nd}_{CHUR} and T^{Sr}_{UR} ages for the two different lithologies are again in excellent agreement, indicating that lithologic type is not important in determining the time of formation of this crustal segment.

Composite samples from Baffin Island and Saskatchewan from different areas of the Churchill Province have been studied. For Baffin Island the T^{Nd}_{CHUR} age is 2.74 ± 0.05 AE, and a T^{Sr}_{UR} age of 2.56 ± 0.03 AE has been obtained. The Saskatchewan composite gives a T^{Nd}_{CHUR} age of 2.68 ± 0.06 AE and a somewhat lower T^{Sr}_{UR} age of 2.43 ± 0.03 AE. These crustal formation ages are much older than the K-Ar ages of ~1.8 to 1.9 AE that are most commonly found in these areas (*26*). In this province, the T^{Sr}_{UR} ages are slightly younger than the T^{Nd}_{CHUR} ages and may have been partially affected by the event or events that reset the K-Ar ages.

Adjacent to the eastern margin of the Superior Province is the Grenville Province. In the southwestern corner of the Grenville Province, the Quebec composite with $\epsilon_{Nd}(0) = -7.1 \pm 0.3$ gives a T^{Nd}_{CHUR} age of 0.80 ± 0.04 AE and a T^{Sr}_{UR} age of 1.01 ± 0.01 AE. The T^{Sr}_{UR} age is consistent with previously determined crystallization ages (*19*, *28*), but the T^{Nd}_{CHUR} age is approximately 0.2 AE

Table 3. Provenance parameters for Nd and Sr.

Sample	$\varepsilon_{Nd}(0)$	$f_{Sm/Nd}$	T^{Nd}_{CHUR} (AE)	$\varepsilon_{Sr}(0)$	$f_{Rb/Sr}$	T^{Sr}_{UR} (AE)	$T_{geologic}$ (AE)
Canadian Shield composites							
New Quebec	−29.4 ± 0.4*†	−0.444	2.66 ± 0.06*‡	345.3 ± 0.8*†	7.48	2.73 ± 0.03*‡	2.5–2.7§
North Quebec	−28.9 ± 0.3	−0.464	2.50 ± 0.05	328.9 ± 1.1	7.74	2.52 ± 0.03	2.5–2.7
Fort Enterprise Gneiss	−24.3 ± 0.4	−0.372	2.62 ± 0.05	369.2 ± 0.8	8.47	2.58 ± 0.03	2.5–2.7
Fort Enterprise Granite	−30.7 ± 0.2	−0.495	2.49 ± 0.04	344.5 ± 0.9	7.99	2.56 ± 0.03	2.5–2.7
Baffin Island	−31.7 ± 0.3	−0.464	2.74 ± 0.05	802.8 ± 0.7	18.6	2.56 ± 0.03	1.8–1.9
Saskatchewan	−32.5 ± 0.4	−0.486	2.68 ± 0.06	566.1 ± 0.9	13.8	2.43 ± 0.03	1.8–1.9
Quebec	− 7.1 ± 0.3	−0.361	0.80 ± 0.04	164.8 ± 0.8	9.81	1.01 ± 0.01	0.9–1.2
Sedimentary rocks							
Baja Shale	+ 0.7 ± 0.4	−0.227	−0.12 ± 0.07	27.0 ± 0.8	55.2	0.030 ± 0.001	0.1‖
San Gabriel Sand	− 9.9 ± 0.4	−0.225	1.77 ± 0.09	59.5 ± 0.8	5.16	0.69 ± 0.02	0.2–1.7
Figtree shale	−28.0 ± 0.4	−0.317	3.53 ± 0.06	4506.7 ± 1.0	90.6	2.94 ± 0.03	2.98
Iowa loess	−14.1 ± 0.5	−0.411	1.38 ± 0.06	181.8 ± 0.7	15.3	0.710 ± 0.01	0.01
Nanking loess	−10.2 ± 0.4	−0.410	1.00 ± 0.05	198.7 ± 1.0	34.3	0.350 ± 0.005	0.01
North American shales	−14.4 ± 0.5	−0.380	1.52 ± 0.07	380.8 ± 1.1	30.1	0.76 ± 0.01	0.5
Birch Creek Schist	−27.0 ± 0.3	−0.464	2.33 ± 0.05	811.8 ± 1.1	68.3	0.714 ± 0.008	0.5–1.8
Deep-sea red clay	− 3.3 ± 0.4	−0.212	0.63 ± 0.08	53.7 ± 1.0	8.41	0.38 ± 0.01	0.01
Australian sediments							
SC-5	−14.5 ± 0.4	−0.443	1.32 ± 0.05	2481.6 ± 0.7	293.0	0.509 ± 0.005	0.44
AO-7	−16.8 ± 0.4	−0.433	1.56 ± 0.05	1130.0 ± 0.6	71.6	0.95 ± 0.01	0.8
MI-1	−23.5 ± 0.3	−0.455	2.07 ± 0.05	6837.5 ± 0.8	264.0	1.55 ± 0.02	1.5
KH44	−28.3 ± 0.5	−0.370	3.06 ± 0.08	928.0 ± 0.8	18.2	3.01 ± 0.03	2.7–3.0
Weathered Morton Gneiss							
Locality 3	−46.7 ± 0.4	−0.522	3.58 ± 0.03	3548.7 ± 3.0	98.7	2.14 ± 0.02	3.2–3.8¶
Locality 5	−36.9 ± 0.3	−0.506	2.92 ± 0.03	2099.4 ± 2.0	69.4	1.80 ± 0.02	3.2–3.8¶
CHUR (Sm/Nd)	0.0	0.0					
UR (Rb/Sr)				0.0	0.0		

*Errors are 2 σ_{mean}. †Measured $^{143}Nd/^{144}Nd$ and $^{87}Sr/^{86}Sr$ values can be calculated from Eqs. 5 and 8, respectively, and the $\varepsilon_{Nd}(0)$ and $\varepsilon_{Sr}(0)$ values listed above. ‡For ^{147}Sm, $\lambda = 6.54 \times 10^{-12}$ year^{-1}; for ^{87}Rb, $\lambda = 1.39 \times 10^{-11}$ year^{-1}. §For the Canadian Shield composites, T_{geol} is the previously determined radiometric age from samples within the same province. ‖For the sedimentary rocks, T_{geol} is the best estimate of the time at which the sediment was formed, based on the stratigraphic age or radiometric age determinations. ¶Radiometric age of fresh Morton Gneiss.

younger. Although there is substantial evidence (*19, 28*) that some rocks in the Grenville Province are remobilized 2.5-AE rocks, particularly at the weld between the Grenville and Superior provinces, the results presented here indicate that the bulk of the area sampled is comprised of much younger crust.

The T^{Nd}_{CHUR} and T^{Sr}_{UR} ages of the Churchill Province are essentially identical to those obtained for the Superior and Slave provinces. Although this was suggested by some previous age determinations (*29*), there now appears to be compelling evidence that the Superior, Slave, and Churchill provinces were all formed as crustal segments within the same period from 2.5 to 2.7 AE. This now poses the problem of how these structural provinces, having relatively distinct boundaries and structural patterns but consisting of materials formed at nearly the same time, were juxtaposed. The good correlation between the K-Ar ages and the structural provinces (*26*) suggests that the K-Ar ages represent the time at which the different provinces were last metamorphosed and deformed and obtained their structural characteristics. If this is the case, the structural characteristics of the Superior and Slave provinces were imposed at the time of or within 0.2 AE of their formation, while those of the Churchill Province were obtained approximately 0.8 AE after its formation. It is not, however, apparent whether the last metamorphism and deformation of the Churchill Province occurred before, during, or after the time when the provinces assumed their present relative positions.

The T^{Nd}_{CHUR} and T^{Sr}_{UR} ages of ~0.8 to 1.0 AE for the Grenville Province composite show that it is markedly younger than the other Canadian Shield composites. This indicates the addition of younger material onto the preexisting Canadian Shield. However, from the T^{Nd}_{CHUR} and T^{Sr}_{UR} ages of the Superior, Slave, and Churchill composites, it is evident that the Canadian Shield contains only a relatively small amount of material that is substantially younger than 2.5 AE. Older structural units are manifest on the North American continent, where rocks of ~3.6 AE old have been found (*30–32*). Ancient cratonic components have also been found in Australia (*33*), Greenland (*34*), Africa (*35*), and possibly the Baltic (*36*) and Ukrainian (*37*) shields. However, considering the wide variety of materials and the distinctive areas that have been sampled, we must conclude that the period 2.5 to 2.7 AE was a major epoch of formation of new continental crust. This has been manifest from the studies of previous workers (*3, 25*), who observed the relatively high frequency of radiometric ages in this period, but it can now clearly be extended to a much broader context. From our present knowledge of the times of formation of continental crust, it appears that the activity around 2.5 to 2.7 AE ago has been unique in geologic history. It also appears certain that some truly major periods of continental crustal growth are sharply episodic. This raises the interesting possibility that the dramatic decrease in the volume of continental crust produced since 2.5 AE ago may have been due to a change in the mechanism rather than only in the rate of crustal formation.

From heat flow data and the chemical composition of exposed lower crustal rocks, it is well known that the upper crustal composition represented by these composites cannot extend to a depth of more than 10 km (*38*). It has been inferred (*38–40*) that the Rb/Sr ratio in the lower crust is at least a factor of 2 smaller than in the upper crust. The T^{Sr}_{UR} ages indicate that this enrichment of Rb/Sr in the upper crust occurred during the period 2.5 to 2.7 AE. Thus the younger events that reset the K-Ar ages in the Churchill Province did not redistribute Rb or Sr over a scale greater than that sampled. Furthermore, the relatively good agreement between the T^{Nd}_{CHUR} and T^{Sr}_{UR} ages (that is, 2.5 to 2.7 AE) requires

that the fractionation of Sm and Nd was contemporaneous with that of Rb and Sr. From these data, the enrichment of Rb/Sr in the upper crust appears to be a primary feature of continental crust, being associated with the formation of new crust, and does not reflect metasomatic or metamorphic processes at later times.

The enrichment factors $f_{Rb/Sr}$ in the Churchill Province composites are approximately a factor of 2 greater than those in the Superior and Slave composites. This distinction may be attributable to more extensive erosion of the Superior and Slave provinces, exposing a greater proportion of a lower crust more depleted in Rb. Consistent with this is the relatively widespread occurrence in the Superior Province of granulite facies rocks (*41*), which are indicative of formation depths greater than ~20 km. An analogous variation of $f_{Sm/Nd}$ is not present in the same composites. Thus, although Sm and Nd were fractionated at the same time as Rb and Sr, their relative elemental distributions through the continental crust do not appear to be correlated.

The Sm-Nd and Rb-Sr isotopic studies of composite samples can, of course, be applied to other continental segments to ascertain average times of formation with relatively few analyses. This approach may be particularly useful where there is little or no other radiometric age information indicative of formation times of new crust, or where complex metamorphic processes make the identification of primary magmatic crystallization ages difficult.

Sediments

In many respects, sedimentary rocks are similar to the Canadian Shield composites. They were originally derived from igneous and metamorphic rocks and often consist of materials from diverse sources. However, although sedimentary rocks cover approximately 80 percent of the continent's surface (*42*), attempts to characterize and identify their provenances by using isotopic tracers have not been extensively pursued (*2*, *43*). This is mainly due to the disturbance of these systems by chemical processes during or after sedimentation. In particular, many trace elements are fractionated as a result of preferential weathering of specific mineral phases and of the formation of authigenic minerals such as clays. However, because of the geochemical coherence and short residence times of REE in seawater, the Sm-Nd isotopic system may be less susceptible to disturbance during sedimentation and diagenesis. This is apparent from Table 3, where the $f_{Sm/Nd}$ values for the sediments are all approximately the same and are also similar to those estimated for the upper crust (Table 1). This suggests that the Sm-Nd isotopic system may remain closed during sedimentation and diagenesis, in which case the T^{Nd}_{CHUR} age would represent the average time of formation of the crust from which the sediments were derived. The sediments could be derived from this crust either directly, or indirectly from recycled materials. In contrast, $f_{Rb/Sr}$ is variable and in some sediments is up to a factor of 30 greater than the average upper crustal estimates in Table 1. These large $f_{Rb/Sr}$ values show loss of Sr relative to Rb in the sediments, probably due to the formation of clay minerals such as illite and montmorillonite, within which Rb is strongly fixed relative to Sr (*22*, *44*). Depending on the relative increase in $f_{Rb/Sr}$ and the initial $^{87}Sr/^{86}Sr$ of the sediment, it would be expected that the T^{Sr}_{UR} age will be less than the time of formation of new crust and will approach the time of deposition or diagenesis of the sediment.

In an attempt to ascertain directly the effect of weathering on the Sm-Nd and Rb-Sr isotopic systems, we analyzed two samples from the weathered profile of the Morton Gneiss in the Minnesota River valley. These samples are the same as those used by Goldich (*45*) in his classic study of rock weathering. The profile consisting predominantly of quartz and kaolinite was developed during the Cretaceous in a humid tropical or subtropical climate by weathering of Precambrian gneisses and igneous rocks. The sample from Goldich's locality 3 has a T^{Nd}_{CHUR} age of 3.58 ± 0.03 AE and a distinctly younger T^{Sr}_{UR} age of 1.80 ± 0.02 AE. The sample from locality 5 has a

T^{Nd}_{CHUR} age of 2.92 ± 0.03 AE and a T^{Sr}_{UR} age of 2.14 ± 0.02 AE. The markedly younger T^{Sr}_{UR} ages and large $f_{Rb/Sr}$ values of 98.7 for locality 3 and 69.4 for locality 5 are probably due to loss of Sr relative to Rb during the weathering, or to earlier metamorphic events (*32*). The K-Ar and Rb-Sr ages of biotites were obtained from the same samples by Goldich and Gast (*46*). These ages are 25 to 75 percent lower than those obtained from biotites in the fresh Morton Gneiss and indicate preferential loss of radiogenic Sr and Ar. In addition, zircons analyzed from locality 3 (*47*) are highly discordant, with a minimum age of 0.455 AE, which has been attributed to bulk loss of lead by leaching (*47*). The T^{Nd}_{CHUR} age from locality 3 is within the age range of 3.2 to 3.8 AE found for fresh Morton Gneiss (*32*), indicating that the Sm-Nd system remained closed during weathering and metamorphism. However, the T^{Nd}_{CHUR} age of 2.92 AE from locality 5 is difficult to interpret, as it could be attributed either to the presence of a large component of younger rocks, which are often associated with the Morton Gneiss (*32*), or to effects of weathering. This cannot be resolved in this geologically complex area and must be addressed by future studies in more carefully defined geologic settings.

To test this approach further, we chose an example of a sediment derived from a relatively young crustal source. We analyzed a shale from the Rosario Formation, Punta San Jose, western Baja California, Mexico (Baja Shale), which contains marine fossils of Maestrichtian age (~ 0.065 AE) and is isolated from older mainland material. Its source was most probably Jurassic or Cretaceous eugeosynclinal rocks, which are predominant in this region. No Precambrian terranes appear to be available as possible source regions. Its $\epsilon_{Nd}(0)$ value of +0.7 ± 0.4 is clearly characteristic of a very young source and markedly different from the large negative $\epsilon_{ND}(0)$ for older sources. The T^{Sr}_{UR} age of 0.030 ± 0.001 AE, although more reasonable than the T^{Nd}_{CHUR} age, is somewhat younger than the time of deposition. These results reflect the sensitivity of rocks with young sources to the detailed assumptions of their evolutionary history. However, both of these results clearly are compatible with the very young age of the crustal sources that constituted the provenance for this shale.

As an example of a young detrital sediment, derived from old source material, we analyzed sand (San Gabriel Sand), which was collected from the mouth of Santa Anita Canyon in the San Gabriel Mountains of Southern California. The rocks in this area are predominantly granitic rocks of Mesozoic age (*48*), although a wedge of Precambrian gneisses is present at the mouth of the canyon (*49*). This sample has $\epsilon_{Nd}(0) = -9.9 \pm 0.4$ and a relatively small value of $f_{Sm/Nd} = -0.225$, giving a T^{Nd}_{CHUR} age of 1.77 ± 0.09 AE. This suggests that most of the sample was derived from the older Precambrian gneisses. However, the $f_{Rb/Sr} = 5.16$ together with the low value of $\epsilon_{Sr}(0) = 59.5 \pm 0.8$ gives a calculated T^{Sr}_{UR} age of 0.69 ± 0.02 AE. The T^{Sr}_{UR} age is markedly younger than the T^{Nd}_{CHUR} age, but the low $f_{Rb/Sr}$ is not consistent with Sr loss or Rb fixation during weathering of this material. Further isotopic characterization of the possible sources of the San Gabriel Sand are required to resolve this problem.

To ascertain the self-consistency of this approach, sediments representing a

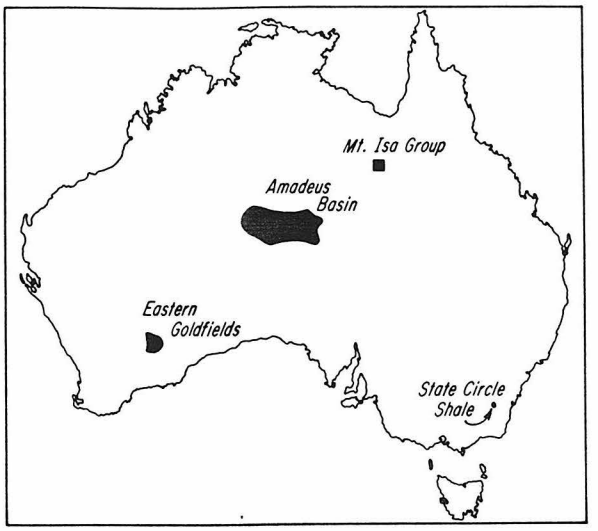

Fig. 4. Map of Australia showing the areas sampled (*50*). The approximate areas of outcrop of the sampled or related units are shaded.

range of depositional ages were studied. These sediments are from the Australian continent, and their locations are shown in Fig. 4. They were part of a REE distribution study by Nance and Taylor (*50*). The Australian sediment with the youngest depositional age is the Silurian State Circle Shale (SC-5). It has a measured $\epsilon_{Nd}(0) = -14.5 \pm 0.4$ and a resulting T^{Nd}_{CHUR} age of 1.32 ± 0.05 AE. However, the nearest exposed Precambrian rocks that could have acted as sources for this sediment are now approximately 720 km to the west. This suggests either that SC-5 was not locally derived or that it was derived from recycled older sedimentary material, which had in turn been derived from Precambrian sources. An exceedingly large enrichment of Rb relative to Sr is found in this sediment, which has $f_{Rb/Sr} = 293$; together with the measured $\epsilon_{Sr}(0)$, this gives a T^{Sr}_{UR} age of 0.509 ± 0.005 AE. This age is only slightly greater than the age of 0.440 ± 0.009 obtained from an Rb-Sr isochron by Bofinger *et al.* (*51*). A shale (AO-7) from the Pertakaka Formation in the Amadeus basin, central Australia, has a depositional age of 0.8 AE (*52*) and $\epsilon_{Nd}(0) = -16.8 \pm 0.4$, giving a T^{Nd}_{CHUR} age of 1.56 ± 0.05 AE. The Musgrave-Mann and Arunta complexes that surround the Amadeus basin have Rb-Sr and K-Ar ages ranging from 1.1 to 1.8 AE (*52*). These ages are compatible with the T^{Nd}_{CHUR} age, which suggests that these complexes could have acted as the source of this sediment. For AO-7 $f_{Rb/Sr} = 71.6$ which, together with the measured $\epsilon_{Sr}(0)$, gives a T^{Sr}_{UR} age of 0.95 ± 0.01 AE, compared with an age of 0.79 AE obtained previously from Rb-Sr studies (*52*). A shale (MI-1) from the Mount Isa Geosyncline, Mount Isa, Queensland, has $f_{Rb/Sr} = 264$ and a T^{Sr}_{UR} age of 1.55 ± 0.02 AE. This is in good agreement with the estimated depositional age of approximately 1.5 AE (*53*), indicating that the massive enrichment of Rb relative to Sr occurred at this time. From the measured $\epsilon_{Nd}(0) = -23.5 \pm 0.3$ a T^{Nd}_{CHUR} age of 2.07 ± 0.05 AE is calculated for MI-1. Zircon and Rb-Sr total rock ages of 1.86 and 1.84 AE, respectively, have been determined (*54*) from the oldest unit in the Mount Isa basement sequence, the Leichardt metamorphics. These ages, in conjunction with the T^{Nd}_{CHUR} age, suggest that the shale could have been derived mainly from this source, but with an additional component of substantially older age.

The application of Sm-Nd isotopic systematics to calculate the T^{Nd}_{CHUR} provenance age may also be particularly useful for older sediments, whose sources may no longer be preserved or recogniz-

able. An example is the graywacke KH44 from Coolgardie, Western Australia, which has a depositional age of approximately 2.6 to 3.0 AE and is part of the Archean granite-greenstone terrain prevalent in this area. The graywacke KH44 has $\epsilon_{Nd}(0) = -28.3 \pm 0.5$, giving a T^{Nd}_{CHUR} age of 3.06 ± 0.08 AE. This is consistent with the younger age limit of 2.76 AE determined by Oversby (*55*) from granitic intrusives in the neighboring areas, but indicates a significant contribution of substantially older crust that has not yet been found, although there are other hints of it (*55*). The T^{Sr}_{UR} age of 3.01 ± 0.03 AE for KH44 is identical, within errors, to the T^{Nd}_{CHUR} age. This agreement may be explained by the fact that the $f_{Rb/Sr}$ value of 18.24 is relatively low compared to those of other sediments.

Another example of a sediment from an Archean granite-greenstone terrain is the Figtree shale from the Swaziland system in South Africa. The Figtree Group conformably overlies the relatively well preserved Onverwacht Group, whose ages as summarized by Jahn and Shih (*35*) range from 3.2 to 3.5 AE. From the measured $\epsilon_{Nd}(0) = -28.0 \pm 0.4$, a T^{Nd}_{CHUR} age of 3.53 ± 0.06 AE is calculated for the Figtree shale. This is consistent with its derivation from the underlying Onverwacht Group, although at the upper limit of the proposed age range (*35*). Allsopp *et al.* (*21*) obtained an Rb-Sr isochron of 2.98 ± 0.02 AE from the Figtree shale. Interpreted as the minimum age of the shale, the isochron clearly demonstrates that redistribution of Rb and Sr has occurred during sedimentation and diagenesis. The T^{Sr}_{UR} age of 2.94 ± 0.03 AE that we obtained for a radiogenic sample with $f_{Rb/Sr} = 90.6$, where the assumptions regarding the initial $^{87}Sr/^{86}Sr$ are relatively unimportant, is consistent with the age of Allsopp *et al.* (*21*). Thus the T^{Nd}_{CHUR} age indicates that the Figtree shale was derived from a source with a mean age of crustal formation of 3.53 AE, and the T^{Sr}_{UR} age in conjunction with the large $f_{Rb/Sr}$ value suggests that the sediment was probably deposited ~ 2.94 AE ago.

For many sedimentary rocks the provenance is obscure or a complete enigma. Classic examples are the loess deposits that cover areas extending from north-central Europe to eastern China and are found in the Mississippi Valley and the northwest United States. Their origin is still controversial (*56*), but they are generally believed to be eolian dust of Pleistocene age derived from desert surfaces, from alluvial valleys, or from unconsolidated glacial or glaciofluvial deposits. In an attempt to characterize their source regions, we analyzed loess deposits from Iowa, United States, and Nanking, China. The Iowa loess has $\epsilon_{Nd}(0) = -14.1 \pm 0.5$ and $f_{Sm/Nd} = -0.411$, giving a T^{Nd}_{CHUR} age of 1.38 ± 0.06 AE. From these data, we infer that a major component of material from the older [$\epsilon_{Nd}(0) = -30$, $T^{Nd}_{CHUR} \sim 2.6$ AE] Canadian Shield is prohibited. However, a composite of Paleozoic North American shales (NAS) of Haskin *et al.* (*57*) having $\epsilon_{Nd}(0) = -14.5 \pm 0.5$ and $T^{Nd}_{CHUR} = 1.52 \pm 0.07$ AE (*6*) is almost identical to the Iowa loess. Hence the Paleozoic sediments, or a source similar to the source of Paleozoic sediments, could have provided materials for the Iowa loess. The penultimate source must, of course, be rocks with a mean crustal formation age of ~1.38 AE. Rocks of this approximate age are not widely exposed, although radiometric ages have been obtained (*58*) in the range 1.0 to 1.7 AE from numerous drill core samples of basement from the midcontinental region of the United States. These data suggest that a substantial component of the Paleozoic

NAS composite was probably derived from this Precambrian basement or from recycled materials derived from this basement. If the Nd isotopic composition [$\epsilon_{Nd}(0)$] and $f_{Sm/Nd}$ of NAS is representative of the average from the midcontinental region of the U.S. crust, then the similarity with the Iowa loess suggests that loess deposits may also be good averages of large areas of continental crust. Hence the Nanking loess with $\epsilon_{Nd}(0) = -10.2 \pm 0.4$ and $f_{Sm/Nd} = -0.410$, giving a T^{Nd}_{CHUR} age of 1.00 ± 0.05 AE, may indicate that this part of the Asian continent is on the average approximately 0.40 AE younger than the North American continent. Only relatively moderate enrichments of Rb relative to Sr have occurred during the formation of these loesses, with $f_{Rb/Sr} = 15.3$ for the Iowa loess and 34.3 for the Nanking loess. As a consequence, the T^{Sr}_{UR} ages of 0.71 ± 0.01 AE for the Iowa loess and 0.350 ± 0.005 AE for the Nanking loess are younger than the time of formation of their provenance as given by the T^{Nd}_{CHUR} age and older than their time of deposition (Pleistocene).

Another example of a rock whose provenance is unknown is the Birch Creek Schist of the Alaska Range which, together with the correlated metasediments in the Yukon-Tanana Upland, constitutes a pervasive formation in this area. It is predominantly a quartz-sericite and quartz-sericite-calcite schist, and its metamorphic grade has been established as greenschist facies (*59*). No original sedimentary structures are preserved, the foliation within the formation being due to alignment of sericite flakes and segregations of quartz and sericite. The Rb-Sr and K-Ar age measurements on micas from the polymetamorphosed Birch Creek Schist indicate that it was locally metamorphosed at 0.12 to 0.18 AE (*60*). Total rock Rb-Sr ages from (*60*) range from 0.664 to 1.17 AE, but do not uniquely indicate a Precambrian age, as they are also compatible with a younger period of metamorphism. A sample of the Birch Creek Schist in the Healy D-4 Quad of Alaska has $\epsilon_{Nd}(0) = -27.0 \pm 0.3$ and $f_{Sm/Nd} = -0.464$, giving a T^{Nd}_{CHUR} age of 2.33 ± 0.05 AE. This is definitive evidence that the Birch Creek Schist was derived predominantly from an ancient Precambrian source, which was probably the adjacent older portion of the Canadian Shield with a small component of younger crustal materials. The age of formation of the schist has not been established, although the T^{Sr}_{UR} age of 0.714 ± 0.008 AE is similar to the total rock Rb-Sr ages of Wasserburg *et al.* (*60*) and is suggestive of an early Paleozoic or late Precambrian depositional or metamorphic age for the schist.

"Red" clay is a sedimentary material predominant in the deeper parts of the ocean basis under surface waters of low biological productivity. The source of red clay is still open to dispute, its formation being attributed to eolian or current-transported continental material and to decomposed volcanic ejecta and pyroclastics (*61*). We analyzed a sample of red clay obtained by the Deep Sea Drilling Project (leg V, hole 37, core 3, section 2, 22 to 24 cm, abyssal hill, northeast Pacific Ocean). For this sample $\epsilon_{Nd}(0) = -3.3 \pm 0.4$ and $f_{Sm/Nd} = -0.212$, giving a T^{Nd}_{CHUR} age of 0.63 ± 0.08 AE, which is consistent with the idea that red clay is composed only of continental material with a mean age of 0.63 AE. This is much younger than the mean age of either the North American or the Asian continent as ascertained from the loess and shale results. It may be more reasonable to assume that the red clay consists of a mixture of oceanic basalt with $\epsilon_{Nd}(0) \approx +10$ and $f_{Sm/Nd} \approx 0$ (*7*), island arc volcanics with $\epsilon_{Nd}(0) = +7$ and $f_{Sm/Nd} \approx -0.28$ (*62*), and continental material such as the Iowa loess with $\epsilon_{Nd}(0) = -14.1$ and $f_{Sm/Nd} = -0.411$. For example, the Sm-Nd isotopic characteristics of this red clay could be accounted for by a mixture of approximately equal proportions of oceanic basalt, island arc volcanics, and Iowa loess. However, regardless of the proportions, the Sm-Nd results require a significant component of continental material. The Rb-Sr isotopic characteristics of the red clay [$\epsilon_{Sr}(0) = +53.7$ and $f_{Rb/Sr} = 8.41$] can al-

so be accounted for by similar proportions of oceanic basalt [$\epsilon_{Sr}(0) \approx -25$ and $f_{Rb/Sr} \approx -0.7$] (*3*), island arc volcanics [$\epsilon_{Sr}(0) \approx -15$ and $f_{Rb/Sr} \approx 0.4$] (*62*), and Iowa loess [$\epsilon_{Sr}(0) = +181.1$ and $f_{Rb/Sr} = 15.3$]. This agreement may, however, be fortuitous as the observed $\epsilon_{Sr}(0)$ value of the red clay may also have been produced by exchange of Sr with seawater, which has $\epsilon_{Sr}(0) = +65$.

For all the sediments that we studied, with only one exception (Baja Shale), the T^{Nd}_{CHUR} ages have been greater than the sedimentation age and less than the "age" of the earth (4.47 AE) (*63*). In addition, where known, the ages of crystallization or formation of likely source areas have been consistent with T^{Nd}_{CHUR} ages. This self-consistency is also apparent in the $f_{Sm/Nd}$ values, which are generally within the same range as those estimated for the upper crust (Table 1). This indicates that for the sedimentary rocks that were studied, the assumptions of no fractionation of Sm/Nd and no exchange of Nd since derivation from the CHUR reservoir are plausible. Possible exceptions may be the San Gabriel Sand and the Baja Shale, whose smaller enrichment factors may reflect fractionation of Sm from Nd during the sedimentary process. However, from previous REE distribution studies (*13–15, 57*) it appears more plausible to assume that these variations in Sm/Nd are simply a result of variations of Sm/Nd in the sediment source. In contrast, massive enrichments of Rb relative to Sr of up to a factor of 30 are often found in the sediments compared to their likely sources. As a consequence, the T^{Sr}_{UR} ages usually approach the time of sedimentation or diagenesis and are generally younger than the corresponding T^{Nd}_{CHUR} age. The calculated T^{Nd}_{CHUR} ages are interpreted to be the average ages of formation of the crustal sources from which the sediments were derived. These formation ages also appear to be retained in recycled sediments such as SC-5. Thus, $\epsilon_{Nd}(0)$ and $f_{Sm/Nd}$ parameters are characteristic of the sediment provenance and T^{Nd}_{CHUR} is the provenance age.

Conclusions

The Sm-Nd and Rb-Sr isotopic systematics, together with plausible assumptions regarding the geochemical evolution of continental crustal materials, have been used to ascertain the times at which new segments of continental crust were formed. The general approach that has been used is to assume that the dominant contribution to the continental crust comes from the emplacement of magmatic rocks derived from a uniform mantle reservoir, and that the differentiation processes that produce the magmatic rocks occur with a marked chemical fractionation of the daughter and parent elements relative to the source region. It is the time of this chemical fractionation from the penultimate provenances that has been dated. These times of formation of new crust have been obtained from an extremely diverse range of rocks, including metamorphic and sedimentary rocks and composites of igneous and metamorphic rocks from different structural provinces of the Canadian Shield.

Analyses of composites representing portions of the Superior, Slave, and Churchill structural provinces indicate that these provinces were all formed within the period 2.5 to 2.7 AE. The times of formation of the Superior and Slave provinces are in agreement with previously determined K-Ar and Rb-Sr ages, but the time for formation of the Churchill Province, as represented by

the Baffin Island and Saskatchewan composites, is approximately 0.8 AE greater than the K-Ar age. From our present knowledge of the times of formation of continental crust, it appears that the activity around the period 2.5 to 2.7 AE is unique in geologic history and that some truly major periods of continental growth are sharply episodic. A younger (1.0 AE) age obtained for the Grenville Province indicates the addition at this time of new crust onto the preexisting Canadian Shield.

Studies of sedimentary rocks indicate that the Sm-Nd isotopic systematics are not substantially disturbed during sedimentation or diagenesis, which has made it possible to determine the mean crustal formation age of their provenances. In contrast, Rb-Sr studies of these sediments have shown pronounced enrichments of Rb relative to Sr (up to a factor of 30). Depending on the relative enrichment, the Rb-Sr ages from the sediments are generally more compatible with the time of sedimentation or diagenesis. The Sm-Nd provenance ages have been used to characterize and, in particular cases, to identify the provenance of the sediment. This has enabled old crust that acted as the source for Archean sediments to be identified in the Yilgarn Block of Western Australia and in the Swaziland System from South Africa. The mean age of large areas of the North American and Asian continents has also been ascertained from the provenance ages of loess deposits. As an example of the characterization of sediment provenances by using Sm-Nd systematics, we showed that deep-sea red clay cannot be produced by only oceanic or island arc volcanism but also requires a significant component of continental material. In addition, a sample of widespread metasediment (Birch Creek Schist) from Alaska has a provenance age indicating derivation from the older portion of the Canadian Shield. Determinations of model crustal formation ages on sediments and on composite samples of well-defined lithologies with a broad distribution may prove to be useful as an aid to geologic mapping and to the better definition of geologic provenances.

References and Notes

1. P. M. Hurley, H. Hughes, G. Faure, H. W. Fairbairn, W. H. Pinson, *J. Geophys. Res.* **67**, 5315 (1962); P. M. Hurley and J. R. Rand, *Science* **164**, 1229 (1969).
2. C. Patterson, in *Isotopic and Cosmic Chemistry*, H. Craig, S. L. Miller, G. J. Wasserburg, Eds. (North-Holland, Amsterdam, 1964), pp. 244–268;_____ and M. Tatsumoto, *Geochim. Cosmochim. Acta* **28**, 1 (1964).
3. S. Moorbath, *Chem. Geol.* **20**, 151 (1977).
4. K. E. Eade and W. F. Fahrig, *Bull. Geol. Surv. Can. 179* (1971); *Geol. Surv. Can. Pap. 72-46* (1973).
5. D. M. Shaw, G. A. Reilly, J. R. Muyssen, G. E. Pattendon, F. E. Campbell, *Can. J. Earth Sci.* **4**, 829 (1967).
6. D. J. DePaolo and G. J. Wasserburg, *Geophys. Res. Lett.* **3**, 249 (1976).
7. _____, *ibid.*, p. 743; *Geol. Soc. Am. Abstr. Programs* **8**, 835 (1976).
8. L. T. Aldrich, G. L. Davis, G. R. Tilton, G. W. Wetherill, *J. Geophys. Res.* **61**, 215 (1956); G. W. Wetherill, G. R. Tilton, G. L. Davis, L. T. Aldrich, *Geochim. Cosmochim. Acta* **9**, 292 (1956); W. Compston, P. M. Jeffery, G. H. Riley, *Nature (London)* **186**, 702 (1960); P. W. Gast, *Ann. N.Y. Acad. Sci.* **91**, 181 (1961); H. W. Fairbairn, P. M. Hurley, W. H. Pinson, *Geochim. Cosmochim. Acta* **23**, 135 (1961).
9. G. J. Wasserburg, D. A. Papanastassiou, E. V. Nenow, C. A. Bauman, *Rev. Sci. Instrum.* **40**, 288 (1969); G. P. Russ III, D. S. Burnett, G. J. Wasserburg, *Earth Planet. Sci. Lett.* **15**, 172 (1972).
10. G. W. Lugmair, N. B. Scheinin, K. Marti, *Earth Planet. Sci. Lett.* **27**, 79 (1975); *Proc. 6th Lunar Sci. Conf.* (1975), pp. 1419–1429.
11. R. K. O'Nions, P. J. Hamilton, N. M. Evensen, *Earth Planet Sci. Lett.* **34**, 13 (1977); P. J. Hamilton, R. K. O'Nions, N. M. Evenson, *ibid.* **36**, 263 (1977)
12. P. Richard, N. Shimizu, C. J. Allegre, *ibid.* **31**, 269 (1976).
13. L. A. Haskin, F. A. Frey, R. A. Schmitt, R. H. Smith, *Phys. Chem. Earth* **7**, 167 (1966).
14. S. R. Taylor, *Geochim. Cosmochim. Acta* **28**, 1273 (1964); *ibid.*, p. 1989.
15. A. B. Ronov, Y. A. Balashov, Y. P. Girin, R. K. Bratishko, G. A. Kazakov, *Geochem. Int.* **9** (No. 6), 987 (1972).
16. D. M. Shaw, J. Dostal, R. R. Keays, *Geochim. Cosmochim. Acta* **40**, 73 (1976).
17. T. H. Green, A. O. Brunfelt, K. S. Heier, *Earth Planet. Sci. Lett.* **7**, 93 (1969).
18. G. W. Wetherill, G. L. Davis, G. R. Tilton, *J. Geophys. Res.* **65**, 2461 (1960); G. J. Wasserburg and M. A. Lanphere, *Geol. Soc. Am. Bull.* **76**, 735 (1965).
19. J. A. Grant, *Science* **146**, 1049 (1964).
20. W. Compston and R. T. Pidgeon, *J. Geophys. Res.* **67**, 3493 (1962); P. R. Whitney and P. M. Hurley, *Geochim. Cosmochim. Acta* **28**, 425 (1964).
21. H. L. Allsopp, T. J. Ulrych, L. O. Nicolaysen, *Can. J. Earth Sci.* **5**, 605 (1968).
22. D. Gebauer and M. Grünenfelder, *Contrib. Mineral. Petrol.* **47**, 113 (1974).
23. D. A. Papanastassiou and G. J. Wasserburg, *Earth Planet. Sci. Lett.* **17**, 324 (1973).
24. D. A. Papanastassiou, D. J. DePaolo, G. J. Wasserburg, *Proc. 8th Lunar Sci. Conf.* (1977), pp. 1639–1672.
25. P. W. Gast, L. J. Kulp, L. E. Long, *Trans. Am. Geophys. Union* **39**, 322 (1958); J. A. Lowdon, *Geol. Surv. Can. Pap. 61-17* (1961); S. S. Goldich, A. O. Nier, H. Baadsgaard, J. H. Hoffman, H. W. Krueger, *Minn. Geol. Surv. Bull. 41* (1961); R. H. Steiger and G. J. Wasserburg, *Geochim. Cosmochim. Acta* **33**, 1203 (1969); S. R. Hart and C. Brooks, *Contrib. Mineral. Petrol.* **61**, 109 (1977).
26. C. H. Stockwell, *Geol. Surv. Can. Pap. 64-17* (1964); J. A. Lowdon, *Geol. Surv. Can. Dep. Mines Tech. Surv. Rep. 63-17* (1963).
27. D. C. Green, H. Baadsgaard, G. L. Cumming, *Can. J. Earth Sci.* **5**, 725 (1968).

28. R. Doig, *Geol. Soc. Am. Bull.* **88**, 1843 (1977); T. E. Krogh and P. M. Hurley, *J. Geophys. Res.* **73**, 7107 (1968).
29. L. C. Coleman, *Can. J. Earth Sci.* **7**, 338 (1970).
30. R. W. Hurst, D. Bridgwater, K. D. Collerson, G. W. Wetherill, *Earth Planet. Sci. Lett.* **27**, 393 (1975).
31. E. J. Catanzaro, *J. Geophys. Res.* **68**, 2045 (1963).
32. S. S. Goldich, C. E. Hedge, T. W. Stern, *Geol. Soc. Am. Bull.* **81**, 3671 (1970); S. S. Goldich and C. E. Hedge, *Nature (London)* **252**, 467 (1974); J. S. Farhat and G. W. Wetherill, *ibid.* **257**, 721 (1975).
33. R. T. Pidgeon, *Earth Planet. Sci. Lett.* **37**, 421 (1978).
34. V. R. McGregor, *Philos. Trans. R. Soc. Lond. Ser. A* **273**, 343 (1973); S. Moorbath, R. K. O'Nions, R. J. Pankhurst, N. H. Gale, V. R. McGregor, *Nature (London) Phys. Sci.* **240**, 78 (1972); H. Baadsgaard, *Earth Planet. Sci. Lett.* **19**, 22 (1973).
35. B. Jahn and C. Shih, *Geochim. Cosmochim. Acta* **38**, 873 (1974).
36. K. O. Kratz, E. K. Gerling, S. B. Lobach-Zhuchenko, *Can. J. Earth Sci.* **5**, 657 (1968).
37. N. P. Semenko, A. P. Shcherbak, A. P. Vinogradov, A. I. Tugarinov, G. D. Eliseeva, F. I. Kotlovskaya, S. G. Demidenko, *ibid.*, p. 661.
38. K. S. Heier, *Nature (London)* **202**, 477 (1964); *Philos. Trans. R. Soc. London Ser. A* **273**, 429 (1973).
39. R. E. Zartman and G. J. Wasserburg, *Geochim. Cosmochim. Acta* **33**, 901 (1969).
40. S. R. Taylor, in *Island Arcs. Deep Sea Trenches and Back-Arc Basins*, M. Talwani and W. C. Pitmann, III, Eds. (American Geophysical Union, Washington, D.C., 1977), pp. 325–335.
41. K. E. Eade, W. F. Fahrig, J. A. Maxwell, *Nature (London)* **211**, 1245 (1966).
42. R. M. Garrels and F. T. Mackenzie, *Evolution of Sedimentary Rocks* (Norton, New York, 1971).
43. T. J. Chow and C. C. Patterson, *Geochim. Cosmochim. Acta* **26**, 263 (1962); M. Tatsumoto and C. Patterson, *J. Geol.* **72**, 232 (1964); E. J. Dasch, *Geochim. Cosmochim. Acta* **33**, 1521 (1969); P. D. Boger and G. Faure, *Geology* **2**, 181 (1974); N. R. Shaffer and G. Faure, *Geol. Soc. Am. Bull.* **87**, 1491 (1976); Z. E. Peterman, C. E. Hedge, R. B. Coleman, P. D. Snavely, *Earth Planet. Sci. Lett.* **2**, 433 (1967).
44. V. M. Goldschmidt, in *Geochemistry*, A. Muir, Ed. (Clarendon, Oxford, 1954), pp. 167–169; E. A. Perry and K. K. Turekian, *Geochim. Cosmochim. Acta* **38**, 929 (1974); G. W. Brass, *ibid.* **39**, 1647 (1975).
45. S. S. Goldich, *J. Geol.* **46**, 17 (1938).
46. _____ and P. W. Gast, *Earth Planet. Sci. Lett.* **1**, 372 (1966).
47. T. W. Stern, S. S. Goldich, M. F. Newell, *ibid.*, p. 369.
48. L. T. Silver, C. R. McKinney, S. Deutsch, J. Bolinger, *J. Geol.* **71**, 196 (1963).
49. L. T. Silver, *Geol. Soc. Am. Abstr. Programs* **3**, 193 (1971).
50. W. B. Nance and S. R. Taylor, *Geochim. Cosmochim. Acta* **40**, 1539 (1976); *ibid.* **41**, 225 (1977).
51. V. M. Bofinger, W. Compston, B. L. Gulson, *ibid.* **34**, 433 (1970).
52. W. Compston and P. A. Arriens, *Can. J. Earth Sci.* **5**, 561 (1968).
53. J. R. Richards, J. A. Cooper, A. W. Webb, *J. Geol. Soc. Aust.* **10**, 299 (1963); R. B. Farquharson and J. R. Richards, *Chem. Geol.* **16**, 73 (1975).
54. R. W. Page, personal communication.
55. V. M. Oversby, *Geochim. Cosmochim. Acta* **39**, 1107 (1975).
56. P. Marosi, in *Loess Lithology and Genesis* (Benchmark Papers in Geology 26), I. J. Smalley, Ed. (Dowden, Hutchinson & Ross, Stroudsburg, Pa., 1975), pp. 402–408; I. J. Smalley, in *ibid.*, pp. 362–370.
57. L. A. Haskin, T. R. Wildeman, F. A. Frey, K. A. Collins, C. R. Reedy, M. A. Haskin, *J. Geophys. Res.* **71**, 6091 (1966).
58. S. S. Goldich, W. R. Muehlberger, E. G. Lidiak, C. E. Hedge, *ibid.*, p. 5375; G. J. Wasserburg, G. W. Wetherill, L. T. Silver, P. T. Flawn, *ibid.* **67**, 4021 (1962).
59. C. Wahrhaftig, *U.S. Geol. Surv. Bull. 1254-E* (1968), pp. E1–E22.
60. G. J. Wasserburg, G. D. Eberlein, M. A. Lanphere, *Geol. Soc. Am. Spec. Pap.* **73**, 258 (abstr.) (1963).
61. P. Biscaye, *Geol. Soc. Am. Bull.* **76**, 803 (1965); J. J. Griffin, H. Windom, E. D. Goldgerg, *Deep-Sea Res.* **15**, 433 (1968); R. A. Copeland, F. A. Frey, D. R. Wones, *Earth Planet. Sci. Lett.* **10**, 186 (1971).
62. D. J. DePaolo and G. J. Wasserburg, *Geophys. Res. Lett.* **4**, 465 (1977).
63. C. C. Patterson, *Geochim. Cosmochim. Acta* **10**, 230 (1956); A. J. Gancarz and G. J. Wasserburg, *ibid.* **41**, 1283 (1977).
64. H. C. Urey, *Q. J. R. Astron. Soc.* **8**, 23 (1967).

65. This article is dedicated to the late A. I. Tugarinov. Many of us have benefited from his scholarship in crustal evolution and geochemistry and from his enthusiasm for science. We are grateful to D. M. Shaw, McMaster University, Hamilton, Ontario, and to W. F. Fahrig, Geological Survey of Canada, for providing us with the important composite samples from the Canadian Shield. S. S. Goldich, G. D. Eberlein, L. A. Haskin, H. A. Lowenstam, and L. T. Silver kindly provided samples of the metamorphic and sedimentary rocks. The sample of the deep-sea red clay was obtained through the courtesy of the Scripps Institution of Oceanography. M.T.M. also thanks D. J. DePaolo for assistance and advice. S. B. Jacobsen, D. J. DePaolo, and the reviewers provided constructive criticism of the manuscript. Special thanks to S. R. Taylor for providing sediments with the same provenance as one of us (M.T.M.). Results of this work were presented at the AIGC-Unesco Second Symposium on the Origin and Distribution of the Elements, held in Paris, 1977. This work has been supported by NSF grant PHY76-83685 and NASA grant NGL05-002-188. This is contribution No. 2975 of the Division of Geological and Planetary Sciences of the California Institute of Technology.

Table 4. Trace element concentrations

Sample	Rb	Sr	Sm	Nd
Canadian Shield Composites				
New Quebec	101	408	2.93	16.5
North Quebec	101	396	4.45	25.9
Fort Enterprise Gneiss	67	242	4.22	21.0
Fort Enterprise Granite	81.7	310	5.55	34.4
Baffin Island	133	231	7.20	42.5
Saskatchewan	104	239	4.48	27.2
Quebec	105	333	6.83	33.4
Sedimentary Rocks				
Baja Shale	69.2	42.1	3.94	15.9
San Gabriel Sand	133	741	6.17	24.3
Figtree Shale	17.3	6.46	2.37	10.8
Iowa Loess	77.0	162	6.78	36.0
Nanking Loess	108	104	6.66	35.2
NAS	47.0	51.9	5.7	31.0
Birch Creek Schist	65.7	32.3	4.06	23.7
Deep Sea Red Clay	16.0	57.8	6.01	24.0
SC-5	198	23.0	7.01	39.3
AO-7	196	91.9	5.85	32.3
MI-1	185	23.4	4.31	24.7
KH44	49.8	88.3	3.14	15.6
Weathered Morton Gneiss				
LOC 3	132	38.1	7.85	51.3
LOC 5	71.8	35.1	16.2	102

APPENDIX 2

Sm-Nd MODEL AGES FROM AN EARLY ARCHEAN TONALITIC GNEISS, NORTHERN MICHIGAN

M.T. McCulloch and G.J. Wasserburg

Lunatic Asylum, Division of Geological and Planetary Sciences
California Institute of Technology
Pasadena, California 91125

Division Contribution No. 3175 (283)

ABSTRACT

Sm-Nd model ages on a whole rock sample of the gneiss at Watersmeet, Michigan, show that these rocks were added to the continental crust about 3600 m.y. ago. These model ages are calculated assuming that the rocks were derived from a mantle reservoir with the Sm/Nd of CHUR which corresponds approximately to the chondritic ratio. These data confirm the U-Th-Pb zircon results of Peterman and others (this volume) which indicated a minimum age of 3410 m.y. and possibly an age of up to 3,800 m.y. This study further illustrates the utility of Sm-Nd model ages in deciphering the history of complex Precambrian terranes.

INTRODUCTION

Peterman and others (this volume) have reported an age based on U-Th-Pb zircon systematics of greater than 3,400 m.y. for a tonalitic gneiss in the Marenisco-Watersmeet area of northern Michigan. In an attempt to confirm this important observation we have determined Sm-Nd model ages on a total rock sample of the gneiss at Watersmeet. Although dependent on the validity of the model assumptions, the Sm-Nd model ages are consistent with the early Archean ages of Peterman and others. This study further illustrates the ability of the Sm-Nd system to obtain primary crustal formation ages, despite the complex history which these rocks have undergone. The utility of this approach should enable formation ages to be determined from other rocks produced during early crustal formation events.

ANALYTICAL PROCEDURE AND RESULTS

A 4 Kg sample of the tonalitic augen gneiss from Watersmeet was provided to us by Z. Peterman, R. Zartman, and P. Sims. The plagioclase-quartz-biotite gneiss has a groundmass grain size of $\sim$ 2 mm with larger 1-2 cm plagioclase porphyroblasts. The sample was pulverized and ground to pass 100 mesh and splits taken. Splits of 0.5 g and 2.5 g were dissolved and totally spiked using ^{147}Sm and ^{150}Nd tracers. Sm and Nd concentrations and $^{143}Nd/^{144}Nd$ isotopic ratios were determined from these solutions using procedures described by Papanastassiou and others (1977). A small difference in the Sm and Nd concentrations is present between the two splits. Although this small difference does not seriously affect the T^{Nd}_{CHUR} age, it does show the difficulty in obtaining representative whole rock samples from polymetamorphic rocks where isotopic redistribution

has probably occurred between mineral phases.

Sm-Nd data for a sample from locality D1042 (see Peterman and others, this volume) are given in Table 1. The model ages from two splits of the same sample are 3620±30 m.y. and 3570±50 m.y. which are the same within analytical error.

DISCUSSION

The Sm-Nd model age (T^{Nd}_{CHUR}) is the time in the past when the major REE fractionation in a rock occurs during its derivation from a mantle reservoir. This is shown schematically in Figure 1 where the $^{143}Nd/^{144}Nd$ evolves as a function of time in the mantle reservoir ($I_{CHUR}(T)$) from 4.5 AE until time T^{Nd}_{CHUR}. At this time (3.6 AE) the magma with a light REE enrichment is derived from the mantle reservoir. This light REE enrichment produces a lower Sm/Nd ratio and the subsequent evolution of $^{143}Nd/^{144}Nd$ in the rock is retarded relative to the mantle reservoir. The T^{Nd}_{CHUR} age is then the intersection of the rock evolution and mantle evolution curves and is given by

$$T^{Nd}_{CHUR} = \frac{1}{\lambda} \ln \left[1 + \frac{\varepsilon_{Nd}(0)\ I_{CHUR}(0) \times 10^{-4}}{f_{Sm/Nd}\ (^{147}Sm/^{144}Nd)_{CHUR}} \right]$$

where

$$f_{Sm/Nd} = \left[\frac{(^{147}Sm/^{144}Nd)_{meas}}{(^{147}Sm/^{144}Nd)_{CHUR}} - 1 \right]$$

and

$$\varepsilon_{Nd}(0) = \left[\frac{(^{143}Nd/^{144}Nd)_{meas}}{I_{CHUR}(0)} - 1 \right] \times 10^4 \quad .$$

$\left(\frac{^{143}Nd}{^{144}Nd}\right)_{meas}$ and $\left(\frac{^{147}Sm}{^{144}Nd}\right)_{meas}$ are the ratios measured in the rock. The mantle reservoir (CHUR) has a Sm/Nd ratio of $\left(\frac{^{147}Sm}{^{144}Nd}\right)_{CHUR} = 0.1936$ and $^{143}Nd/^{144}Nd$ ratio today of $I^{Nd}_{CHUR}(0) = 0.511836$. The evolution of $^{143}Nd/^{144}Nd$ and of Sm/Nd in the mantle reservoir were first described by DePaolo and Wasserburg (1976). The model age arguments presented here are directly dependent on the validity of the mantle reservoir characteristic which they outlined and which have been further substantiated in Archean rocks by Hamilton and others (1977, 1978). A detailed discussion of Sm-Nd model ages from a wide variety of crustal rock types is given by McCulloch and Wasserburg (1978) and Jacobsen and Wasserburg (1978).

In Table 2 the Sm-Nd parameters from the gneiss at Watersmeet are compared with the Amitsoq Gneiss (DePaolo and Wasserburg, 1976) and a composite sample (New Quebec) from the Superior Province of the Canadian Shield (McCulloch and Wasserburg, 1978). The Canadian shield composite, which represents a large segment of the Superior Province has a light REE enrichment ($f_{Sm/Nd} < 0$) and a negative $\varepsilon_{Nd}(0)$ value. These characteristics are even more evident in the older 3600 m.y. Amitsoq Gneiss and the gneiss at Watersmeet. The $\varepsilon_{Nd}(0) = -55$ from the gneiss at Watersmeet is the most primitive $^{143}Nd/^{144}Nd$ so far reported. For comparison, a sample which has been Sm free during the earth's history would today have an $\varepsilon_{Nd}(0) = -114$. Thus, even without correction for ^{147}Sm decay the primitive $^{143}Nd/^{144}Nd$ ratio in

the gneiss shows unequivocally that this is a very ancient rock.

In a manner analogous to that discussed for Sm and Nd, Rb-Sr model ages (T_{UR}^{Sr}) can also be calculated (see McCulloch and Wasserburg, 1978). Using the data from Peterman and others (this volume), the T_{UR}^{Sr} model ages from the gneiss at Watersmeet range from 2090 m.y. to an impossible 6130 m.y. For the sample studied, T_{UR}^{Sr} = 3160 m.y., which is distinctly younger than the T_{CHUR}^{Nd} age. This difference is probably due to redistribution of Rb and Sr at younger times, as indicated by the wide range in T_{UR}^{Sr} ages.

The gneiss at Watersmeet has had a complex history and shows evidence of cataclasis and recrystallization (Sims and Peterman, 1976). As shown by Peterman and others (this volume), this later metamorphism has resulted in highly disturbed Rb-Sr and complexly discordant U-Th-Pb zircon systems. Despite the intensive study by these workers, a definitive primary age of the gneiss at Watersmeet could not be established, although a minimum age of 3410 m.y. was clearly indicated from the zircon study. In contrast, the Sm-Nd model age appears to indicate that the whole rock Sm-Nd system has remained closed since 3,600 m.y. This is probably due to the geochemical coherence and relative immobility of the REE elements. As already pointed out, this age is dependent on model assumptions. However, a relatively large deviation in the initial $^{143}Nd/^{144}Nd$ of 1 part in 10^4 would produce an error of only 70 m.y.

The presence of 3600 m.y. crust in western Greenland, Labrador, Minnesota (Moorbath and others, 1972; Baadsgaard, 1973; Barton, 1975; Hurst and others, 1975; Catanzaro, 1963; Goldich and others, 1970; and Goldich and Hedge, 1974), and now in northern Michigan suggests that this

may be a period of major and widespread crustal formation. Although this event is relatively poorly documented compared to the younger 2600 m.y. - 2800 m.y. event, the application of Sm-Nd model ages may enable identification of other rocks of this age, even in complex polymetamorphic terranes.

ACKNOWLEDGMENTS

We thank R. Zartman, Z. Peterman, and P. Sims for the sample of the gneiss at Watersmeet from northern Michigan. Their endeavors provided the impetus for this study. This study was supported by NSF Grant PHY 76-02724 and NGL 05-002-188.

REFERENCES CITED

Baadsgaard, H., 1973, U-Th-Pb dates on zircons from the early Precambrian Amitsoq Gneisses, Godthaab district, West Greenland: Earth and Planetary Science Letters, v. 19, p. 22-28.

Barton, J. M., Jr., 1975, Rb-Sr isotopic characteristics and chemistry of the 3.6 b.y. Hebron Gneiss, Labrador: Earth and Planetary Science Letters, v. 27, p. 427-435.

Catanzaro, E. J., 1963, Zircon ages in Southwestern Minnesota: Journal of Geophysical Research, v. 68, p. 2045-2049.

DePaolo, D. J., and Wasserburg, G. J., 1976, Nd isotopic variations and petrogenetic models: Geophysical Research Letters, v. 3, p. 249-254.

Goldich, S. S., Hedge, C. E., and Stern, T. W., 1970, Age of Morton and Montevideo Gneisses and related rocks, southwestern Minnesota: Geological Society of America Bulletin, v. 81, p. 3671-3696.

Goldich, S. S., and Hedge, C. E., 1974, 3,800 Myr granitic gneiss in southwestern Minnesota: Nature, v. 252, p. 467-468.

Hamilton, P. J., O'Nions, R. K., and Evensen, N. M., 1977, Sm-Nd dating of Archean basic and ultrabasic volcanics: Earth and Planetary Science Letters, v. 36, p. 263-268.

Hamilton, P. J., O'Nions, R. K., and Evensen, N. M., 1978, Sm-Nd isotopic investigations of Isua supracrustals and implications for mantle evolution: Nature, v. 272, p. 41-43.

Hurst, R. W., Bridgwater, D., Collerson, K. D., and Wetherill, G. W., 1975, 3600 m.y. Rb-Sr ages from very early Archean gneisses from Saglek Bay, Labrador: Earth and Planetary Science Letters, v. 27, p. 393-403.

Jacobsen, S. B. and Wasserburg, G. J., 1978, Interpretation of Nd, Sr and Pb isotope data from Archean migmatites in Lofoten-Vesterålen, Norway: Earth and Planetary Science Letters, v. 41, p. 245-253.

McCulloch, M. T. and Wasserburg, G. J., 1978, Sm-Nd and Rb-Sr chronology of continental crust formation: Science, v. 200, p. 1003-1011.

Moorbath, S., O'Nions, R. K., Pankhurst, R. J., and Gale, N. H., 1972, Further rubidium-strontium age determinations on the very early precambrian rocks of the Godthaab district, west Greenland: Nature Physical Science, v. 240, p. 78-82.

Papanastassiou, D. A., DePaolo, D. J., and Wasserburg, G. J. 1977, Rb-Sr and Sm-Nd chronology and genealogy of mare basalts from the sea of tranquility: Proceedings of the Eighth Lunar and Planetary Science Conference, v. 1, p. 1639-1672.

Peterman, Z. E., and Zartman, R. E., and Sims,P. K., 1978, Tonalitic gneiss of early Archean age from northern Michigan: This volume.

Sims, P. K., and Peterman, Z. E., 1976, Geology and Rb-Sr ages of reactivated gneisses and granite in the Marenisco-Watersmeet area, northern Michigan: U.S. Geological Survey Journal of Research, v. 4, p. 405-414.

TABLE 1. Sm-Nd DATA FOR THE GNEISS AT WATERSMEET

Sample	Weight g.	Sm (ppm)	Nd (ppm)	$\frac{^{147}Sm}{^{144}Nd}$	$\frac{^{143}Nd}{^{144}Nd}$	$T^{Nd}_{CHUR\ AE}$
D1042 Split a	2.56	5.05	41.38	0.07383	0.509011±37	3.57±0.05
D1042 Split b	0.54	5.11	40.50	0.07632	0.509027±22	3.62±0.03

TABLE 2. Sm-Nd EVOLUTIONARY PARAMETERS

Sample	$\varepsilon_{Nd}(0)$	$f_{Sm/Nd}$	$T^{Nd}_{CHUR\ AE}$
Watersmeet Gneiss*	-55.0±0.5	-0.612	3.60±0.04
Amitsoq Gneiss†	-35.4±0.6	-0.390	3.62±0.09
New Quebec Comp.§	-29.4±0.3	-0.444	2.66±0.06

* *Average from Table 1.*

† *DePaolo and Wasserburg (1976).*

§ *McCulloch and Wasserburg (1978).*

Figure 1. Evolution of $^{143}Nd/^{144}Nd$ in the gneiss at Watersmeet (to scale). The T^{Nd}_{CHUR} age is given by the intersection of the sample evolution line with that in the mantle reservoir (CHUR).

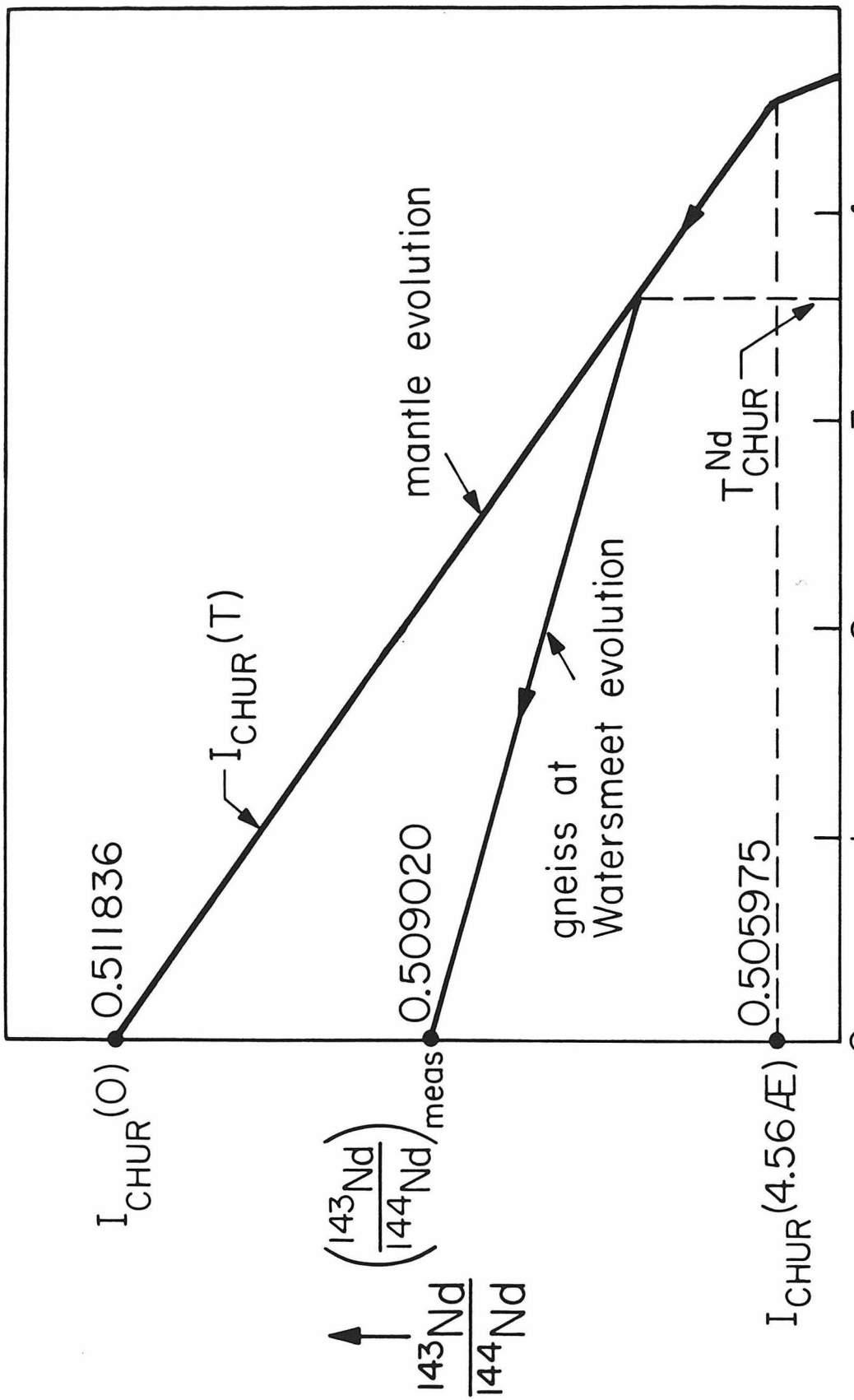
0.511836
$I_{CHUR}(T)$
mantle evolution
0.509020
gneiss at
Watersmeet evolution
T^{Nd}_{CHUR}
0.505975
$I_{CHUR}(0)$
$\left(\frac{^{143}Nd}{^{144}Nd}\right)_{meas}$
$\frac{^{143}Nd}{^{144}Nd}$
$I_{CHUR}(4.56 Æ)$
0
1
2
3
4
T AGE (Æ)

Fig. 1

APPENDIX 3

Sm-Nd, Rb-Sr, AND $^{18}O/^{16}O$ ISOTOPIC SYSTEMATICS IN AN OCEANIC CRUSTAL SECTION: EVIDENCE FROM THE SEMAIL OPHIOLITE

Malcolm T. McCulloch, Robert T. Gregory,
G. J. Wasserburg, and Hugh P. Taylor, Jr.

Division of Geological and Planetary Sciences
California Institute of Technology
Pasadena, California 91125

Division Contribution No. 3303 (317)

Abstract

Using Sm-Nd, Rb-Sr, and $^{18}O/^{16}O$ isotopic systems, it has been possible to distinguish between the effects of sea floor hydrothermal alteration and primary magmatic isotopic variations. The Sm-Nd isotopic system is essentially unaffected by seawater alteration while the Rb-Sr and $^{18}O/^{16}O$ systems are sensitive to hydrothermal interactions with seawater. Sm-Nd mineral isochrons from the cumulate gabbros of the Semail ophiolite have an initial $^{143}Nd/^{144}Nd$ ratio of $\varepsilon_{Nd} = 7.8\pm0.3$, which clearly substantiates the oceanic affinity of this complex. The initial $^{143}Nd/^{144}Nd$ ratios for the harzburgite, plagiogranite, sheeted diabase dikes, and basalt units have a limited range in ε_{Nd} of from 7.5 to 8.6, indicating that all the lithologies have distinctive oceanic affinities although there is also some evidence for small isotopic heterogeneities in the magma reservoirs. The Sm-Nd mineral isochrons give crystallization ages of 130±12 m.y. from Ibra and 100±20 m.y. from Wadi Fizz which is approximately 300 km N.W. of Ibra. These crystallization ages are interpreted as the time of formation of the oceanic crust and are older than the geologically inferred emplacement age of 65-80 m.y. This indicates that mature oceanic crust was obducted. The $^{87}Sr/^{86}Sr$ initial ratios on the same rocks has an extremely large range of from 0.7030 to 0.7065 and the $\delta^{18}O$ values vary from 2.6 to 12.9. These large variations clearly demonstrate hydrothermal interaction of oceanic crust with seawater.

1.0 Introduction

The purpose of this study is to compare and contrast the neodymium, strontium, and oxygen isotopic characteristics of the Semail ophiolite. This ophiolite consists of (from bottom to top) tectonized peridotite (dominantly harzburgite), layered gabbro, sheeted dikes, pillow basalts, and pelagic sediments. These rocks are of significance as it is now generally recognized that ophiolites represent allochthonous fragments of oceanic crust and upper mantle that were emplaced upon continental margins [1-5] and therefore provide a unique opportunity to study in detail an exposed cross section of oceanic crust.

Studies of oceanic crustal rocks are extremely important because of their volumetric extent and the fact that a large proportion of the oceanic crust has been recycled into the mantle at subduction zones. This recycling of oceanic crust probably had profound effects on the evolution of the upper mantle and the composition of island arc and active continental margins which are overriding subduction zones. In addition, during the course of geologic time the isotopic composition of oxygen and strontium in seawater has also been strongly affected by hydrothermal interaction with the oceanic crust [6-9].

Many previous studies of oceanic crust have relied on rocks collected directly from the ocean floor either by dredging or drilling. These methods are not ideal due to the lack of stratigraphic control during dredging and the difficulty of drilling into igneous rocks. An alternative approach is to study oceanic crust preserved in ophiolite complexes. The Semail ophiolite, Sultanate of Oman, was chosen for this study because as described by Coleman [10] "it is perhaps the largest (30,000 km^3) and the best exposed section of ancient oceanic crust

within the world." In addition the Semail ophiolite is also one of the best preserved and its thickness compares favorably [10] to geophysical estimates of "typical" oceanic crustal thickness [11]. It is therefore possible to sample an essentially complete stratigraphic section of "typical" oceanic crust and also to contrast variations within a single tectonic unit over a large distance ($\sim$ 300 km).

In this study we have examined the Nd, Sr, and O isotopic characteristics from identical samples of harzburgites, gabbros, plagiogranites, sheeted dikes, and basalt units. The $^{18}O/^{16}O$ and Rb-Sr isotopic systems are sensitive to hydrothermal interaction with seawater [14-25] and therefore provide an opportunity to study the nature and extent of hydrothermal exchange of seawater with the oceanic crust on these two systems. Using $\delta^{18}O$ variations as criteria, samples were selected which showed no measurable effects of hydrothermal exchange, as well as samples in which the $\delta^{18}O$ indicated varying amounts of both high and low temperature exchange. In addition, by analyzing both fresh and altered samples as identified from the oxygen and Sr data we could then test for the degree of disturbance of seawater contamination on the Sm-Nd system. We will show that the Sm-Nd system is apparently unaffected by hydrothermal seawater interaction, and therefore we have been able to obtain crystallization ages and initial $^{143}Nd/^{144}Nd$ ratios from these units. The ability to determine crystallization ages from ophiolitic rocks using Sm-Nd has many potential applications as most ophiolitic material is unsuitable or only marginally suitable for isotopic age determinations by conventional techniques. This is due to the low K and Rb concentrations and to deformation and metamorphism

that is usually associated with their formation at ocean ridges and later during their tectonic emplacement upon continental margins. A possible exception is the dating by U-Pb of zircons sometimes found in the more siliceous but relatively rare members of an ophiolite suite such as plagiogranites and high level hornblende gabbros [12,13]. In contrast, Sm-Nd ages can in principle be obtained from the major minerals plagioclase (low Sm/Nd) and clinopyroxene (high Sm/Nd) which are common constituents of all the gabbros, diabases, and basalts. The determination of the time of ophiolite formation (crystallization) together with the time of ophiolite emplacement is important in our understanding of the time/space relationships between the ophiolite and its tectonic environment.

The initial $^{143}Nd/^{144}Nd$ ratios can also provide valuable constraints on the primary petrogenetic relationships among different lithologic units. This is particularly useful, as other criteria, such as those based on major and trace elements, are not always applicable due to modification by seawater. This problem has been particularly severe in highly tectonized units such as the harzburgites which have been subject to serpentinization and major changes in their trace element concentrations.

Isotopic studies of a few other ophiolite complexes have been reported [18-20, 22-27] with the Troodos massif of Cyprus at present being one of the better documented examples. $^{18}O/^{16}O$ [18, 22], $^{87}Sr/^{86}Sr$ [17, 19, 20] and trace and major element studies [26, 30, 33] have confirmed its similarity to oceanic crust and identified the effects of seawater circulation in the pillow basalts, sheeted dikes, and uppermost gabbro complexes. The seawater has also to a large degree

altered the primary $^{87}Sr/^{86}Sr$ ratios [17,19,20] and it has therefore not been possible to infer genetic relations between the different units within the complex using Sr isotopic data. A preliminary Nd isotopic study by Richard et al. [34] of single whole-rock gabbro samples from the Troodos, Semail, and several other ophiolite complexes has shown that the measured $^{143}Nd/^{144}Nd$ ratios are similar to those found in young ocean floor basalts [35-38].

Previous studies of the Semail ophiolite and its surrounding complex have been summarized by Coleman [10] and important contributions include papers by Reinhardt [39], Allemann and Peters [40], and Glennie [41,42]. Currently, detailed and systematic geological, geochemical, and geophysical studies in the southeastern Oman mountains are being undertaken by a group led by C. Hopson and R. Coleman. The samples analyzed in this study were collected as part of this cooperative study, and mainly come from one of the standard ophiolite sections near Ibra, southeastern Oman (see Fig. 1). Samples collected from the same outcrops are currently being studied by other collaborators.

2.0 Geology and Sampling

The Semail ophiolite forms a major part of the 700 km long arcuate Oman Mountains which are on the eastern edge of the Arabian Peninsula (Fig. 1). A detailed geologic map of the Ibra section in southeastern Oman has been prepared by Bailey, Hopson, Coleman, Pallister, and Gregory [43]. A suite of samples representing the different lithologic units in the Ibra section were chosen on the basis of their oxygen isotopic properties as described by Gregory and Taylor [44,45]. In addition, two cumulate gabbro samples (OM251 and OM28) from the Rustac

and Wadi Fizz localities (Fig. 1) were also analyzed to check for regional isotopic and age variations within similar lithologies of the ophiolite on a scale of several hundred kilometers.

A minimum age for the emplacement of the ophiolite is provided by Maestrichtian-Tertiary shallow-water limestones which unconformably overlies parts of the ophiolite. A maximum age is given by Campanian sediments which underlie the ophiolite [42]. These constraints are consistent with K-Ar ages of 83±5 m.y. reported by Allemann and Peters [40] from metamorphic biotites in amphibolites from the contact aureole at base of the Semail thrust sheet. Until now, evidence for the age of production of the oceanic crust is sparse, although Glennie and others [42] estimated a minimum age limit based on middle to late Cretaceous sediments which overlie the pillow lavas in northern Oman.

2.1 Sample Descriptions

The stratigraphic locality of the Ibra samples is shown in Fig. 12.

Basalt G54 (Ibra): Microphyric basalt with acicular laths of plagioclase (An25). Groundmass is altered to palagonite, zeolites, saponite, and calcite. The calcite is present as 1-2 cm amygdules and also as smaller blebs dispersed throughout the rock. A whole rock sample which was free of large amygdules and an amygdule were analyzed. The mineralogy and oxygen isotope data (whole rock $\delta^{18}O = 12.9$) are consistent with low temperature alteration (100°C-200°C).

Diabase Dike G10 (Ibra): Ophitic texture with turbid albitized plagioclase (An20). Alteration products include epidote and chlorite and actinolite-tremolite pseudomorphs after pyroxene, quartz, carbonate, and leucoxene. The mineralogy indicates alteration in the green schist facies.

Diabase Dike K1 (Ibra): Ophitic texture with turbid plagioclase

(An25), clinopyroxene and opaques. Alteration products include chlorite, actinolite, uralite, and quartz, and suggest an alteration at greenschist facies.

Plagiogranite G224-3 (Ibra): Granophyric texture with zoned plagioclase (core An30, rim An27), hornblende, quartz, magnetite, and trace amounts of apatite. Hornblende is partially altered to chlorite. The plagiogranite was collected from a non-chilled dike which cross-cuts uralite gabbro G224-2 approximately 500 meters below the gabbro-diabase contact.

Uralite Gabbro G224-2 (Ibra): Poikalitic hornblende enclosing zoned plagioclase (core An40, rim An20) and opaques. Alteration products include rare prehnite, chlorite, and fibrous amphibole pseudomorphs after hornblende. The mineralogy and oxygen isotope data (whole rock $\delta^{18}O = 3.7$, plagioclase $\delta^{18}O = 4.5$, and $\delta^{18}O$ uralite = 2.6) suggest relatively high temperatures of alteration ($> 400°$ C).

Gabbro K9 (Ibra): Adcumulate with igneous lamination; 72% plagioclase (An75), 20% clinopyroxene, 7% olivine, and 1% hornblende. The brown hornblende is a minor alteration product of the clinopyroxene. The mineralogy and oxygen isotope data (whole rock $\delta^{18}O = 5.8$, plagioclase $\delta^{18}O = 60$, and clinopyroxene $\delta^{18}O = 5.3$) indicate that this is one of the least altered samples.

Gabbro OM251 (Wadi Fizz, northern Oman): Late cumulate pyroxene poikalitically enclosing plagioclase; 77% plagioclase (An80), 25% clinopyroxene, and 3% olivine. The olivine has been partially serpentinized. Although the olivine is serpentinized, the oxygen data (plagioclase $\delta^{18}O = 6.4$ and clinopyroxene $\delta^{18}O = 5.8$) indicate that the plagioclase and clinopyroxene have exchanged only slightly with an ^{18}O shifted seawater-derived hydrothermal fluid.

Gabbro OM28 (Rustaq): Adcumulate with igneous laminations; 72% plagioclase (An75), 15% clinopyroxene, 10% amphibole, and 3% serpentine, talc alteration pseudomorphing olivine. In contrast to the other cumulate gabbros, in this sample the oxygen isotope data (plagioclase $\delta^{18}O = 4.7$, and whole rock $\delta^{18}O = 5.2$) indicates significant exchange of plagioclase and pyroxene with seawater.

Harzburgite K22 (Ibra): Porphyroclastic texture with tectonite fabric; 40% orthopyroxene, 30% olivine, 30% serpentine, and trace amounts of spinel. Serpentine is pseudomorphing olivine.

3.0 Experimental Procedures

Samples were prepared by removing exterior surfaces with a rock splitter and crushing interior chunks. Only mechanical means were used for mineral separations and involved a combination of handpicking and magnetic separations. These procedures produced high purity ($\sim$ 100%) plagioclase separates and pyroxene separates of greater than 95% purity. The small amount of impurity in the pyroxene separate generally consisted of olivine which is unimportant as it contains extremely low trace element concentrations.

Oxygen was extracted and analyzed from approximately 20 mg of sample using the procedures outlined by Taylor and Epstein [47]. For Nd and Sr, approximately 200 mg of sample was dissolved using HF and $HClO_4$. After complete dissolution an aliquot consisting of about 10% of the solution was spiked and concentrations of K, Rb, Sr, Sm, and Nd were determined. From approximately 100 mg of the remaining unspiked solution, Nd and Sr were separated using ion exchange chemistry [35]. For several samples (see Table 1) both Sm and Nd concentrations and $^{143}Nd/^{144}Nd$ ratios were obtained from the same spiked sample. Under our

spiking conditions the number of ^{150}Nd tracer atoms was about equal to ^{150}Nd in the sample, and the net correction to $^{143}Nd/^{144}Nd$ is 0.001, for which the uncertainty is insignificant. For the plagioclase separate from the gabbro K9, the $^{143}Nd/^{144}Nd$ ratio was obtained from both spiked and unspiked samples and was the same within experimental error. The Sr isotopic composition was measured using a single oxidized tantalum filament [48] and typically $\sim$ 150 ratios were collected. The Nd isotopic composition was determined by measuring NdO on a single rhenium filament and normalized to $^{150}Nd/^{142}Nd = 0.2096$ [35]. The 2σ (mean) errors quoted for the $^{143}Nd/^{144}Nd$ ratio were generally obtained from about 250 ratios. For the above procedures the blanks were Rb = 0.01 ng, Sr = 0.1 ng, Sm = 0.006 ng, and Nd = 0.02 ng and are negligible for the data presented here.

For the harzburgite, the lower Sr and Nd concentrations required the use of a slightly modified procedure to enable the precise determination of the isotopic compositions. Approximately 400 mg of the harzburgite was dissolved, and split into 3 equal portions after removing a 10% aliquot for concentrations. The 3 portions were passed separately through a cation column and Sr and rare earths separated. The rare earth fractions were combined and loaded on the lactic acid column and Nd separated [35]. Using this procedure, a total of 10 ng of Nd was obtained from the harzburgites K22, with a Nd blank of $\sim$ 0.06 ng. This blank is less than 0.6% of the total Nd and is therefore still insignificant. For 10 ng of Nd the precision of the $^{143}Nd/^{144}Nd$ ratio is still better than 5 parts in 10^5.

4.0 Data representation

The oxygen data are given in the conventional notation of

$$\delta^{18}O = \left(\frac{^{18}O/^{16}O_{SAMPLE} - ^{18}O/^{16}O_{SMOW}}{^{18}O/^{16}O_{SMOW}} \right) 10^3$$

where $^{18}O/^{16}O_{SMOW}$ is standard mean ocean water [50]. Following DePaolo and Wasserburg [35] an analogous notation is used here for Nd and Sr, with the reference reservoir evolving with time. This gives

$$\varepsilon_{Nd}^{(T)} = \left(\frac{^{143}Nd/^{144}Nd_{INIT}(T) - ^{143}Nd/^{144}Nd_{CHUR}(T)}{^{143}Nd/^{144}Nd_{CHUR}(T)} \right) 10^4$$

and

$$\varepsilon_{Sr}^{(T)} = \left(\frac{^{87}Sr/^{86}Sr_{INIT}(T) - ^{87}Sr/^{86}Sr_{UR}(T)}{^{87}Sr/^{86}Sr_{UR}(T)} \right) 10^4$$

The $^{143}Nd/^{144}Nd_{INIT}(T)$ and $^{87}Sr/^{86}Sr_{INIT}(T)$ are the measured ratios corrected for decay since the time of crystallization T. The $^{143}Nd/^{144}Nd_{CHUR}(T)$ and $^{87}Sr/^{86}Sr_{UR}(T)$ ratios are those in the standard reservoirs [35,36] at the time T.

5.0 Oxygen isotopic characteristics

The oxygen isotopic systematics of the Semail ophiolite are discussed in detail in the companion paper [45]. The three general categories of samples are: (1) lower cumulate gabbros which exhibit close to "normal" ^{18}O characteristics (K9, OM251), (2) rocks below the diabase-gabbro contact which exhibit ^{18}O depletions (G224-2, G224-3, OM28), and (3) rocks above the diabase-gabbro contact which exhibit ^{18}O enrichments, relative to a primary magmatic reservoir $\delta^{18}O = 5.7$ [6].

The dichotomy between $\delta^{18}O$ values of the rocks above or below the diabase-gabbro contact is a result of differing alteration environments which depend upon temperature, water/rock ratio and the history of the exchanging fluid.

In order to understand the ^{18}O variation due to temperature effects, let us consider the ^{18}O fractionation between rock and fluid defined as

$$\Delta^{18}O_{rock - H_2O} \equiv \delta^{18}O_{rock} - \delta^{18}O_{H_2O} \quad , \tag{1}$$

which is a function of temperature given by [94]:

$$\Delta^{18}O_{rock - H_2O} = \frac{A}{T^2} + B \quad , \tag{2}$$

where A,B are constants.

In the basalt-seawater system, temperatures of alteration in the vicinity of 200°C to 250°C produce no ^{18}O shifts in the rocks as a result of hydrothermal exchange (i.e., $\Delta^{18}O_{rock - H_2O} \approx 5.7$).

The gabbros which are altered at temperatures greater than 400°C are depleted in $\delta^{18}O$ (i.e., $\Delta^{18}O_{rock - H_2O} < 5.7$). The subsolidus alteration event is characterized by isotopic disequilibrium between

coexisting plagioclases and clinopyroxenes and water/rock ratios < 0.5 [45]. The Semail gabbro-water interactions are analogous to those observed in continental layered complexes such as the Skaergaard intrusion which have suffered meteoric hydrothermal exchange [49, 99]. The major difference between the continental and marine environments is the contrast between the initial compositions of the hydrothermal fluids, ≈ -15 and ≈ 0, respectively. Therefore, in the continental environment the contrast between fluid and rock is large $\approx 20‰$, so that the hydrothermal exchange produces almost exclusively ^{18}O depletions in the intrusion and its surrounding country rock over a wide range of temperatures. In the marine case because seawater is isotopically close to the initial rock composition, the combined effects of temperature and water/rock ratio can shift the rocks above or below their magmatic value.

Considering temperature alone, the diabase dikes with greenschist to lower amphibolite mineral assemblages are expected to be depleted in ^{18}O. However, G10 = 8.5 and K1 = 6.8 are, to the contrary, enriched in ^{18}O. This contradiction requires that these diabases have exchanged with an ^{18}O shifted hydrothermal fluid. The fluids that have path lines through the solidified cumulate gabbro are likely candidates as the gabbro section is a region of high temperature alteration and low water/rock ratio--ideal for producing fluid phase ^{18}O enrichments. Fluids discharging from the gabbros into the diabases at the edge of the magma chamber have calculated ^{18}O shifts from $\approx +2$ to $\approx +9‰$ [45]. Because seawater is only $\approx 6‰$ lighter than the rock, shifts of this magnitude can modify upper greenschist facies rocks ($2 \leqslant \Delta \leqslant 6$) from ^{18}O depleted (if the fluid was pristine seawater $\delta^{18}O \approx -0.5$) to ^{18}O enriched hydrothermally altered rocks such as the diabases.

6.0 Trace element abundances

The K, Rb, Sr, Sm, and Nd abundances are listed in Table 2. The most obvious feature is the contrast in K, Rb, Sm, and Nd concentrations between the layered gabbros (K9, OM28, and OM251) which are a factor of ten to one-hundred times lower than those in the upper sequence (plagiogranite, uralite gabbro, sheeted dikes, and basalts). This feature is due to the mineralogy (clinopyroxene, plagioclase, and olivine) and cumulate origin of the layered gabbros. The K, Rb, Sm, and Nd mineral/liquid partition coefficients of $D_{OLIVINE} \ll 1$, $D_{CPX} < 1$, and $D_{PLAG} < 1$ result in these cumulate minerals having lower concentrations relative to the melt from which they crystallized. The resulting melt which is enriched in these elements is presumably represented at least in part by the upper sequence with higher concentrations. It is unlikely that any particular rock group represents the primitive melt composition [51,52]. In contrast, the Sr concentration is relatively uniform throughout the layered gabbros and upper sequence. In the layered gabbros this is due to its high concentration in plagioclase ($D^{Sr}_{PLAG} \sim 2$) which compensates for the lower concentrations in the other cumulate minerals olivine ($D^{Sr}_{OL} \ll 1$) and clinopyroxene ($D^{Sr}_{CPX} \ll 1$) and leaves Sr in the melt approximately constant.

Significant variations in concentrations also exist within the same lithologic units. The gabbro K9 has approximately a factor of four higher concentration of Sm and Nd and a factor of approximately two higher K and Sr concentrations than the gabbro OM251 (see Table 1). Similar variations have also been observed in the gabbros from the Troodos ophiolite [30] and have been interpreted by Kay and Senechal [30] as differences in the amount of trapped liquid in the cumulates. However, an alternative

explanation is that these differences are due to variation of composition of the melt from which these phases crystallized [52]. For example, assuming that OM251 represents a crystallization product of the initial melt and K9 the final melt, then to account for the lower concentration in OM251 CPX compared to K9 CPX, a simple Rayleigh fractionation model requires that the fraction of melt crystallized is from 80% to 90%. A similar result is obtained using the OM251 and OMK9 plagioclase data. However, the problem is more complex, as the composition of the melt in the magma chamber depends upon both the fractionation and replenishment history. In the Semail ophiolite evidence for multiple cycles of primitive magma replenishment within the gabbro complex has been documented by Hopson and Pallister [53] and Pallister and Hopson [54]. This is apparently a normal feature of ophiolite complexes [56], as well as of layered gabbro intrusions emplaced in continental rift environments, such as the Muskox and Great Dike intrusions [57,58]. It has been shown [51,52,55] that mixing between unfractionated primitive magma and a magma that is more highly evolved gives higher concentrations of incompatible elements than are predicted by Rayleigh fractionation. This enrichment of incompatible elements is somewhat analogous to that produced by zone refining. Thus the 80% to 90% fractional crystallization calculated using a Rayleigh model for K9 and OM251 is an upper limit for these two samples, although neither may represent

crystallization products from the most primitive or evolved end members.

As mentioned, the Sm and Nd concentrations in the upper sequence are significantly higher than in the cumulate gabbros. In addition Smewing and coworkers [59] have found variations of approximately a factor of two between the upper and lower pillow lavas in the Semail ophiolite at Wadi Jizzi. The highest concentrations are in the lower pillow lavas or "axis sequence" notation of Gass and Smewing [60] and correspond approximately to concentrations measured in this study at Ibra. The upper pillow lavas at Wadi Jizzi have lower concentrations [59] which are more consistent with "typical" ocean ridge tholeiites. These variations within the pillow lavas have been studied more extensively in the Troodos ophiolite by Smewing and others [31]. It has been suggested by these authors to be partly due to variations in the compositions of primary magmas away from the ridge axis and to smaller amounts of fractionation that the uppermost lavas have undergone.

Some trace element concentration variations, particularly alkali elements within the upper sequence, may be due to the effects of seawater alteration. For example, within the upper sequence, the K concentration decreases systematically from top to bottom. Rb shows a similar trend to K with the exception of the plagiogranite (G224-3). However, the Sr, Sm, and Nd concentrations do not show any similar systematic trends. This could indicate that the higher K and Rb concentrations are due to low-temperature seawater alteration and are not primary. This is consistent with other studies [21,61-63] and observation of K-rich alteration minerals in oceanic basalts [64]. For example, the original 300°C water issuing from submarine hot springs at the Galapagos spreading center, which last equilibrated with the rocks at 300°C [65], was probably enriched in K and Rb relative to normal seawater [106]. These data suggest that K

and Rb may have been leached from the deeper levels of the ophiolite complex and preferentially fixed in the upper part of the sequence. Despite the effects of alteration, the low K and to a lesser extent Rb concentrations of the basaltic rocks are still consistent with an oceanic affinity. The K/Rb ratios of 620 to 2420 and Sr/Rb ratios of 27 to 373 of the diabase dikes and basalt in the Semail ophiolite are roughly comparable to the average MOR tholeiite ratios of K/Rb $\simeq$ 1300 and Sr/Rb $\simeq$ 130 [66-68]. Although the Sm and Nd concentrations in the Ibra section of the Semail ophiolite are somewhat higher, the Sm/Nd ratios are within the range of typical MOR tholeiites [68-70] and are not greatly different from the chondritic ratio.

Another important feature is the distinctly lower trace element concentrations in the harzburgite compared to the rest of the ophiolite (Table 2). These extremely low levels of incompatible elements have also been observed in metamorphic peridotites from other ophiolites and have been interpreted as evidence that the harzburgite tectonite is a residual fraction left after partial melting [71, 72]. However, because of the effects of serpentinization detailed modeling of these trace element abundances (with the exception of the REE [71]) is not possible.

We will now test whether the Sm and Nd concentrations are compatible with the hypothesis of the harzburgite being a residue from partial melting. Assuming that the composite of the cumulate gabbros, diabase dikes, and pillow basalts represents the primary unfractionated magma, we estimate that this magma had Nd $\approx$ 4 ppm and Sm $\approx$ 15 ppm. Then from the measured concentrations in the harzburgite residue K22 (Nd = 0.035 ppm, Sm = 0.013 ppm) and for 15% partial melting, mass balance gives an estimated initial concentration in the source of Nd $\approx$ 0.63 ppm and Sm $\approx$ 0.24 ppm. These concentrations are approximately consistent with those calculated for

batch melting of a spinel lherzolite source material. For comparison, spinel lherzolites in the Beni Bouchera, Lherz, and Lizard peridotites have similar concentrations with Nd $\leqslant$ 0.65 ppm and Sm $\leqslant$ 0.26 ppm (Loubet et al. [73]). Thus, these results are consistent with the hypothesis that the harzburgite is a cogenetic residue after the partial melting which produced the rest of the ophiolite section. However, considering the large uncertainties in this type of calculation (for example, the amount of partial melting, distribution coefficients and composition of source material) a more definitive conclusion is provided by the Nd isotopic data.

7.0 Crystallization age and initial $^{143}Nd/^{144}Nd$

Although current models for the formation of ophiolites at spreading centers indicate that within a single section all the igneous rocks, with perhaps the exception of the basal peridotites, should be of approximately the same age, there may still be significant variations in initial $^{143}Nd/^{144}Nd$ ratios due to mantle source heterogeneities. For this reason, analyses of only whole rock samples from different parts of an ophiolite may have variable initial $^{143}Nd/^{144}Nd$ ratios and may not define an isochron. In addition, there may not be an adequate spread in Sm/Nd of total rocks to define an age for such young samples. We therefore determined crystallization ages and initial ratios by using the coexisting mineral phases from gabbros. These are then compared with whole rock analyses from the same section and analyses of other gabbros from widely different localities.

7.1 Sm-Nd gabbro mineral isochrons

In the Semail ophiolite, apart from the basal periodotite, the

gabbros are volumetrically the most important unit, being approximately 4-6 kilometers in thickness (Fig. 12). We obtained Sm-Nd mineral isochrons from three gabbros (K9, G224-2, OM251) using plagioclase, clinopyroxene, and uralite mineral separates. The gabbro K9 from the Ibra section contains plagioclase, clinopyroxene, and olivine and is extremely fresh, with only a minor amount of alteration (section 2.1). It can be seen in Table 1 and Fig. 2 that the $^{143}Nd/^{144}Nd$ ratio is enriched in the clinopyroxene from K9 by 2 parts in 10^4 relative to the plagioclase. The clinopyroxene also has a higher $^{147}Sm/^{144}Nd$ ratio of 0.320 compared to 0.129 for the plagioclase. Assuming that these minerals and the whole rocks have remained closed systems since forming from an isotopically homogeneous melt, these data indicate a crystallization age of 128±20 m.y. with an initial $^{143}Nd/^{144}Nd$ ratio of $\varepsilon_{Nd} = 7.7\pm0.3$. As the age and initial ratio for this gabbro are only defined by two independent points, the interpretation of this "isochron" as the time of crystallization is not unique. For example, sub-solidus alteration of the Nd isotopic composition in only the plagioclase would for a single rock still define a linear array but give an erroneous age and initial $^{143}Nd/^{144}Nd$. To eliminate the possibility of two component mixing producing this array, three or more distinct mineral phases would have to be analyzed. This is not possible in this sample, as no other REE bearing mineral phase is present (olivine contains negligible REE). This is substantiated by the whole rock analysis which is colinear with the other points and has Sm and Nd concentrations which are consistent with the modal abundances of plagioclase, clinopyroxene, and olivine.

To check the self consistency of this approach, we analyzed a

second gabbro from the upper part of the same gabbro unit as K9. This gabbro (G224-2) contains uralite as a late-stage replacement of pyroxene and primary hornblende. The low $\delta^{18}O$ values for both plagioclase and uralite indicate that this sample has exchanged with seawater at high temperatures ($>$ 400° C). The Sm-Nd data from G224-2 are shown in Table 1 and Fig. 3. The uralite has the highest $^{147}Sm/^{144}Nd$ and $^{143}Nd/^{144}Nd$ ratios and together with the plagioclase gives an age of 150±40 m.y. and an initial $^{143}Nd/^{144}Nd$ ratio of ε_{Nd} = 7.8±0.4. The larger uncertainty in the age and initial ratio for this gabbro compared to K9 is due to the smaller difference between the $^{147}Sm/^{144}Nd$ ratios in the plagioclase and uralite mineral separates. However, within this uncertainty both samples have the same age and initial $^{143}Nd/^{144}Nd$ ratio. In addition, the results from G224-2 show that the Sm-Nd systematics are not affected by the presence of hydrous alteration minerals such as uralite. Three distinct and pure mineral separates from two gabbros now give the same age and initial ratio within experimental uncertainty. This is evidence that the correlated variations of $^{143}Nd/^{144}Nd$ and $^{147}Sm/^{144}Nd$ ratios in these minerals represents an isochron rather than an accidental mixing line. As these samples are also part of the same gabbro section (Ibra) it is justified to combine the Sm-Nd data for K9 and G224-2. The combined data are shown in Fig. 4 and give an age of 130±12 m.y. and ε_{Nd} = 7.8±0.2. This will be used as a reference isochron for comparison of other data from the Ibra section.

In order to determine whether there exist any lateral variations in either the age or initial $^{143}Nd/^{144}Nd$ ratio, we analyzed the gabbro OM251 which was collected in Wadi Fizz approximately 300 km NW from the

Ibra section (see Fig. 1). In Fig. 4 it can be seen that the plagioclase and clinopyroxene data points from this gabbro show a similar relationship as in K9, with the clinopyroxene having the highest $^{143}Nd/^{144}Nd$ and $^{147}Sm/^{144}Nd$ ratios. These two points give an age of 100±20 m.y. and an initial of $\varepsilon_{Nd} = 7.6\pm0.3$. This initial ratio is slightly lower than that obtained from the Ibra section and the crystallization age appears to be about 30 m.y. younger (note, however, that the error bars on the two isochron ages overlap). The isochrons from Ibra and Wadi Fizz together with a gabbro whole rock from Rustaq (~ 180 km NW of Ibra) are compared in Fig. 5. From this figure and the errors given, it can be seen that although the age difference appears to be significant, more precise measurements will be required for this to be definitively established.

7.2 Sm-Nd whole rock analyses of basalts, sheeted dikes, plagiogranite, and harzburgite

Sm-Nd whole rock analyses were obtained from a plagiogranite (G224-3), sheeted dikes (G10, K1), and a basalt (G54) from the Ibra section. In addition, a calcite amygdule from the basalt G54 was also analyzed for Sm-Nd. From the $\delta^{18}O$ values and petrography, these samples show varying degrees and conditions of alteration and metamorphism ranging from zeolite to greenschist facies (see section 2). With the exception of the basalt, only a single data point was obtained for each sample and it is therefore not possible to independently calculate both the age and initial ratio for each sample. Therefore, in Fig. 6 these data are compared with the mineral isochron defined by the gabbros from Ibra. Apart from the sheeted dike K1, the data all lie within analytical error of the gabbro reference isochron. This is consistent with these samples having the same

crystallization age (130 m.y.) and initial $^{143}Nd/^{144}Nd$ ratio. This can be seen from the ε_{Nd} values given in Table 1, which for an age of 130 m.y. range from 7.5±0.4 to 8.3±0.3 compared to ε_{Nd} = 7.8±0.2 for the two Ibra gabbros. The plagiogranite G224-3, with ε_{Nd} = 8.2±0.3 has a clear affinity with these rocks and must represent a later first or second stage differentiate from the same type of oceanic magma source and cannot be a product of melting of any older continental basement.

The tectonized harzburgite K22 with ε_{Nd} = 8.3±0.4 is also within analytical uncertainty of the Ibra reference isochron. This suggests that the harzburgite is genetically related to the rest of the ophiolite (i.e., cumulate gabbro and high level volcanics) and that the serpentization of the harzburgite (section 2.1) has not disturbed the Sm-Nd system.

The Sm-Nd analysis of the diabase dike K1 does not overlap with the reference isochron. This cannot be explained by seawater alteration as the more altered samples are consistent with the reference isochron. This small deviation of K1 could be due to variations in both initial $^{143}Nd/^{144}Nd$ ratio and the crystallization age. As it is unlikely that significant age differences exist within the same section, the deviation of K1 is most probably due to a variation in its initial $^{143}Nd/^{144}Nd$ ratio. For an age of 130 m.y. this corresponds to ε_{Nd} = 8.6±0.4 for K1 compared to ε_{Nd} = 7.8±0.2 for the Ibra gabbros and indicates the presence of small but significant isotopic heterogeneities in the magma reservoirs.

In an attempt to directly ascertain the Nd isotopic characteristics of the interacting fluid, we analyzed a calcite amygdule from the basalt G54. The amygdule has ε_{Nd} = 8.1±0.6 which is within error the same as the host basalt. This indicates that while the solution that deposited the

calcite which was most likely derived from seawater with an initially negative ε_{Nd} value [75,76] the final fluid must have obtained the Nd from the parent rock and not from an exotic source.

8.0 Implications of Sm-Nd

The presence in the Semail ophiolite of only small variations in the initial $^{143}Nd/^{144}Nd$ ratios from different localities and stratigraphic units appears to indicate a relatively uniform isotopic source regions. It is therefore useful to compare these initial ratios with those found in young ocean ridge, ocean island, island arc, and continental basalts. In Fig. 7 it can be seen that ocean ridge and island arc tholeiites have ε_{Nd} values which overlap, with ocean ridge tholeiites having a range of +7 to +13 [35-38,77,78] and island arcs ranging from +7 to +10 [37,38, 74,77,78]. These values are distinctive from the ocean island range of $\sim$ +4 to +8 [37,38,74]. The ε_{Nd} for oceanic rocks are very different from young continental tholeiitic basalts which have $\varepsilon_{Nd} \sim 0$ [35,36,77,79] and older continental crust having $\varepsilon_{Nd}(0) \ll 0$ [35,80]. The Semail ophiolite with $\varepsilon_{Nd} = 7.8$ has clearly an oceanic affinity and is in the lower limit of the island arc and ocean ridge basalt range and the uppermost limit of the ocean island range. Unfortunately, because of the overlap shown on Fig. 7, the Nd isotopic data by themselves cannot at present be used to definitely distinguish among various possible genetic models such as mid-ocean ridge, back-arc basin, ocean island, or island-arc origin for the Semail ophiolite. However, the lack of light REE enriched samples and alkalic volcanism usually associated with ocean island and island arc environments suggests that the most reasonable scenario for its formation is in an ocean basin.

The somewhat lower value of ε_{Nd} = 7.8 in the Semail ophiolite compared to "typical" MORB with $\varepsilon_{Nd} \approx 10$, may be due to either its older age of 130 m.y. compared to the zero age basalts plotted in Fig. 6 or simply reflects the overall variability present today in ocean ridge basalts. The dispersion in ε_{Nd} observed today in oceanic basalts is to some extent correlated with chemistry, with alkalic rocks generally having lower values than MOR tholeiites [77]. However, several oceanic tholeiites with relatively low ε_{Nd} on the range of +7.0 to 8.5 have also been found, for example, in the Atlantic (113152 [35] and ARP75 [38]) and Pacific (BD17-1 [36]) oceans. These samples do not appear to be chemically of tectonically distinctive although the isotopic data indicate an origin from a less depleted source and it appears that they are not uncommon. Tectonically distinctive oceanic settings which may be modern day analogues of the environment in which the Semail ophiolite was formed are the Lau marginal basin and Scotia Sea back arc. The ε_{Nd} values from these two areas [77,78] are shown in Fig. 6 and define a relatively narrow range in ε_{Nd} of 8.1 to 9.0. These initial ratios are also somewhat low compared to normal MORB samples and are very similar to the Semail ophiolite.

The other possibility is that the slightly lower ε_{Nd} value of the Semail ophiolite compared to "typical" oceanic crust, may be due to the evolution of $^{143}Nd/^{144}Nd$ in the oceanic mantle reservoirs after the formation of the Semail oceanic crust. The evolution of ε_{Nd} in the oceanic mantle required to account for the apparently lower ε_{Nd} of the Semail ophiolite is illustrated by the clinopyroxene from the gabbro K9. This sample has $^{147}Sm/^{144}Nd = 0.322$ and a measured $^{143}Nd/^{144}Nd$ ratio of $\varepsilon_{Nd}(0) = 9.9$ (Fig. 2), which is similar to $\varepsilon_{Nd} \approx 10$ for typical MORB today.

Thus for the initial ratios to be compatible, during the last 130 m.y. the typical MORB source reservoir is required to have $^{107}Sm/^{144}Nd \approx 0.32$. Although this high $^{147}Sm/^{144}Nd$ ratio in the MORB source region cannot be discounted, partial melting calculations (see section 6.0) suggest that a more plausible value is $^{147}Sm/^{144}Nd \sim 0.24$. For this lower value of $^{147}Sm/^{144}Nd$, the typical MORB source reservoir evolves by ~ 0.6 ε_{Nd} units per 100 m.y. and would have $\varepsilon_{Nd} \sim 9.2$ at the time the Semail ophiolite was being produced (i.e., 130 m.y. ago). Thus the initial Nd of the Semail ophiolite is only about ~ 1 ε_{Nd} unit below the center of the MORB distribution and is therefore fully consistent with a MORB affinity. In addition these results indicate a dispersion in the initial $^{143}Nd/^{144}Nd$ of Mesozoic oceanic crust.

The relationship of the basal peridotite to the rest of the ophiolite sequence has up to now been obscure due to the effects of alteration and deformation which have largely destroyed the primary geologic structures and relationships. Various hypotheses have considered the harzburgite as a (1) cogenetic lowermost cumulate, (2) older accidental mantle substrate which is not petrogenetically linked to the rest of the ophiolite, or (3) a cogenetic refractory residue remaining from the partial melting which produced the rest of the ophiolite [10]. The initial Nd value of $\varepsilon_{Nd} = 8.3 \pm 0.4$ for the tectonized harzburgite K22 is the same within error the same as the rest of the ophiolite. This result, together with the low trace element concentrations in K22 indicates that this harzburgite is probably a cogenetic residue after partial melting from which the rest of the ophiolite section was produced. However, considering the complexity of the Semail ophiolite peridotite (Boudier and Coleman [81]), the generalization of this result must await a more complete characterization of the peridotite.

The Sm-Nd crystallization age of 130±12 m.y. from Ibra appears to be approximately 30 m.y. older than the 100±20 m.y. crystallization age from the more northern Rustaq, Wadi Fizz localities. This age difference suggests a tectonic break, for example, a transform fault, with a large lateral offset. Such a structure conceivably might be located in the Semail gap (Fig. 1). For a half spreading rate of 1 cm year, a 30 m.y. age difference across a "fossil" transform fault would correspond to a displacement of 300 km from the spreading axis. If the ocean basin was to the east of the Semail ophiolite (i.e., what is now the Gulf of Oman) this would suggest an approximately NW-SE oriented spreading axis. The principal strike direction of the sheeted dike complex in the Semail ophiolite is in fact approximately N15°W.

From the geologic constraints discussed in section 2, there is good evidence that the Semail ophiolite was emplaced onto the Oman continental margin between 65 m.y. to 80 m.y. which is significantly younger than the Sm-Nd crystallization ages. It therefore appears that the Semail ophiolite is an example of relatively mature, oceanic crust being obducted onto a continental margin. Although the mechanisms for emplacement of ocean crust onto continents are still uncertain, it has been suggested [82] that an important condition is for a region of high heat flow as now observed over midocean ridges and behind volcanic arcs [83,84]. In these areas the lithosphere is thinned, less dense, and may be more easily detached onto continental margins [1,8]. However, the indications of a relatively mature oceanic crust and the lack of geologic evidence for island-arc volcanism indicates that the above obduction model is not applicable to the Semail ophiolite. Determination of crystallization ages using the Sm-Nd method should provide a test for the validity of this hypothesis in other ophiolites.

9.0 Comparison of Rb-Sr and Sm-Nd

The most obvious contrast between the Sr and Nd isotopic systems is the larger variability of the $^{87}Sr/^{86}Sr$ ratios ranging from 0.70296 (ε_{Sr} =-19.7) to 0.70650 (ε_{Sr} = +30.5) compared to a range in ε_{Nd} of from only 7.5 to 8.6. The lowest $^{87}Sr/^{86}Sr$ ratios are found in the plagioclase separates from the layered cumulate gabbros K9 and OM251. In K9, the plagioclase has a $^{87}Sr/^{86}Sr$ ratio of 0.70926±2. However, the coexisting clinopyroxene has a distinctly higher value of 0.70313±3. In Fig. 7 reference isochrons of 150 m.y. and 4550 m.y are shown. The 130 m.y. isochron corresponds to the near horizontal line and shows that the change in $^{87}Sr/^{86}Sr$ from ^{87}Rb decay is negligible in these samples. It can be seen that a line connecting the clinopyroxene and plagioclase from K9 give an impossibly old age of > 4.5 AE. In the high level gabbro G224-2 there is a similar disparity between the plagioclase and uralite. The uralite has an $^{87}Sr/^{86}Sr$ ratio of 0.70426±3 compared to 0.70352±4 for the coexisting plagioclase. As in K9, these isotopic variations cannot be accounted for by radiogenic decay since crystallization. Instead, this isotopic relationship between the coexisting mineral phases indicates partial exchange with a source of high $^{87}Sr/^{86}Sr$. The enrichment in $^{87}Sr/^{86}Sr$ is more pronounced in the clinopyroxene and uralite and is anticipated as they have a factor of 5 lower Sr concentration than the plagioclase. This enrichment is also consistent with the petrography (section 2.1) as the uralite is clearly an alteration product and the clinopyroxene contains $\sim$ 5% of secondary hornblende. These results are in distinct contrast to Sm-Nd, where all mineral phases plot on a 130 m.y. isochron.

The highest $^{87}Sr/^{86}Sr$ ratios found in the Semail ophiolite are in the upper sequences consisting of basalts, sheeted dikes, and plagiogranites. The higher $^{87}Sr/^{86}Sr$ ratios in these rocks is consistent with a greater degree of exchange with seawater having a high $^{87}Sr/^{86}Sr$ ratio. In an attempt to determine the $^{87}Sr/^{86}Sr$ ratio in seawater, we analyzed a calcite amygdule from the basalt OMG54. This has $^{87}Sr/^{86}Sr = 0.7065$ which is significantly higher than that found for any of the igneous rocks and may be compared to 0.7076 estimated for Cretaceous seawater [7,8]. These observations are clearly consistent with hydrothermal interaction with seawater. The slightly lower ratio in the amygdule compared to Cretaceous seawater is probably due to the lowering of $^{87}Sr/^{86}Sr$ in the fluid by interaction with the rock. There is also an approximate correlation between high $^{87}Sr/^{86}Sr$ and stratigraphic height (see Fig. 12) which suggests that water/rock ratios increased upward in the section.

Due to the overprinting of rock Sr with seawater Sr, it is not possible to unambiguously determine the primary magmatic $^{87}Sr/^{86}Sr$ ratio in these rocks. An upper limit is given by the lowest $^{87}Sr/^{86}Sr$ value of 0.70296 found in the plagioclase from the gabbro K9. This may be close to its magmatic value as the coexisting clinopyroxene with a lower Sr concentration has only a slightly greater $^{87}Sr/^{86}Sr$ ratio. The $^{87}Sr/^{86}Sr$ ratios in the clinopyroxene and plagioclase from the gabbro OM251 also have very different Sr concentrations but have the same $^{87}Sr/^{86}Sr$ ratio within error and should thus also represent a primary value. The difference between the plagioclase separates from K9 and OM251 of 0.70296 ± 2 and 0.70311 ± 5 could therefore indicate a small but real difference in the $^{87}Sr/^{86}Sr$ ratios of these samples and apparently of the original magmas from which they crystallized. This demonstrates that small $^{87}Sr/^{86}Sr$ mantle isotopic

heterogeneities have been preserved during the formation of the Semail ophiolite, because the same effect is also apparent in the Nd isotopic data (Table 1). In fact these two samples OM251 and K9 plot right on the MOR correlation line in the ε_{Sr}-ε_{Nd} diagram of Fig. 9.

The Rb-Sr isochron diagram of Fig. 8 also illustrates the importance of distinguishing between seawater alteration effects and mantle isotopic variations. In this figure, seawater alteration has produced an approximate correlation between Rb/Sr and $^{87}Sr/^{86}Sr$. If interpreted literally, this correlation would imply that Rb/Sr heterogeneities have existed for at least several billion years in the mantle reservoirs of the Semail ophiolite. Similar correlations and interpretations have been suggested in other ophiolites [17], oceanic basalts [87,89], and ocean islands [90-92]. Although some of these correlations are undoubtedly due to mantle variations, the ^{18}O data from the Semail ophiolite indicate that this Rb/Sr - $^{87}Sr/^{86}Sr$ correlation is clearly an artifact of seawater alteration.

A useful criterion to distinguish between isotopic variations due to either primary magmatic or seawater alteration effects is the ε_{Nd},ε_{Sr} diagram. In Fig. 9 the ε_{Nd} and ε_{Sr} values from the Semail ophiolite are shown. They have an origin at the mantle correlation line [36,37,74] and form a horizontal trajectory to the higher ε_{Sr} values. Although this general effect has been shown by previous workers [36,37,74], the present results provide a spectacular example of how the Nd isotopic composition is unaffected by seawater contamination while the Sr composition is shifted drastically. It is illustrative to compare the observed ε_{Nd},ε_{Sr} values, with those calculated for contamination of oceanic crust by Cretaceous

seawater. Assuming a simple closed system model for mixing of Sr and Nd in seawater with oceanic crust, mass balance between the initial and final products gives:

$$w\ \varepsilon^{i}_{H_2O} + r\ \varepsilon^{i}_{rock} = w\ \varepsilon^{f}_{H_2O} + r\ \varepsilon^{f}_{rock} \qquad (3)$$

where w and r are the atomic proportions of Nd or Sr in the water and rock systems respectively and ε^{i}_{rock} = initial ε_{Nd} or ε_{Sr} value in rock before exchange; ε^{f}_{rock} = final modified rock ε_{Nd} or ε_{Sr} value; $\varepsilon^{i}_{H_2O}$ = initial ε_{Nd} or ε_{Sr} value in water before exchange; and $\varepsilon^{f}_{H_2O}$ = final modified water ε_{Nd} or ε_{Sr} value. For equilibrium exchange of water and rock, $\varepsilon^{f}_{H_2O} = \varepsilon^{f}_{rock}$ and from equation (3) the water/rock ratio by <u>weight</u> is given by

$$\frac{W}{R} = \left(\frac{\varepsilon^{f}_{rock} - \varepsilon^{i}_{rock}}{\varepsilon^{i}_{H_2O} - \varepsilon^{f}_{rock}}\right) \frac{C^{i}_{rock}}{C^{i}_{H_2O}} \qquad (4)$$

where C^{i}_{rock} = concentration of Sr or Nd in initial rock and $C^{i}_{H_2O}$ = concentration of Sr or Nd in seawater.

For Sr the parameters used in this equation are $\varepsilon^{i}_{rock} = -20$, $\varepsilon^{i}_{H_2O} = +47$ [8], and $C^{i}_{H_2O} = 8$ ppm [93]. ε^{f}_{rock} values are given in Table 2. As Sr concentrations are not subject to major changes [59], we take the initial Sr concentration in the rock (C^{i}_{rock}) is the same as the final measured concentration (Table 1). A similar equation has also been given (incorrectly) by Spooner <u>et al.</u> [19]. For Nd the parameters used in equation (2) are $\varepsilon^{i}_{rock} = +8.0$, $\varepsilon^{i}_{H_2O} = -7$, and $C^{i}_{H_2O} = 2.8 \times 10^{-6}$ ppm [76]. The C^{i}_{rock} and ε^{f}_{rock} values are given in Tables 1 and 2.

Using equation (2) and the Sr and Nd parameters, the ε_{Nd} and ε_{Sr} values in the rock resulting from mixing of different proportions of

seawater with oceanic crust have been calculated. The ε_{Nd},ε_{Sr} mixing line is shown in Fig. 9, together with the water/rock ratios for $C^{i}_{rock}Sr$ = 180 ppm and $C^{i}_{rock}Nd$ = 10 ppm. From Fig. 9 it can be seen that the ε_{Nd} values are far less sensitive to seawater contamination than the ε_{Sr} values. This is due to the significantly lower concentration of Nd in seawater of 2.8×10^{-6} ppm compared to 8 ppm for Sr. As an example, from equation (4) the Sr data indicate that the sample with the highest water/rock ratio is the diabase dike K1 with W/R = 43 (Table 3). Using the same equation, but with the Nd parameters, the same water/rock ratio causes only an insignificant change of ε_{Nd} = -0.0001. To produce a measurable shift in ε_{Nd}, of, for example, ε_{Nd} = 0.5, a water/rock ratio of W/R = 1.6×10^{5} would be required. Thus relative to the most altered rock an increase in the water/rock ratio of $\sim 4 \times 10^{3}$ would be required before seawater contamination would measurably change the ε_{Nd} values. A detailed analysis of the effects of seawater interaction using ε_{Sr} and $\delta^{18}O$ variations will be given in section 10.1.

The above calculations were based on a closed system model which assumes continuous recirculation and cyclic re-equilibration of the water with the rock. However, some of the heated water will be lost from the system, for example by escape to the ocean. In the extreme open system case in which each increment of water makes only a single pass through the system, it has been shown by Taylor [98] that the integrated water/rock ratios are lower or equal to those in the closed system model. The W/R ratios calculated from the Sr data using both open and closed system models give similar results, except for samples with high W/R ratios such as K1 where W/R (open) = 31 compared to W/R (closed) = 43. In addition, both the

open and the closed system models give significantly lower W/R ratios in the gabbros (0.5-3) than in the upper sequence (11-43). These W/R ratios are only minimum values because, for example, an appreciable volume of water may move through fractures in the rocks without exchanging.

The ε_{Nd} and ε_{Sr} values of mid-ocean ridges, island arc, and ocean island basalts which define the correlation line are also shown in Fig. 9. This correlation of ε_{Nd} and ε_{Sr} has been discussed by other workers [36,37] and has been interpreted as an important mantle feature. For example [36], it may represent mixing between undepleted continental mantle ($\varepsilon_{Nd} = 0$) and depleted oceanic mantle ($\varepsilon_{Nd} = +12$). In the Semail ophiolite, the gabbro K9 has the lowest ε_{Sr} value and together with the ε_{Nd} value plots on the correlation line is therefore consistent with a mantle origin. The somewhat lower ε_{Nd} and higher ε_{Sr} values compared to "typical oceanic crust" indicates that the Semail ophiolite was probably derived from a less depleted oceanic mantle [79]. As both the ε_{Nd} and ε_{Sr} values from the Semail ophiolite plot in a position where the fields for MOR, ocean island, and island arc basalts overlap, the ε_{Sr}-ε_{Nd} diagram cannot be used in this case to discriminate between the different oceanic environments.

10.0 Comparison of $^{87}Sr/^{86}Sr$ and $\delta^{18}O$

It has already been shown that $^{87}Sr/^{86}Sr$ and $\delta^{18}O$ values are sensitive to hydrothermal alteration. The correlated effects of alteration on both these systems is shown in the initial $^{87}Sr/^{86}Sr$, $\delta^{18}O$ diagram of Fig. 10. In this figure there appear to be at least two distinct trends which are centered about the primary values of $\delta^{18}O \approx +6$ and $^{87}Sr/^{86}Sr \approx 0.7030$. The most obvious trend is the approximate inverse correlation corresponding to depleted $\delta^{18}O$ and high $^{87}Sr/^{86}Sr$ ratios. The second, less distinctive, feature is the association of heavy $\delta^{18}O$ values with high $^{87}Sr/^{86}Sr$ ratios in the sheeted dikes and basalt. In an attempt to understand these features, we will now consider simple models for the exchange of Sr and O with seawater.

10.1 Modeling of $^{87}Sr/^{86}Sr$ and $\delta^{18}O$ variations

Let us consider a simple closed system model for the exchange of Sr and O with seawater as has already been discussed for Sr and Nd. Using this model, the water/rock ratio (by weight) calculated using $\delta^{18}O$ variations is given by Taylor [94]:

$$\frac{W}{R} = \left(\frac{\delta^{f}O_{rock} - \delta^{i}O_{rock}}{\delta^{i}O_{H_2O} - (\delta^{f}O_{rock} - \Delta)} \right) \frac{C^{i}O_{rock}}{C^{i}O_{H_2O}} \qquad (5)$$

where

$\delta^{f}O_{rock}$ = final modified rock $\delta^{18}O$ value

$\delta^{i}O_{rock}$ = initial rock $\delta^{18}O$ value

$\delta^{i}O_{H_2O}$ = initial $\delta^{18}O$ in water

$\Delta = {}^{18}O/{}^{16}O_{mineral} - {}^{18}O/{}^{16}O_{H_2O}$

$C^{i}O_{rock}$ = concentration O in rock

and $C^{i}O_{H_2O}$ = concentration O in water.

This equation is identical to that used for Sr, apart from the temperature dependent fractionation factor Δ. Let us now assume that only a particular fraction of the rock exchanges with seawater. This may, for example, be the case for the more easily exchanged minerals such as feldspar. The effective water/rock ratio (W/R(effective)) is then given by

$$\frac{W}{R}(\text{effective}) = \frac{W}{R} \times \frac{1}{q} \tag{6}$$

where q is the fraction (by weight) of rock that exchanged with seawater. A similar equation can also be written for the Sr water/rock ratio, where in this case let us assume that different fractions of the rock, q^1 exchanged with seawater. Therefore the relationship between the Sr and O water/rock ratios is given by

$$\frac{W}{R}(\text{strontium})\ \frac{1}{q^1} = \frac{W}{R}(\text{oxygen})\ \frac{1}{q} \tag{7}$$

Using this relationship, equations (4) and (5) can now be combined to give

$$\frac{\varepsilon^f Sr_{rock} - \varepsilon^i Sr_{rock}}{\delta^f O_{rock} - \delta^i O_{rock}} = \left(\frac{\varepsilon^i Sr_{H_2O} - \varepsilon^f Sr_{rock}}{\delta^i O_{H_2O} - (\delta^f O_{rock} - \Delta)} \right) \times C \tag{8}$$

where $$C = \frac{C^i Sr_{H_2O}/C^i O_{H_2O} \times q^1/q}{C^i Sr_{rock}/C^i O_{rock}}$$

Equation 8 is now similar to mixing equations derived previously for mixing of Sr, Nd, and Pb, and other trace elements [95-97]. An example of a mixing line using equation 8 is shown in Fig. 11a for $\Delta = 0$. It can be seen that the mixing line is a hyperbola with the curvature determined by

the constant C. For $q^1/q = 1$ and using average concentrations of Sr and O in the rock and seawater, C = 0.022, which is the curve shown in Fig. 11a. Using this arbitrary value of C, the effect of the oxygen water-rock fractionation factor Δ is shown in Fig. 11b. In this figure the resultant $^{87}Sr/^{86}Sr$ and $\delta^{18}O$ variations are shown for $\Delta = +2$ and $\Delta = +8$ and $\Delta = +2$. The value of Δ depends on the temperature of exchange and is given by equation 2 (section 5). Thus for different temperatures no simple correlation of $\delta^{18}O$ and $^{87}Sr/^{86}Sr$ would be expected. In fact for $\Delta = 6$ corresponding to a temperature of $\sim 250°$ C there can be changes in $^{87}Sr/^{86}Sr$ without any change in the $\delta^{18}O$ (Fig. 11b).

For $\Delta > 0$ the $\delta^{18}O$ value of the water is different from the $\delta^{18}O$ value of the rock, being related by $\Delta = \delta^{f}O_{rock} - \delta^{f}O_{H_2O}$. The curves are shown in Fig. 11c for the respective Δ values. In Fig. 11c it can be seen that for $\Delta < 6$ the water will be enriched in $\delta^{18}O$ (i.e., $\delta^{18}O_{H_2O} > 0$) and for $\Delta > 6$ the water will be depleted. Subsequent interaction of this exchanged water will result in another set of mixing curves. Evidence has been found in the diabase dikes for exchange with ^{18}O-enriched water (section 5) indicating that this water has had a history of high temperature (> 300° C) exchange.

In Fig. 11d, mixing lines are shown which could account for the Sr isotopic disequilibrium observed for example between the plagioclase and uralite in the gabbro G224-2. The mixing lines are different for each mineral as they have different Sr concentrations and presumably different exchange rates (i.e., different values of q^1/q). As the factor q^1/q is unknown, the mixing lines that are shown are arbitrary, but they appear to account for the observed $^{87}Sr/^{86}Sr$ and $\delta^{18}O$ values in the minerals of G224-2.

From this discussion it is apparent that the production of water with $\delta^{18}O_{H_2O} > 0$ results from water-rock interaction at high temperatures (i.e., with $\Delta < 6$). This implies that the $\delta^{18}O$ effects in the sheeted dikes were produced by upward convection at the distal edges of the magma chamber of seawater already enriched in ^{18}O, by exchange with the underlying gabbros at higher temperature as shown by Gregory and Taylor [45]. This ^{18}O shifted fluid would also presumably be shifted in $^{87}Sr/^{86}Sr$ ($\sim$ 0.704 suggested by uralite from G224-2) and may have equilibrated with the diabases already altered over the ridge axis. This implies that there are at least two temperature and spatial regimes where exchange of oxygen and Sr occurs. The first is at the ridge axis above the magma chamber where fluid path lines do not cross the diabase-magma contact. It is in this environment that ^{18}O-depleted rocks and $^{87}Sr/^{86}Sr$ enriched rocks could be produced with a high water/rock ratio. Subsequently, with continued production of oceanic crust, these rocks are transported away from the ridge into a cooler regime at the distal edges of the magma chamber where interaction between isotopically shifted fluids and the diabases occurs. This high ^{18}O and $^{87}Sr/^{86}Sr$ fluid discharges from a second hydrothermal system which operates under the wings of the ridge magma chamber [45]. This "hydrothermal reworking" of oceanic crust may also explain the generally more altered nature of ophiolite pillow basalts compared to those dredged from ocean ridges. It is apparent, however, that to adequately interpret these data more quantitative models are required, as for example described in the Skaergaard intrusion by Norton and Taylor [99].

10.2 Significance of $^{87}Sr/^{86}Sr$ and $\delta^{18}O$ variations

An important category of theories for the origin of island arcs and continental margin magmatic rocks involves the partial melting of subducted oceanic crust [100-103]. It is therefore of interest to compare the $^{87}Sr/^{86}Sr$ and $\delta^{18}O$ characteristics of these rocks with those found in the Semail ophiolite.

Recently it has been found that a positive correlation between $\delta^{18}O$ and initial $^{87}Sr/^{86}Sr$ is present in the Peninsular Ranges batholith of southern and Baja California [104], in the Banda arc of Indonesia [105], and in the Peruvian volcanic rocks of the Andes [104]. The approximate $\delta^{18}O$ and $^{87}Sr/^{86}Sr$ values of whole rock samples from the Peninsular Ranges batholith areas are delimited by the dashed lines in Fig. 10, together with the $^{87}Sr/^{86}Sr$ and $\delta^{18}O$ data points from the Semail ophiolite. It can be seen that the batholith samples have $\delta^{18}O$ and $^{87}Sr/^{86}Sr$ values which overlap to some extent with those from the Semail ophiolite. This suggests that these rocks could plausibly be derived by partial melting of hydrothermally altered pillow basalts and sheeted dike complexes. However, it is apparent from Fig. 10 that there is no overlap with the ^{18}O-depleted rocks. This may not be a serious objection, as most of the ^{18}O-depleted rocks in the Semail ophiolite are the virtually anhydrous cumulate gabbros [45] which represent liquidus phases and therefore require higher melting temperatures. The strongly ^{18}O-depleted uralite gabbro G224-2 forms only a minor proportion (< 10%) of the ophiolite.

Another possible objection is that some lavas [105] have higher $^{87}Sr/^{86}Sr$ ratios (~ 0.740) than can possibly be accounted for by seawater contamination. For these examples a special case of contamination by a high $^{87}Sr/^{86}Sr$ source must be made. However, an even more profound objection is that the $^{87}Sr/^{86}Sr$ and $\delta^{18}O$ values from the Peninsular Ranges batholith are much more strongly correlated than would be expected for magmas derived by partial melting of a subducted, hydrothermally altered, oceanic crust (section 10.2). In addition, the high K and other incompatible element concentrations in the batholith probably would require unrealistically small amounts of partial melting. Thus although partial melting of subducted oceanic crust may be an important process, in terms of isotope systematics the general applicability of such a process still has many difficulties. It is apparent that Nd isotopic studies on these circum-Pacific andesites and batholithich bodies could provide useful additional constraints.

11.0 Summary and Conclusions

(1) In this study we have established the crystallization age of the Semail ophiolite by obtaining Sm-Nd mineral isochrons from gabbros. The gabbros from the southern part of the ophiolite in Ibra give an age of 130±12 m.y. while a gabbro from Wadi Fizz in the northern part of Oman gives a somewhat younger age of 100±20 m.y. These results show that the Sm-Nd technique can be used to determine and to resolve differences in crystallization ages within large ophiolite complexes. In addition, it should be possible to use Sm-Nd crystallization ages, together with emplacement ages of ophiolites, to further refine and reconstruct plate motions and relative spreading rates.

(2) The initial $^{143}Nd/^{144}Nd$ ratio of gabbros, plagiogranite, diabase dikes, and a basalt from the Semail ophiolite have a narrow range in ε_{Nd} of from 7.5 to 8.6 (Fig. 12). For an increase in the MORB source reservoirs of $\varepsilon_{Nd} \approx 0.6$ units per 100 m.y., the center of the MORB distribution, 130 m.y. ago, would be at $\varepsilon_{Nd} \sim 9.2$ compared to $\varepsilon_{Nd} \sim 10$ today. Therefore the Semail ophiolite is only about 1 ε_{Nd} unit below the center of the Mesozoic MORB distribution which probably has a spread of about 4 ε_{Nd} units. This clearly demonstrates an oceanic affinity for the Semail ophiolite and indicates that all of its lithologies are comagmatic. Unfortunately, because of the overlap (Fig. 7) the Nd (and Sr) isotopic data cannot by themselves be used at present to definitely distinguish among various genetic models such as MOR, back-arc basin, or island-arc origin for the Semail ophiolite.

(3) The tectonized harzburgite has $\varepsilon_{Nd} = 8.3$ which is also consistent with the rest of the ophiolite. This result, together with its low trace

element concentrations, indicate that the harzburgite is a cogenetic residue after partial melting which produced the rest of the ophiolite section. However, considering the complexity and heterogeneous character of the peridotite in the Semail ophiolite [81] generalization of this result must await a more complete characterization of the peridotite.

(4) In contrast to the initial $^{143}Nd/^{144}Nd$ ratios, the initial $^{87}Sr/^{86}Sr$ ratios have an extremely large range of from 0.7030 to 0.7065. This large variation is consistent with hydrothermal interaction of seawater with oceanic crust. In addition, the $^{87}Sr/^{86}Sr$ ratios generally decrease downwards (Fig. 12), suggesting downwardly decreasing water/rock ratios. These results indicate extreme caution must be employed before variations in initial $^{87}Sr/^{86}Sr$ ratios of ophiolitic rocks can be attributed to primary magmatic variations. In this study we have in fact found small variations in initial $^{87}Sr/^{86}Sr$ of gabbro plagioclase separates of from 0.70296±2 to 0.70311±5 which we have attributed to primary magmatic variations. However, this interpretation is supported by corresponding variations in the initial $^{143}Nd/^{144}Nd$ ratios and by analysis of coexisting pyroxenes.

(5) The complete ^{18}O profile from Gregory and Taylor [45] is also shown in Fig. 12. From this figure it can be seen that with respect to the "normal" value of $\delta^{18}O = 5.7$ there are both ^{18}O depleted and enriched rocks. The depletions are probably a result of high temperature hydrothermal alteration whereas the ^{18}O enrichments are due to hydrothermal exchange with either strongly ^{18}O-shifted waters at high temperature or less ^{18}O-shifted waters at much lower temperatures.

In Fig. 12 it can be seen that above the diabase-gabbro contact there is an approximate linear correlation between high ^{18}O and high

$^{87}Sr/^{86}Sr$ ratios. Below this contact the correlation is approximately inverse, corresponding to depleted ^{18}O and high $^{87}Sr/^{86}Sr$ ratios. These relationships are primarily due to the temperature dependence of the oxygen water-rock interactions. Due to this temperature effect, it has been shown that in general no simple relationship between ^{18}O and $^{87}Sr/^{86}Sr$ variations would be expected. In fact at the appropriate temperature of hydrothermal interaction (200°C - 250°C) it is possible to have $^{87}Sr/^{86}Sr$ enrichments while retaining apparently normal ^{18}O values.

Table 1. Nd, Sr, and O isotopic data from the Semail ophiolite.

Samples	$\frac{^{87}Rb}{^{86}Sr}$	$\frac{^{147}Sm}{^{144}Nd}$	$\frac{^{87}Sr}{^{86}Sr}$	$\frac{^{143}Nd}{^{144}Nd}$	ε_{Sr}	ε_{Nd}	$\delta^{18}O$
Basalt							
G54 WR	0.104	0.192	0.70491±4	0.512219±19	5.1±0.6[a]	7.5±0.4[a]	12.7
CALCITE	0.0042	0.209	0.70650±15	0.512265±29	30.5±2.1	8.1±0.6	
Sheeted Dikes							
G10	0.029	0.209	0.70535±4	0.512250±25	13.5±0.6	7.8±0.5	8.5
K1	0.008	0.194	0.70519±4	0.512275±20	11.7±0.6	8.6±0.4	6.8
Plagiogranite							
G224-3	0.035	0.187	0.70362±4	0.512249±18	-11.3±0.6	8.2±0.3	5.2
Gabbros							
G224-2 WR	0.010	0.201	0.70370±3	0.512251±19	-9.5±0.4	8.0±0.4	3.7
PLAG	0.008	0.151	0.70352±4	0.512196±18	-12.5±0.6	7.8±0.3	4.5
URAL	0.014	0.241	0.70426±3	0.512285±19	-1.6±0.4	8.0±0.4	2.6
K9 WR	0.0008	0.271	0.70304±5	0.512310±18	-18.6±0.7	8.0±0.3	5.7
PLAG	0.0005	0.129	0.70296±2	0.512180±25	-19.7±0.3	7.8±0.5	6.0
				0.512181±19[b]		7.8±0.4	
CPX	0.0008	0.322	0.70313±3	0.512341±15	-17.3±0.4	7.7±0.3	5.3
OM251 PLAG	0.0010	0.159	0.70311±5	0.512203±22	-18.0±0.7	7.6±0.4	6.4
	0.0018	0.377	0.70315±5	0.512346±25[b]	-17.5±0.7	7.6±0.5	5.8
OM28 WR	0.0014	0.264	0.70383±5	0.512274±22[b]	-7.8±0.7	7.7±0.4	5.2
Harzburgite							
K22		0.216		0.512278±23		8.3±0.4	

[a] ε_{Sr} and ε_{Nd} values calculated for a crystallization age of 130 m.y. except for OM251 and OM28 for which an age of 100 m.y. was used.

[b] $^{143}Nd/^{144}Nd$ determined from spiked sample.

Table 2. Trace element abundances from the Semail ophiolite (ppm)

Samples	K	Rb	Sr	Sm	Nd	$\frac{Sr}{Rb}$	$\frac{K}{Rb}$	$\frac{Sm}{Nd}$
Basalt								
G54 WR	4470	7.16	198	5.03	15.9	28	624	0.316
G54 CALCITE	76	0.009	6.12	0.043	0.126	680	8440	0.341
Sheeted Dikes								
G10	3950	1.63	162	3.85	11.2	99	2420	0.344
K1	2290	1.04	388	4.16	13.0	370	2201	0.320
Plagiogranite								
G224-3	2200	2.31	192	5.36	17.3	83	952	0.310
Gabbros								
G224-2 WR	1320	0.674	196	2.78	8.36	290	1960	0.333
PLAG	1800	0.950	330	0.563	2.25	350	1890	0.250
URAL	740	0.280	58.7	3.79	9.51	210	2640	0.399
K9 WR	117	0.052	188	0.441	0.986	3610	2250	0.447
PLAG	161	0.050	311	0.085	0.399	6220	3220	0.213
CPX	29	0.023	24.8	1.401	2.630	1080	1260	0.533
OM251								
PLAG	77	0.055	156	0.021	0.081	2840	1400	0.259
CPX	20	0.034	54.2	0.256	0.411	1590	588	0.623
OM28 WR	126	0.066	132	0.168	0.385	2000	1910	0.436
Harzburgite								
K22	6	0.023	0.43	0.013	0.035	19	261	0.371
Average MOR Tholeiite [62-64]	1400	1	140	2.7	8	140	1400	0.34

Acknowledgments

We express our gratitude to the Directorate General of Petroleum and Minerals of the Ministry of Agriculture, Fisheries, Petroleum, and Minerals, Sultanate of Oman for their support of this project. Some of the samples were provided by R. G. Coleman. Field work was conducted with the U. S. Geological Survey--National Science Foundation Oman project and we would particularly like to thank E. H. Bailey, R. G. Coleman, C. A. Hopson, and J. S. Pallister.

This work has been supported by NSF Grant PHY 76-83685.

FIGURE CAPTIONS

Figure 1. Simplified geologic map of the Semail ophiolite, Oman (after Glennie et al. [42]), showing sample localities. The Semail ophiolite (solid) is an allochtonous body which is in thrust contact with the underlying rocks.

Figure 2. Sm-Nd evolution diagram for the cumulate gabbro K9, from the Ibra section, Oman. The uncertainty in the age determination is largely controlled by the difference between the $^{147}Sm/^{144}Nd$ ratios of the coexisting clinopyroxene and plagioclase.

Figure 3. Sm-Nd evolution diagram for the high level uralite gabbro G224-2, from the Ibra section, Oman. The larger uncertainty in the age determination compared to the gabbro K9 is due to the smaller spread in $^{147}Sm/^{144}Nd$ ratios of the plagioclase and uralite. The uralitization process must have occurred close to the time of crystallization of the gabbro and does not appear to have disturbed the Sm-Nd systematics.

Figure 4. Sm-Nd evolution diagram for the cumulate gabbro OM251, from Wadi Fizz, Arab Emirates.

Figure 5. Sm-Nd evolution diagram showing the data for the gabbros from Ibra and the gabbros from Wadi Fizz and Rustag. Although at the limit of our resolution, the gabbros from Ibra appear to be approximately 30 m.y. older than those from the more northern Wadi Fizz-Rustaq area.

Figure 6. Sm-Nd evolution diagram showing whole rock data for basalt, sheeted dikes, and plagiogranite from the Ibra section, Oman. With the exception of the sheeted dike K1, the data from the other samples are consistent with the same crystallization age and initial $^{143}Nd/^{144}Nd$ ratio as the gabbros from Ibra. The deviation of K1 indicates the presence of small but significant isotopic heterogeneities in the magma reservoirs. The tectonite harzburgite K22 is within analytical uncertainty of the Ibra reference isochron. This is consistent with the harzburgite being a cogenetic residue, remaining from the partial melting which produced the rest of the ophiolite.

Figure 7. Histogram comparing ε_{Nd} values from the Semail ophiolite measured in this study with mid-ocean ridge basalts (MORB) [35-38], marginal basins (Lau, Scotia Sea) [78], island arcs [77], ocean islands [37,38,74], and continental flood basalts [35,36,77,79]. The Semail ophiolite clearly has an oceanic affinity, although because of the overlap, the Nd isotopic data by themselves cannot at present be used to definitely distinguish among the various possible oceanic environments.

Figure 8. Rb-Sr evolution diagram showing whole rock and mineral data from the Semail ophiolite. The near horizontal line is a 130 m.y. isochron and the steeper line is for an isochron of 4550 m.y. The lack of correlation between $^{87}Rb/^{86}Sr$ and $^{87}Sr/^{86}Sr$ and the high $^{87}Sr/^{86}Sr$ is attributed to contamination by seawater.

Figure 9. ε_{Nd} and ε_{Sr} values for the Semail ophiolite. The arrows indicate the effect of contamination with Cretaceous seawater for different water/rock ratios and show that $W/R > 10^5$ is required before ε_{Nd} values are affected. The ε_{Nd} and ε_{Sr} values of uncontaminated samples plot on the "mantle correlation" line and are consistent with derivation from a less depleted MORB source region. As these ε_{Nd} and ε_{Sr} values plot in a position where the fields for MOR, ocean island, and island arc basalts overlap, this diagram cannot be used in this case to discriminate between the oceanic environments in which the Semail ophiolite formed.

Figure 10. Initial $^{87}Sr/^{86}Sr$ versus $\delta^{18}O$ values of whole rocks and minerals from the Semail ophiolite. The dashed lines delimit the $^{87}Sr/^{86}Sr$ and $\delta^{18}O$ values of the Peninsular Ranges batholith [104] of southern and Baja California and are much more strongly correlated than would be expected for magmas derived by partial melting of a subducted, hydrothermally altered, oceanic crust.

Figure 11.a. ε_{Nd} and $\delta^{18}O$ mixing lines of rock and seawater for oxygen fractionation factor $\Delta = 0$ and $C = 0.022$ (see equation 7). Arrows show direction of increasing water/rock ratio.

b. ε_{Sr} and $\delta^{18}O$ values in the rock for $C = 0.022$ and $\Delta = 2$ (line A), $\Delta = 6$ (line C), and $\Delta = 8$ (line B). For $\Delta = 6$ which corresponds to a temperature of 300°C, there can be shifts in ε_{Sr} without any change in $\delta^{18}O$.

c. ε_{Sr} and $\delta^{18}O$ values in water for $\Delta = 2$, $\Delta = 6$, and $\Delta = 8$

(solid lines). Given by $\delta^{18}O_{H_2O} = \delta^{18}O_{rock} - \Delta$ and $\varepsilon_{Sr_{H_2O}} = \varepsilon_{Sr_{rock}}$. For $\Delta < 6$ which corresponds to temperature > 300° C, ^{18}O-enriched water (i.e., $\delta^{18}O_{H_2O} > 0$) will be produced. For $\Delta > 6$ (< 300° C) ^{18}O-depleted waters will be produced. The dashed lines show the ε_{Sr} and $\delta^{18}O$ values in the rock (from Fig. 11b).

d. Example of mixing lines consistent with ε_{Sr} and $\delta^{18}O$ values in the uralite gabbro.

Figure 12. $\delta^{18}O$, ε_{Sr} and ε_{Nd} values from a composite stratigraphic profile of the Semail ophiolite, Ibra section. The stratigraphic profile was compiled from the geologic map of Bailey et al. [43]. The symbol V = volcanics, SD = sheeted dikes, Pg = plagiogranite, HG = high level gabbros, G = cumulate gabbros, WG = wehlite gabbros, D = dunite, and H = harzburgite. It can be seen that the ε_{Nd} values are in general within error of the primary magmatic value of $\varepsilon_{Nd} = 78$. In contrast, the $\delta^{18}O$ (from Gregory et al. [45] and this study) and ε_{Sr} values show large deviations from their primary magmatic values of $\delta^{18}O = 5.7$ and $\varepsilon_{Sr} = -19.5$. These large variations in $\delta^{18}O$ and ε_{Sr} are indicative of hydrothermal interaction of seawater.

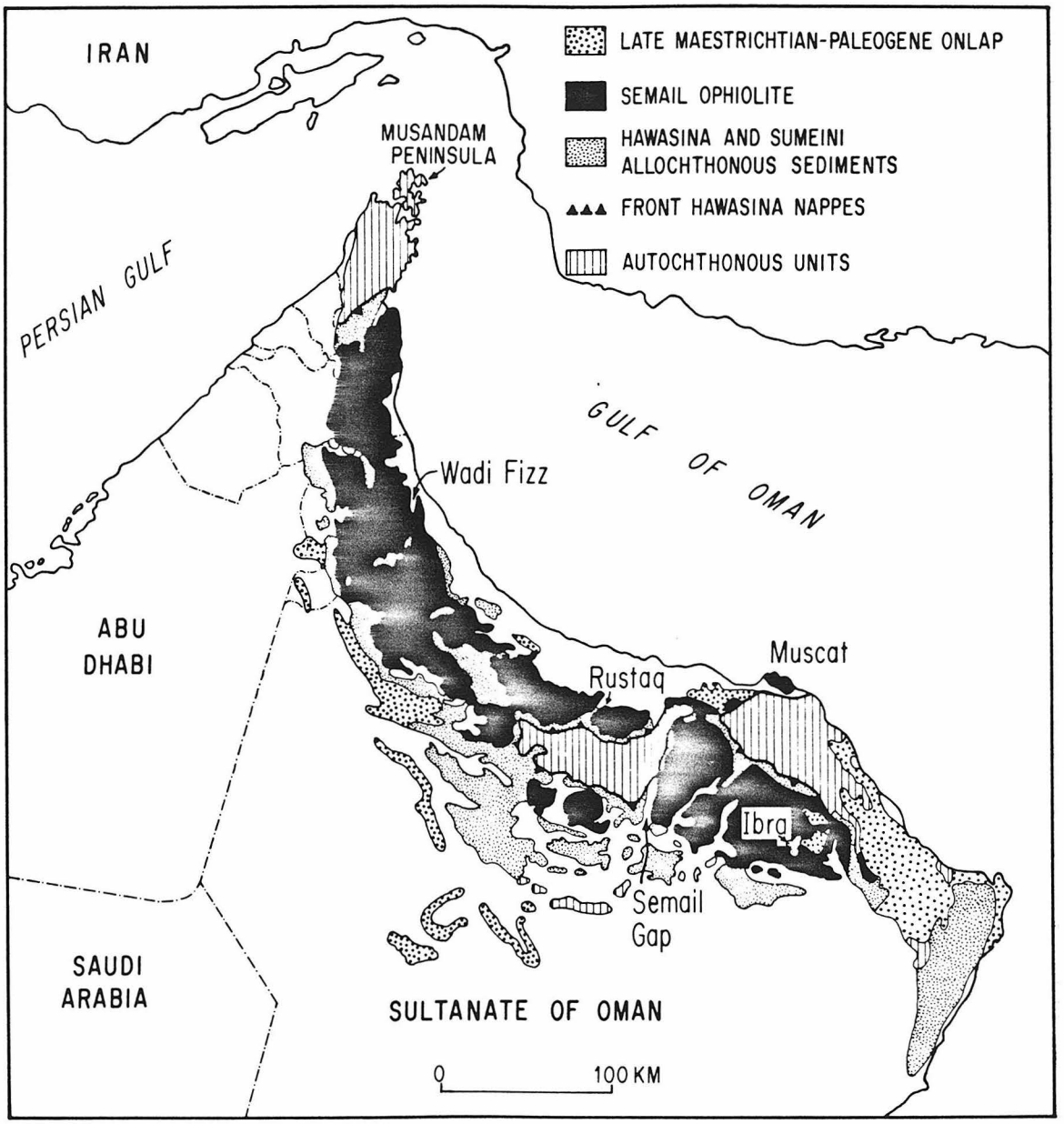
IRAN
LATE MAESTRICHTIAN-PALEOGENE ONLAP
SEMAIL OPHIOLITE
HAWASINA AND SUMEINI ALLOCHTHONOUS SEDIMENTS
FRONT HAWASINA NAPPES
AUTOCHTHONOUS UNITS
MUSANDAM PENINSULA
PERSIAN GULF
GULF OF OMAN
Wadi Fizz
ABU DHABI
Rustaq
Muscat
Ibra
Semail Gap
SAUDI ARABIA
SULTANATE OF OMAN
0
100 KM

Fig. 1

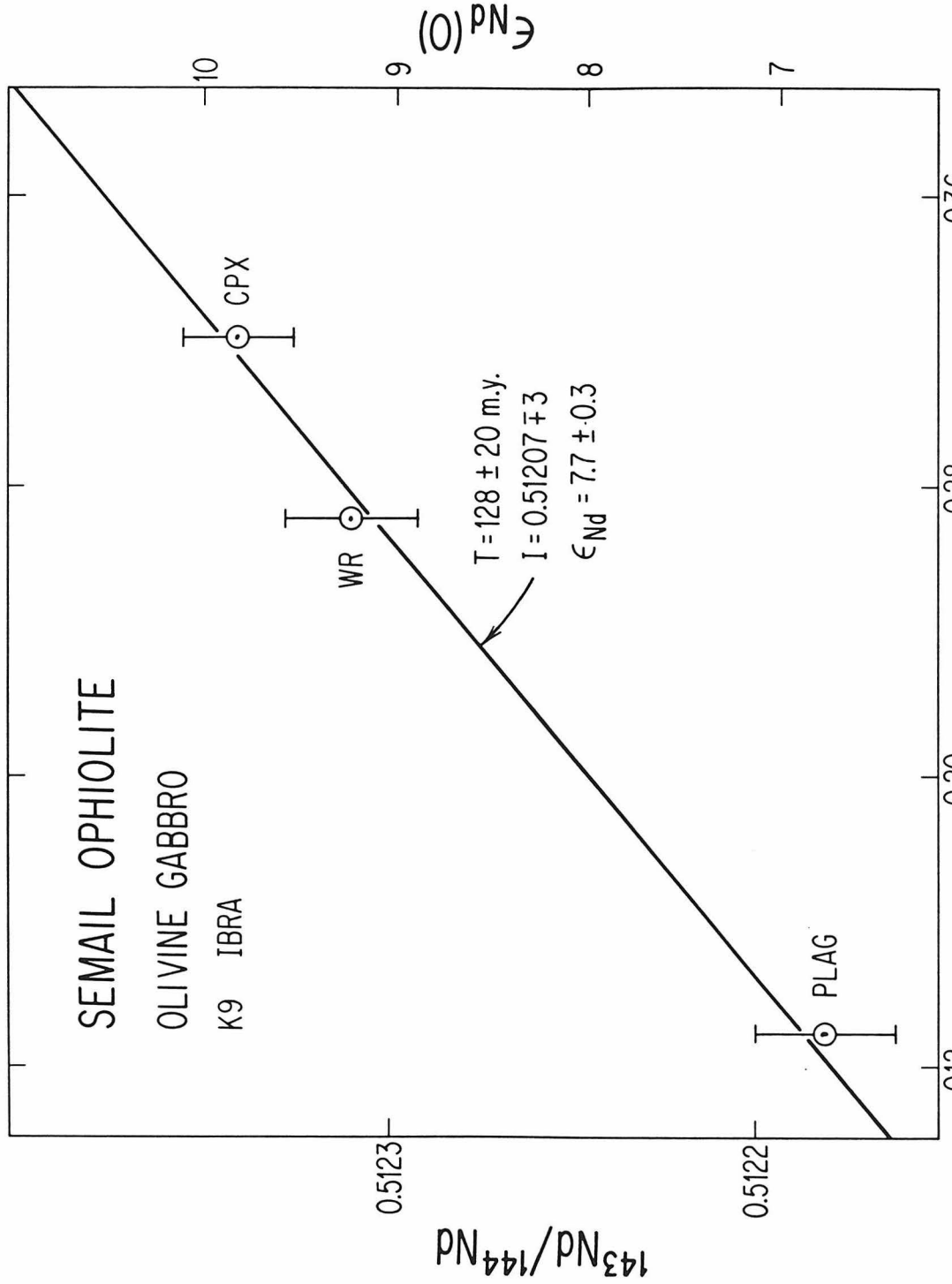
SEMAIL OPHIOLITE
OLIVINE GABBRO
K9 IBRA
CPX
WR
PLAG
T = 128 ± 20 m.y.
I = 0.51207 ∓ 3
ϵ_{Nd} = 7.7 ± 0.3
$^{143}Nd/^{144}Nd$
$^{147}Sm/^{144}Nd$
$\epsilon_{Nd}(0)$
0.5123
0.5122
0.12
0.20
0.28
0.36
10
9
8
7

Fig. 2

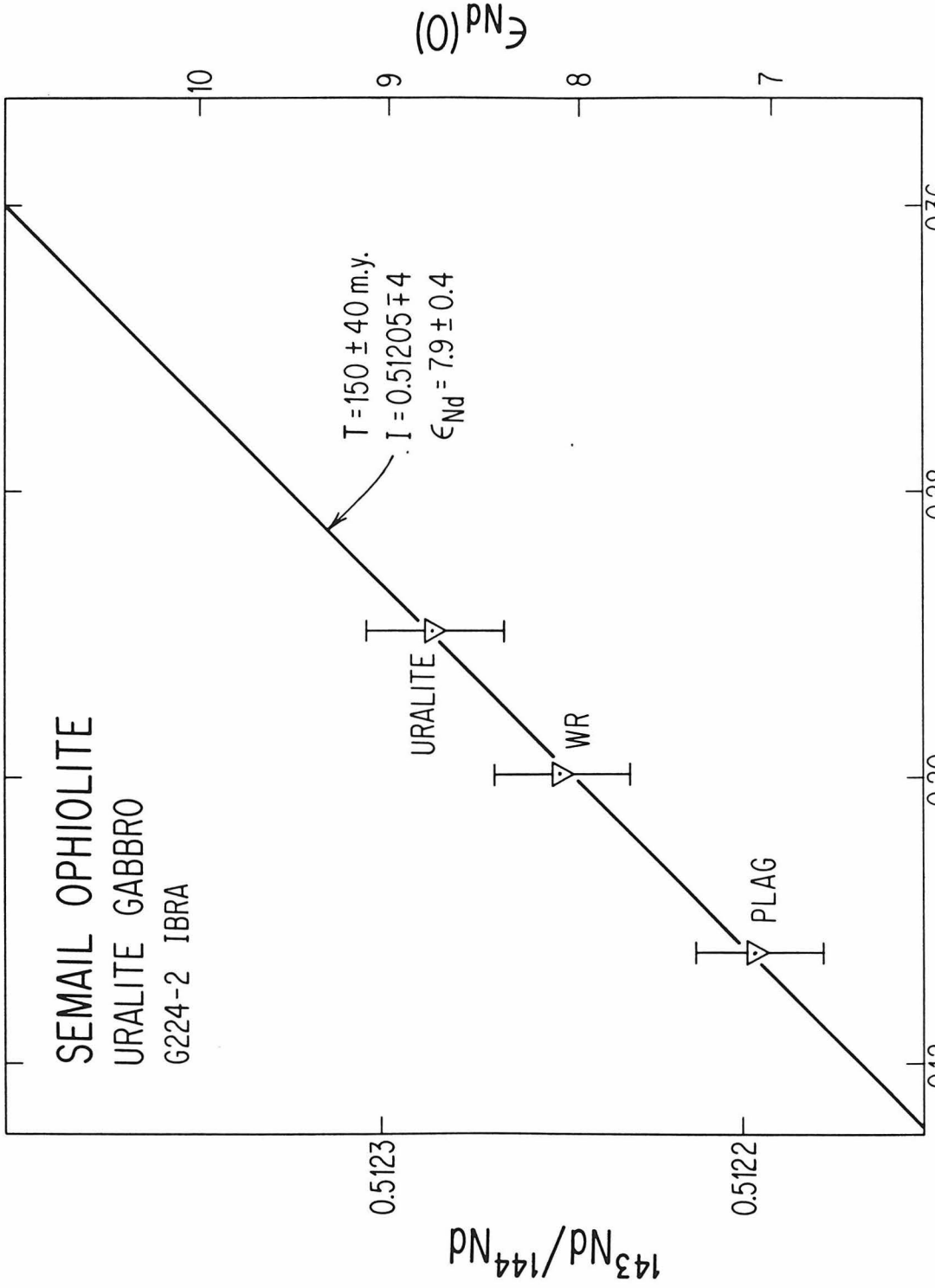
SEMAIL OPHIOLITE
URALITE GABBRO
G224-2 IBRA
T = 150 ± 40 m.y.
I = 0.51205 ∓ 4
ϵ_{Nd} = 7.9 ± 0.4
URALITE
WR
PLAG
0.5123
0.5122
0.12
0.20
0.28
0.36
10
9
8
7
$^{143}Nd/^{144}Nd$
$^{147}Sm/^{144}Nd$
$\epsilon_{Nd}(0)$

Fig. 3

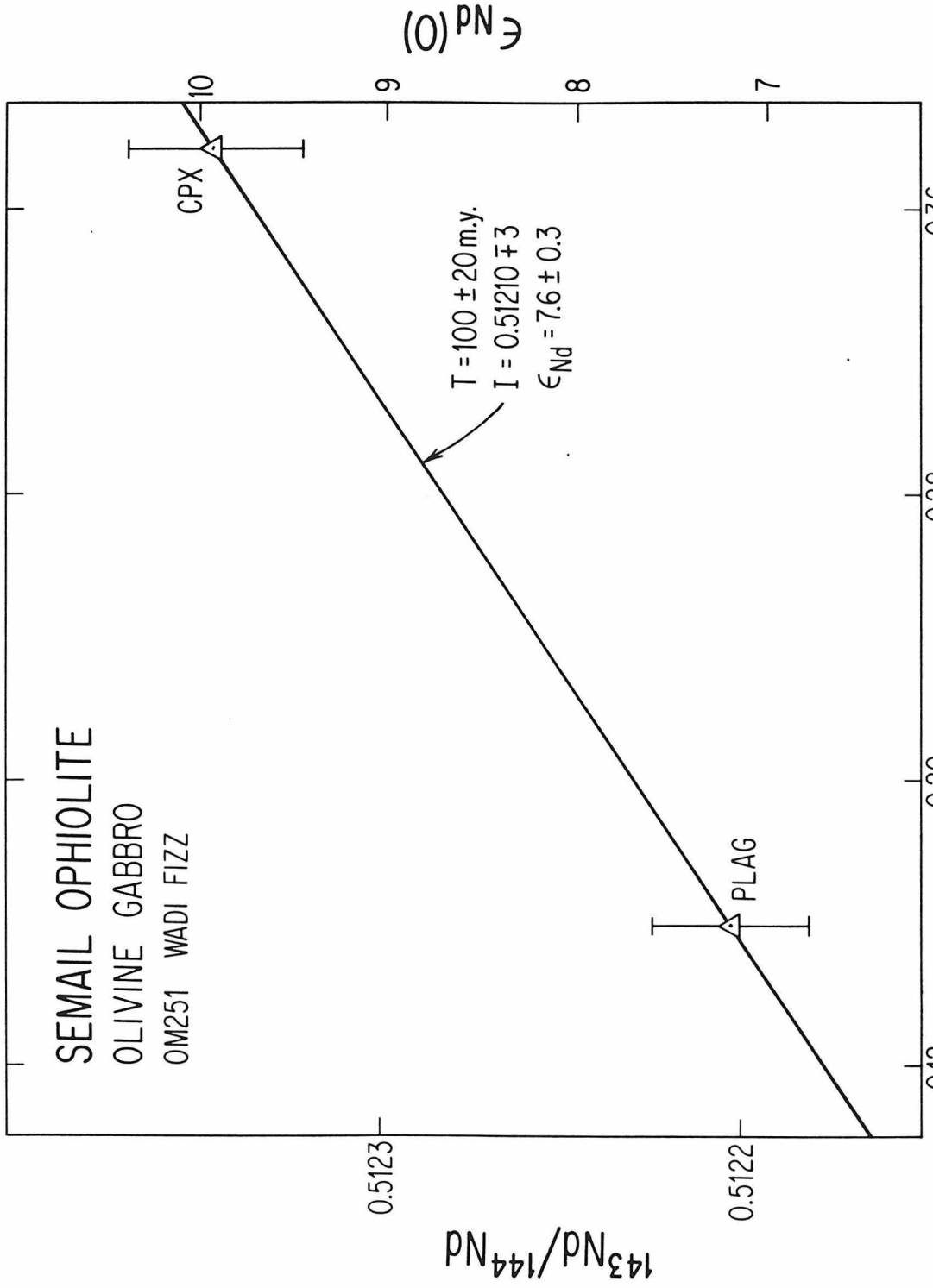
SEMAIL OPHIOLITE
OLIVINE GABBRO
OM251 WADI FIZZ
CPX
PLAG
T = 100 ± 20 m.y.
I = 0.51210 ∓ 3
ϵ_{Nd} = 7.6 ± 0.3
$^{143}Nd/^{144}Nd$
$^{147}Sm/^{144}Nd$
$\epsilon_{Nd}(0)$
0.5123
0.5122
0.12
0.20
0.28
0.36
10
9
8
7

Fig. 4

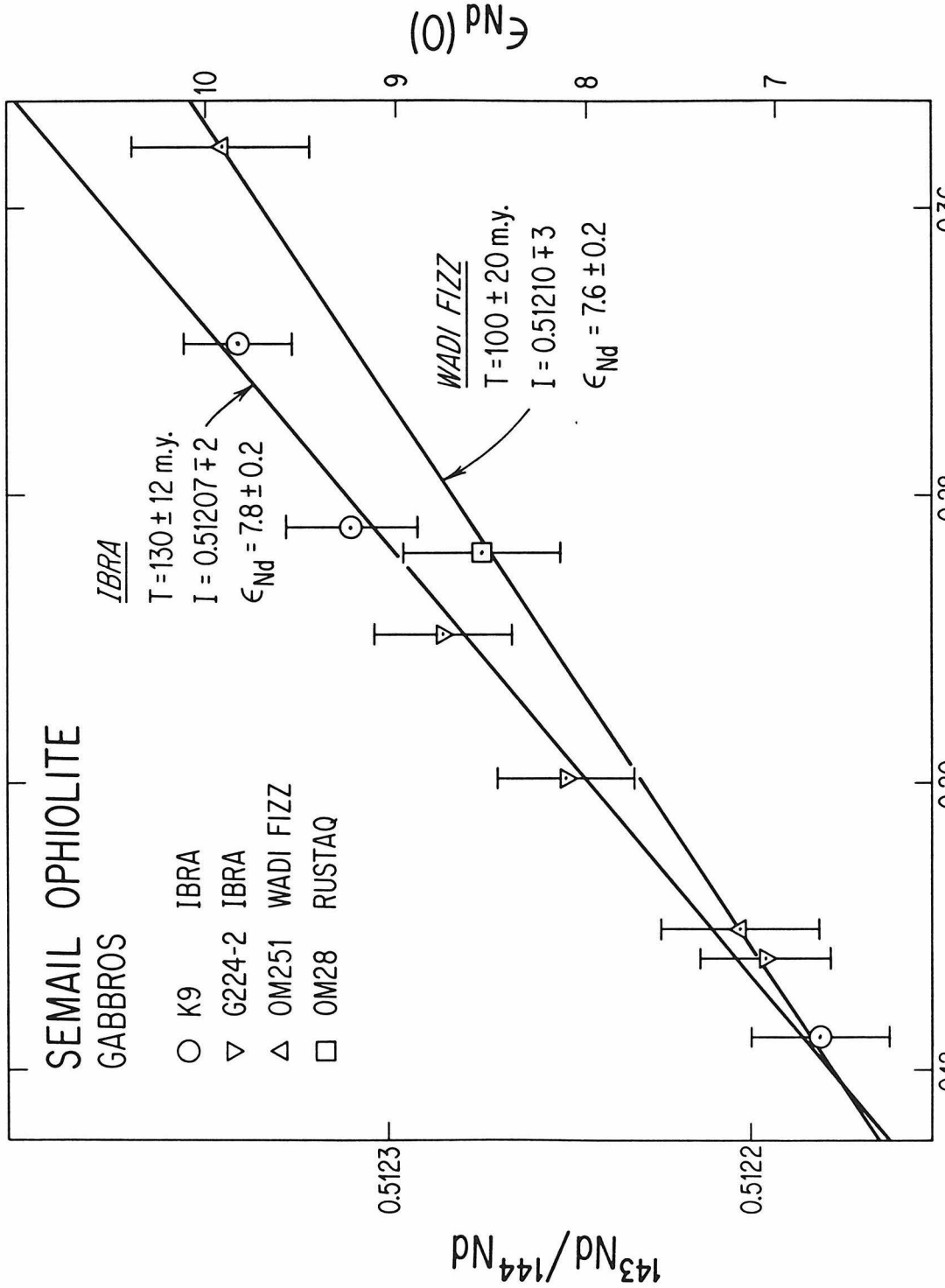
SEMAIL OPHIOLITE
GABBROS
K9 IBRA
G224-2 IBRA
OM251 WADI FIZZ
OM28 RUSTAQ
IBRA
T = 130 ± 12 m.y.
I = 0.51207 ∓ 2
ε_Nd = 7.8 ± 0.2
WADI FIZZ
T = 100 ± 20 m.y.
I = 0.51210 ∓ 3
ε_Nd = 7.6 ± 0.2
143Nd/144Nd
147Sm/144Nd
εNd(0)
0.5123
0.5122
0.12
0.20
0.28
0.36
10
9
8
7

Fig. 5

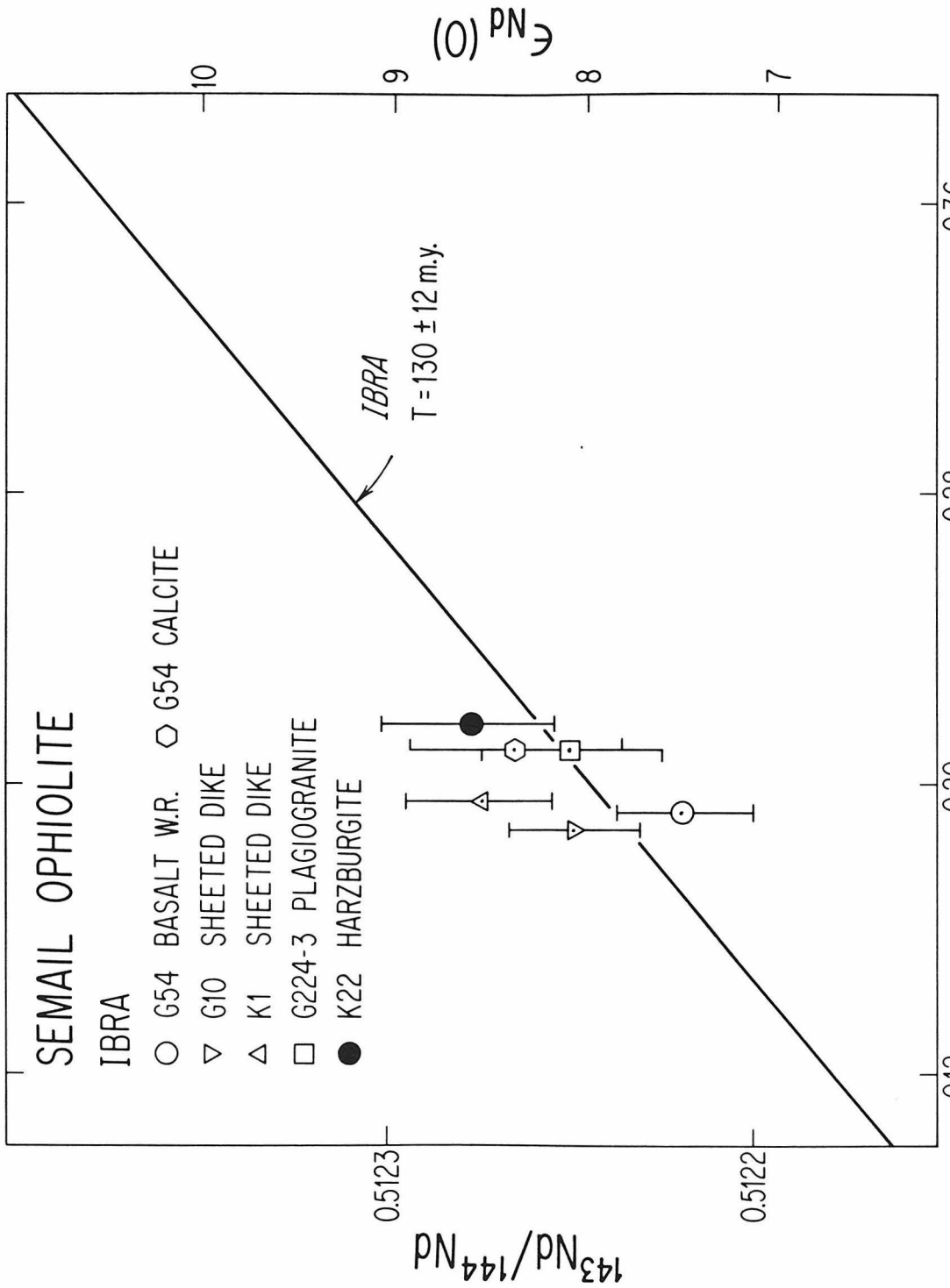
SEMAIL OPHIOLITE
IBRA
○ G54 BASALT W.R. ⬡ G54 CALCITE
▽ G10 SHEETED DIKE
△ K1 SHEETED DIKE
□ G224-3 PLAGIOGRANITE
● K22 HARZBURGITE
IBRA
T = 130 ± 12 m.y.
0.5123
0.5122
0.12
0.20
0.28
0.36
10
9
8
7
$^{143}Nd/^{144}Nd$
$^{147}Sm/^{144}Nd$
$\varepsilon_{Nd}(0)$

Fig. 6

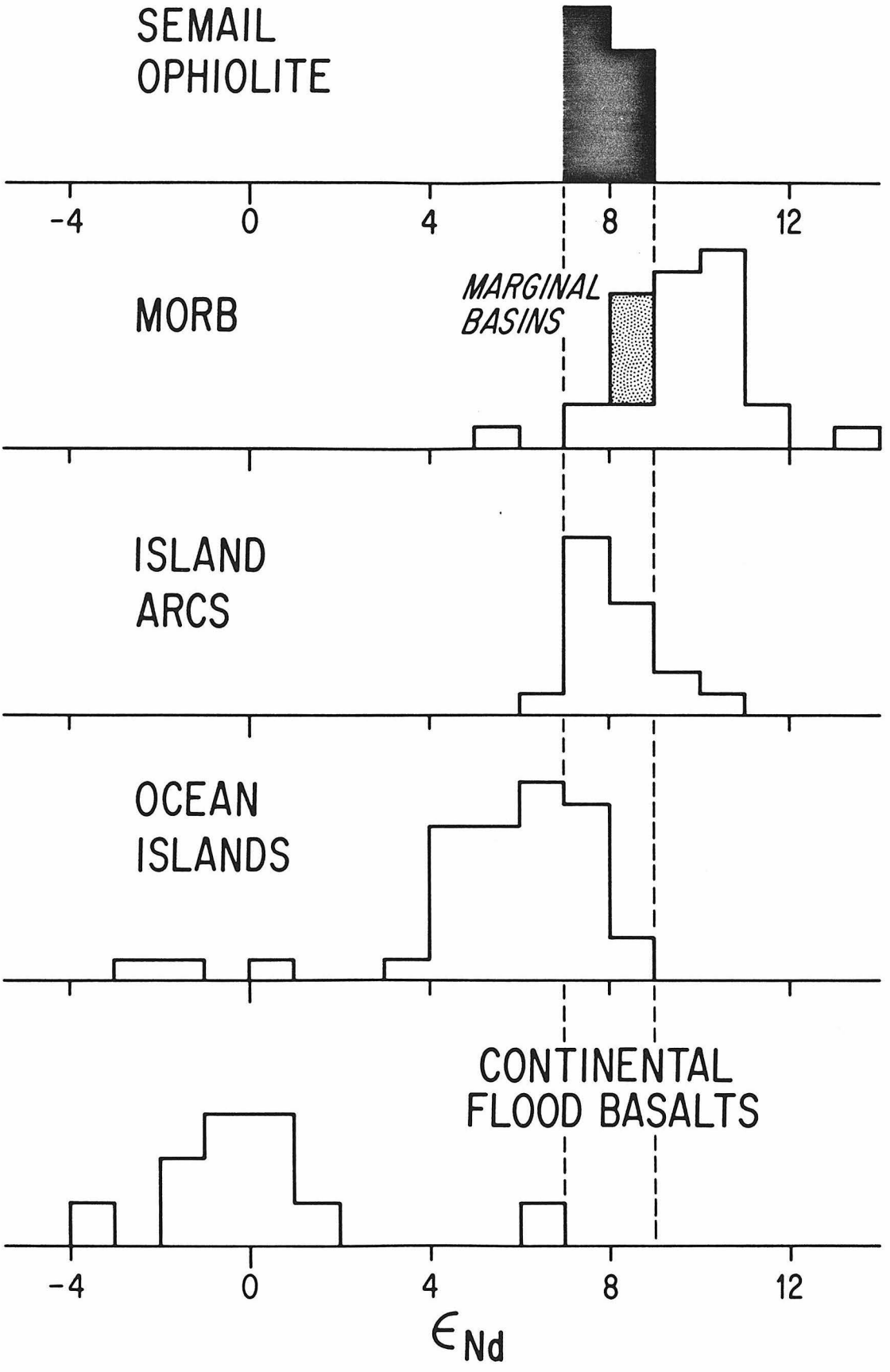
SEMAIL
OPHIOLITE
-4
0
4
8
12
MORB
MARGINAL
BASINS
ISLAND
ARCS
OCEAN
ISLANDS
CONTINENTAL
FLOOD BASALTS
-4
0
4
8
12
ϵ_{Nd}

Fig. 7

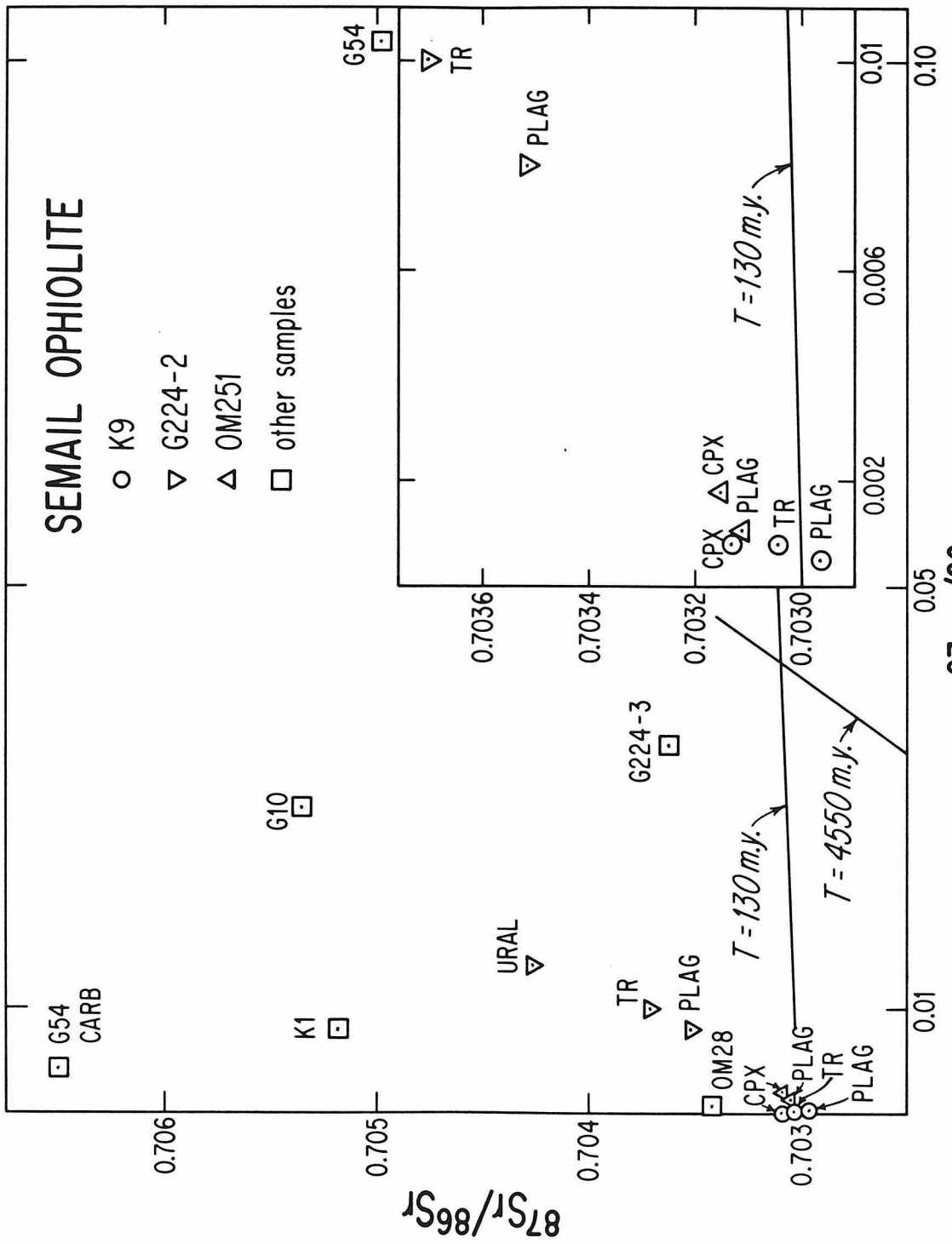
SEMAIL OPHIOLITE
K9
G224-2
OM251
other samples
G54
CARB
K1
G10
URAL
TR
PLAG
G224-3
OM28
CPX
PLAG
TR
PLAG
T = 130 m.y.
T = 4550 m.y.
T = 130 m.y.
0.706
0.705
0.704
0.703
0.7036
0.7034
0.7032
0.7030
0.01
0.05
0.10
0.002
0.006
0.01
$^{87}Sr/^{86}Sr$
$^{87}Rb/^{86}Sr$

Fig. 8

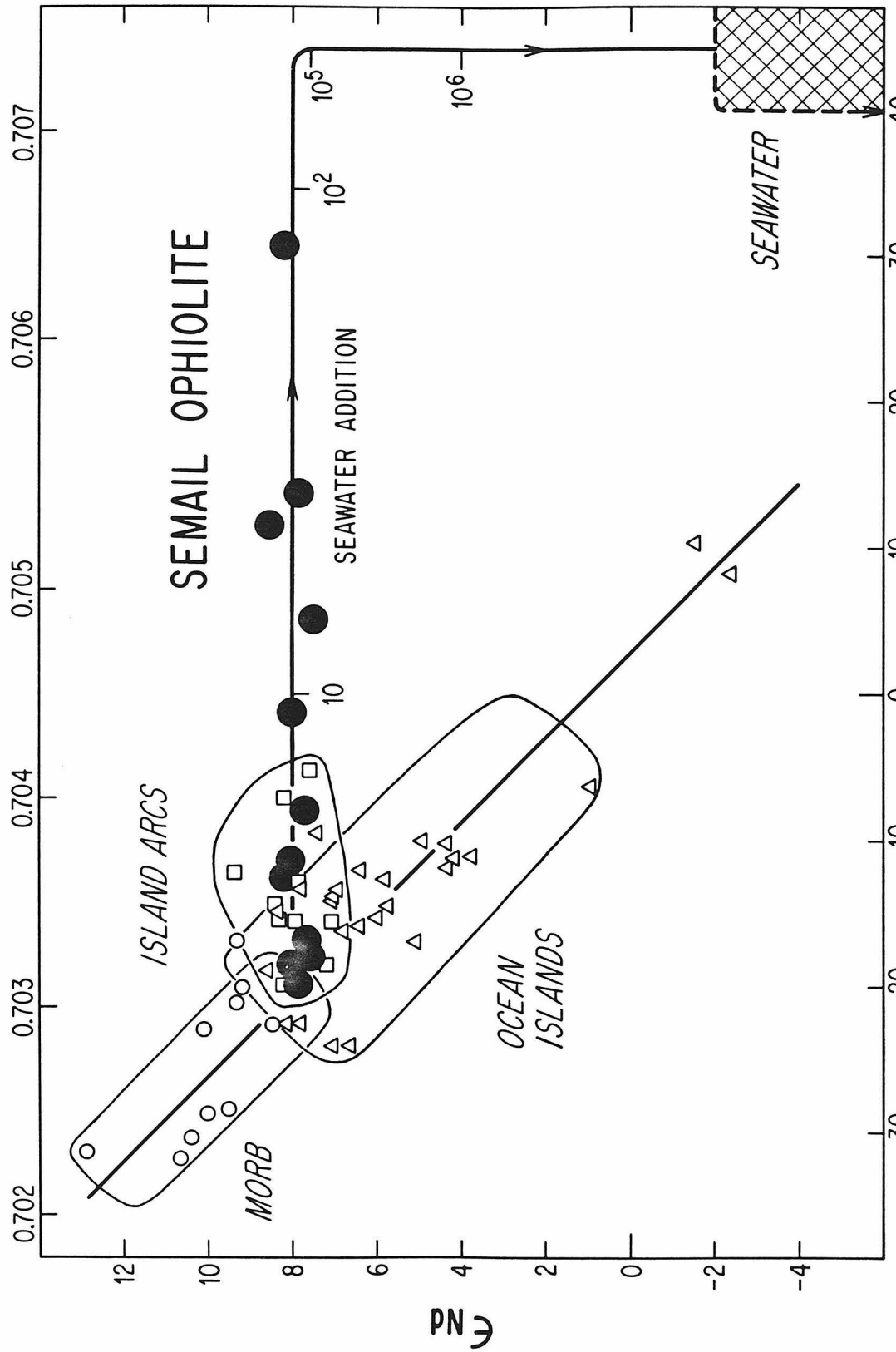
SEMAIL OPHIOLITE
SEAWATER ADDITION
SEAWATER
ISLAND ARCS
MORB
OCEAN ISLANDS
ϵ_{Nd}
ϵ_{Sr}
0.702
0.703
0.704
0.705
0.706
0.707
12
10
8
6
4
2
0
-2
-4
40
30
20
10
0
-10
-20
-30
10^2
10^5
10^6

Fig. 9

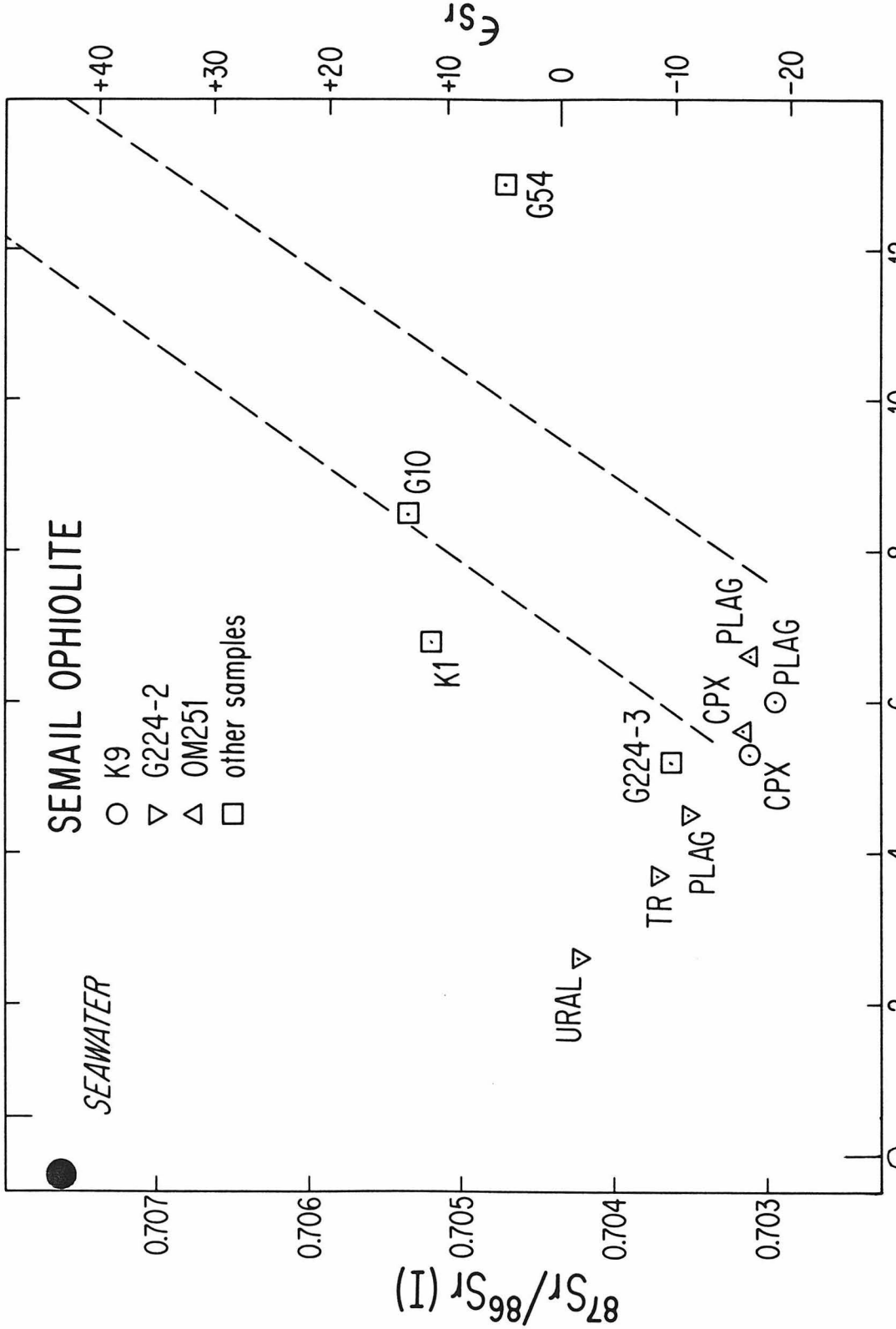
SEMAIL OPHIOLITE
K9
G224-2
OM251
other samples
SEAWATER
G10
K1
G54
G224-3
TR
PLAG
URAL
CPX
PLAG
CPX
PLAG
$^{87}Sr/^{86}Sr$ (I)
$\delta^{18}O$
ϵ_{Sr}
0.707
0.706
0.705
0.704
0.703
0
2
4
6
8
10
12
+40
+30
+20
+10
0
-10
-20

Fig. 10

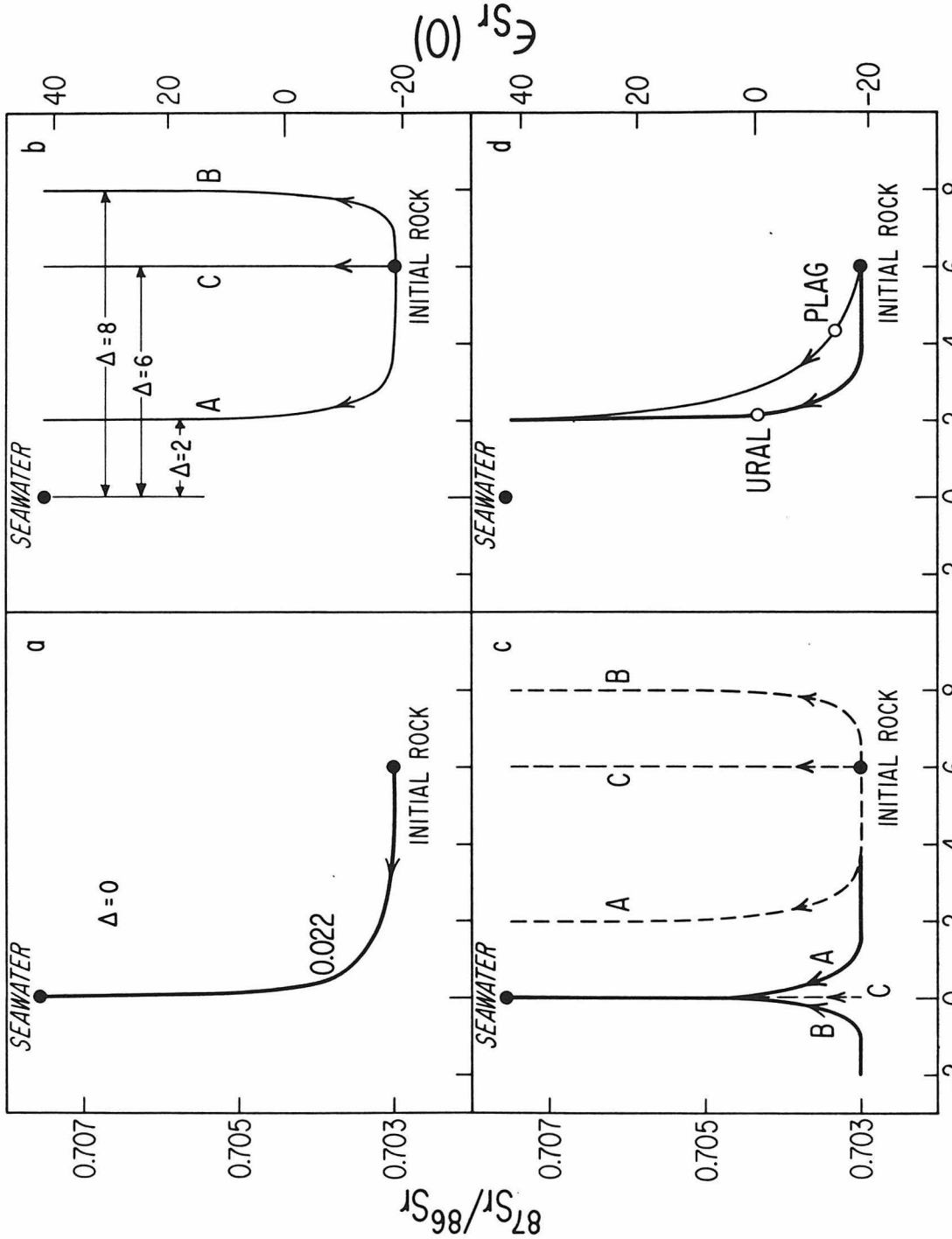
a
b
c
d
SEAWATER
INITIAL ROCK
Δ = 0
0.022
Δ = 8
Δ = 6
Δ = 2
A
B
C
URAL
PLAG
0.707
0.705
0.703
$^{87}Sr/^{86}Sr$
40
20
0
-20
ε_{Sr} (0)
8
6
4
2
0
-2
$\delta^{18}O$

Fig. 11

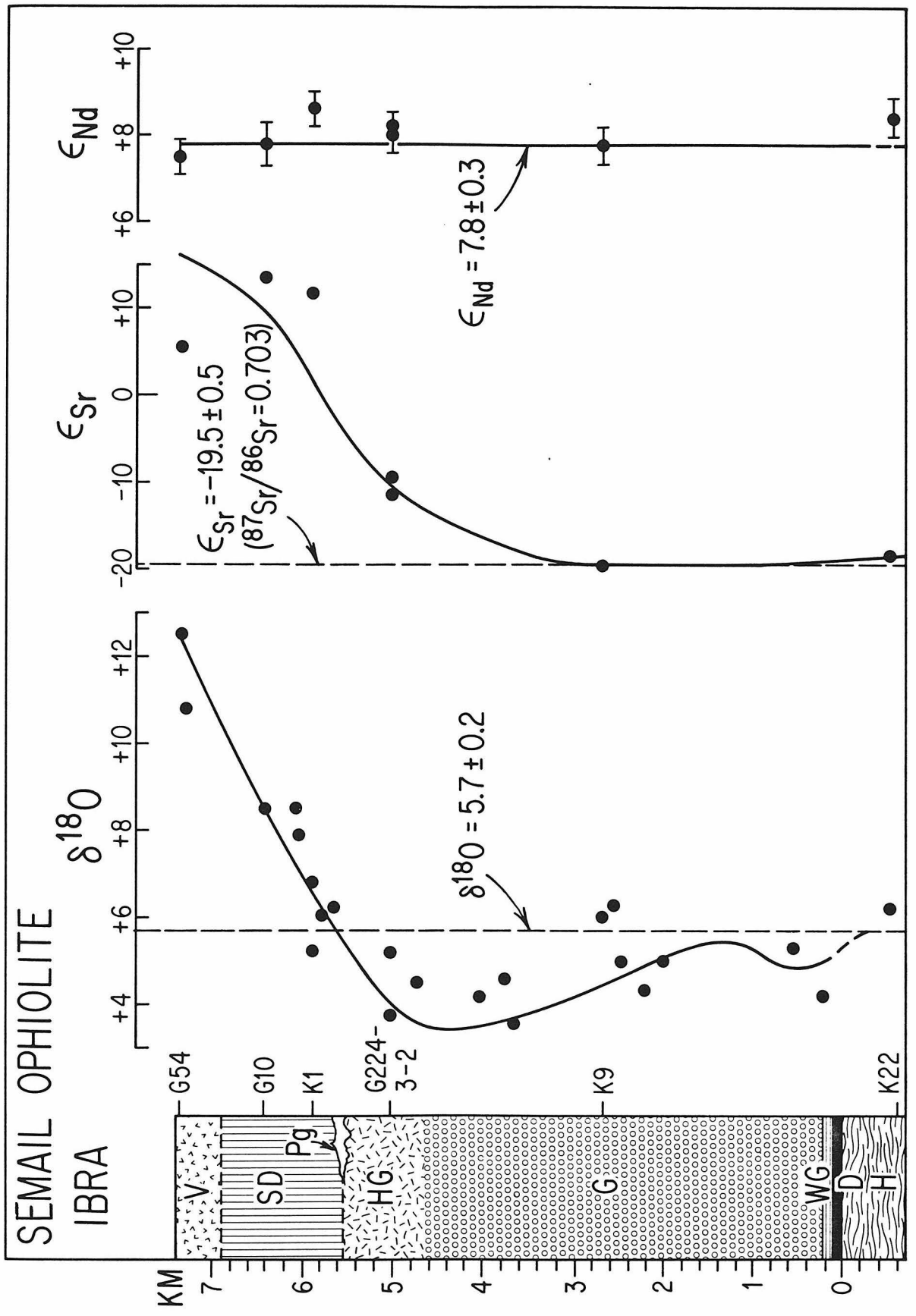
SEMAIL OPHIOLITE
IBRA
KM
7
6
5
4
3
2
1
0
V
SD
Pg
HG
G
WG
D
H
G54
G10
K1
G224-3-2
K9
K22
$\delta^{18}O$
+4
+6
+8
+10
+12
$\delta^{18}O = 5.7 \pm 0.2$
ϵ_{Sr}
-20
-10
0
+10
$\epsilon_{Sr} = -19.5 \pm 0.5$
$(^{87}Sr/^{86}Sr = 0.703)$
ϵ_{Nd}
+6
+8
+10
$\epsilon_{Nd} = 7.8 \pm 0.3$

Fig. 12

REFERENCES

1. R. G. Coleman, Plate tectonic emplacement of upper mantle peridotites along continental edges, J. Geophys. Res., 76 (1971) 1212.
2. J. F. Dewey and J. M. Bird, Origin and emplacement of the ophiolite suite: Appalachian ophiolites in Newfoundland, J. Geophys. Res. 76 (1971) 3179.
3. I. G. Gass, Is the Troodos massif of Cyprus a fragment of Mesozoic ocean floor? Nature 220 (1968) 39.
4. E. M. Moores and F. J. Vine, The Troodos Massif, Cyprus and other ophiolites as oceanic crust: Evaluation and implications, Phil. Trans. R. Soc. Lond. A. 268 (1971) 443.
5. W. R. Church, Ophiolite: Its definition, origin as oceanic crust, and mode of emplacement in orogenic belts, with special reference to the Appalachians, Canada Department of Energy, Mines and Resources Earth Physics Branch Publications 42 (1971) 71.
6. K. Muehlenbachs and R. N. Clayton, Oxygen isotope composition of the oceanic crust and its bearing on seawater, J. Geophys. Res. 81 (1976) 4365.
7. J. Veizer and W. Compston, $^{87}Sr/^{86}Sr$ composition of seawater during the Phanerozoic, Geochim. Cosmochim. Acta 38 (1974) 1461.
8. Z. E. Peterman, C. E. Hedge, and H. Tourtelot, Isotopic composition of Sr in seawater throughout Phanerozoic time, Geochim. Cosmochim. Acta 34 (1970) 105.
9. E. T. C. Spooner, The isotopic composition of seawater, and seawater-oceanic interaction, Earth Planet. Sci. Lett. 31 (1976) 1121.
10. R. G. Coleman, Ophiolites ancient oceanic lithosphere? Springer-Verlag (1977).

11. N. I. Christensen and M. H. Salisbury, Structure and constitution of the lower oceanic crust, Rev. Geophys. Space Physics 13 (1975) 57.

12. J. M. Mattinson, Early Paleozoic ophiolite complexes of Newfoundland: Isotopic ages of zircons, Geology 3 (1975) 181.

13. J. B. Saleeby, Fracture zone tectonics, continental margin fragmentation and emplacement of the Kings-Kaweah ophiolite belt, southwest Sierra Nevada, California, in R. G. Coleman and W. P. Irwin eds. North American ophiolites, Oregon Dept. Geol. Min. Indust. Bull. 95 (1977) 141.

14. H. P. Taylor, Jr., The oxygen isotope geochemistry of igneous rocks, Contrib. Mineral. Petrol. 19 (1968) 1.

15. D. G. Garlick and J. R. Dymond, Oxygen isotope exchange between volcanic materials and ocean water, Geol. Soc. Amer. Bull. 81 (1970) 2137.

16. K. Muehlenbachs and R. N. Clayton, Oxygen isotope studies of fresh and weathered submarine basalts, Can. J. Earth Sci. 9 (1972) 172.

17. Z. E. Peterman, R. G. Coleman, and R. A. Hildreth, $^{87}Sr/^{86}Sr$ in mafic rocks of the Troodos massif, Cyrpus, U.S. Geol. Surv. Prof. Pap. 750-D (1971) 157.

18. E. T. C. Spooner, R. D. Beckinsale, P. C. England, and A. Senior, Hydration, ^{18}O enrichment and oxidation during ocean floor hydrothermal meta-morphism of ophiolitic metabasic rocks from E. Liguria, Italy, Geochim. Cosmochim. Acta 41 (1977) 857.

19. E. T. C. Spooner, H. J. Chapman, and J. D. Smewing, Strontium isotopic contamination and oxidation during ocean floor hydrothermal

metamorphism of the ophiolitic rocks of the Troodos, Cyprus, Geochim. Cosmochim. Acta 41 (1977) 873.

20. H. J. Chapman and E. T. C. Spooner, ^{87}Sr enrichment of ophiolitic sulphide deposits in Cyprus confirms ore formation by circulating seawater, Earth Planet. Sci. Lett. 35 (1977) 71.

21. S. R. Hart, A. J. Erlank, and E. J. D. Kable, Sea floor basalt alteration: some chemical and Sr-isotopic effects, Contrib. Mineral. Petrol. 44 (1974) 219.

22. T. H. E. Heaton and S. M. F. Sheppard, Hydrogen and oxygen isotope evidence for sea-water-hydrothermal alteration and ore deposition, Troodos complex, Cyprus, in: Volcanic processes in ore genesis (Institution of Mining Metallurgy and Geological Society, London), (1977) 42.

23. D. B. Wenner and H. P. Taylor, Oxygen and hydrogen isotope studies of the serpentinization of ultramafic rocks in oceanic environments and continental ophiolite complexes, Am. J. Sci. 273 (1973) 207.

24. M. Magaritz and H. P. Taylor, Jr., Oxygen and hydrogen studies of serpentinization in the Troodos Ophiolite Complex, Cyprus, Earth Planet. Sci. Lett. 23 (1974) 8.

25. M. Magaritz and H. P. Taylor, Oxygen, hydrogen, and carbon isotope studies of the Franciscan formation, Coast Ranges, California, Geochim. Cosmochim. Acta 40 (1976) 215.

26. R. G. Coleman and Z. E. Peterman, Oceanic Plagiogranite, J. Geophys. Res. 80 (1975) 1099.

27. C. L. Chou, H. J. Lo, J. H. Chen, and V. C. Juan, Rare earth element and isotopic geochemistry of Kuanshan igneous complex, Taiwan, Proc. Geol. Soc. China 21 (1978) 13.

28. C. R. Stern, M. J. deWit, and J. R. Lawrence, Igneous and metamorphic processes associated with the formation of Chilean ophiolites and their implication for ocean floor metamorphism, seismic layering, and magnetism, J. Geophys. Res. 81 (1976) 4370.

29. M. A. Lanphere, Strontium isotopic relations in the Canyon Mountain, Oregon and Red Mountain, California ophiolites, Trans. Am. Geophys. Union 54 (1973) 1220.

30. R. W. Kay and R. G. Senechal, The rare earth geochemistry of the Troodos ophiolite complex, J. Geophys. Res. 81 (1976) 964.

31. J. D. Smewing, K. O. Simonian, and I. G. Gass, Meta-basalts from the Troodos Massif, Cyprus: Genetic implication deduced from petrography and trace element geochemistry, Contrib. Mineral. Petrol. 51 (1975) 49.

32. J. D. Smewing and P. J. Potts, Rare-earth abundances in basalts and metabasalts from the Troodos Massif, Cyprus, Contrib. Mineral. Petrol. 57 (1976) 245.

33. J. A. Pearce, Basalt geochemistry used to investigate past tectonic environments on Cyprus, Tectonophysics 25 (1975) 41.

34. P. Richard, D. Rousseau, and C. J. Allegre, Nd and Sr systematics in ophiolites, Short papers of the 4th internat. conf. geochron. cosmochron. isotope geol. Geol. Surv. Open-File report 78-701 (1978) 350.

35. D. J. DePaolo and G. J. Wasserburg, Inferences about magma sources and mantle structure from variations of $^{143}Nd/^{144}Nd$, Geophys. Res. Lett. 3 (1976) 743.

36. D. J. DePaolo and G. J. Wasserburg, Nd isotopic variations and petrogenetic models, Geophys. Res. Lett. 3 (1976) 249.

37. R. K. O'Nions, P. J. Hamilton, and N. M. Evensen, Variations in $^{143}Nd/^{144}Nd$ and $^{87}Sr/^{86}Sr$ ratios in oceanic basalts, Earth and Planet. Sci. Lett. 34 (1977) 13.

38. P. Richard, N. Shimizu, and C. J. Allegre, $^{143}Nd/^{146}Nd$, a natural tracer: An application to oceanic basalts, Earth Planet. Sci. Lett. 31 (1976) 269.

39. B. M. Reinhardt, On the genesis and emplacement of ophiolites in the Oman Mountains geosyncline, Schweizer. Mineralog. Petrog. Mitt. 49 (1969) 1.

40. F. Allemann and T. J. Peters, The ophiolite-radiolarite belt of the North-Oman Mountains: Eclogae Geol. Helvetiae 65 (1972) 657.

41. K. W. Glennie, M. G. A. Boeuf, M. W. Hughes Clarke, M. Moody-Stuart, W. F. H. Pilaar, and B. M. Reinhardt, Late Cretaceous nappes in Oman Mountains and their geologic evolution, Am. Assoc. Petr. Geol. Bull. 57 (1973) 5.

42. K. W. Glennie, M. G. A. Boeuf, M. W. Hughes-Clarke, M. Moody-Stuart, W. F. H. Pilaar, and B. M. Reinhardt, Geology of the Oman Mountains, Geol. Mijb. Gen. Ver. Verh. 31 (1974) 423.

43. E. H. Bailey, R. G. Coleman, C. A. Hopson, J. S. Pallister, and R. T. Gregory, Geologic section through the Semail ophiolite in the Ibra region, southeastern Oman Mountains, in preparation.

44. R. T. Gregory and H. P. Taylor, Jr., $^{18}O/^{16}O$ variations in gabbro, diabase and volcanic sections in Semail ophiolite, southeastern Oman Mountains and the nature of hydrothermal alteration in the oceanic crust, Abstracts, International Ophiolite Symposium Nicosia-Cyprus (1979) 32.

45. R. T. Gregory and H. P. Taylor, Jr., An oxygen isotope profile in a section of Cretaceous oceanic crust, Semail Ophiolite, Oman: evidence for $\delta^{18}O$-buffering of the oceans by deep (> 5 km) seawater-hydrothermal circulation at mid-ocean ridges, J. Geophys. Res., companion paper this issue.

46. R. T. Gregory and H. P. Taylor, Jr., Oxygen isotope and field studies applied to the origin of oceanic plagiogranites, Abstracts, International Ophiolite Symposium Nicosia-Cyprus (1979).

47. H. P. Taylor, Jr. and S. Epstein, Relationship between $^{18}O/^{16}O$ ratios in coexisting minerals of igneous and metamorphic rocks. Part 1: Principles and experimental results, Geol. Soc. Am. Bull. 73 (1962) 461.

48. D. A. Papanastassiou and G. J. Wasserburg, Initial strontium isotopic differences and the resolution of small time differences in the formation of planetary objects, Earth Planet. Sci. Lett. 5 (1969) 361.

49. H. P. Taylor and R. W. Forester, An oxygen and hydrogen isotope study of the Skaergaard intrusion and its country rocks: A description of a 55-m.y. old fossil hydrothermal system, J. Petrology (in press).

50. H. Craig, Isotopic variations in meteoritic waters, Science 133 (1961) 1702.

51. M. J. O'Hara, Non-primary magmas and dubious mantle plume beneath Iceland, Nature 243 (1973) 507.

52. M. J. O'Hara, Geochemical evolution during fractional crystallisation of a periodically refilled magma chamber, Nature 266 (1977) 503.

53. C. A. Hopson and J. S. Pallister, Semail ophiolite magma chamber: I, Evidence from gabbro phase variation, internal structure and layering, Abstracts, International Ophiolite Symposium Nicosia-Cyprus 1979) 37.

54. J. S. Pallister and C. A. Hopson, Semail ophiolite magma chamber: II, Evidence from the cryptic variation and mineral chemistry, Abstracts, International Ophiolite Symposium Nicosia-Cyprus (1979) 38.

55. M. A. Dungan and J. M. Rhodes, Residual glasses and melt inclusions in basalts from DSDP Legs 45 and 46: Evidence for magma mixing, Contrib. Mineral. Petrol. 67 (1978) 417.

56. E. M. Moores, Petrology and structure of the Vourinos ophiolite complex, northern Greece: Geol. Soc. America Spec. Paper, 118 (1969).

57. E. D. Jackson, The cyclic unit in layered intrusions, Geol. Soc. South Africa Spec. Pub. 1 (1970) 391.

58. E. D. Jackson, Ultramafic cumulates in the Stillwater, Great Dyke, and Bushveld intrusion, in Ultramafic and related rocks, P. J. Wyllie ed.; New York, John Wiley and Sons, Inc. (1961) 20.

59. J. D. Smewing, K. O. Simonian, I. M. Elboushi, and I. G. Gass, Mineralized fault zone parallel to the Oman ophiolite spreading axis, Geology 5 (1977) 534.

60. I. G. Gass and J. D. Smewing, Intrusion, extrusion and metamorphism at constructive margins: evidence from the Troodos massif, Cyprus, Nature 242 (1973) 26.

61. R. A. Hart, Chemical exchange between seawater and deep ocean basalts, Earth Planet. Sci. Lett. 9 (1970) 269.

62. S. R. Hart, K, Rb, Sc, Sr, and Sr isotope ratios of ocean floor basalts, Phil.Trans. R. Soc. Lond. A. 268 (1971) 57.

63. J. D. Macdougall, R. C. Finkel, J. Carlson, and S. Krishnaswami, Isotopic evidence for uranium exchange during low-temperature alteration of oceanic basalt, Earth Planet. Sci. Lett. 42 (1979) 27.

64. W. E. Seyfried, W. C. Shanks, and W. E. Dibble, Clay mineral formation in DSDP leg 34 basalt, Earth Planet. Sci. Lett. 41 (1978) 265.

65. J. B. Corliss, J. Dymond, L. J. Gordon, J. M. Edmond, R. P. von Herzen, R. D. Ballard, K. Green, D. Williams, A. Bainbridge, K. Crane, T. H. van Andel, Submarine thermal springs on the Galapagos rift, Science 203 (1979) 1073.

66. A. E. J. Engel, C. G. Engel, and R. G. Havens, Chemical characteristics of oceanic basalts and the upper mantle, Geol. Soc. Am. Bull. 76 (1965) 719.

67. M. Tatsumoto, C. E. Hedge, and A. E. J. Engel, Potassium, rubidium, strontium, thorium, uranium, and the ratio of Sr-87 to Sr-86 in oceanic tholeiitic basalt, Science 150 (1965) 886.

68. R. W. Kay, N. J. Hubbard, and P. W. Gast, Chemical characteristics and origin of ocean ridge volcanic rocks, J. Geophys. Res. 75 (1970) 1585.

69. R. W. Kay, Trace elements in ocean ridge basalts, Earth Planet. Sci. Lett. 38 (1978) 95.

70. J. G. Schilling, Sea-floor evolution: rare-earth evidence, Phil. Trans. Roy. Soc. Lond. A. 268 (1971) 663.

71. C. J. Allegre, R. Montigny, and Y. Bottinga, Cortege ophiolitique et cortege oceanique, geochimie comparee et mode degenese. Bull. Soc. Geol. France 15 (1973) 461.

72. R. Montigny, H. Bougault, Y. Bottinga, and C. J. Allegre, Trace element geochemistry and genesis of the Pindos ophiolite suite, Geochim. Cosmochim. Acta 37 (1973) 2135.

73. M. Loubet, N. Shimizu, and C. J. Allegre, Rare earth elements in alpine peridotites, Contrib. Mineral. Petrol. 53 (1972) 1.

74. D. J. DePaolo and G. J. Wasserburg, The sources of island arcs as indicated by Nd and Sr isotopic studies, Geophys. Res. Lett. 4 (1977) 465.

75. R. K. O'Nions, S. R. Carter, R. S. Cohen, N. M. Evensen, and P. J. Hamilton, Pb, Nd, and Sr isotopes in oceanic ferromanganese deposits and ocean floor basalts, Nature 273 (1978) 435.

76. D. J. Piepgras, G. J. Wasserburg, and E. J. Dasch, The isotopic composition of Nd in different ocean masses, submitted to Science (1979).

77. R. W. Carlson, J. D. Macdougall, and G. W. Lugmair, Differential Sm/Nd evolution in oceanic basalts, Geophys. Res. Lett. 5 (1978)229.

78. C. J. Hawkesworth, R. K. O'Nions, R. J. Pankhurst, P. J. Hamilton, and N. M. Evensen, A geochemical study of island-arc and back-arc tholeiites from the Scotia Sea, Earth Planet. Sci. Lett. 36 (1977) 253.

79. G. J. Wasserburg and D. J. DePaolo, Nd in flood basalts from the Siberian platform and models of earth structure, submitted to Contrib. Mineral. Petrol. (1979).

80. M. T. McCulloch and G. J. Wasserburg, Sm-Nd and Rb-Sr chronology of continental crust formation, Science 200 (1978) 1003.

81. F. Boudier and R. G. Coleman, Cross section through the peridotite in the Semail ophiolite, Oman, Abstracts, International Ophiolite Symposium Nicosia-Cyprus (1979) 18.

82. R. L. Armstrong and H. J. B. Dick, A model for the development of thin overthrust sheets of crystalline rock, Geology 2 (1974) 35.

83. D. P. McKenzie and J. G. Sclater, Heat flow inside the island arcs of the northwestern Pacific, J. Geophys. Res. 73 (1968) 3173.

84. E. R. Oxburgh and D. L. Turcotte, Thermal structure of island arcs, Geol. Soc. Am. Bull. 81 (1970) 1665.

85. J. F. Dewey and J. M. Bird, Origin and emplacement of the ophiolite suite: Appalachian ophiolites in Newfoundland, J. Geophys. Res. 76 (1971) 3179.

86. M. M. Menzies and V. R. Murphy, Strontium isotope geochemistry of Alpine tectonite lherzolites: data compatible with a mantle origin, Earth Planet. Sci. Lett. 38 (1978) 346.

87. C. Brooks, S. R. Hart, A. Hofmann, and D. E. James, Rb-Sr mantle isochrons from oceanic regions, Earth Planet. Sci. Lett. 32 (1976) 51.

88. C. E. Hedge, Strontium isotopes in basalts from the Pacific Ocean basin, Earth Planet. Sci. Lett. 38 (1978) 88.

89. W. M. White and J. G. Schilling, The nature and origin of geochemical variation in Mid-Atlantic ridge basalts from the central north Atlantic, Geochim. Cosmochim. Acta 42 (1978) 1501.

90. S. S. Sun and G. N. Hanson, Evolution of the mantle: geochemical evidence from alkali basalt, Geology 3 (1975) 297.

91. R. A. Duncan and W. Compston, Sr-isotopic evidence for an old mantle source region for French Polynesian volcanism, Geology 4 (1976) 728.

92. D. J. Whitford, W. Compston, I. A. Nicholls, and M. J. Abbott, Geochemistry of late Cenozoic lavas from eastern Indonesia, Role of subducted sediments in petrogenesis, Geology 5 (1977) 571.

93. E. D. Goldberg, Minor elements in sea water, in: Riley J. P., Skirrow, G. (eds.): Chemical Oceanograph, vol. 1, New York, Academic Press (1965) 162.

94. H. P. Taylor, Jr., The application of oxygen and hydrogen isotope studies to problems of hydrothermal alteration and ore deposition, Econ. Geol. 69 (1974) 843.

95. R. Vollmer, Rb-Sr and U-Th-Pb systematics of alkaline rocks: the alkaline rocks from Italy, Geochim. Cosmochim. Acta 40 (1976) 283.

96. C. H. Langmuir, R. D. Vocke, G. N. Hanson, and S. R. Hart, A general mixing equation with applications to Icelandic basalts, Earth Planet. Sci. Lett. 37 (1978) 380.

97. D. J. DePaolo and G. J. Wasserburg, Petrogenetic mixing models and Nd-Sr isotopic patterns, Geochim. Cosmochim. Acta 43 (1979) 615.

98. H. P. Taylor, Water/rock interactions and the origin of H_2O in granitic batholiths, J. Geol. Soc. Lond. 133 (1977) 509.

99. D. Norton and H. P. Taylor, Jr., Quantitative simulation of the hydrothermal systems of crystallizing magmas on the basis of transport theory and oxygen isotope data: An analysis of the Skaergaard intrusion. J. Petrology (in press).

100. T. H. Green and A. E. Ringwood, Genesis of the calcalkaline igneous rock suite, Contrib. Mineral. Petrol. 18 (1968) 105.

101. T. H. Green, Crystallization of calc-alkaline andesite under controlled high-pressure hydrous conditions, Contrib. Mineral. Petrol. 34 (1972) 150.

102. A. E. Ringwood, The petrological evolution of island arc systems, J. Geol. Soc. London 130 (1974) 183.

103. I. A. Nicholls, Liquids in equilibrium with peridotitic mineral assemblages of high water pressures, Contrib. Mineral. Petrol. 45 (1974) 289.

104. H. P. Taylor Jr. and L. T. Silver, Oxygen isotope relationships in plutonic igneous rocks of the peninsular ranges batholith, southern and Baja California, Short papers of the 4th internat. conf. geochron. cosmochron. isotope geol. Geol. Surv. Open-File report 78-701 (1978) 423.

105. M. Magaritz, D. J. Whitford, and D. E. James, Oxygen isotopes and the origin of high $^{87}Sr/^{86}Sr$ andesites, Earth Planet. Sci. Lett. 40 (1978) 220.

106. W. Seyfried and J. L. Bischoff, Hydrothermal transport of heavy metals by seawater: The role of seawater/basalt ratio, Earth Planet. Sci. Lett. 34 (1977) 71.

APPENDIX 4

A NEODYMIUM, STRONTIUM, AND OXYGEN ISOTOPIC STUDY OF THE CRETACEOUS SAMAIL OPHIOLITE AND IMPLICATIONS FOR THE PETROGENESIS AND SEAWATER-HYDROTHERMAL ALTERATION OF OCEANIC CRUST

[1]Malcolm T. McCulloch, Robert T. Gregory,
[1]G. J. Wasserburg, and Hugh P. Taylor, Jr.

Division of Geological and Planetary Sciences
California Institute of Technology
Pasadena, California 91125

[1]The Lunatic Asylum of the Charles Arms Laboratory
Division Contribution No. 3309 (325)

ABSTRACT

In the Samail Ophiolite, ^{147}Sm-^{143}Nd, ^{87}Rb-^{87}Sr, and $^{18}O/^{16}O$ isotopic systems have been used to distinguish between sea-floor hydrothermal alteration and primary magmatic isotopic variations. The Rb-Sr and $^{18}O/^{16}O$ isotopic systems clearly exhibit sensitivity to hydrothermal interactions with seawater while the Sm-Nd system appears essentially undisturbed. Internal isochrons have been determined by the ^{147}Sm-^{143}Nd method using coexisting plagioclase and pyroxene and give crystallization ages of 130 $\pm$ 12 m.y. from Ibra and 100 $\pm$ 20 m.y. from Wadi Fizh. These ages are interpreted as the time of formation of the Samail oceanic crust and are older than the inferred emplacement age of 65 - 85 m.y. The initial $^{143}Nd/^{144}Nd$ ratios for a tectonized harzburgite, cumulate gabbros, plagiogranite, sheeted dikes and a basalt have a limited range in ε_{Nd} of from 7·5 to 8·6 for all lithologies, demonstrating a clear oceanic affinity and supporting earlier interpretations based on geologic observations and geochemistry. The $^{87}Sr/^{86}Sr$ initial ratios on the same rocks have an extremely large range of from 0.70296 to 0.70650 (ε_{Sr} = -19.7 to +30.5) and the $\delta^{18}O$ values vary from 2.6 to 12.7. These large variations are clearly consistent with hydrothermal interaction of seawater with the oceanic crust. A model is presented for the closed system exchange of Sr and O, that in principle illustrates how the Sr isotopic data may be utilized to estimate the water/rock ratio and subsequently used to evaluate the temperature of equilibration between the water and silicates from the $^{18}O/^{16}O$ water-rock fractionation.

1.0 Introduction

This report presents the results of a neodymium, strontium and oxygen isotopic study of a profile through Cretaceous oceanic crust, as represented by the Samail Ophiolite, Oman. The Samail ophiolite consists of (from bottom to top) tectonized peridotite (dominantly harzburgite), layered gabbro, sheeted dikes, pillow basalts, and pelagic sediments. These rocks represent allochthonous fragments of oceanic crust and upper mantle that were emplaced upon the Arabian continental margin in the late Cretaceous [1-4]. The Samail ophiolite crops out in a desert region and, therefore, provides a unique opportunity to study in detail an exceptionally well exposed and preserved cross section of oceanic crust. The characterization of oceanic crust is important as it presently represents over two thirds of Earth's surface and because nearly all of the oceanic crust created over Earth's history has been recycled into the mantle at zones. This recycling of oceanic crust probably has had profound effects both on the geochemical evolution of the mantle and on the composition of island arcs and active continental margins. In addition, during the course of geologic time, the isotopic composition of oxygen and strontium in seawater has been affected strongly by hydrothermal interaction with the oceanic crust [5-8].

The aims of this present study are:

a). To determine the crystallization age of this complex by using Sm-Nd mineral isochrons;

b). To determine the initial Nd and Sr ratios of the magma source which produced the Samail ophiolite and to compare these with

possible modern-day analogues such as mid-ocean ridge basalts (MORB), island arcs and back arc basins;

c). To compare the effects of seawater-hydrothermal alteration on the Nd, Sr and O isotopic systems. A more comprehensive report of the results of these studies will be published elsewhere (Gregory and Taylor [9], and McCulloch et al. [10]).

Isotopic studies of a few other ophiolite complexes have been reported [11 - 19] with the Troodos massif of Cyprus at present being one of the better documented examples. $^{18}O/^{16}O$ [13, 14], $^{87}Sr/^{86}Sr$ [11, 15, 16] and trace and major elements studies [12, 20 - 22] confirm its similarity to oceanic crust and identify the effects of seawater circulation in the pillow basalts, sheeted dikes, and uppermost gabbro complexes. As seawater also has largely altered the primary $^{87}Sr/^{86}Sr$ ratios, it has therefore not been possible to infer genetic relations between the different units within the complex using Sr isotopic data. A preliminary Nd isotopic study by Richard et al. [23] of single whole-rock gabbro samples from the Troodos, Samail, and several other ophiolite complexes has shown that the measured $^{143}Nd/^{144}Nd$ ratios are similar to those found in young ocean floor basalts.

2.0 Geology and Sampling

The Samail ophiolite forms a major part of the 700 km long arcuate Oman Mountains on the eastern edge of the Arabian Peninsula (Fig. 1). Individual members of the ophiolite pseudostratigraphy are essentially internally undeformed [1] and have thicknesses comparable to geophysical estimates of modern-day oceanic crust [24].

The Samail ophiolite formed during Cretaceous spreading in the Hawasina ocean basin, which was a portion of the Tethys seaway [2,3].

A minimum age for the emplacement of the ophiolite is provided by Maestrichtian-Tertiary shallow-water limestones, which unconformably overlie parts of the ophiolite. A maximum age is given by Campanian sediments which underlie the ophiolite [3]. These constraints are consistent with K-Ar ages of 83 ± 5 m.y. [25] from metamorphic biotites in amphibolites from the contact aureole at the base of the Samail thrust sheet. Until now, no radiometric age determinations on any of the ophiolite members have been reported, although Glennie and others [3] estimated a minimum crystallization age based on middle to late Cretaceous sediments which overlie the pillow lavas in northern Oman.

Samples representing the different lithologic units were chosen on the basis of their oxygen isotopic properties as described by Gregory and Taylor [9, 26]. Most of these samples were collected from one of the standard ophiolite sections near Ibra as part of a cooperative study led by C. A. Hopson and R. G. Coleman. A detailed geologic map of the Ibra section in southeastern Oman Mountains has been prepared by Hopson, Coleman, Bailey, Pallister, and Gregory [27].

G54 is a microphyric basalt from the pillow lava section which exhibits igneous textures despite extensive recrystallization during hydrothermal alteration in the zeolite facies. The mineralogy and oxygen isotopic composition of the whole rock ($\delta^{18}O = 12.7$), are consistent with low temperature alteration by a hydrothermal fluid derived from seawater. G10 and K1 are from the sheeted dike complex; they have an ophitic texture and have been hydrothermally altered under greenschist facies conditions (K1 whole rock $\delta^{18}O = 6.8$, and G10 whole rock $\delta^{18}O = 8.5$). G224-3 is a plagiogranite with a granophyric texture and consists of plagioclase, hornblende, quartz,

magnetite and trace amounts of apatite. Hornblende is altered partially to chlorite. This plagiogranite was collected from an unchilled dike which cross-cuts the uralite gabbro G224-2, approximately 500 meters below the gabbro-diabase contact. The gabbro G224-2 contains poikilitic hornblende enclosing zoned plagioclase laths; alteration products include both chlorite and fibrous amphibole pseudomorphs after hornblende and rare retrograde prehnite. The mineralogy and oxygen isotope data of G224-2 (whole rock $\delta^{18}O = 3.7$, plagioclase $\delta^{18}O = 4.5$ and uralite $\delta^{18}O = 2.6$) suggest relatively high temperatures of alteration (>400°C). K9 is a sample from the cumulate gabbros and consists predominantly of cumulate plagioclase, clinopyroxene, and olivine. Trace amounts of brown hornblende are present as a minor alteration product of the clinopyroxene. This sample was chosen for Rb-Sr and Sm-Nd analysis as the mineralogy and oxygen data (whole rock $\delta^{18}O = 5.8$, plagioclase $\delta^{18}O = 6.0$ and clinopyroxene $\delta^{18}O = 5.3$) indicate that this is one of the least altered samples.

To check for possible isotopic and age variations, two additional gabbros (OM251 and OM28) were analyzed from widely spaced areas north of the Samail gap. OM251 is from Wadi Fizh (Fig. 1) and consists of cumulate plagioclase, clinopyroxene, and a minor amount of cumulate olivine. Although the olivine is partially serpentinized, the oxygen data (plagioclase $\delta^{18}O = 6.4$ and clinopyroxene $\delta^{18}O = 5.8$) indicate that these minerals have exchanged only slightly. OM28 is a cumulate gabbro from the Rustaq area (Fig. 1) containing plagioclase and clinopyroxene. Olivine has been replaced by serpentine and talc. Secondary amphibole is also present. The oxygen data for OM28 (whole rock $\delta^{18}O = 5.2$ and plagioclase $\delta^{18}O = 4.7$)

indicate significant exchange of plagioclase and clinopyroxene with seawater. To test the hypothesis that the basal peridotite is residual upper mantle produced by partial melting and separation of a basaltic liquid, a tectonized harzburgite (K22) from Ibra was analyzed. This sample consists of olivine, orthopyroxene, trace amounts of spinel, and serpentine pseudomorphing olivine.

3.0 Results and Discussion

Oxygen was extracted and analyzed using the procedures outlined by Taylor and Epstein [28]. Detailed descriptions of the chemical and mass spectrometric procedures for Nd and Sr are given by Papanastassiou et al. [29].

The oxygen results are reported in δ-notation in parts per 10^3 where: $\delta^{18}O = \left[(^{18}O/^{16}O)_{sample} / (^{18}O/^{16}O)_{standard} - 1 \right] 10^3$

Following DePaolo and Wasserburg [30,31] an analogous notation is used for Nd with the initial $^{143}Nd/^{144}Nd$ ratio of a rock of age T reported in the ε-notation in parts per 10^4 where:

$$\varepsilon_{Nd} = \left[(^{143}Nd/^{144}Nd)^{T}_{INIT} / (^{143}Nd/^{144}Nd)^{T}_{CHUR} - 1 \right] 10^4$$

and

$$(^{143}Nd/^{144}Nd)^{T}_{CHUR} = (^{143}Nd/^{144}Nd)^{0}_{CHUR} - (^{147}Sm/^{144}Nd)^{0}_{CHUR} (e^{\lambda_{Sm} T} - 1).$$

Present-day reference values are $(^{143}Nd/^{144}Nd)^{0}_{CHUR} = 0.511836$, and $(^{147}Sm/^{144}Nd)^{0}_{CHUR} = 0.1936$ [30]; $\lambda_{Sm} = 6.54 \times 10^{-12} yr.^{-1}$. $(^{143}Nd/^{144}Nd)^{T}_{INIT}$ is the measured ratio in the rock, corrected for decay since the time of crystallization T. An equivalent notation is used for Sr with $(^{87}Sr/^{86}Sr)^{0}_{UR} = 0.7045$, $(^{87}Rb/^{86}Sr)^{0}_{UR} = 0.0827$ [31,40], and $\lambda_{Rb} = 1.42 \times 10^{-11}$ yr.$^{-1}$.

3.1 Crystallization Age and Initial Nd

In an attempt to determine the crystallization age of the Samail ophiolite, we have analyzed Sm and Nd in coexisting mineral phases from the gabbros. In principle Sm-Nd ages can be obtained from the major minerals plagioclase and clinopyroxene. These minerals differ greatly in their Sm/Nd ratios and are common constituents of all gabbros, unaltered diabases and phyric basalts. Using other conventional techniques it often is difficult to determine the crystallization ages of mafic or ultramafic rocks due to lack of adequate parent-daughter fractionation, later thermal disturbances, or contamination by seawater. A possible exception is U-Pb zircon dating of siliceous late-stage differentiates. However these bodies are volumetrically insignificant, not present everywhere, and their relationship to the mafic or ultramafic rocks is sometimes controversial [32, 33]. The success of the Sm-Nd technique for the dating of mafic rocks has been demonstrated by Lugmair [34, 35] Papanastassiou et al. [29] and Nakamura et al. [36] for meteoritic and lunar rocks and by Hamilton et al. [37, 38] and DePaolo and Wasserburg [39] for terrestrial rocks.

In Table 1 and Fig. 2, the results of the analysis of whole rocks and mineral separates of plagioclase, clinopyroxene and uralite from gabbros are shown. The data form two approximately linear arrays. The upper array is defined by two gabbros K9 and G224-2 from the Ibra locality. The gabbro K9 is extremely fresh with only clinopyroxene exhibiting minor alteration to brown hornblende. The clinopyroxene from K9 has a significantly higher Sm/Nd and $^{143}Nd/^{144}Nd$ ratio than the coexisting plagioclase; together they indicate a crystallization age of 128 $\pm$ 20 m.y. with an initial $^{143}Nd/^{144}Nd$ ratio of $\varepsilon_{Nd} = 7.7 \pm 0.3$.

The other gabbro (G224-2) is from the upper part of the same gabbro unit as K9. This gabbro contains uralite as a late - stage replacement of both pyroxene and primary hornblende. The uralite has the highest $^{147}Sm/^{144}Nd$ and $^{143}Nd/^{144}Nd$ ratios for this rock, and together with the plagioclase gives an age of 150 $\pm$ 40 m.y. and an initial $^{143}Nd/^{144}Nd$ ratio of $\varepsilon_{Nd} = 7.8 \pm 0.4$. The larger uncertainty in the age for this gabbro compared to K9 is due to the smaller difference in the $^{147}Sm/^{144}Nd$ ratios for the plagioclase and uralite. Both gabbros have the same age and initial ratio within analytical uncertainty,and the Sm-Nd systematics do not appear to be disturbed by the presence of hydrous alteration products such as uralite. The combined data are shown in Fig. 2 and give a crystallization age of 130 $\pm$ 12 m.y. and $\varepsilon_{Nd} = 7.8 \pm 0.2$.

The lower array shown in Fig. 2 is defined by the gabbros OM251 and OM28. These two gabbros were collected from Wadi Fizh and Rustaq,which are located north of the Samail gap (Fig. 1). The clino-pyroxene and plagioclase from OM251 give an age of 100 $\pm$ 20 m.y. and an $\varepsilon_{Nd} = 7.6 \pm 0.3$. Although the isochron ages from Ibra and Wadi Fizh overlap within analytical uncertainty, the Sm-Nd results suggest that there may be an age difference of approximately 30 m.y. between these two areas. More precise measurements will be required for this to be established definitively, but the present results clearly indicate that these rocks crystallized in the time interval from 100 m.y. to 130 m.y. These crystallization ages are greater than the time of emplacement of the Samail ophiolite onto the Oman continental margin which occurred between 65 m.y. to 85 m.y. [25]. This suggests that relatively mature ($>$ 15 m.y old) oceanic crust was obducted.

The initial $^{143}Nd/^{144}Nd$ ratios from the gabbros, together with those determined from a plagiogranite, sheeted dikes, basalt and a

tectonized harzburgite from the peridotite, are shown in the histogram in Fig. 3. The latter samples are all from the Ibra area and their initial ratios were calculated assuming a crystallization age of 130 m.y. Most of the samples have ε_{Nd} values within an extremely narrow range of from 7.5 to 8.2 (Table 1), indicating derivation from an isotopically uniform light REE depleted (depleted in Nd relative to Sm) source region. The sheeted dike K1 has $\varepsilon_{Nd} = 8.6 \pm 0.4$ compared to the mean ε_{Nd} of 7.8 ± 0.2 for the Ibra gabbros. This small deviation in ε_{Nd} of K1 cannot be explained by seawater alteration as more altered samples have consistent ε_{Nd} values, but it suggests the presence of small but significant isotopic heterogeneities in the oceanic mantle magma reservoirs.

The initial value of $\varepsilon_{Nd} = 8.3 \pm 0.4$ obtained from the tectonized harzburgite is also, within error, the same as the rest of the ophiolite. This result, together with the low trace element concentrations (Table 1), supports the hypothesis that the harzburgite is probably a cogenetic upper mantle residue produced by partial melting and removal of a basaltic liquid from which the rest of the ophiolite section formed.

In Fig. 3 the ε_{Nd} values from the Samail ophiolite are compared with those found in MORB (+7 to +13), marginal basins (+8 to +9), island arcs (+7 to +10), ocean islands (+4 to +8) and continental basalts ($\sim$0). The ε_{Nd} values from the Samail ophiolite clearly have an oceanic affinity. The Nd isotopic data alone cannot be used to distinguish definitively among the various possible tectonic settings for this ophiolite because of the overlap in ε_{Nd} between MORB, marginal basins, island arcs and to a lesser degree ocean islands (Fig. 3). However, the lack of light REE enriched samples [10, 47] and of widespread alkalic volcanism usually associated with ocean island and island arc environments plus geologic arguments [27] suggests that

the most reasonable scenario for the formation of the Samail ophiolite is at a ridge axis spreading center in an ocean basin.

The initial Nd value of the Samail ophiolite with an average of $\varepsilon_{Nd} = 7.9 \pm 0.2$, is somewhat lower than the "typical" MORB with $\varepsilon_{Nd} \simeq 10$. To some extent this is due to its older age compared to the zero age MORB samples shown in Fig. 3. A more exact comparison requires correction for the evolution of Nd in the Samail ophiolite source region during the past 130 m.y. Assuming that the composite of the cumulate gabbros, diabase dikes, and pillow basalts represents the primary unfractionated magma of the Samail ophiolite, we estimate [10] that this magma had $^{147}Sm/^{144}Nd = 0.24 \pm 0.02$. This also probably represents the $^{147}Sm/^{144}Nd$ ratio in the source region, as both Nd and Sm are strongly partitioned into the melt during partial melting. For this value of $^{147}Sm/^{144}Nd$, the Samail ophiolite source region today would have $\varepsilon_{Nd} \simeq 8.8$ which is only 1 ε_{Nd} unit below the center of the present MORB distribution and is therefore fully consistent with a MORB affinity. The lower ε_{Nd} value of the Samail ophiolite compared to typical MORB indicates derivation from a slightly less light REE depleted oceanic mantle source.

3.2 Comparison of Nd and Sr

A striking contrast exists between the Sr and Nd isotopic systems, with an extremely large range in $^{87}Sr/^{86}Sr$ ratios from 0.70296 ($\varepsilon_{Sr} = -19.7$) to 0.70650 ($\varepsilon_{Sr} = +30.5$) compared to a narrow range in ε_{Nd} values of from only 7.5 to 8.6. The highest $^{87}Sr/^{86}Sr$ ratios are found in the petrographically more altered rocks (basalts, sheeted dikes, high level gabbros, and plagiogranites). This approximate correlation between high $^{87}Sr/^{86}Sr$ and stratigraphic height (see Fig. 5) indicates that these rocks exchanged with Cretaceous seawater, the only geologically reasonable source of high $^{87}Sr/^{86}Sr$.

In Fig. 4 the ε_{Nd} and ε_{Sr} values from the Samail ophiolite are plotted. They have an origin at the mantle correlation line [31,40] and produce a horizontal trajectory to higher ε_{Sr} values. Although this general effect has been shown by previous workers [40,43], the present results provide a spectacular example of how the Nd isotopic composition is unaffected by seawater contamination, despite the large shifts in the Sr isotopic composition. To illustrate further the effects of seawater addition, in Fig. 4, a mixing line for Sr and Nd is shown for the closed system exchange of seawater with oceanic crust for various water/rock ratios. For closed system exchange of seawater and rock the Sr water/rock ratio (by weight) is given by

$$\frac{W}{R} = \left(\frac{\varepsilon^{f}_{Rock} - \varepsilon^{i}_{Rock}}{\varepsilon^{i}_{H_2O} - \varepsilon^{f}_{Rock}} \right) \frac{C^{i}_{Rock}}{C^{i}_{H_2O}} \qquad (1)$$

where i = initial value

f = final value

C^{i}_{Rock} = concentration of Sr in rock

and $C^{i}_{H_2O}$ = concentration of Sr in seawater.

The parameters used in this equation are $\varepsilon^{i}_{Rock} = -20$, $\varepsilon^{i}_{H_2O} = +47$ [7,8], and $C^{i}_{H_2O} = 8$ ppm [48]. ε^{f}_{Rock} values are given in Table 1. It is assumed that the initial Sr concentration in the rock (C^{i}_{Rock}) is the same as the final measured concentration (Table 1). With these parameters, W/R ratios of 15 to 40 are required to account for the observed $^{87}Sr/^{86}Sr$ ratios in the sheeted dikes and basalt. For the gabbros lower W/R ratios of 0 to 4 are indicated, suggesting that W/R ratios increase upward in the section.

The significantly lower concentration of Nd in seawater of 3×10^{-6} ppm [48, 49] requires a W/R ratio exceeding 2×10^5 to produce a measureable shift in ε_{Nd}.

Due to the overprinting of rock Sr with seawater Sr, it is not possible to determine unambiguously the primary magmatic $^{87}Sr/^{86}Sr$ ratio in these rocks. An upper limit is given by the lowest $^{87}Sr/^{86}Sr$ value of 0.70296 ± 2 found in the plagioclase from the gabbro K9. This may be close to its magmatic value as the coexisting clinopyroxene with a lower Sr concentration has only a slightly greater $^{87}Sr/^{86}Sr$ ratio of 0.70313 ± 3. The $^{87}Sr/^{86}Sr$ ratios in the clinopyroxene and plagioclase from the gabbro OM251 also have very different Sr concentrations but have the same $^{87}Sr/^{86}Sr$ ratio within error (0.70315 ± 5 and 0.70311 ± 5), and may also represent a primary value. The difference between the plagioclase separates from K9 and OM251, may suggest a small but real difference in the $^{87}Sr/^{86}Sr$ ratios of these samples and of the original magmas from which they crystallized. This small $^{87}Sr/^{86}Sr$ isotopic heterogeneity is also consistent with the ε_{Nd} values for these two gabbros as both plot right on the correlation line in the ε_{Sr}-ε_{Nd} diagram of Fig. 4. The correlation line shown in Fig. 4 is defined by the ε_{Nd} and ε_{Sr} values of MORB, island arcs and ocean islands [30, 31, 40-45]. This correlation of ε_{Nd} and ε_{Sr} has been interpreted as an important mantle feature [31, 40, 45]. For example, the correlation may represent mixing between two reservoirs [31]; an undepleted "continental" type mantle with $\varepsilon_{Nd} \sim 0$ and $\varepsilon_{Sr} \sim 0$ and a LIL depleted "oceanic" type mantle with $\varepsilon_{Nd} = +10$ and $\varepsilon_{Sr} = -27$.

3.3 Comparison of Sr and ^{18}O

The data presented in Fig. 5 and in Table 1 show that: a) measured $^{87}Sr/^{86}Sr$ in altered samples shifts from the primary magmatic value of $\sim$0.7030 towards the higher values of Cretaceous seawater of 0.7076 [7, 8] and b) $\delta^{18}O$ values of samples above the diabase-gabbro contact are enriched (relative to the primary magmatic value), whereas samples below the diabase-gabbro contact have depleted $\delta^{18}O$ values. These data, therefore, indicate that both the Sr and ^{18}O isotopic systems have been affected by exchange with a seawater derived hydrothermal fluid. The major difference between the two systems is that during hydrothermal exchange, only oxygen isotopes are significantly affected by temperature dependent fractionation. Oxygen water-rock fractionation factor Δ is defined as $\Delta = \delta^{18}O_{rock} - \delta^{18}O_{water}$ and is temperature dependent ($\Delta \propto 1/T^2$). For zeolite facies alteration, $\Delta > 6$, and for greenschist or higher facies alteration, $\Delta < 6$ [50]. As extremely steep thermal gradients are present near the ridge axis spreading center, a wide range of Δ's ($-2 < \Delta < +20$) is possible. In addition, since seawater is only 6‰ lighter in $\delta^{18}O$ than the initial magmatic reservoir, the changes in the alteration temperature regimes at active spreading environments can produce both ^{18}O enrichments or depletions [9].

For closed system exchange of seawater and rock, the oxygen water/rock ratio (by weight) is given by [50]:

$$\frac{W}{R} = \left(\frac{\delta^{f}_{Rock} - \delta^{i}_{Rock}}{\delta^{i}_{H_2O} - (\delta^{f}_{Rock} - \Delta)} \right) \frac{C^{i}_{Rock}}{C^{i}_{H_2O}} \qquad (2)$$

This is identical to the Sr exchange equation (equation 1) apart from the fractionation factor Δ. In principle the combined Sr and O approach may be used as a geothermometer with the $^{87}Sr/^{86}Sr$ ratios being utilized to estimate the W/R ratio. Using this W/R ratio and the $\delta^{18}O$ values, the fractionation factor Δ and hence the final temperature of water-rock equilibration can be evaluated. This approach may be particularly useful in systems with relatively low water/rock ratios where equilibrium closed system exchange prevails and the Sr and O water-rock exchange rates are probably similar. Mixing lines can be calculated by combining equations 1 and 2 [10]. The effect of changing Δ on the calculated mixing lines is shown in Fig. 5. Since there are many different alteration temperature regimes, no simple correlation between $\delta^{18}O$ and $^{87}Sr/^{86}Sr$ would be expected for the entire ophiolite.

4.0 Conclusions

Using the Sm-Nd method, internal isochrons were obtained from three gabbros establishing a Cretaceous crystallization age for the Samail ophiolite. These results appear to be highly consistent in spite of extensive hydrothermal exchange which has altered the primary $^{87}Sr/^{86}Sr$ and $^{18}O/^{16}O$ ratios. Gabbros from Ibra give an age of 130±12 m.y., and a gabbro in the northern part of Oman gives an age of 100±20 m.y. These results show that the Sm-Nd technique can be used to determine crystallization ages of relatively young, Mesozoic and Cenozoic mafic complexes.

The initial $^{143}Nd/^{144}Nd$ ratios for all of the major lithologic

units of the Samail ophiolite have a narrow range in ε_{Nd} values indicating that they are derived from a common mantle source which has been depleted in Nd relative to Sm (light REE depleted) for at least a billion years or more. These data clearly demonstrate an oceanic affinity for this complex. The Nd and Sr isotopic data cannot by themselves be used to distinguish definitively among the various possible settings such as mid-ocean ridge, back-arc basin, or island-arc.

In contrast to the small range in initial Nd with ε_{Nd} = 7.5 to 8.6, the same samples have an extremely large range in initial $^{87}Sr/^{86}Sr$ and $\delta^{18}O$ with $^{87}Sr/^{86}Sr$ (I) = 0.7030 to 0.7065 and $\delta^{18}O$ = +2.6 to +12.7. These large variations in both Sr and O are consistent with hydrothermal exchange of oceanic crust with seawater initially having a high $^{87}Sr/^{86}Sr$ ratio and $\delta^{18}O \simeq 0$. The initial $^{87}Sr/^{86}Sr$ ratios generally decrease downward suggesting that the ratio of seawater to rock decreases with depth. As the ^{18}O shifts depend upon W/R ratio and temperature, both ^{18}O-depleted and ^{18}O-enriched rocks have been produced. Utilizing a relatively simple model for relating the exchange of Sr and O, it may be possible to use the Sr data to estimate W/R ratios and subsequently to evaluate the temperature of equilibration between the water and silicates by using the $^{18}O/^{16}O$ water-rock fractionation.

Acknowledgments

Field work was conducted in collaboration with the National Science Foundation - U.S. Geological Survey Oman project organized by R. G. Coleman and C. A. Hopson. Their help and support have been invaluable. This work has benefited from discussions with R. G. Coleman, C. A. Hopson, E. H. Bailey, J. S. Pallister, J. Chen, and M. A. Lanphere. R. G. Coleman provided additional samples from northwest of Ibra which greatly broadened the scope of this study. S. B. Jacobsen and the reviewers provided helpful comments on the manuscript. We appreciate Marvin Lanphere's indulgence in matters regarding an easily exchanged element. We express our gratitude to the Directorate General of Petroleum and Minerals, Sultanate of Oman, particularly Mohammed Kassim and Ismail M. El Boushi, for their support of this project. This work has been supported by N.S.F. grants PHY 76-83685, EAR-76-21310, EAR-7816874, and also indirectly by a N.S.F. grant to C. A. Hopson.

References

1. R. G. Coleman, Ophiolites ancient oceanic lithosphere? Springer-Verlag (1977).

2. B. M. Reinhardt, On the genesis and emplacement of ophiolites in the Oman Mountains geosyncline, Schweizer Mineralog. Petrog. Mitt. 49 (1969) 1.

3. K. W. Glennie, M. G. A. Boeuf, M. W. Hughes-Clarke, M. Moody-Stuart, W. F. H. Pilaar, and B. M. Reinhardt, Geology of the Oman Mountains, Geol. Mijb. Gen. Ver. Verh. 31 (1974) 423.

4. K. W. Glennie, M. G. A. Boeuf, M. W. Hughes Clarke, M. Moody-Stuart, W. F. H. Pilaar and B. M. Reinhardt, Late Cretaceous nappes in Oman Mountains and their geologic evolution, Am. Assoc. Petr. Geol. Bull. 57 (1973) 5.

5. E. T. C. Spooner, The isotopic composition of seawater, and seawater-oceanic crust interaction, Earth Planet. Sci. Lett. 31 (1976) 1121.

6. K. Muehlenbachs and R. N. Clayton, Oxygen isotope composition of the oceanic crust and its bearing on seawater, J. Geophy. Res. 81 (1976) 4365.

7. Z. E. Peterman, C. E. Hedge and H. Tourtelot, Isotopic composition of Sr in Seawater throughout Phanerozoic time, Geochim. Cosmochim. Acta 34 (1970) 105.

8. J. Veizer and W. Compston, $^{87}Sr/^{86}Sr$ composition of seawater during the Phanerozoic, Geochim. Cosmochim. Acta 38 (1974) 1461.

9. R. T. Gregory and H. P. Taylor, An oxygen isotope profile in a section of Cretaceous oceanic crust, Samail ophiolite, Oman:Evidence

for $\delta^{18}O$ - buffering of the oceans by deep (> 5 km) seawater - hydrothermal circulation at mid-ocean ridges, submitted to J. Geophys. Res. (1979).

10. M. T. McCulloch, R. T. Gregory, G. J. Wasserburg, and Hugh P. Taylor, Jr., Sm-Nd, Rb-Sr and $^{18}O/^{16}O$ isotopic systematics in an oceanic crustal section: evidence from the Samail ophiolite, Submitted to J. Geophys. Res. (1979).

11. Z. E. Peterman, R. G. Coleman and R. A. Hildreth, $^{87}Sr/^{86}Sr$ in mafic rocks of the Troodos massif, Cyprus, U.S. Geol. Surv. Res. 750-D (1971) D157.

12. R. G. Coleman and Z. E. Peterman, Oceanic Plagiogranite, J. Geophys. Res. 80 (1975) 1099.

13. M. Magaritz and H. P. Taylor, Jr., Oxygen and hydrogen studies of serpentinization in the Troodos Ophiolite Complex, Cyprus, Earth Planet. Sci. Lett., 23 (1974) 8.

14. T. H. E. Heaton and S. M. F. Sheppard, Hydrogen and oxygen isotope evidence for sea-water - hydrothermal alteration and ore deposition, Troodos complex, Cyprus, in: Volcanic Processes in Ore Genesis, Spec. Paper No. 7, Geol. Soc. London (1977) 42.

15. H. J. Chapman and E. T. C. Spooner, ^{87}Sr enrichment of ophiolitic sulphide deposits in Cyprus confirms ore formation by circulating seawater, Earth Planet. Scl. Lett. 35 (1977) 7.

16. E. T. C. Spooner, H. J. Chapman and J. D. Smewing, Strontium isotopic contamination and oxidation during ocean floor hydrothermal metamorphism of the ophiolitic rocks of the Troodos, Cyprus, Geochim. Cosmochim. Acta 41 (1977) 873.

17. E. T. C. Spooner, R. D. Beckinsale P. C. England and A. Senior, Hydration, ^{18}O enrichment and oxidation during ocean floor hydrothermal meta morphism of ophiolitic metabasic rocks from E. Liguria, Italy, Geochim. Cosmochim. Acta 41 (1977) 857.

18. C. R. Stern, M. J. deWit and J.R. Lawrence, Igneous and metamorphic processes associated with the formation of Chilean ophiolites and their implication for ocean floor metamorphism, seismic layering, and magnetism, J. Geophys. Res. 81 (1976) 4370.

19. C. L. Chou, H. J. Lo, J. H. Chen and V. C. Juan, Rare earth element and isotopic geochemistry of Kuanshan igneous complex, Taiwan, Proc. Geol. Soc. China 21 (1978) 13.

20. J. A. Pearce, Basalt geochemistry used to investigate past tectonic environments on Cyprus, Tectonophysics 25 (1975) 41.

21. J. D. Smewing, K. O. Simonian and I. G. Gass, Meta-basalts from the Troodos Massif, Cyprus: Genetic implication deduced from petrography and trace element geochemistry, Contrib. Mineral. Petrol. 51 (1975) 49.

22. R. W. Kay and R. G. Senechal, The rare earth geochemisty of the Troodos ophiolite complex, J. Geophys, Res. 81 (1976) 964.

23. P. Richard, D. Rousseau and C. J. Allegre, Nd and Sr systematics in ophiolites, short papers of the 4th Internat. Conf. Geochron. Cosmochron. Isotope Geol. U.S. Geol. Surv. open-file report 78-701 (1978) 350.

24. N. I. Christensen and M. H. Salisbury, Structure and constitution of the lower oceanic crust, Rev. Geophys. Space Phys. 13 (1975) 57.

25. F. Allemann and T. J. Peters, The ophiolite-radiolarite belt of the North-Oman Mountains, Eclogae Geol. Helvetiae 65 (1972) 657.

26. R. T. Gregory and H. P. Taylor, Jr., $^{18}O/^{16}O$ variations in gabbro, diabase and volcanic sections in Samail ophiolite, southeastern Oman Mountains and the nature of hydrothermal alteration in the oceanic crust (Abstract) International Ophiolite Symposium Nicosa - Cyprus (1979) 32.

27. C. A. Hopson, R. G. Coleman, E. H. Bailey, J. S. Pallister and R. T. Gregory, Geologic section through the Samail ophiolite near Ibra, southeastern Oman Mountains, Submitted to J. Geophys. Res. (1979).

28. H. P. Taylor, Jr. and S. Epstein, Relationship between $^{18}O/^{16}O$ ratios in coexisting minerals of igneous and metamorphic rocks. Part I: Principles and experimental results, Geol. Soc. Amer. Bull. 73 (1962) 461.

29. D. A. Papanastassiou, D. J. DePaolo and G. J. Wasserburg, Rb-Sr and Sm-Nd chronology and genealogy of basalts from the Sea of Tranquility, Proc. Eighth Lunar Sci. Conf. (1977) 1639.

30. D. J. DePaolo and G. J. Wasserburg, Nd isotopic variations and petrogenetic models, Geophys. Res. Lett. 3 (1976) 249.

31. D. J. DePaolo and G. J. Wasserburg, Inferences about magma sources and mantle structure from variations of $^{143}Nd/^{144}Nd$, Geophys. Res. Lett. 3 (1976) 743.

32. J. M. Mattinson, Early paleozoic ophiolite complexes of Newfoundland: isotopic ages of zircons, Geology 3 (1975), 181.

33. J. B. Saleeby, Fracture zone tectonics, continental margin fragmentation and emplacement of the Kings-Kaweah ophiolite belt, southwest Sierra Nevada, California, in "North American Ophiolites", Oregon Dept. Geol. Min. Indust. Bull. 95 (1977) 141.

34. G. W. Lugmair, Sm-Nd ages: a new dating method, (Abstract) Meteoritics 9 (1974) 369.

35. G. W. Lugmair, K. Marti, J. P. Kurtz, N. B. Scheinin, History and genesis of lunar troctolite 76535 or: how old is old? Proc. Seventh Lunar Sci. Conf. (1976) 2009.

36. N. Nakamura, M. Tatsumoto, P. D. Nunes, D. M. Unruh, A. P. Schwab and T. R. Wildman, 4.4 b.y.-old clast in Boulder 7, Apollo 17: A comprehensive chronological study in U-Pb, Rb-Sr and Sm-Nd methods, Proc. Seventh Lunar Sci. Conf. (1976) 2309.

37. P. J. Hamilton, R. K. O'Nions and N. M. Evensen, Sm-Nd dating of Archean basic and ultrabasic volcanics, Earth Planet. Sci. Lett. 36 (1977) 263.

38. P. J. Hamilton, N. M. Evensen, R. K. O'Nions, H. S. Smith and A. J. Erlank, Sm-Nd dating of Onverwacht group volcanics, southern Africa, Nature 279 (1979) 298.

39. D. J. DePaolo and G. J. Wasserburg, Sm-Nd age of the Stillwater Complex and the mantle evolution curve for neodymium, Geochim. Cosmochim. Acta, 43 (1979) 999.

40. R. K. O'Nions, P. J. Hamilton and N. M. Evensen, Variations in $^{143}Nd/^{144}Nd$ and $^{87}Sr/^{86}Sr$ ratios in oceanic basalts, Earth Planet. Sci. Lett. 34 (1977) 13.

41. P. Richard, N. Shimizu and C. J. Allegre, $^{143}Nd/^{146}Nd$, a natural tracer: an application to oceanic basalts, Earth Planet. Sci. Lett. 31 (1976), 269.

42. R. W. Carlson, J. C. MacDougall and G. W. Lugmair, Differential Sm/Nd evolution in oceanic basalts, Geophys. Res. Lett. 5 (1978) 229.

43. D. J. DePaolo and G. J. Wasserburg, The sources of island arcs as indicated by Nd and Sr isotopic studies, Geophys. Res. Lett. 4 (1977) 465.

44. C. J. Hawkesworth, R. K. O'Nions, R. J. Pankhurst, P. J. Hamilton and N. M. Evensen, A geochemical study of island-arc and back-arc tholeiites from the Scotia Sea, Earth Planet. Sci. Lett. 36 (1977) 253.

45. C. J. Hawkesworth, M. J. Norry, J. C. Roddick and R. Vollmer, $^{143}Nd/^{144}Nd$ and $^{87}Sr/^{86}Sr$ ratios from the Azores and their significance in LIL-element enriched mantle, Nature 280 (1979) 28.

46. D. J. DePaolo and G. J. Wasserburg, Neodymium isotopes in flood basalts from the Siberian Platform and inferences about their mantle sources. Proc. Natl. Acad. Sci. 76 (1979) 3056.

47. J. D. Smewing, K. O. Simonian, I. M. Elboushi and I. G. Gass, Mineralized fault zone parallel to the Oman ophiolite spreading axis, Geology 5 (1977) 534.

48. E. D. Goldberg, Minor elements in seawater, in Chemical Oceanography, Vol. I, p. 162 (J. P. Riley and G. Skirrow, eds.), Academic Press, New York. 1965.

49. D. J. Piepgras, G. J. Wasserburg and E. J. Dasch, The isotopic composition of Nd in different ocean masses, Earth Planet. Sci. Lett. (in press).

50. H. P. Taylor, Jr., The application of oxygen and hydrogen isotope studies to problems of hydrothermal alteration and ore deposition, Econ. Geol. 69 (1974) 843.

FIGURE CAPTIONS

Figure 1. Generalized geologic map of the Samail ophiolite, Oman (after Glennie et al. [3]), showing sample localities. The Samail ophiolite (solid) is an allochthonous body which is in thrust contact with the underlying rocks.

Figure 2. Sm-Nd evolution diagram showing the data for whole rocks and coexisting pyroxene-plagioclase and uralite-plagioclase pairs for gabbros from Ibra, Wadi Fizh and Rustaq. The gabbros from Ibra give an age of 130±12 m.y. and ε_{Nd} = 7.8±0.2. The gabbro from north of the Samail gap gives an age of 100±20 m.y. and ε_{Nd} = 7.6±0.2. These ages are considered to be the times of formation of the oceanic crust that was formed in the Hawasina ocean basin and is now preserved as the Samail ophiolite.

Figure 3. Histogram comparing initial ε_{Nd} values from the Samail ophiolite measured in this study with modern-day mid-ocean ridge basalts (MORB)[30, 31, 40-42], marginal basins (Lau, Scotia Sea) [42, 44], island arcs [43, 44], ocean islands [31, 40, 41, 45], and continental flood basalts [30, 31, 42, 46]. The small range in ε_{Nd} for marginal basins (shaded) may be an artifact of the limited data (the smallest vertical division represents one sample). The Samail ophiolite clearly has an oceanic affinity. The initial ε_{Nd} values of the Samail ophiolite (solid) give an average of ε_{Nd} = 7.9, which is somewhat lower than typical modern-day MORB with $\varepsilon_{Nd} \simeq 10$. Correcting

for differential evolution in the Samail ophiolite source region relative to the bulk earth during the past 130 m.y. increases the ε_{Nd} values of the Samail ophiolite (delimited by dashed lines) to give a modern-day average of $\varepsilon_{Nd} = 8.8$, which is well within the MORB and marginal basin range.

Figure 4. ε_{Nd} and ε_{Sr} values for the Samail ophiolite. The arrows indicate the effect of contamination with Cretaceous seawater for different water/rock ratios and show that $W/R > 10^5$ is required before ε_{Nd} values are affected. The ε_{Nd} and ε_{Sr} values of uncontaminated samples plot on the "mantle correlation" line [31, 40] and are consistent with derivation from a less depleted MORB source region. The ε_{Nd} and ε_{Sr} values plot in a position where the fields for MORB and island arc basalts overlap, and hence do not discriminate between the oceanic environments in which the Samail ophiolite formed.

Figure 5. Initial $^{87}Sr/^{86}Sr$ and $\delta^{18}O$ values of whole rocks (solid) and minerals (open) from the Samail ophiolite. The approximate stratigraphic depth is given in parentheses. The curves describe the $\delta^{18}O$ and $^{87}Sr/^{86}Sr$ values in mixtures of seawater and oceanic crust for different temperatures of ^{18}O exchange. The oxygen water-rock fractionation factor Δ is temperature dependent ($\Delta \propto 1/T^2$), being approximately equivalent to zeolite facies for $\Delta = 11$, to greenschist facies for $\Delta = 6$, and to upper amphibolite facies for $\Delta = 0$. The water/rock ratios on the right ordinate are calculated

assuming closed system exchange of Sr (equation 1) in Cretaceous seawater ($^{87}Sr/^{86}Sr$ = 0.7076, Sr = 8 ppm) with Sr in oceanic crust ($^{87}Sr/^{86}Sr$ = 0.7030, Sr = 160 ppm). The arrows on the mixing lines show the direction of increasing W/R ratios. These lines illustrate that W/R ratios are higher while alteration temperatures are lower for the diabases and basalts (K1, G10, G54). The curves also show that the gabbros (G224-2, OM28) were altered at higher temperatures and lower W/R ratios. In principle, the Sr and O isotopic systems can be used together as a geothermometer for hydrothermal interactions.

Table 1. Nd, Sr, and O isotopic data from the Samail ophiolite.

Samples	Nd (ppm)	Sr (ppm)	$\frac{^{87}Rb}{^{86}Sr}$	$\frac{^{147}Sm}{^{144}Nd}$	$\frac{^{87}Sr}{^{86}Sr}$	$\frac{^{143}Nd}{^{144}Nd}$	ε_{Sr}	ε_{Nd}	$\delta^{18}O$
Basalt									
G54 WR	15.9	198	0.104	0.192	0.70491±4[a]	0.512219±19[a]	5.3[b]	7.5[b]	12.7
CALCITE	0.126	6.12	0.004	0.209	0.70650±15	0.512265±29	30.5	8.1	-
Sheeted Dikes									
G10	11.2	162	0.029	0.209	0.70535±4	0.512250±25	13.5	7.8	8.5
K1	13.0	388	0.008	0.194	0.70519±4	0.512275±20	11.7	8.6	6.8
Plagiogranite									
G224-3	17.3	192	0.035	0.187	0.70362±4	0.512249±18	-11.3	8.2	5.2
Gabbros									
G224-2 WR	8.36	196	0.010	0.201	0.70370±3	0.512251±19	-9.5	8.0	3.7
PLAG	2.25	330	0.008	0.151	0.70352±4	0.512196±18	-12.0	7.8	4.5
URAL	9.51	58.7	0.014	0.241	0.70426±3	0.512285±19	-1.6	8.0	2.6
K9 WR	0.986	188	0.001	0.271	0.70304±5	0.512310±18	-18.6	8.0	5.7
PLAG	0.399	311	0.001	0.129	0.70296±2	0.512180±25	-19.7	7.8	6.0
						0.512181±19[c]		7.8	
CPX	2.630	24.8	0.001	0.322	0.70313±3	0.512341±15	-17.3	7.7	5.3
OM251 PLAG	0.081	156	0.001	0.159	0.70311±5	0.512203±22	-18.0	7.6	6.4
CPX	0.411	54.2	0.002	0.377	0.70315±5	0.512346±25[c]	-17.5	7.6	5.8
OM28 WR	0.385	132	0.001	0.264	0.70383±5	0.512274±22[c]	-7.8	7.7	5.2
Harzburgite									
K22	0.035	0.43	0.150	0.216	0.70313±9	0.512278±23	-21.2	8.3	-

[a] Errors are in the last figures given and represent ±2σ mean. These errors correspond to typical uncertainties in ε_{Sr}, and ε_{Nd} of ±0.6 and ±0.4 ε units, respectively. The uncertainty in $\delta^{18}O$ is ±0.1‰.

[b] ε_{Sr} and ε_{Nd} values calculated for a crystallization age of 130 m.y. except for OM251 and OM28 for which an age of 100 m.y.was used.

[c] $^{143}Nd/^{144}Nd$ determined from spiked sample.

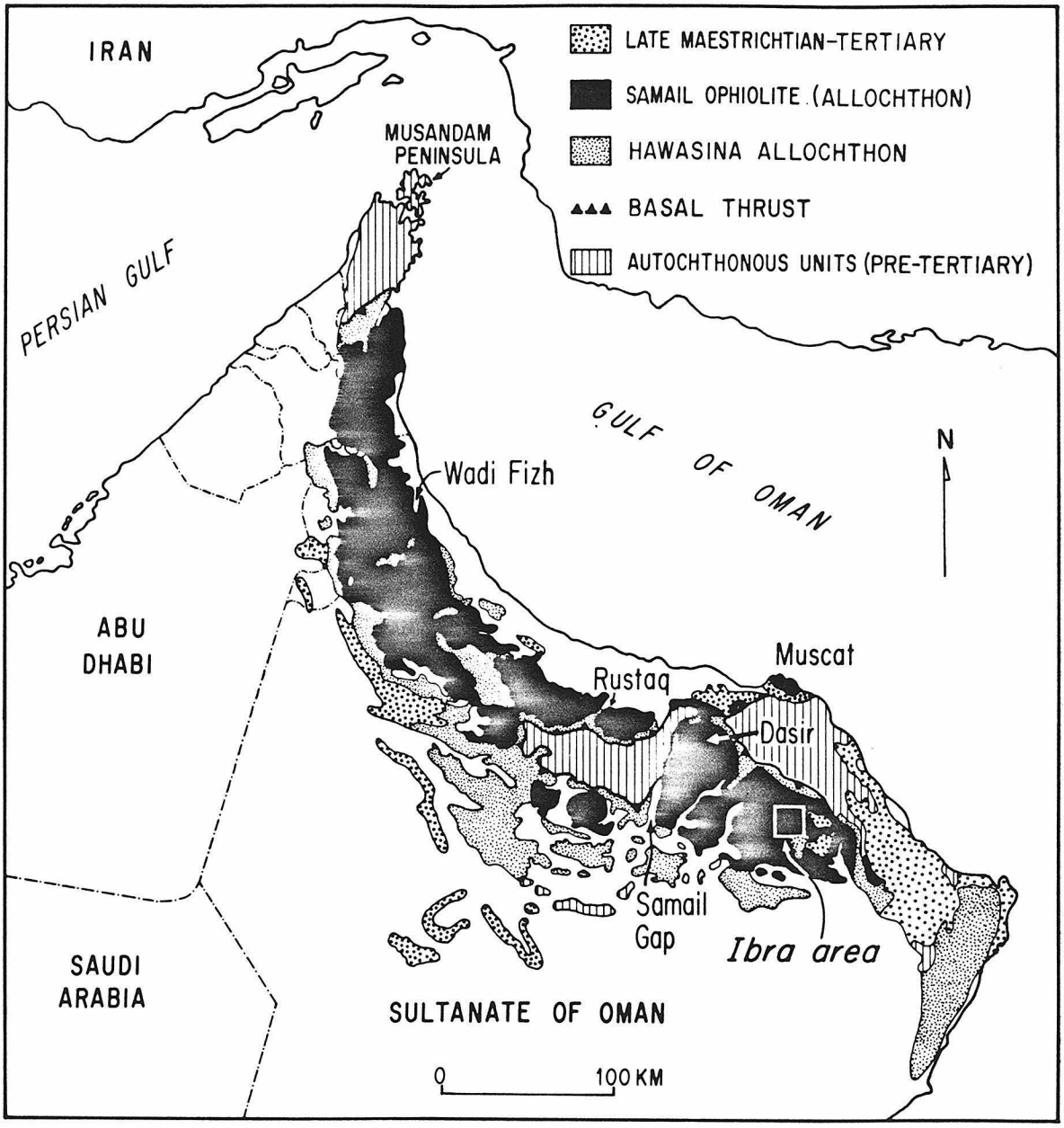
IRAN
MUSANDAM PENINSULA
PERSIAN GULF
GULF OF OMAN
N
LATE MAESTRICHTIAN-TERTIARY
SAMAIL OPHIOLITE (ALLOCHTHON)
HAWASINA ALLOCHTHON
BASAL THRUST
AUTOCHTHONOUS UNITS (PRE-TERTIARY)
Wadi Fizh
ABU DHABI
Muscat
Rustaq
Dasir
Samail Gap
Ibra area
SAUDI ARABIA
SULTANATE OF OMAN
0
100 KM

Fig. 1

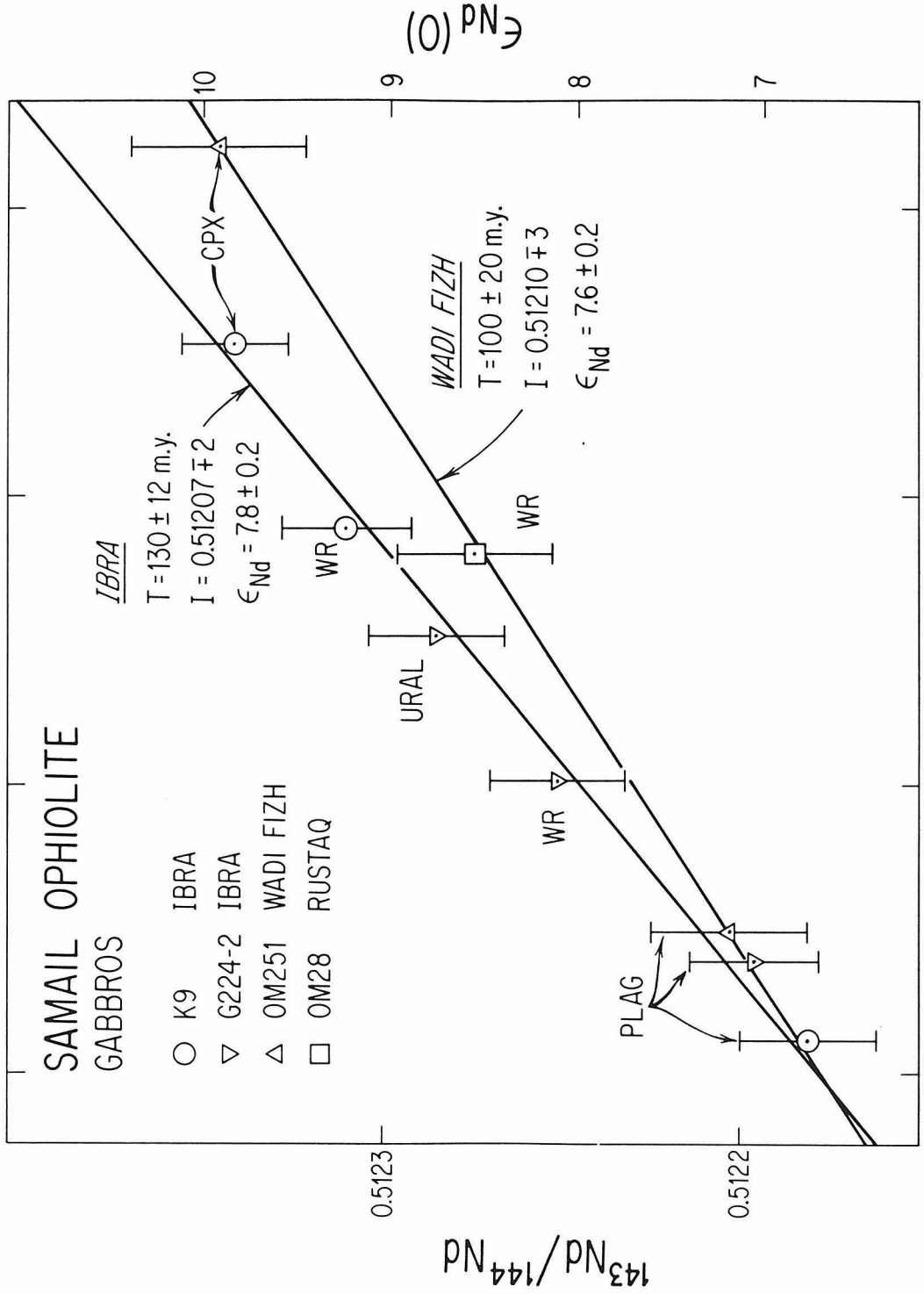
SAMAIL OPHIOLITE
GABBROS
K9 IBRA
G224-2 IBRA
OM251 WADI FIZH
OM28 RUSTAQ
IBRA
T = 130 ± 12 m.y.
I = 0.51207 ∓ 2
ε_Nd = 7.8 ± 0.2
WADI FIZH
T = 100 ± 20 m.y.
I = 0.51210 ∓ 3
ε_Nd = 7.6 ± 0.2
CPX
WR
WR
WR
URAL
PLAG
0.5123
0.5122
0.12
0.20
0.28
0.36
10
9
8
7
143Nd/144Nd
147Sm/144Nd
εNd(0)

Fig. 2

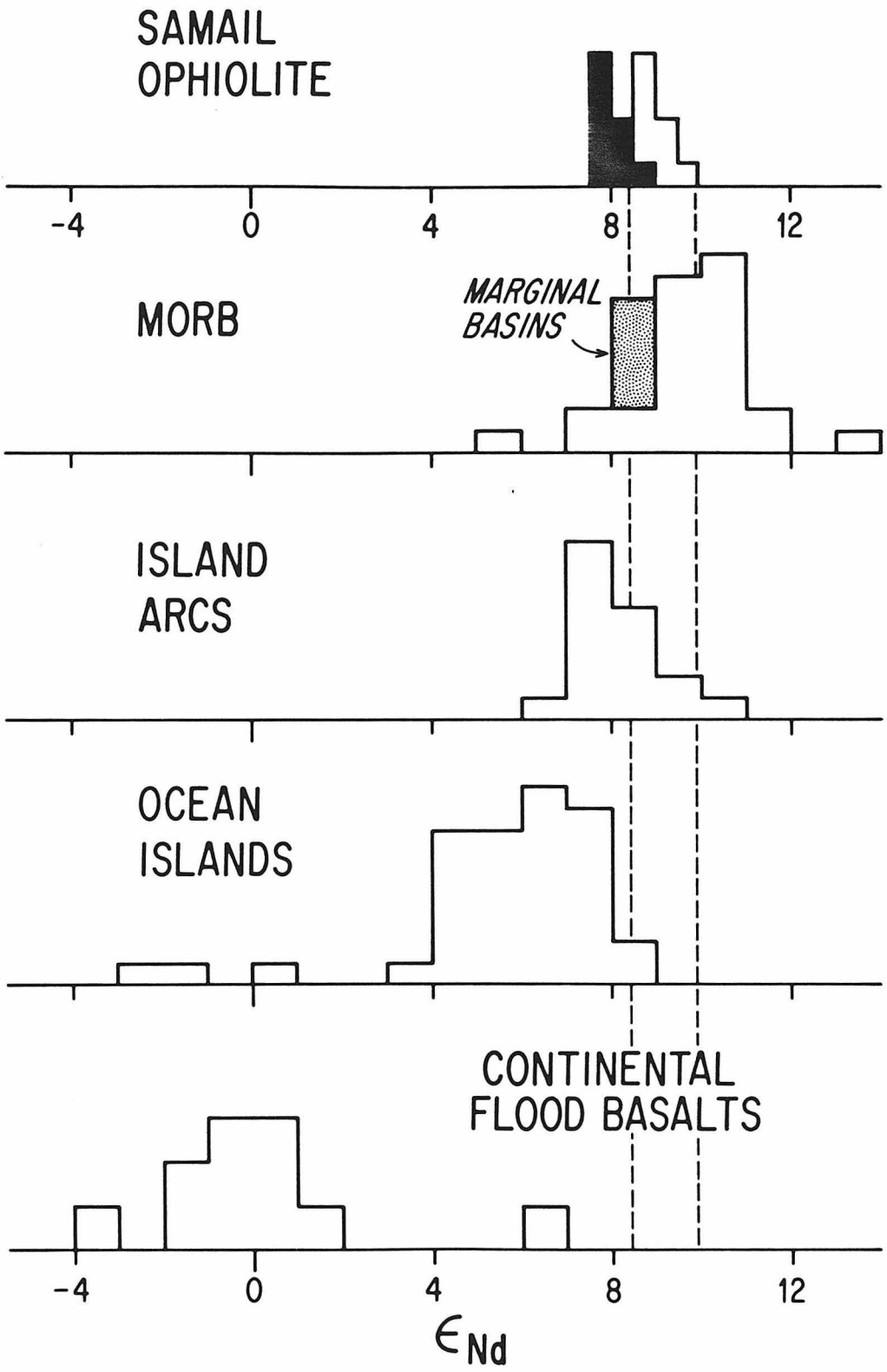
SAMAIL
OPHIOLITE
-4
0
4
8
12
MORB
MARGINAL
BASINS
ISLAND
ARCS
OCEAN
ISLANDS
CONTINENTAL
FLOOD BASALTS
-4
0
4
8
12
ϵ_{Nd}

Fig. 3

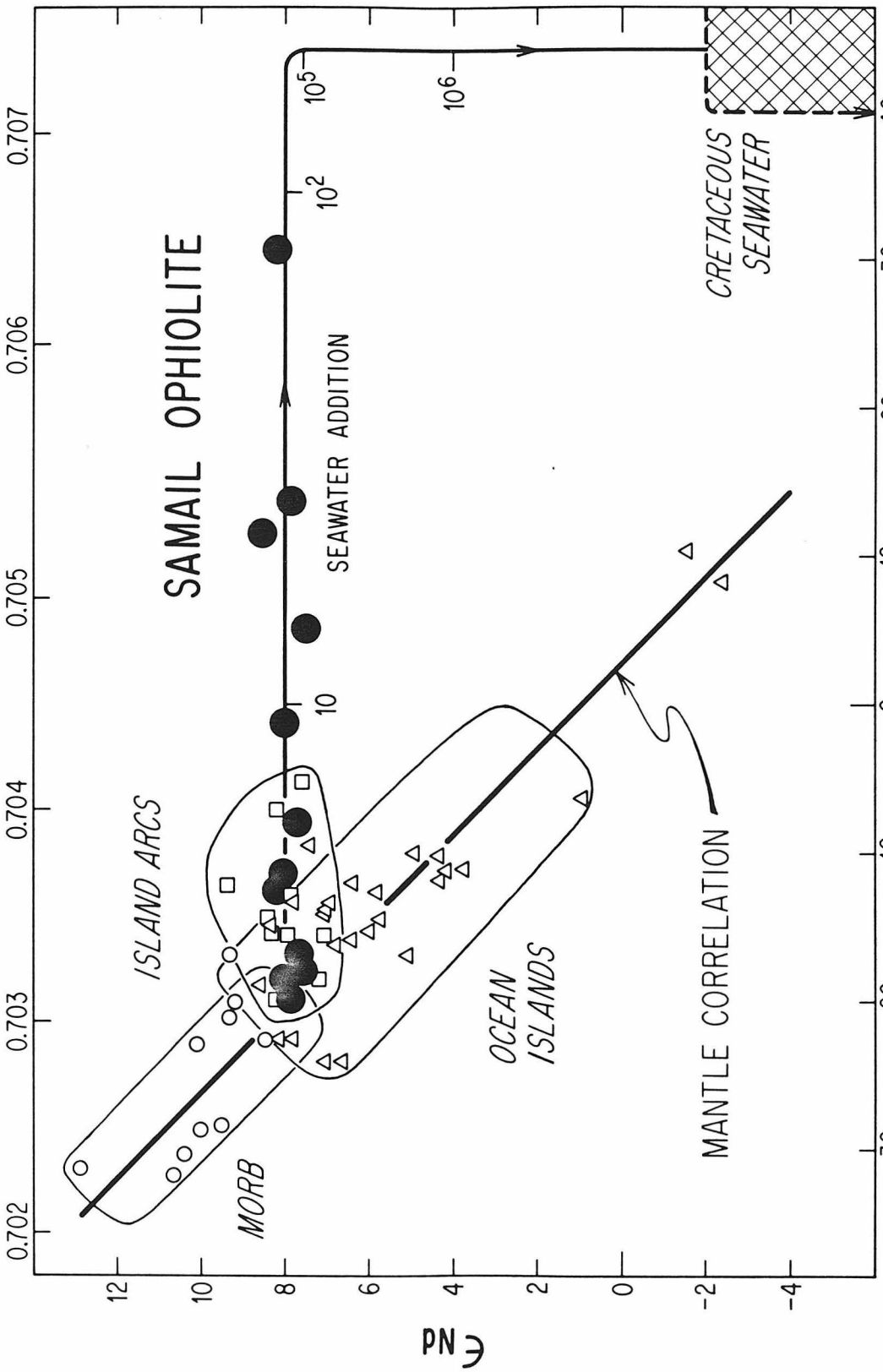
SAMAIL OPHIOLITE
SEAWATER ADDITION
ISLAND ARCS
MORB
OCEAN ISLANDS
MANTLE CORRELATION
CRETACEOUS SEAWATER
10^2
10^5
10^6
10
0.702
0.703
0.704
0.705
0.706
0.707
12
10
8
6
4
2
0
-2
-4
40
30
20
10
0
-10
-20
-30
ϵ_{Nd}
ϵ_{Sr}

Fig. 4

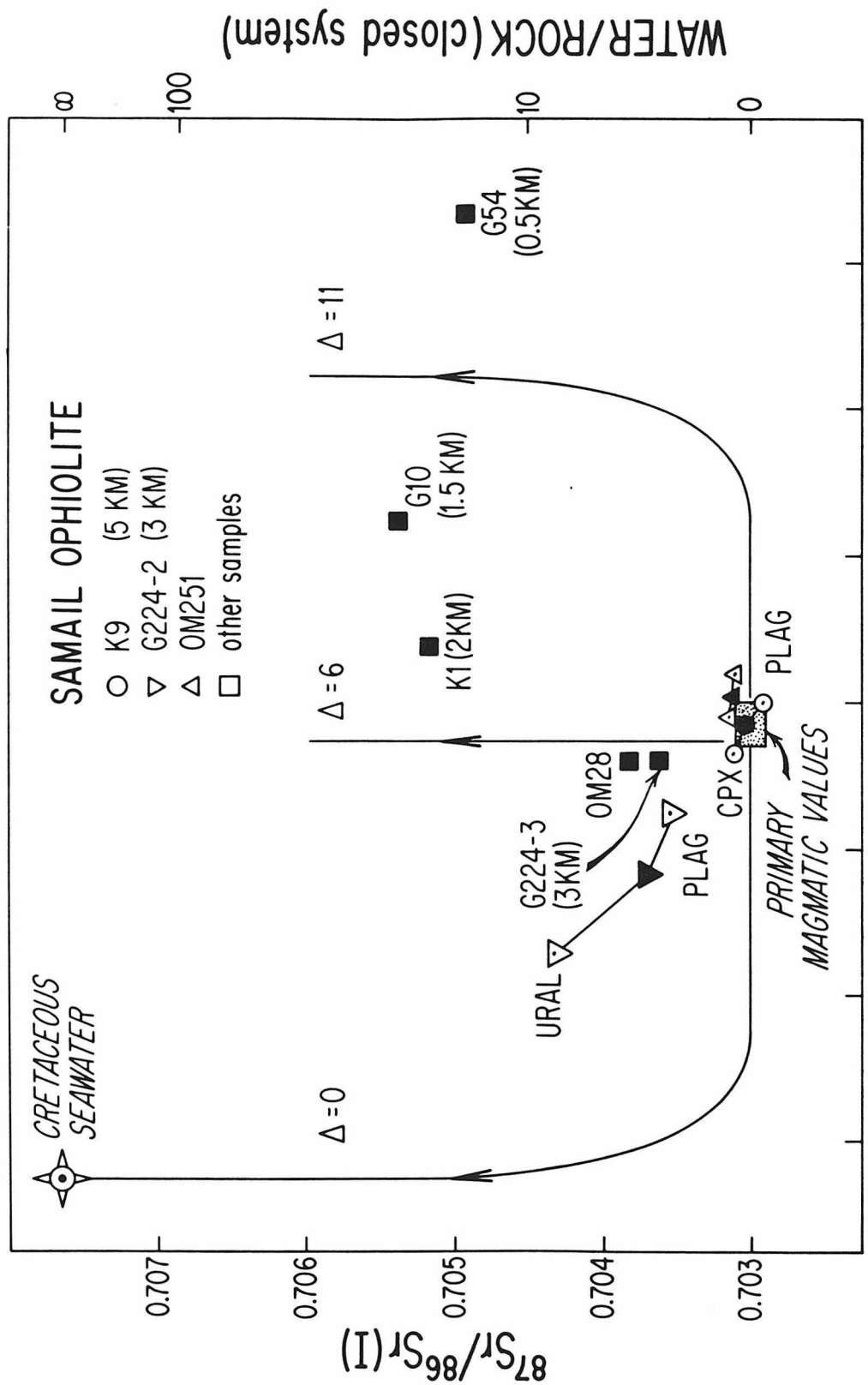
WATER/ROCK (closed system)
∞
100
10
0
SAMAIL OPHIOLITE
K9 (5 KM)
G224-2 (3 KM)
OM251
other samples
CRETACEOUS SEAWATER
Δ=0
Δ=6
Δ=11
G54 (0.5KM)
G10 (1.5 KM)
K1(2KM)
OM28
G224-3 (3KM)
URAL
PLAG
CPX
PLAG
PRIMARY MAGMATIC VALUES
0.707
0.706
0.705
0.704
0.703
87Sr/86Sr(I)
0
2
4
6
8
10
12
δ18O

Fig. 5

Appendix 5. MINNESOTA RIVER VALLEY: GEOLOGY, FIELD NOTES, AND SAMPLE DESCRIPTIONS

GEOLOGY

The Archean rocks of the Minnesota River Valley in S.W. Minnesota are exposed in three main areas. These are the Morton-Delhi area, the Granite Falls-Montevideo area, and the Ortonville-Odessa area. In this study most of the samples were collected from the first two areas.

In the Morton-Delhi area the principal rock is the Morton gneiss within which Lund (1956) distinguished three rock types. These are:

(1) Basic or mafic amphibolitic xenoliths which range in chemistry from tholeiitic to komatiitic (Wooden et al., 1979).

(2) Gray tonalitic gneisses which have variable textures and structures. They range from fine to very coarse grained, thin to thick layered, and straight banded to highly contorted and convoluted rocks. Gradations in composition from predominantly tonalitic to granodioritic are also present.

(3) Pink granitic rocks which are the neosome or leucosome of the Morton gneiss. They range from a coarse grained pegmatitic gneiss to a finer grained relatively undeformed adamellite. Resembling this least deformed phase is the Sacred Heart granite which outcrops in the area south of Sacred Heart and locally intrudes the Morton gneiss (Lund, 1956).

The second area that was studied is in the vicinity of Granite

Figure A5-1. Geologic map of the Granite Falls and Montevideo areas showing principal geologic units and location of samples (adopted from Himmelberg, 1968).

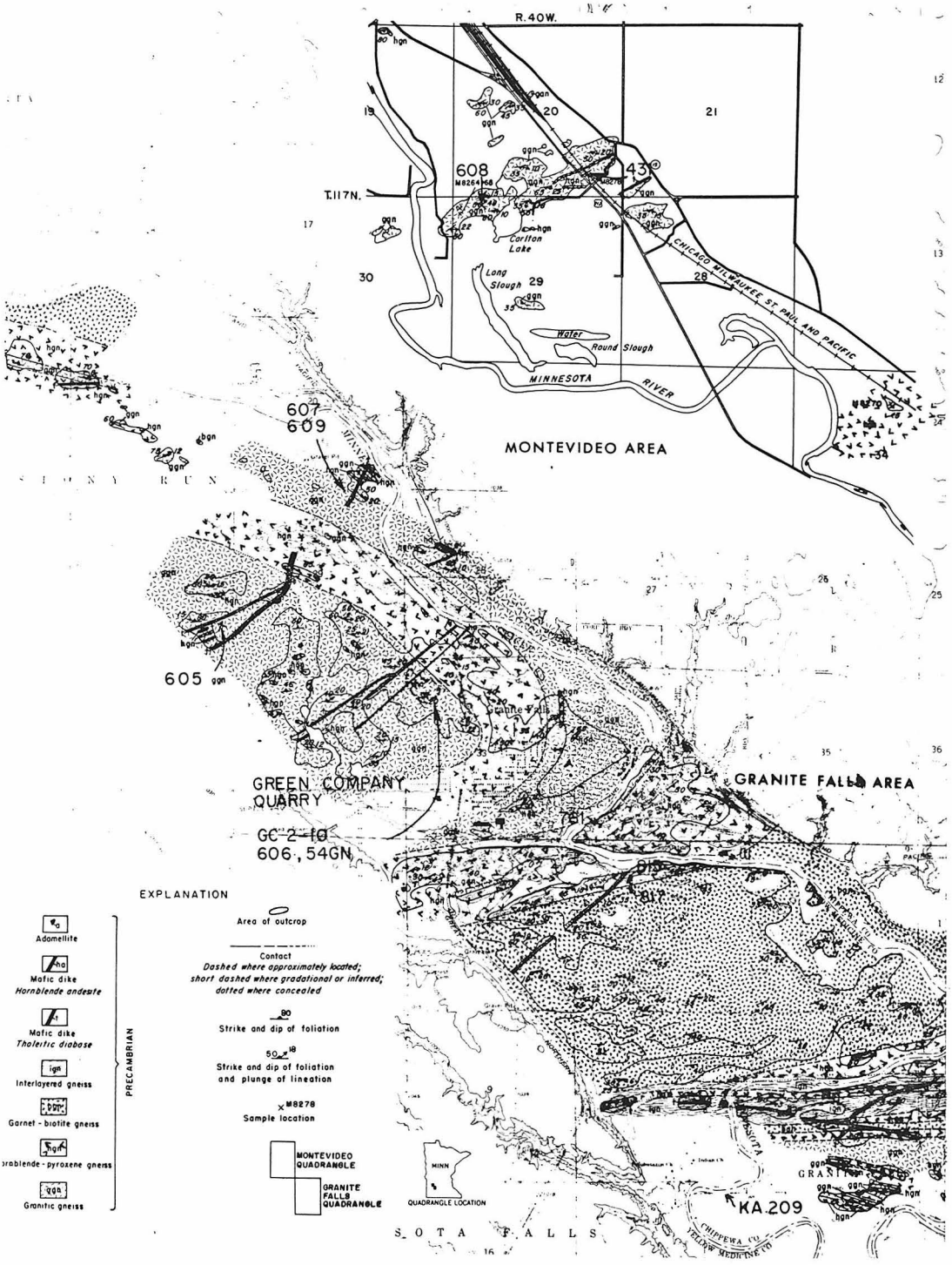
R.40W.
T.117N.
MONTEVIDEO AREA
GRANITE FALLS AREA
GREEN COMPANY QUARRY
GC-2-10
606, 54GN
607
609
605
608
Carlton Lake
Long Slough
Round Slough
MINNESOTA RIVER
CHICAGO, MILWAUKEE, ST. PAUL AND PACIFIC
EXPLANATION
Area of outcrop
Contact
Dashed where approximately located; short dashed where gradational or inferred; dotted where concealed
Strike and dip of foliation
Strike and dip of foliation and plunge of lineation
Sample location
Adamellite
Mafic dike
Hornblende andesite
Mafic dike
Tholeiitic diabase
Interlayered gneiss
Garnet - biotite gneiss
Granitic gneiss
PRECAMBRIAN
MONTEVIDEO QUADRANGLE
GRANITE FALLS QUADRANGLE
QUADRANGLE LOCATION
KA 209

Fig. A5-1

Falls and Montevideo and contains the largest area of exposure and most diverse lithologies. Lund (1956) and Himmelberg (1968) classified the rocks in this area according to the following divisions (Fig. A5-1):

(1) hornblende-pyroxene gneiss

(2) garnet-biotite gneiss

(3) interlayered gneiss

(4) granitic or Montevideo gneiss.

In this area, most of the samples that were studied were from the Montevideo gneiss. Within the Montevideo or granitic gneiss, Goldich and Hedge (1974) and Goldich et al. (1979) have further recognized three principal rock types. These are:

(1) predominantly granodioritic but including some tonalitic gneisses,

(2) adamellite gneiss including minor leucocratic and pegmatitic phases, and

(3) minor amounts of amphibolitic xenoliths and rafts which are similar to, but less abundant than, those found in the Morton gneiss.

The main difficulty in deciphering the complex history of the Morton and Montevideo gneisses is in obtaining samples which are representative of the pure and end-member components of the tonalite-granodiorite and adamellite gneisses. The main field criteria for identifying the adamellite is its characteristic red-brown color. This is associated with hematite and feldspar and may be due to hydrothermal alteration which has affected the adamellite more severely than the

finer grained granodioritic and tonalitic gneisses. Where crosscutting relationships are preserved, the adamellite is the younger phase. This suggests that the adamellite invaded the gneiss in a lit-par-lit fashion, but locally truncated the structure with later deformation affecting both phases and developing boudins of granodioritic gneiss with adamellite separations. The adamellite also has a distinctive geochemical signature (Goldich et al., 1979) having higher K, Rb, Ba, K/Na, and Rb/Sr and lower Sr/Ba ratios than the granodiorite gneiss.

The granodioritic gneiss is a gray to dark-gray, fine to medium grained, thin layered rock with well-aligned biotite. Apart from its distinctive gray color it contains a higher proportion of more sodic plagioclase. In the Morton area and occasionally in the Granite Falls area, the gneiss is a tonalite and is thus readily distinguished from the adamellite. Due to the limited exposures and deformed character of granodioritic gneisses, no field relationships have been recognized which constrain the number of generations and time interval during which these rocks were formed and emplaced.

FIELD NOTES AND SAMPLE DESCRIPTIONS

During the course of this study, rocks in the Minnesota River Valley were examined in three separate visits. The first two visits were in October 1977 and August 1978. These trips were mainly of a familiarization and reconnaissance nature insofar as localities which had already been sampled by Goldich et al. (1970) and Goldich and Hedge (1974) were mainly visited. After Sm-Nd analytical data were obtained from a number of samples supplied by S. S. Goldich from these localities, it was decided to revisit and resample some of these localities in October 1978. This latter sampling was undertaken with G. J. Wasserburg, S. S. Goldich together with assistance from R. Beltrame, and D. Bergstrom from the Minnesota Geological Survey. The following descriptions include both field and laboratory notes. Modes and chemical analyses of samples (from Goldich et al., 1979) are summarized in Tables A5-1 to A5-8.

Figure A5-2. a) GC-2:-Thin layered gray granodioritic gneiss from Green Company Quarry. The lighter portions are quartz, feldspar rich segregations.

b) GC-3:- Medium grained homogeneous amphibolite from Green Company Quarry.

c) GC-4:- Medium grained red-brown adamellite from Green Company Quarry.

d) GC-7:- Heterogeneous rock consisting of adamellite (darker) interlayered with granodiorite gneiss (lighter), from Green Company Quarry.

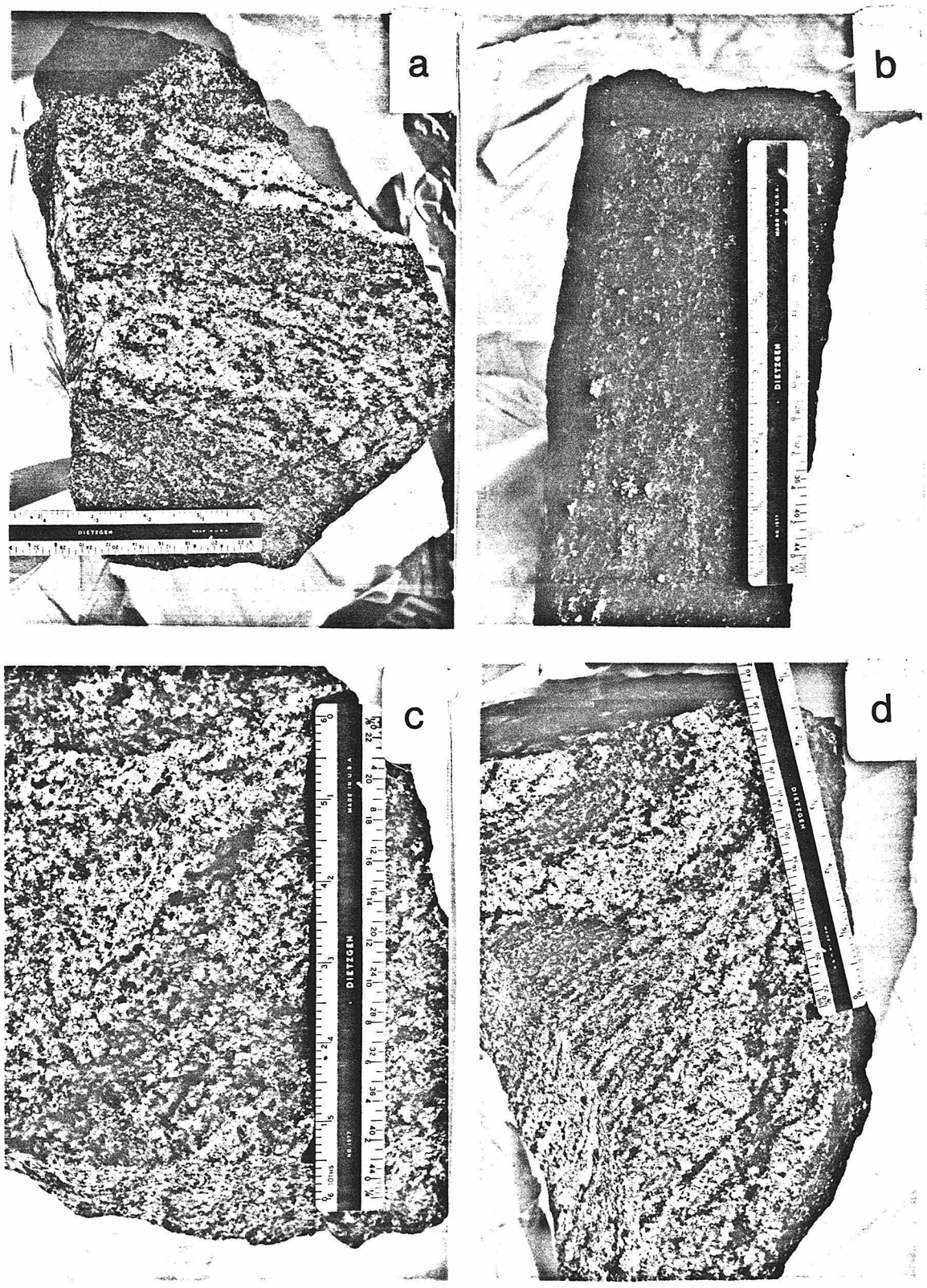

Fig. A5-2

Figure A5-3. a) GC-9:- Massive uniform plagioclase-quartz-pyroxene-biotite gneiss from Green Company Quarry. This lithology typically has a green caste and is equivalent to the pyroxene gneiss described by Himmelberg (1968).

b) S-1:- Light gray coarse grained tonalitic gneiss from Schumacher Farm. This sample is part of the Morton gneiss.

c) 649-2:- Dark gray, coarse grained and thinly banded gneiss from Morton

d) SH-1:- Sacred Heart granite. Although inclusions of the Morton gneiss are occasionally found in the Sacred Heart granite, in this photograph the darker feature is due to a shadow.

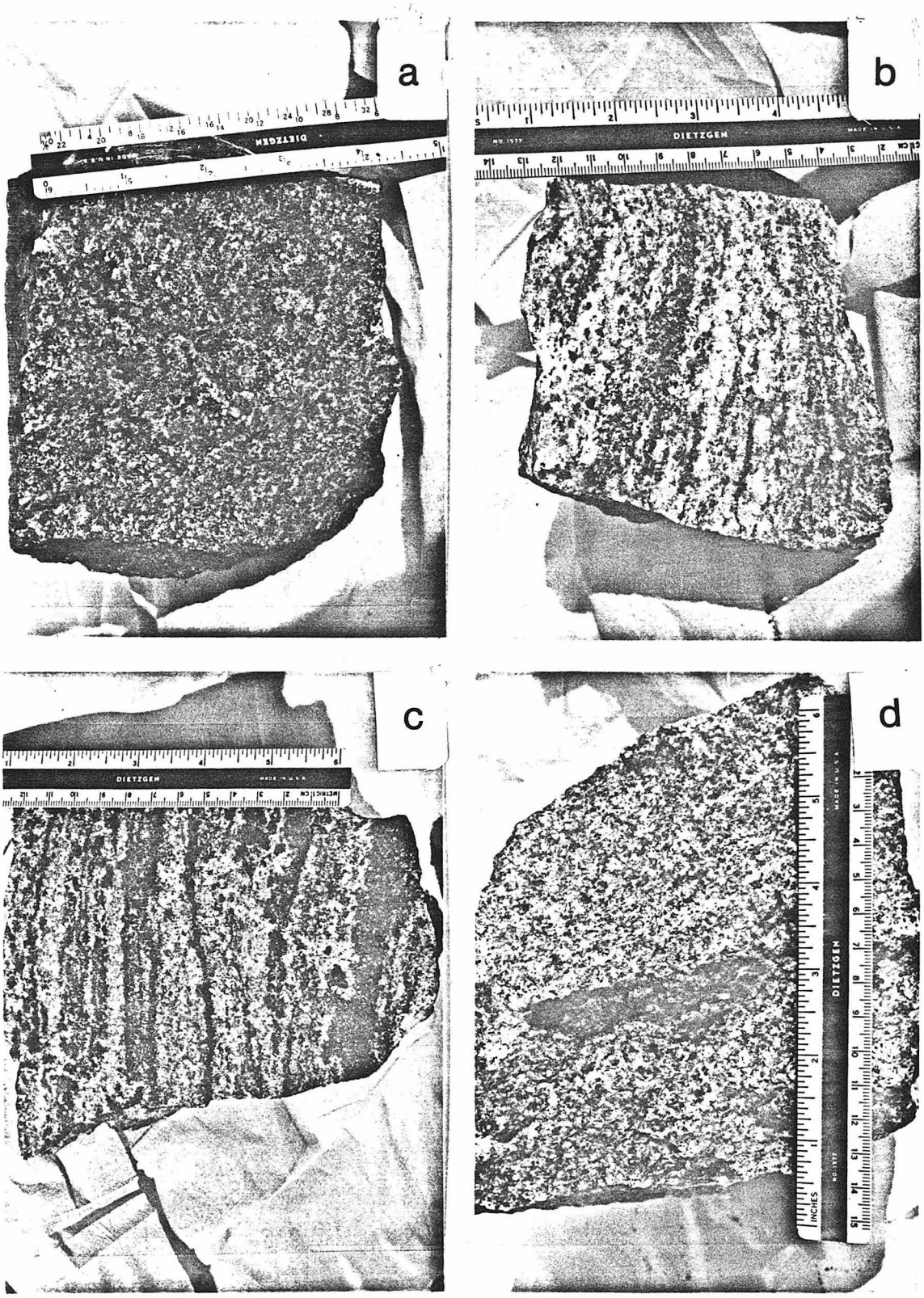

Fig. A5-3

October 14-19, 1978

15th October 1978, Sunday

Collected samples from the active Green Company Quarry in Granite Falls (see Fig. A5-1). From the geologic map of Himmelberg (1968)(Fig. A5-1), it can be seen that the quarry is mostly within the "Montevideo gneiss" defined by Lund (1956) and Himmelberg (1968) However, it is adjacent to the contact of the mafic hornblende-pyroxene gneiss body and is crosscut by younger hornblende diabase dikes.

In the latter part of the day exposures of the Montevideo gneiss in the roadcut along highway 212 were examined in the vicinity of the township of Montevideo. Outcrops of the garnet-biotite gneiss (metasediment?) and the hornblende-pyroxene gneiss near Memorial Park Granite Falls were examined on the return trip.

Sample GC-2. Green Company Quarry middle west wall. (Collected sample from boulder with sledge hammer)(sample 833 of S. S. Goldich). See Figs. A5-1 and A5-2.

Field. Dark grey thin layered gneiss which is fine to medium grained and has a relatively uniform foliation defined by biotite-qtz + feld layers. In addition, there are several leucocratic feldspathic 1-2 cm layers which are coarser grained ($\sim$ 1 cm). Spects of pyrite are visible in hand specimen suggesting some alteration.

Laboratory. Equigranular, cataclystic texture with qtz, plag, K-spar, biotite. Some of the biotite is partially altered to hematite.

This is a relatively pure chunk of the granodioritic gneiss which appears to be free of any adamellite contamination. One half of the sample ($\sim$ 6 kg) was pulverized and ground to $<$ 50 mesh and split for W.R. sample.

Sample GC-3. Green Company Quarry N-W wall (collected with sledge hammer). See Figs. A5-1 and A5-2b.

Field. Black massive and very uniform amphibolite. In hand specimen appears to consist almost entirely of hornblende. Collected from quarry face. Appears to be crosscut by adamellite and itself crosscuts hornblende-pyroxene gneiss, i.e., younger than hornblende-pyroxene gneiss, older than adamellite.

Laboratory. Consists of predominantly hornblende with less than 10% orthopyroxene and plagioclase. The orthopyroxene and plagioclase occur interstitially suggesting that they are late stage crystallization products.

Sample GC-4. Green Company Quarry same locality as GC-3 (collected with sledge hammer) (sample 828 of S.S. Goldich). See Figs. A5-1 and A5-2c.

Field. Dark red-brown equigranular medium grained adamellite. Uniform red K-feldspars with dark grey quartz grains $\sim$ 2mm in diameter. This is a relatively pure chunk of the adamellite gneiss which appears to be free of any contamination from the granodioritic gneiss.

Laboratory. In thin section it is apparent that this sample is more altered insofar as most of the feldspar is cloudy and is being

replaced by sericite. Hematite is also replacing the biotite. Approximately 1-2 kg of this relatively uniform rock was ground to < 50 mesh and split for W.R. sample.

Sample GC-5. Green Company Quarry. Approximately 200 yards S.W. of GC-3 (collected with sledge hammer). See Fig. A5-1.

Field. Distinctive thin layered granodioritic gneiss with a granoblastic texture and local porphyroblasts of hornblende which are aligned with the biotite. Crosscutting the gneiss is a fine grained aplite vein which grades into a coarser grained pegmatite. These distinctive lithologies were not recognized in the quarry walls and it is possible that the large boulder from which the sample was taken is a glacial erratic.

Sample GC-6. Green Company Quarry adjacent to GC-5 (collected with sledge hammer). See Fig. A5-1.

Field. Collected from a boulder near the quarry wall and is typical of the samples in the quarry wall. Consists of coarse (3-4 cm) and finer (~ 1 cm) bands of adamellite interlayered with granodiorite. This sample was collected as it contains both granodiorite and adamellite and therefore age relationships between the two units can be directly ascertained.

Sample GC-7. Green Company Quarry; same location as GC-6 (collected from boulder with sledge hammer). See Figs. A5-1 and A5-2d.

Field. Similar sample to GC-6 in that it is typical of the wall rocks and contains both adamellite and granodiorite. Collected

for the same reason.

Sample GC-8. Green Company Quarry, same location as GC-3. See Fig. A5-1.

Field. Mixed sample consisting of a 3-4 cm layer of adamellite between a mafic pyroxene gneiss. The layering is parallel to the foliation defined by biotites.

Sample GC-9. Green Company Quarry, same location as GC-3. See Fig. A5-3a.

Field. Massive relatively undeformed pyroxene-gneiss with a greenish caste. This sample is probably equivalent to the hornblende-pyroxene gneiss mapped by Himmelburg (1968) as the contact is close to where the sample was collected.

Laboratory. Contains quartz, plagioclase, and orthopyroxene. Some of the feldspar contains antiperthitic blebs. The pyroxene is partially altered to chlorite.

Sample GC-10. Green Company Quarry. See Fig. A5-1.

Field. Diabase dike, contains small phenocrysts of plagioclase. This sample is part of the younger dike complex which dissects the quarry and is undeformed. K-Ar and zircons from similar dikes give an age of 1800 m.y.

Laboratory. Composed of plagioclase laths which are poikalitically enclosed by altered hornblende-pyroxene aggregates. There are also large zoned plagioclase phenocrysts indicating at least a two-stage cooling history.

October 16th, 1978

Quarried sample of the Morton gneiss from Shumacher Farm (Map 1). Also collected sample of amphibolite and aplite dike from the same locality. Later in the day visited the Sacred Heart quarry with B. Beltrame and collected samples of Sacred Heart granite. G. J. Wasserburg left for Minneapolis in the early afternoon.

Sample S-1. Map 1 Shumacher Farm (sample obtained by air-drilling and wedging)(Sample 835 of S.S. Goldich). See Fig. A5-3b.

Field. Light gray, coarse grained, layered tonalitic gneiss from the ledge east of the large aplite dike. As this sample has irregular banding consisting of quartzo feldspathic layers (1-2 cm) a large 18" x 18" block of the gneiss was collected. In hand specimen brown stained sphenes are apparent. No adamellite or younger granitic material present.

Laboratory. In thin section the gneiss contains mostly plagioclase plus some quartz, biotite, microcline, and traces of sphene and apatite. Some of the plagioclase is slightly sericitized. Approximately 1/2 of the rock was crushed and ground to a fine powder (< 100 mesh) and split for a whole rock sample.

Sample S-2. Shumacher Farm (collected by sledge hammer).

Field. Amphibolite collected from an approximately 30' x 15' raft of amphibolite. The amphibolite consists mainly of hornblende with some plagioclase phenocrysts and is somewhat altered to chlorite and serpentine (?). Small 1-2 cm quartzo-feldspathic veins

are present in the amphibolite raft but were not present in the sample.

Sample S-3. Shumacher Farm (collected by sledge hammer).

Field. Large aplite dike which crosscuts the tonalitic gneiss (S-1). Pinkish-gray, sugary textured, fine-grained biotite aplite. The aplite has large grains of altered allanite and has a weak secondary foliation.

Sample SH-1. Sacred Heart granite (collected by sledge hammer). See Fig. A5-3d.

Field. Collected fresh pieces from an abandoned quarry which is approximately 1/2 mile S. of Minnesota River along Redwood County Road 9. This sample is relatively undeformed medium-grained gray-to-red colored fairly uniform rock containing ~ 40% K-spar, 30% plag, 20% quartz, and ~ 10% biotite and accessory minerals. In an adjacent outcrop there are inclusions of mafic rocks and tonalitic gneisses which are almost certainly pieces of the Morton gneiss. This indicates that Sacred Heart granite is younger than Morton gneiss. Zircons from Sacred Heart give an upper intercept age of ~ 2530 m.y. (Goldich et al., 1970). Initial Sr = 0.702.

October 17th, 1978

Quarried sample of the Morton gneiss from an inactive quarry (#4) in the vicinity of Morton. In the afternoon collected samples from the Ellison Farm area which is also in the vicinity of

Morton.

Sample 649-2. Morton Quarry #4 (quarried sample using drill and wedges). See Fig. A5-3c. (S.S.Goldich sample KA 811).

Field. Dark gray, coarse-grained, thinly-banded (1-4 mm) hornblende-biotite gneiss with a cataclastic texture. The hornblende is porphyroblastic. Collected a single chunk ~ 12" x 12". This sample is thought to be representative of the uncontaminated tonalite gneiss.

Laboratory. In transferring samples to permanent container split sample into 2 pieces. In the center of one of the pieces are some K-spar and granitic pods suggesting contamination by granitic material.

Sample EF-1. Ellison Farm, Morton, collected with drill and wedges.

Field. This rock contains 3 distinct lithologies:

(1) dark gray, medium-grained biotite tonalite gneiss;

(2) leucocratic fine-grained aplite dike which crosscuts the foliation of the tonalitic gneiss;

(3) finely layered pink-gray granodioritic gneiss. This may represent a mixture of sheared adamellite and tonalite gneiss. This sample was collected as it preserves contact relations for the three different lithologies.

Sample EF-2. Ellison Farm Morton. Collected with drill and wedges.

Field. Gray to pink, medium grained, relatively undeformed biotite adamellite. Has a weak foliation with minor sheared quartz veins and pods.

October 1977 and August 1978

Sample MIN. 1 Shumacher Farm. Amphibolite dike in Morton gneiss which is approximately parallel to the gneissic foliation. Chemical analyses by S. S. Goldich indicates that it has an approximately komatiitic composition.

Sample MIN. 2 Lunds type locality on highway 212 approximately 1 mile SE of Montevideo. Same outcrop as KA431 (Fig. A5-1). Fine to medium grained partially sheared oligoclase-microcline-quartz adamellite. Has a pink to red coloration which is probably due to alteration of biotite.

Sample MIN. 3 Same locality as MIN. 2. Fine to medium grained very homogeneous hornblende-plagioclase amphibolite. Has tholeiitic chemistry. Three chunks were collected.

Sample MIN. 4 Same locality as MIN. 2. Sheared Montevideo gneiss with layers of brick-red granulated pegmatite and dark-gray granodioritic gneiss layers. Some of the granodioritic layers appear to form sharp anticlinal type folds; however, in general, the foliation is parallel to the regional trend.

Sample MIN. 5 Memorial Park Granite Falls (same outcrop as 817, Map 2). Medium grained massive and homogeneous garnet-pyroxene

("graywacke") gneiss. This is part of the mafic series which Lund postulated may have been the older basement intruded by the Montevideo gneiss.

Sample MIN. 6 Granite Falls (same outcrop as 761, Fig. A5-1). Medium to coarse grained dark gray quartz-pyroxene-hornblende-plagioclase gabbro. Some of the mafic minerals are altered to chlorite and actinolite.

Sample MIN. 7 Green Company Quarry Granite Falls (Fig. A5-1). Massive, medium to coarse grained pyroxene-quartz-plagioclase gneiss with a distinct greenish caste. This sample is very similar to GC-9.

Sample MIN. 8 Same location as MIN. 7. Sample consists predominantly of medium to coarse grained pyroxene-gneiss with a green caste. In the centre of the sample is an $\sim$ 1" layer of medium grained adamellite with a red brown caste. The adamellite layer is concordant with the gneissic foliation.

Sample MIN. 9 Same locality as MIN. 7. Mixed sample consisting of mainly red-brown medium grained adamellite together with the pyroxene-gneiss.

Sample MIN. 10 Same outcrop as KA209 (Fig. A5-1). Gray to red-brown medium grained, thin layered well-foliated granodioritic gneiss.

Sample MIN. 11 Abandoned quarries near Montevideo (Fig. A5-1). Red-brown medium grained, coarsely layered adamellite gneiss.

Sample MIN. 12 Redwood Falls State Park. Light-brown residual clay sample from regolith resulting from late Cretaceous weathering of the Morton gneiss. Consists principally of kaolinite and quartz.

Sample MIN. 13 Morton Quarry #5. Light pink medium to coarse grained adamellite. Contains garnet which is an unusual occurrence. Described by S. S. Goldich as "infolded adamellite" as it occurs as highly deformed and irregularly shaped bodies.

Sample MIN. 14 Morton Quarry #2. Black, medium grained hornblende rich amphibolite. Partially intruded by pink veins of pegmatite.

Sample MIN. 15 Active Quarry, Morton. Large (1' x 2') slab of Morton gneiss from active quarry waste pile. Consists of coarse layers of light gray granodioritic gneiss and pink pegmatitic layers. Also contains an amphibolite xenolith.

Sample MIN. 16 Bruekutes Farm Morton. Dark gray, medium grained, thinly layered garnet-muscovite-quartz paragneiss.

Sample MIN. 17 1/2 mile S. of Delphi, same outcrop as 339 of SSG. Gray, medium grained, finely layered and highly contorted sample of granodioritic gneiss.

Goldich and Hedge (1974) and Goldich et al. (1979) Samples

Sample 431

Along Highway 212 (Fig. A5-1) and railroad tracks, 2.6 km SE of Montevideo.

Leuco-adamellite gneiss. Bright red, medium grained, oligoclase-microcline-quartz, minor biotite. Collected along railroad track east of highway.

Sample KA-608

Same locality as 431 (Fig. A5-1).

Granodiorite gneiss. Pinkish-gray, medium to coarse grained (0.5 - 1.0 mm), banded with fine-grained biotitic and coarse-grained quartz-feldspar layers. Collected by R. L. Bauer (Goldich and Hedge, 1974).

Sample KA-605

3.6 km northwest of Granite Falls on Peterson Farm (Fig. A5-1).

Granodiorite gneiss. Pinkish-gray, medium to coarse grained (2-3 mm) oligoclase-quartz-microcline-biotite, similar to KA-608. Collected by R. L. Bauer.

Sample KA-607

3.2 km NW of Granite Falls, west side of river (Fig. A5-1).

Tonalitic gneiss. Grayish-pink, medium grained (1-2 mm), foliated oligoclase-quartz-biotite gneiss. Minor idioblastic

hornblende. Plagioclase is commonly antiperthite. Collected by R. L. Bauer.

Sample 609

Same locality as KA-607 (Fig. A5-1).

Granodiorite gneiss. Light gray, medium-grained plagioclase-quartz- microcline.

Sample 54CGN

Granite Falls Green Company Quarry (Fig. A5-1).

Layered mafic gneiss with dark gray bands, 0.5-2.0 mm thick, andesine-clinopyroxene-orthopyroxene-hornblende-magnetite-ilmenite; light bands 0.5-4 mm thick, largely andesine, quartz, and minor mafites.

Sample KA-606

Same locality as 54CGN (Fig. A5-1).

Granodiorite gneiss. Light to dark reddish-gray, medium grained (0.5-1.5 mm), banded, folded oligoclase-quartz-microcline-biotite gneiss. Collected by R. L. Bauer.

Sample KA-54GN

Same locality as 54CGN (Fig. A5-1).

Granodiorite gneiss, pinkish-gray, medium grained (0.5-1.5 mm), thinly banded (2 mm) plagioclase-quartz-microcline-biotite with minor hornblende.

Sample 815

Memorial Park, Granite Falls (Fig. A5-1).

Metagraywacke. Dark gray, fine-to-medium grained, massive to weakly foliated andesine-pyroxene-quartz gneiss.

Sample 817

Same locality as 815 (Fig. A5-1).

Metagraywacke. Dark gray, fine-to-medium grained (0.2-1.0 mm) thinly layered andesine-quartz-biotite-pyroxene-garnet gneiss.

Sample 761

East edge of Granite Falls (Fig. A5-1).

Metagabbro. Dark gray, sheared, and recrystallized anorthositic gabbro.

Sample 649

Morton Quarry #4.

Tonalitic gneiss. Dark gray, coarse-grained, contorted structure, some amphibolite contamination.

Sample 659

Located SE of Franklin.

Granodioritic gneiss. Dark gray, coarse-grained.

Sample 673

NE of Delphi, Shumacher Farm.

Tonalitic gneiss, gray, fine-to-medium grained.

Sample 339

N of Delphi.

Large sample of gray, banded and contorted gneiss.

Table A5-1. Modes of Montevideo Gneiss, Granite Falls Area

Sample	608	605	609	606	54GN	607	GC-2	GC-5
Quartz	28	32	40	31	28	35	35	35
Plagioclase	48	41	39	46	47	55	40	35
Microcline	20	18	17	13	16	x	15	15
Biotite	2	6	3	8	7	9	8	5
Muscovite	-	-	-	-	-	-	2	-
Hornblende	-	x	-	x	0.6	x	x	10
Opaque	x	x	x	x	x	x	x	x
Allanite	-	x	-	-	-	-	-	-
Apatite	-	x	-	x	x	x	x	x
Sphene	-	x	-	-	-	-	x	-
Zircon	x	x	-	x	x	x	x	x
Chlorite	x	x	-	x	0.8	x	x	x
Epidote	x	-	-	-	x	x	-	-
Garnet	x	-	-	-	-	-	-	-
Sericite	x	x	x	x	x	x	x	x
Hematite	x	x	x	x	x	-	x	x

x = less than 0.5 percent.

Table A5-2. Modes of Layered Mafic Gneisses

Granite Falls Area

Sample	815	817	GC-3	GC-9	761	54CGN
Quartz	8	26	-	20	8.8	6.6
Plagioclase	77	49	4	52	63.4	50.4
Antiperthite	-	-	-	10	-	-
Microcline	x	x	-	-	-	x
Biotite	x	14	1	2	-	x
Opaque	3	1.0	x	3	-	7.0
Hornblende	0.8	-	85	2	19.8	11.4
Orthopyroxene	1	3	10	10	x	4.8
Clinopyroxene	9	4	-	1	8	18.8
Apatite	x	x	x	x	-	x
Sphene	x	x	-	-	-	-
Zircon	x	x	-	-	-	-
Secondary Amphibole	-	-	-	-	x	-
Garnet	-	3	-	-	-	-
Chlorite	x	-	x	x	x	-
Sericite	x	x	-	x	x	x

x = less than 0.5 percent

Table A5-3. Modes of Adamellite, Granite Falls Area and younger samples

Sample	431	GC-4	Sacred Heart (SH-1)	Diabase Dike (GC-10)
Quartz	36	40	30	35
Plagioclase	28	34	20	-
Microcline	31	20	40	-
Biotite	x	5	9	5
Hornblende	-	-	-	-
Actinolite	-	-	-	35
Opaque	10	1	1	10
Apatite	x	-	x	-
Sphene	-	-	-	-
Zircon	x	-	-	-
Calcite	x	-	-	-
Chlorite	-	x	x	10
Epidote	-	-	-	-
Garnet	1.4	-	-	-
Hematite	x	x	x	5
Sericite	x	x	x	x

x = less than 0.5 percent

Table A5-4. Modes of Morton Gneiss

Sample	649	673	339	S-1	659
Quartz	27	5	34	10	29
Plagioclase	53	79	48	73	43
Microcline	x	3	3	5	21
Biotite	9.2	9	14	10	4
Hornblende	10.6	2	-	1	1
Hyperthene	-	-	-	-	1
Opaque	x	0.6	x	0.5	0.3
Allanite	x	x	-	x	-
Apatite	x	0.7	x	0.5	x
Sphene	x	1.4	x	0.5	x
Zircon	x	0.1	x	x	x
Calcite	x	-	-	-	-
Chlorite	x	x	x	x	x
Epidote	x	x	0.7	x	x
Rutite	-	x	x	-	x
Sericite	x	x	x	x	x

x = less than 0.5 percent

Table A5-5. Chemical Analyses of Montevideo Gneiss Granite Falls Area (from Goldich et al., 1979a,b).

Sample	608	605	609	606	54GN	607
SiO_2	73.7	72.3	74.3	72.9	71.8	70.0
Al_2O_3	14.6	14.5	14.3	14.6	14.7	15.9
TiO_2	0.12	0.25	0.15	0.22	0.28	0.32
Fe_2O_3	0.65	0.56	0.57	0.59	0.84	0.74
FeO	0.48	1.58	0.43	1.13	1.57	1.86
MnO	0.02	0.03	0.02	0.02	0.04	0.03
MgO	0.19	0.74	0.20	0.59	0.82	0.83
CaO	1.57	2.27	1.53	2.28	2.77	3.06
Na_2O	4.93	4.29	4.61	4.23	4.39	5.15
K_2O	3.35	2.72	3.39	3.21	2.53	1.27
P_2O_5	0.05	0.08	0.05	0.10	0.09	0.09
H_2O^+	0.09	0.19	0.04	0.09	0.20	0.38
H_2O^-	0.09	0.12	0.07	0.10	0.05	0.12
CO_2	0.0	0.07	0.0	0.0	0.04	0.11
F	0.02	0.03	0.01	0.03	0.03	0.02
Total	99.8_5	99.6_8	99.6_3	100.0_7	100.1_4	99.9_3
ppm						
Rb	92.7	89.1	71.7	89.1	75	41.5
Sr	308	257	339	257	270	379
Ba	390	720	715	720	590	585
Sm	3.68	3.17	0.911	3.26	2.47	3.73
Nd	18.0	18.8	6.66	18.8	17.9	29.3
K/Rb	300	283	392	299	280	253
Rb/Sr	0.30	0.28	0.21	0.35	0.28	0.110
Sr/Ba	0.79	0.36	0.47	0.36	0.46	0.65
Ba/Rb	4.2	9.9	10	8.1	7.8	14.1
Sm/Nd	0.204	0.169	0.137	0.173	0.138	0.127

Table A5-6. Chemical Analyses of Adamellite Gneiss Granite Falls Area (from Goldich et al., 1979b).

Sample	431
SiO_2	73.7
Al_2O_3	14.4
TiO_2	0.14
Fe_2O_3	0.64
FeO	0.53
MnO	0.01
MgO	0.18
CaO	1.27
Na_2O	4.12
K_2O	4.45
P_2O_5	0.03
H_2O^+	0.12
H_2O^-	0.07
CO_2	0.08
F	0.03
Total	99.84
ppm	
Rb	139
Sr	170
Ba	620
Sm	193
Nd	11.28
K/Rb	265
Rb/Sr	0.82
Sr/Ba	0.27
Ba/Rb	4.5
Sm/Nd	0.171

Table A5-7. Chemical Analyses of Layered Mafic Gneisses Granite Falls Area (from Goldich et al., 1979a,b)

Sample	815 (metased)	817 (metagabbro)	761 (metagabbro)	54CGN (metagabbro)
SiO_2	53.7	66.3	53.9	59.2
Al_2O_3	17.4	15.2	20.3	14.5
TiO_2	1.62	0.65	0.39	1.19
Fe_2O_3	4.02	0.47	1.16	3.31
FeO	9.02	4.96	4.85	6.38
MnO	0.19	0.06	0.10	0.19
MgO	2.44	2.80	4.52	3.28
CaO	5.96	3.43	11.1	7.84
Na_2O	4.10	3.53	2.62	2.74
K_2O	1.08	1.96	0.59	0.73
P_2O_5	0.32	0.13	0.04	0.12
H_2O^+	0.14	0.41	0.52	0.40
H_2O^-	0.09	0.12	0.08	0.09
CO_2	0.21	0.04	0.16	0.02
F	0.05	0.06	0.04	-
Total	100.3_2	100.0_9	100.3_5	99.9_9
ppm				
Rb	17.3	55.2	1.92	8.0
Sr	414	324	279	298
Ba	610	660	20	350
Sm	-	-	-	-
Nd	-	-	-	-
K/Rb	518	295	2550	759
Rb/Sr	0.042	0.17	0.007	0.027
Sr/Ba	0.68	0.49	1.4	0.85
Ba/Rb	35	12	104	44
Sm/Nd	-	-	-	-

Table A5-8 , Chemical Analyses of Morton Gneiss (from Goldich et al., 1979b)

Sample	649	673	339	659
SiO_2	65.0	60.6	72.0	71.7
Al_2O_3	15.9	21.1	15.4	14.8
TiO_2	0.52	0.68	0.21	0.30
Fe_2O_3	1.61	0.77	0.38	0.13
FeO	3.12	1.53	1.44	2.12
MnO	0.09	0.04	0.02	0.02
MgO	1.92	0.79	0.64	0.74
CaO	4.63	5.03	2.22	2.49
Na_2O	4.93	7.10	5.80	3.96
K_2O	1.28	1.40	1.71	3.50
P_2O_5	0.21	0.31	0.01	0.10
H_2O^+	0.44	0.32	0.32	0.24
H_2O^-	0.07	0.06	0.05	0.09
CO_2	0.03	0.03	n.d.	0.06
F	0.07	0.05	n.d.	0.06
Total	99.7_9	99.7_9	100.2	100.2_8
ppm				
Rb	67	61.4	38.8	86.4
Sr	362	1448	588	283
Ba	240	330	650	750
Sm	8.89	2.41	1.32	2.33
Nd	51.4	16.8	12.1	19.6
K/Rb	159	189	366	336
Rb/Sr	0.19	0.042	0.066	0.31
Sr/Ba	1.5	4.4	0.90	0.38
Ba/Rb	3.6	5.4	17	8.7
Sm/Nd	0.173	0.143	0.109	0.119

REFERENCES

Goldich, S. S., C. E. Hedge, and T. W. Stern, Age of the Morton and Montevideo gneisses and related rocks, southwestern Minnesota, Geol. Soc. America Bull., 81, 3671-3695, 1970.

Goldich, S. S., and C. E. Hedge, 3,800-Myr granitic gneiss in southwestern Minnesota, Nature, 252, 467-468, 1974.

Goldich, S. S., C. E. Hedge, T. W. Stern, J. L. Wooden, J. B. Bodkin, and R. M. North, Archean rocks of the Granite Falls area, southwestern Minnesota, In press, Geol. Soc. America Memoirs, 1979 .

Goldich, S. S., and J. L. Wooden, Origin of the Morton gneiss, southwestern Minnesota, Part III. Geochronology, In press, Geol. Soc. America Memoirs, 1979 .

Himmelberg, G. R., Geology of Precambrian rocks, Granite Falls-Montevideo area, southwestern Minnesota, Minnesota Geol. Survey Spec. Pub. Ser., SP-5, 33p, 1968.

Lund, E. H., Igneous and metamorphic rocks of the Minnesota River Valley, Geol. Soc. America Bull., 67, 1475-1490, 1956.

Wooden, J. L., S. S. Goldich, and N. H. Suhr, Origin of the Morton gneiss, southwestern Minnesota, Part II. Geochemistry, In press, Geol. Soc. America Memoirs, 1979.

PART II. Ba, Nd AND Sm ISOTOPIC ANOMALIES IN THE ALLENDE METEORITE

CHAPTER 3. Ba, Nd, Sm AND Sr ISOTOPIC ANOMALIES IN THE ALLENDE METEORITE

INTRODUCTION

To produce heavy elements with $Z \geq 29$, it has been recognized (see for example Burbidge et al., 1957) that at least three distinct nucleosynthetic processes are required. These are (1) the s-process which involves the capture of neutrons on a long time scale ($>$ 10 years) compared to the β decay rates; (2) the r-process which involves the capture of neutrons on a rapid time scale compared to the β decay rates; and (3) the p-process which is required to produce the neutron-poor isotopes and may involve proton or (γ,n) reactions (Woosley and Howard, 1978).

Although the presently observed isotopic abundances are undoubtedly a result of complex combination of these processes and multiple recycling of material, it is possible that variable isotopic abundances reflecting different mixes of nucleosynthetic components may still be preserved within some parts of the solar system. Meteorites are the most likely candidates to have preserved isotopic heterogeneities as they are relatively "pristine" having largely escaped the chemical and physical reprocessing characteristic of larger planetary bodies. During the last twenty years a number of studies of the isotopic composition of elements in meteorites have been undertaken in an attempt to find these anomalies. With the exception of the rare gases in which there is some evidence for nucleosynthetic anomalies (see for example Reynolds and Turner, 1964 and Lewis et al., 1975), most studies have shown that the isotopic composition of elements in meteorites is remarkably homogeneous and is identical to

Figure 3-1. Chart of the nuclides showing the nucleosynthetic processes involved in the production of Ba isotopes. The heavy line shows the s-process path which is controlled by the relatively slow neutron capture rate (years) versus the β decay rate. The dashed line shows the branching in the s-process due to the intermediate β decay rate of ^{134}Cs. The diagonal arrows show the contributions from the r-process which involves neutron capture on a rapid time scale. The p-process isotopes are produced by proton or γ,n reaction. It can be seen that ^{130}Ba and ^{132}Ba are p-process only and ^{134}Ba and ^{130}Ba are s-process only, as these isotopes are shielded from the r-process by Xe isotopes. ^{135}Ba, ^{137}Ba, and ^{138}Ba have contributions from both the s- and r-processes.

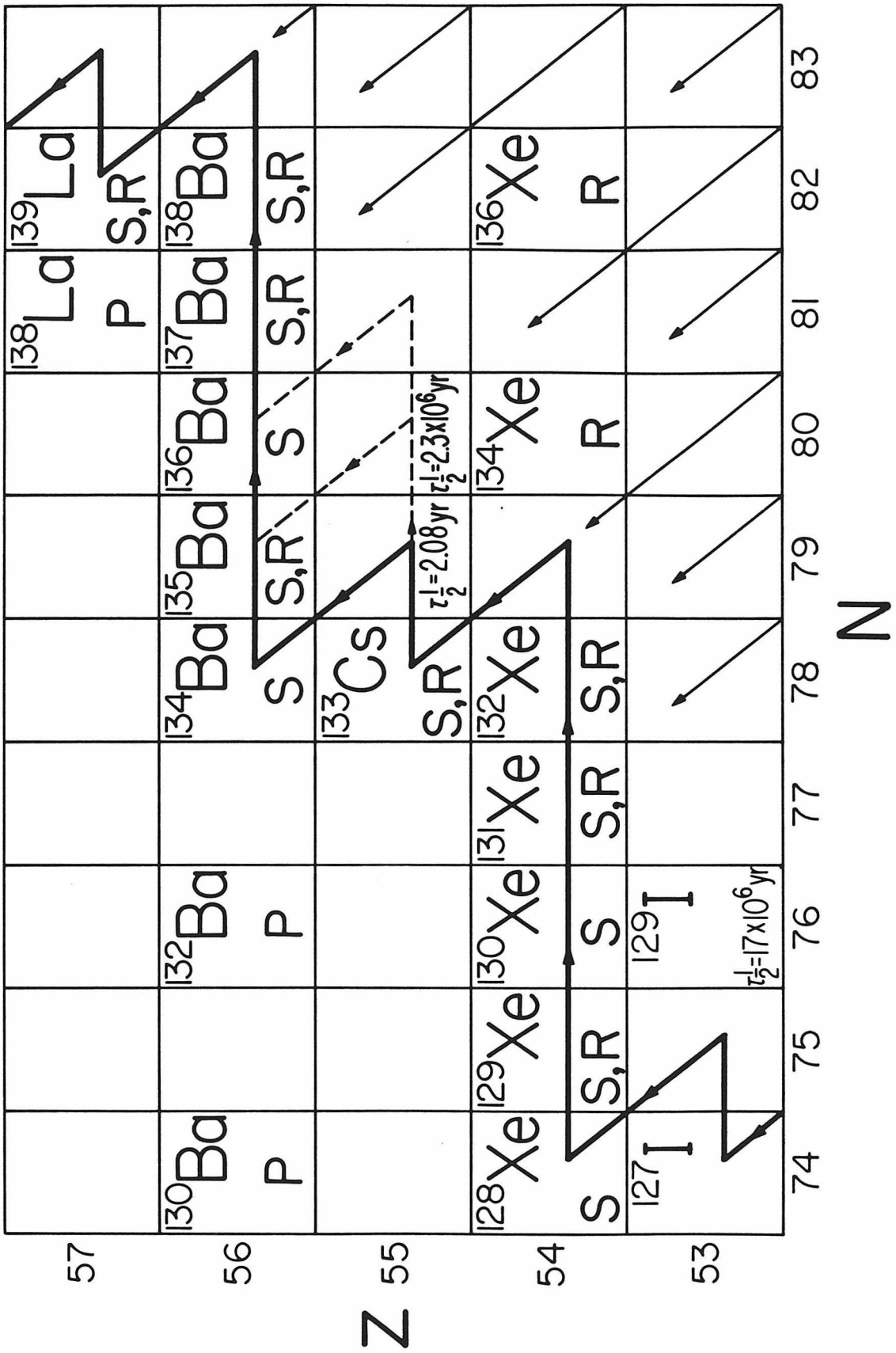
^{139}La
S,R
^{138}La
P
^{138}Ba
S,R
^{137}Ba
S,R
^{136}Ba
S
^{135}Ba
S,R
^{134}Ba
S
^{136}Xe
R
^{134}Xe
R
^{132}Ba
P
^{130}Ba
P
^{133}Cs
$\tau_{\frac{1}{2}}=2.08$yr
$\tau_{\frac{1}{2}}=2.3\times10^{6}$yr
S,R
^{132}Xe
S,R
^{131}Xe
S,R
^{130}Xe
S
^{129}Xe
S,R
^{128}Xe
S
^{129}I
$\tau_{\frac{1}{2}}=17\times10^{6}$yr
^{127}I
74
75
76
77
78
79
80
81
82
83
N
53
54
55
56
57
Z

Fig. 3-1

Figure 3-2. Relative abundances and proportions of the s-, r-, and p-processes involved in the production of the barium isotopes. It can be seen that ^{138}Ba is the most abundant isotope having the largest s-process component due to its "magic" neutron number of N = 82.

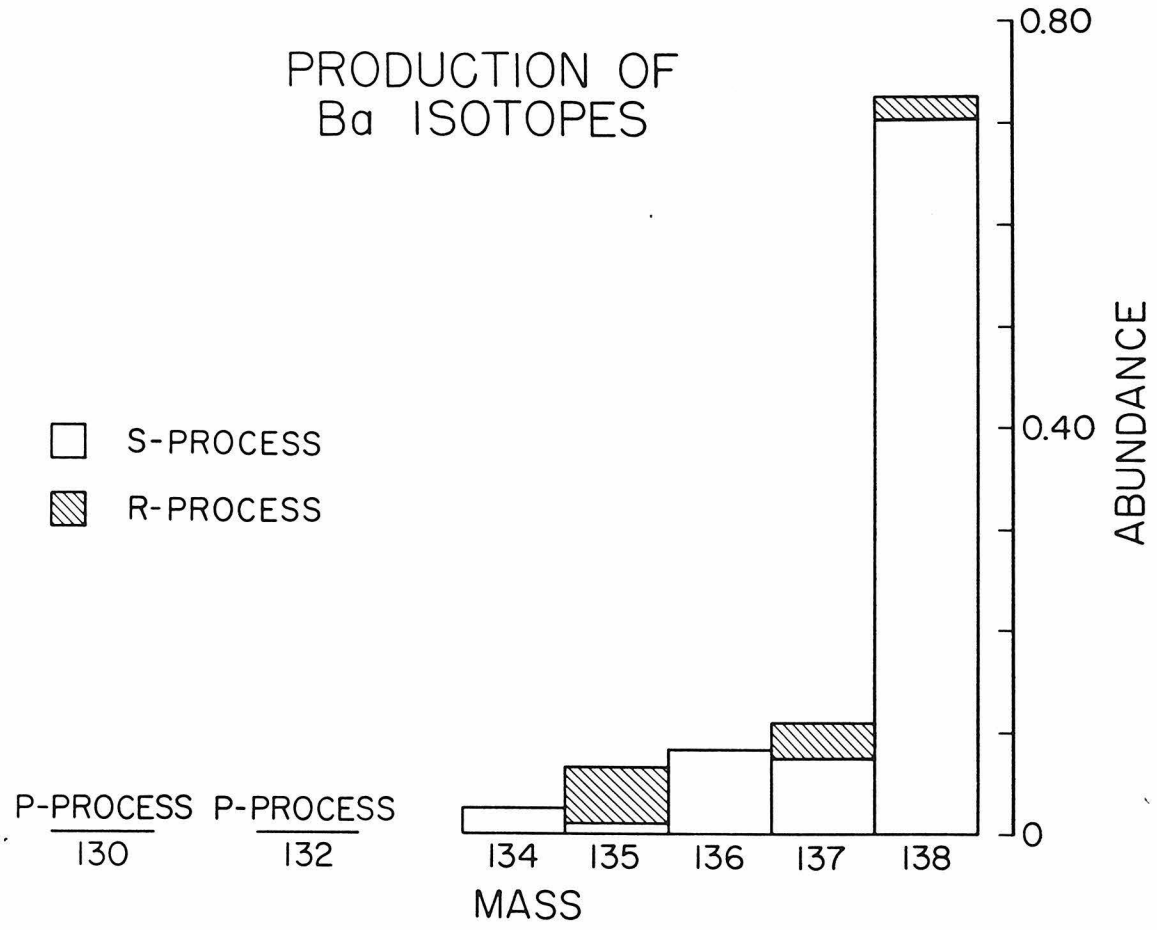
PRODUCTION OF
Ba ISOTOPES
S-PROCESS
R-PROCESS
P-PROCESS
130
P-PROCESS
132
134
135
136
137
138
MASS
0.80
0.40
0
ABUNDANCE

Fig. 3-2

terrestrial elements. There have been a few claims of the existence of isotopic anomalies (for example Ba anomalies by Umemoto, 1962) but these have always been shown (Eugster et al., 1969; DeLaeter and Date, 1973) to be artifacts of the measuring procedures.

With the fall of the Allende meteorite in 1969 and the subsequent discovery of extremely primitive Sr (Gray et al., 1973) oxygen isotopic anomalies (Clayton et al., 1973) and ^{26}Mg decay products from ^{26}Al (Lee et al., 1976, 1977), we decided to re-investigate the problem of isotopic anomalies in the high Z elements. Barium was initially chosen for this study as it is enriched in many of the inclusions by a factor of 10 to 20 compared to chondritic concentrations and high precision analyses could be obtained from small quantities (< 20 ng) of material. In addition, the Ba isotopes are produced by all the major nucleosynthetic processes. This is shown in Figures 3-1 and 3-2 with ^{134}Ba and ^{136}Ba being s-process only, ^{130}Ba and ^{132}Ba p-process only, and ^{138}Ba, ^{137}Ba, and ^{135}Ba having contributions from both the s- and r-processes. During the course of this investigation isotopic anomalies were found in Ba and Nd (McCulloch and Wasserburg, 1978a) and later Sm (McCulloch and Wasserburg, 1978b and Lugmair et al., 1978) and Sr (Papanastassiou and Wasserburg, 1978). These findings will be reviewed together with the results of an extensive survey of the Ba isotopic composition (McCulloch et al., 1976).

EXPERIMENTAL PROCEDURES

In this study we analyzed a number of different elements from the same sample. This required the adoption and combination of a number of different chemical separation procedures which had previously been designed for separation of individual elements. This was particularly important in this study as there was only an extremely limited quantity of material available (< 20 mg).

To separate Sr, Ba, Sm, Nd and the heavy REE the following procedure was adopted (see Figure 3-3).

(1) Ba, REE, and the major elements are separated by using a 1cm x 17cm cation exchange column with Dowex 50-8x, 100-200 mesh resin. Although Ba and the REE are separated to some extent, Ba and Nd overlap and must be separated by using an additional column.

(2) Ba and Nd are separated by using the same ion exchange column as in step 1 but by using only 4N HCl elution. Although there is a reasonable separation of Ba from Nd and the heavy REE, the light REE, Ce, and La overlap into the Ba fraction. The presence of Ce and La in the Ba fraction is not a problem as Ce and La run as oxides in the mass spectrometer and therefore do not interfere with the Ba element. However, in order to separate Ce and La for future isotopic composition determinations and to eliminate the possibility of any interference to Ba another column separation step was introduced.

(3) Ce and La are separated from Ba by using micro-cation column and eluting with lactic acid of ph = 5.3 to remove La and Ce, followed by 4N HCl elution to remove Ba. As shown in Figure3 -3,

Figure 3-3. Flow diagram illustrating the steps required for the separation of Sr, Ba, La and Ce, Sm, Nd, and heavy REE using ion exchange procedures. The procedure uses four columns: 2.5 N HCL, 4N HCl, and lactic acid columns of ph 5.3 and 4.6. The dashed line shows an alternate procedure where the 4N HCl column is bypassed and the Ba and REE fractions are separated by using the lactic acid column of ph 5.3.

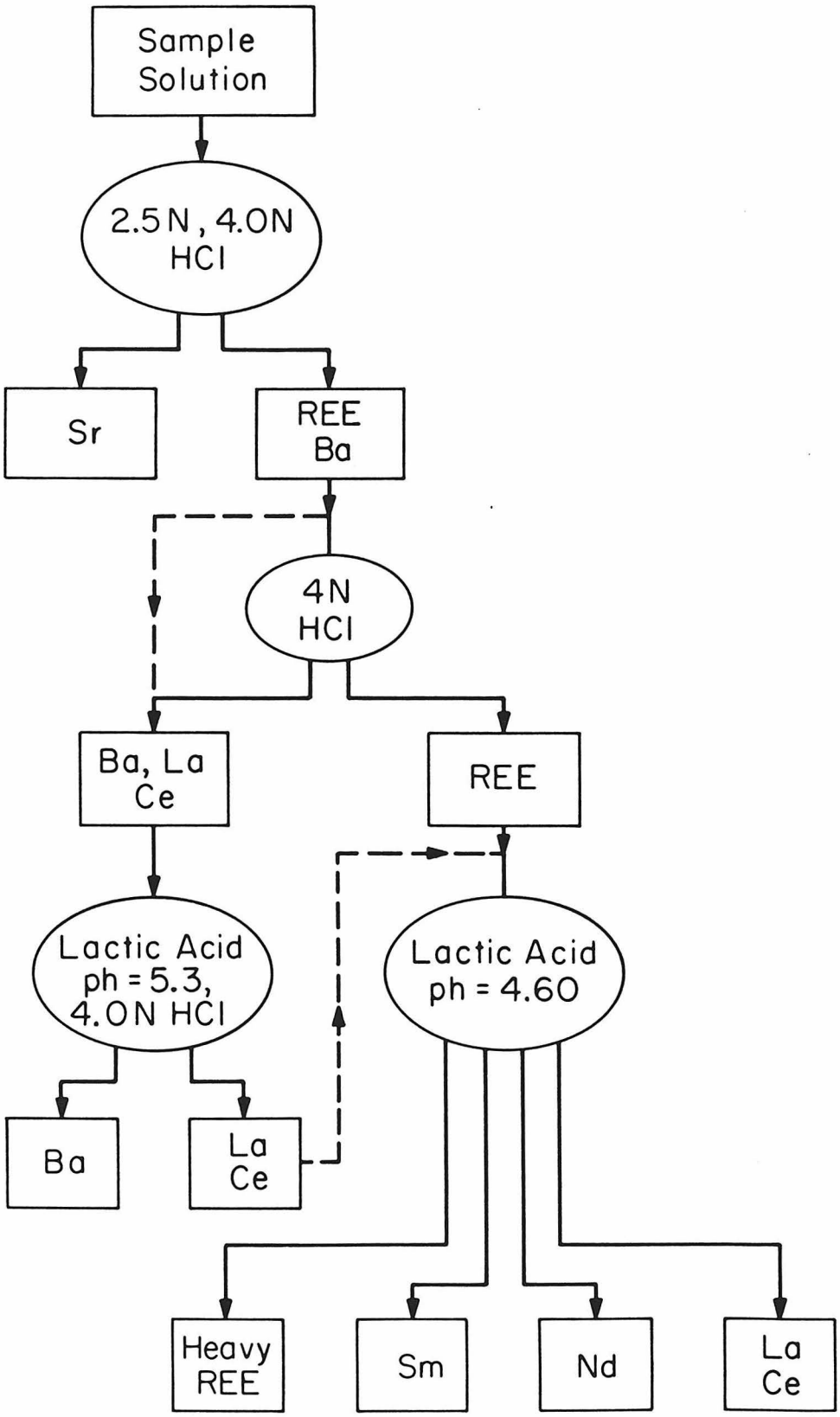
Sample Solution
2.5N, 4.0N HCl
Sr
REE Ba
4N HCl
Ba, La Ce
REE
Lactic Acid ph = 5.3, 4.0N HCl
Lactic Acid ph = 4.60
Ba
La Ce
Heavy REE
Sm
Nd
La Ce

Fig. 3-3

step 2 could be bypassed with this column.

(4) Sm and Nd are separated by using a 40 cm long, 2 mm internal diameter capillary tube with Dowex 50 - 8x, > 400 mesh resin adjusted to the NH_4^+ form. The REE are eluted with 0.2M lactic acid of ph = 4.60. The ph is adjusted for the optimum separation of Sm and Nd and to separate for example the heavier REE Gd, a ph of 4.0 would be required.

To ascertain our ability to resolve small isotopic variations, a series of terrestrial Ba standards were enriched in ^{137}Ba and ^{134}Ba. Table 3-1 shows the data obtained from mass spectrometric measurements and the calculated enrichments from gravimetry. Figures 3-4 and 3-5 show the measured versus calculated values for the enriched standards. The enrichment relative to the terrestrial standard is expressed in parts per ten thousand, and is given by:

$$\varepsilon_{137}^{S,G} = \frac{\left(\frac{^{137}Ba}{^{138}Ba}\right)^{S,G} - \left(\frac{^{137}Ba}{^{138}Ba}\right)_{std}}{\left(\frac{^{137}Ba}{^{138}Ba}\right)_{std}} \times 10^4$$

where the superscript may be either S or G. G stands for the expected enrichment from gravimetry and S for the enrichment measured on the mass spectrometer. $\varepsilon_{134}^{S,G}$ is an analogous expression. From the deviations of the means off the 45° line and the extent of the error bars (2σ mean) for the enriched samples and reference standards, we conclude that we can resolve 0.008% in $^{137}Ba/^{138}Ba$ and 0.02% in $^{134}Ba/^{138}Ba$. Although enrichment experiments have not been performed for the remaining isotopes, the resolution of variations in these

Table 3-1. Comparison of enriched standards: Gravimetric (G) and Spectrometric (S)

Standard	S ε_{137}	G ε_{137}	$^{137}Ba/^{138}Ba$ x10^4	S ε_{134}	G ε_{134}	$^{134}Ba/^{138}Ba$ x10^4
0	0.00±.03	0.00	1565.18±.07 1565.15±.06	0.00	0.00	337.11±.05 337.08±.03
I	0.83±.64	0.90	1565.30±.10	0.9±1.8	0.81	337.13±.06
II	3.58±.45	3.83	1565.73±.07	5.0±1.2	3.56	337.27±.04
III	7.99±.58	7.93	1566.42±.09	7.4±1.5	7.10	337.35±.05
IV	11.48±.45	11.99	1566.97±.07	10.7±1.5	10.73	337.46±.05
V	26.71±.51	27.03	1569.35±.08	25.8±1.8	24.19	337.97±.06

Figure 3-4. Measured enrichments in ^{137}Ba of a terrestrial standard versus calculated enrichments. ε^{S}_{137} is the measured deviation from normal in parts in ten thousand and ε^{G}_{137} is that calculated from gravimetry. It can be seen that there is good agreement between measured and calculated enrichments.

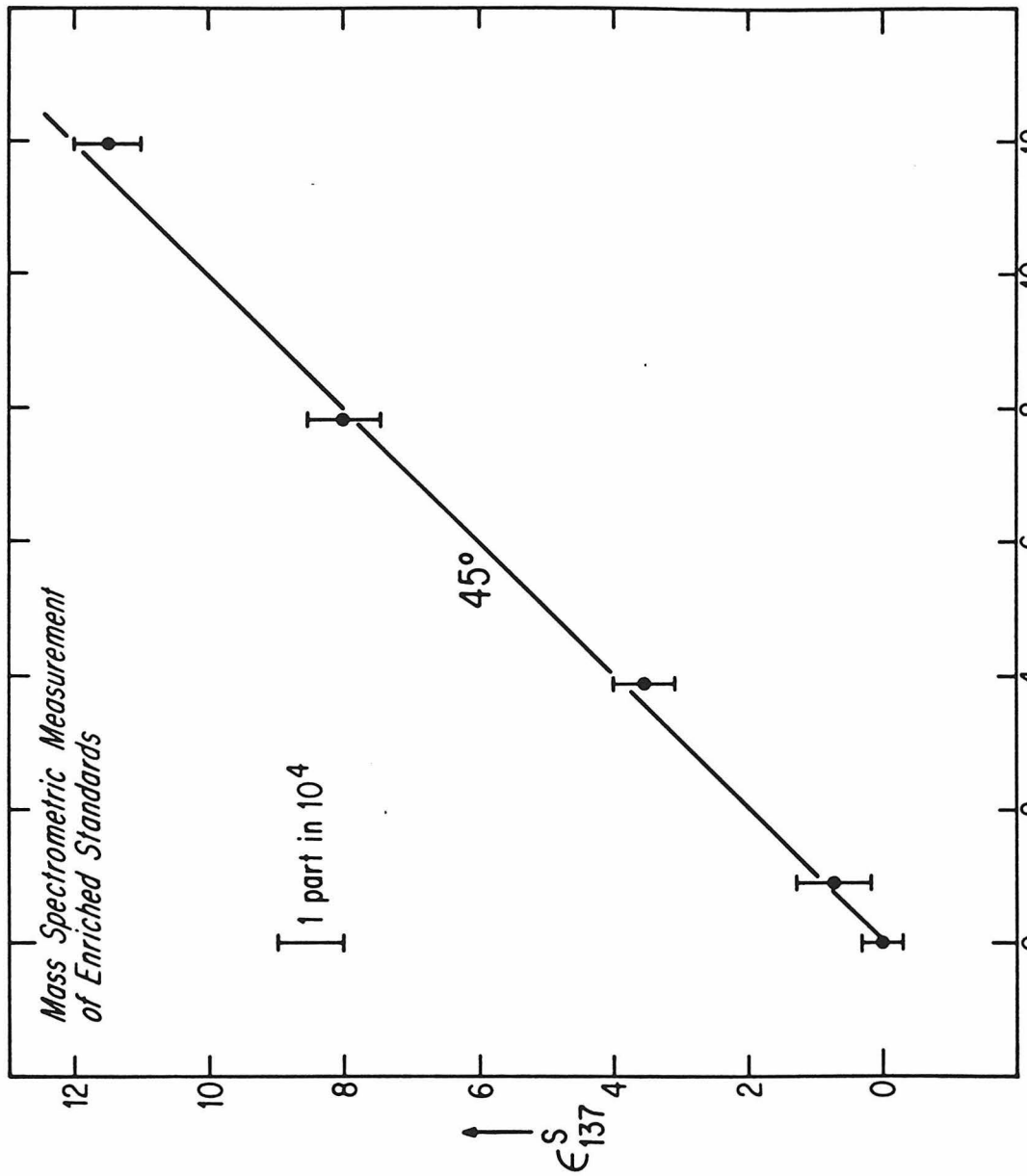
Mass Spectrometric Measurement
of Enriched Standards
1 part in 10^4
45°
ϵ^S_{137}
ϵ^G_{137}
0
2
4
6
8
10
12

Fig. 3-4

Figure 3-5. Measured enrichments of ^{134}Ba versus enrichments calculated from gravimetry. Due to the lower abundance of ^{134}Ba compared to ^{137}Ba (see Figure 3-2) the errors for ε^{S}_{134} are larger, but there is again good agreement between the measured and calculated enrichments.

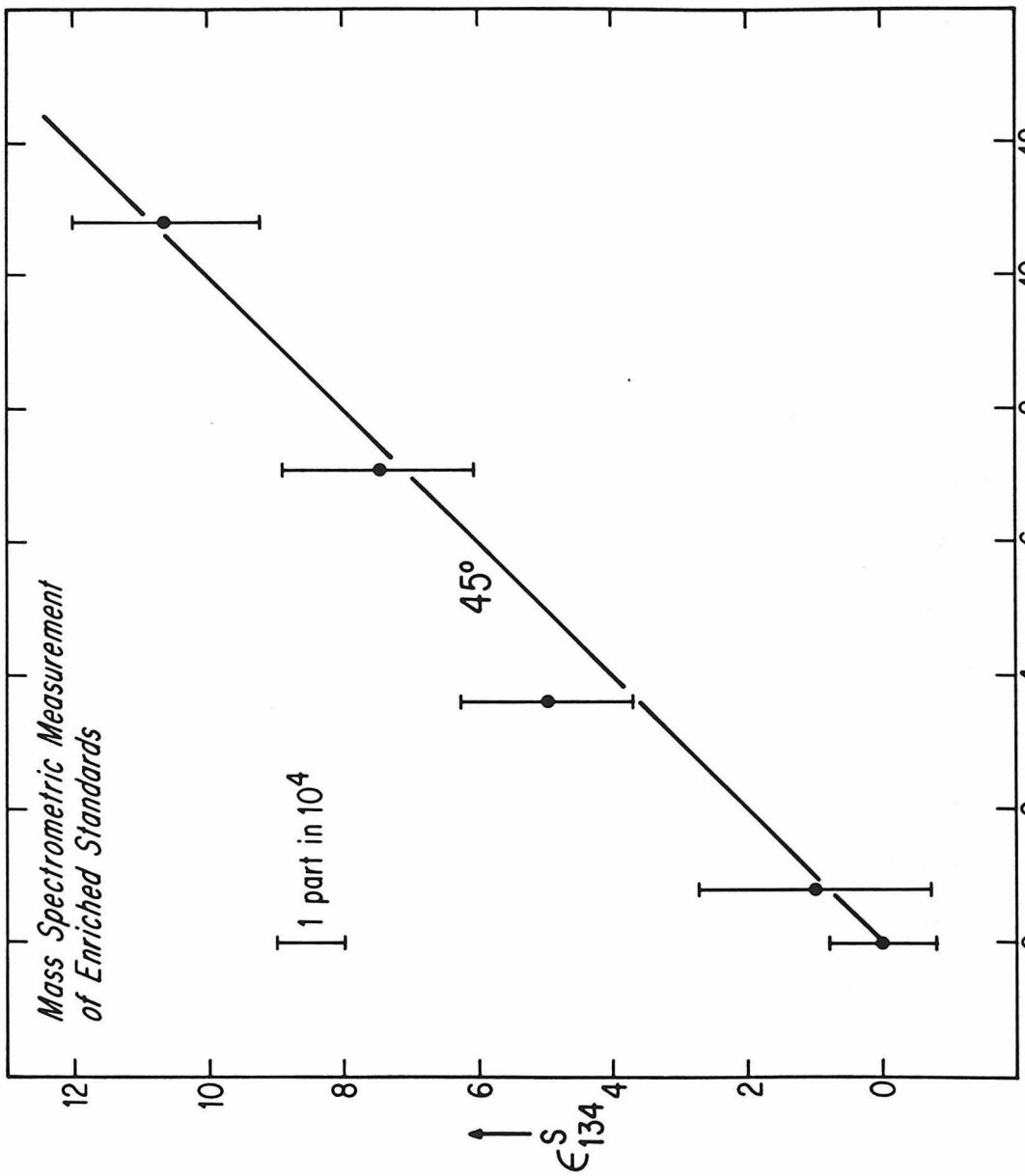
Mass Spectrometric Measurement
of Enriched Standards
1 part in 10^4
45°
ϵ^S_{134}
ϵ^G_{134}
0
2
4
6
8
10
12

Fig. 3-5

isotopes is estimated to be 0.01% for $^{136}Ba/^{138}Ba$, 0.015% for $^{135}Ba/^{138}Ba$, and 0.2% for $^{132}Ba/^{138}Ba$ and $^{130}Ba/^{135}Ba$.

Mg, O, AND Hg ISOTOPIC CHARACTERISTICS OF SAMPLES

In this study we analyzed Ca-Al-rich inclusions which are typical of the type considered as high-temperature condensation products from the solar nebular (see Grossman, 1972). Many of these inclusions had previously been shown to contain Mg (Lee et al., 1977) and O (Clayton et al., 1977) anomalies. In addition matrix from the Allende meteorite which had been shown to contain Hg anomalies (Jovanovic and Reed, 1976) was also analyzed.

1. Mg Isotopic Characteristics

In Table 3-4 and Figure 3-6, the Mg isotopic characteristics of the samples analyzed in this study is tabulated. In the first two columns, the unnormalized $\delta^{25}Mg$ and $\delta^{26}Mg$ values from Wasserburg et al. (1977) are listed. These are the deviations in parts per thousand of the raw measured $^{25}Mg/^{24}Mg$ and $^{26}Mg/^{24}Mg$ ratios from their normal values. It can be seen that the deviations for B29, C1, and EK1-4-1 are approximately proportional to the mass difference, with $\delta^{26}Mg = 2\ \delta^{25}Mg$. This indicates that the anomalous Mg is probably due to mass fractionation effects (see Wasserburg et al., 1977). Assuming that "normal" is defined by terrestrial samples, then the negative fractionation observed in B29 suggests that this inclusion may represent the complementary component of C1 and EK1-4-1.

In the third column of Table 3-4, the $\delta^{26}Mg$ values corrected for mass fractionation are listed. The large positive deviation of $\delta^{26}Mg$ in the plagioclase from the inclusion WA together with its high

Table 3-2. Samples with Magnesium, Oxygen, and Mercury Isotopic Variations

Sample	$\delta^{25}Mg$ (unnormalized ‰)	$\delta^{26}Mg$ (unnormalized ‰)	$\delta^{26}Mg$ [a] (normalized ‰)	$\delta^{18}O$ (‰)	$\delta^{17}O$ [b] (‰)	$\frac{(^{202}Hg/^{196}Hg)_{meas}}{(^{202}Hg/^{196}Hg)_{normal}}$ [c]
WA plag	-	-	85±3	-	-	-
WAf	-	-	0.1±0.2	-	-	-
A2	-	-	0.02±0.74	-18.5	-22.0	-
BG10	-	-	1.9	-	-	-
BG1	-	-	0.9	-	-	-
BG3-13f	-	-	1.1±0.6 [d]	-	-	-
B31	-	-	1.11±0.29	-	-	-
B29	-9	-15	2.7±0.3	-12.6	-16.3	-
C1S1	29	59	-1.5±0.2	-1.7	-11.3	-
C1S1	28	57	-1.7±0.3	-3.0	-13.2	-
EK1-4-1 SP	19	34	-3.9±0.5	-20.8	-31.9	-
EK1-4-1 PYX	21	39	-3.6±0.3	-17.9	-27.8	-
54-2	-	-	-	-	-	1.17

[a] Data from Lee and Papanastassiou (1974), Lee *et al.* (1976), and Wasserburg *et al.* (1977).

[b] Data from Clayton *et al.* (1977) and Clayton and Mayeda (1977).

[c] Data from Jovanovic and Reed (1976).

[d] Pyroxene coexisting with anorthite having $\delta^{26}Mg = 8.1±0.3$.

Figure 3-6. Magnesium isotopic composition of Allende inclusions showing raw measured data as deviations in percent from the mean $^{25}Mg/^{24}Mg$ and $^{26}Mg/^{24}Mg$ of normal terrestrial Mg. Mass-fractionation effects are proportional to the mass difference and are shown by the solid line where $\delta^{26}Mg/^{24}Mg = 2\ \delta^{25}Mg/^{24}Mg$. It can be seen that the FUN samples C1 and EK1-4-1 plot near the mass-fractionation correlation line but show small but significant deviations from the line suggesting additional nuclear effects or a non-linear mass fractionation law. The sample C1 has a larger fractionation than EK1-4-1 but smaller nuclear anomalies. The inclusion B29 has an apparently complementary fractionation pattern (assuming that C1 and EK1-4-1 were fractionated from "normal" material) but does not have any nuclear anomalies. Effects due to ^{26}Mg enrichment from ^{26}Al decay move samples to the right along a horizontal line as shown by the anorthite from inclusion WA. (after Wasserburg et al., 1977)

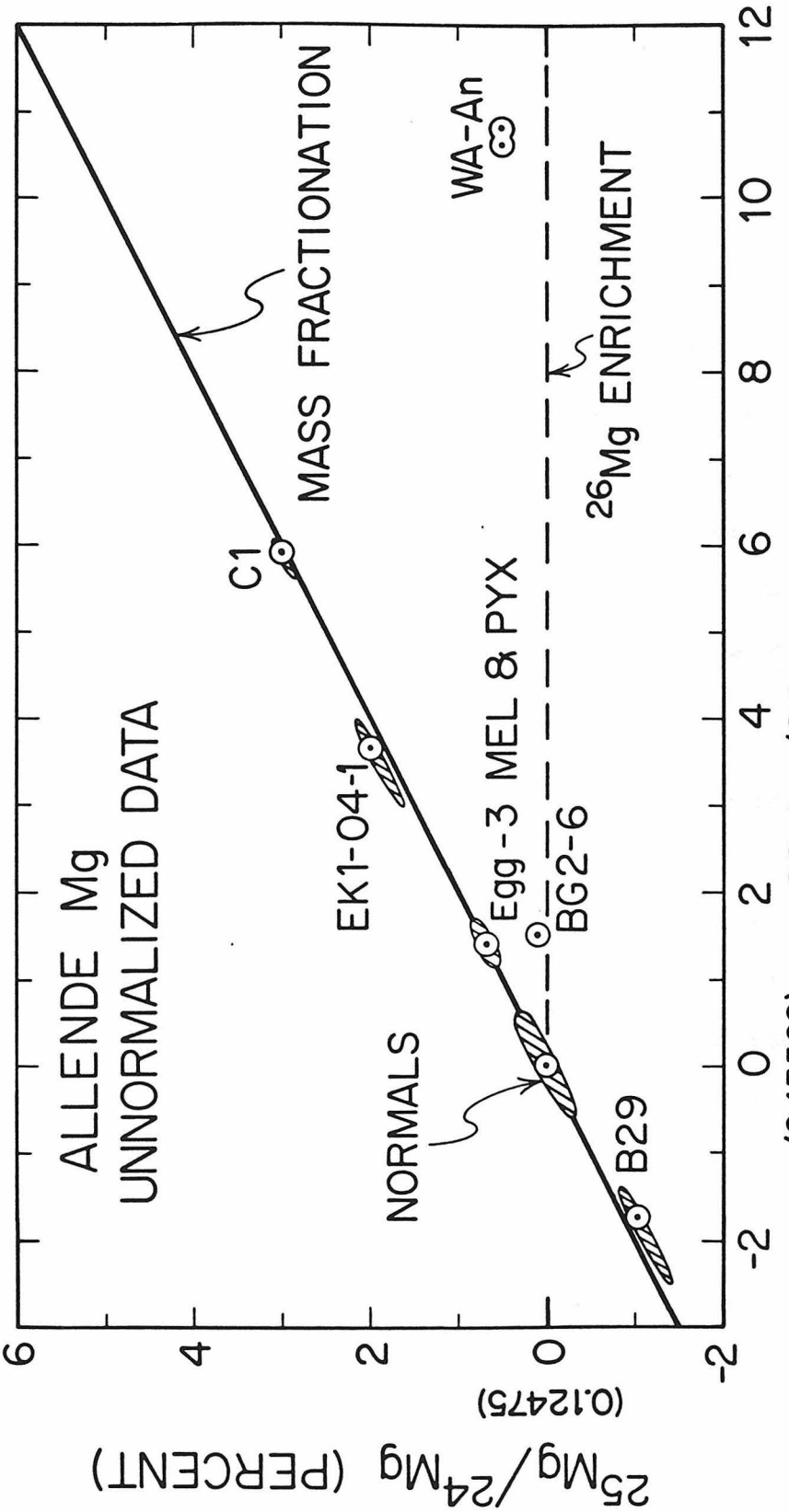
ALLENDE Mg
UNNORMALIZED DATA
MASS FRACTIONATION
NORMALS
^{26}Mg ENRICHMENT
C1
EK1-04-1
Egg-3 MEL & PYX
BG2-6
B29
WA-An
^{25}Mg/^{24}Mg (PERCENT)
(0.12475)
^{26}Mg/^{24}Mg (PERCENT)
(0.13569)
6
4
2
0
-2
-2
0
2
4
6
8
10
12

Fig. 3-6

Al/Mg ratio is consistent with in situ decay of ^{26}Al (Lee et al., 1977). The smaller deviation of BG10 is also consistent with ^{26}Al decay. These samples are particularly important as they provide an opportunity to directly test if the production of ^{26}Al also produces concomitant anomalies in the heavy elements. It can also be seen that the mass-fractionated inclusions C1 and EK1-4-1 after correction for fractionation, have residual negative $\delta^{26}Mg$ effects. Although it is possible that this may be due to an artifact of the mass-fractionation correction procedure, the most plausible explanation is that these effects are due to nuclear anomalies. This has led to the designation of these inclusions as FUN, signifying Fractionated Unknown Nuclear.

2. Oxygen Isotopic Characteristics

In the Allende meteorite there are basically two categories of anomalous oxygen samples (Clayton et al., 1977). By far the most common trend is shown by the line AD in Figure 3-7 which has a slope in the $\delta^{18}O$, $\delta^{17}O$ diagram of approximately unity. This is distinctly different from the terrestrial mass-fractionation line and may be due to mixing between an almost pure ^{16}O component and a more "normal" ^{18}O, ^{18}O enriched component. The samples that we have analyzed and are known to have these oxygen isotopic characteristics are the inclusions B29 and A2 (Table 3-4 and Figure 3-7).

The second and relatively rare type of anomalous oxygen is represented by the FUN inclusions C1 and EK1-4-1 (Clayton and Mayeda, 1977). In Figure 3-7 it can be seen that these inclusions lay

Figure 3-7. Oxygen isotopic composition of some of the inclusions analyzed in this study. There are basically two types of anomalies; those such as B29 and A2 which fall on the line AD and the FUN samples C1 and EK1-4-1 which fall to the right of the line AD. The line AD has a slope of approximately unity and is consistent with mixing between pure ^{16}O and a more normal ^{17}O, ^{18}O, ^{16}O component. The melilite from EK1-4-1 is on the line AD and suggests later exchange with oxygen of composition D. The oxygen in EK1-4-1 with an isotopic compositon of B, can be obtained by mass fractionation from the mixing line AD, assuming an initial oxygen of composition A. A similar mass-fractionation explanation could also account for the C1 oxygen, with C1 being fractionated by about a factor of two more than EK1-4-1 which is similar to the relationship observed for the Mg fractionations. It is noted, however, that although B29 has a Mg fractionation, it shows no evidence of an oxygen fractionation. (after Clayton et al., 1977)

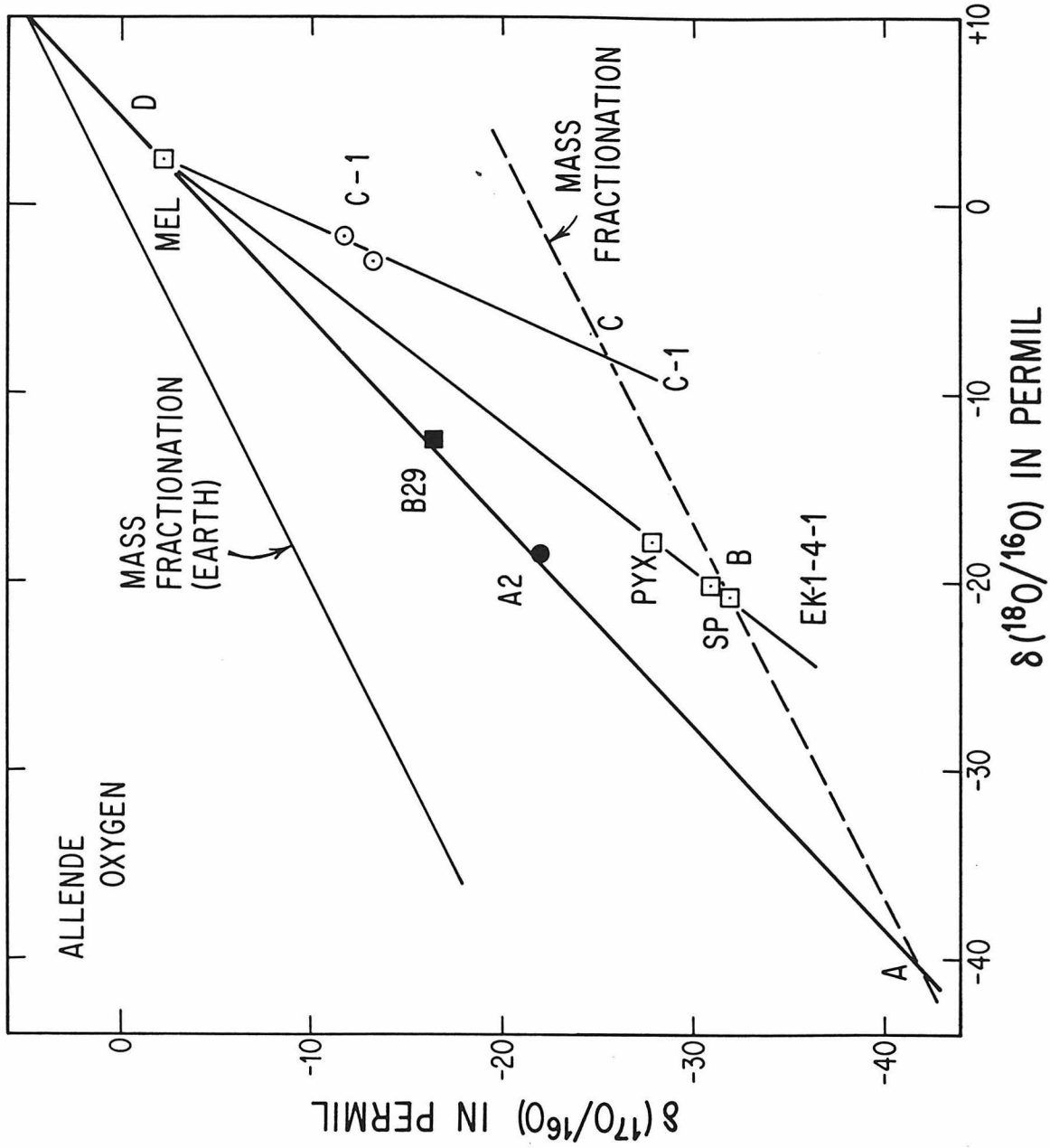
ALLENDE
OXYGEN
MASS
FRACTIONATION
(EARTH)
MASS
FRACTIONATION
D
MEL
C-1
C
C-1
B29
A2
PYX
SP
B
EK1-4-1
A
0
-10
-20
-30
-40
+10
0
-10
-20
-30
-40
δ (17O/16O) IN PERMIL
δ (18O/16O) IN PERMIL

Fig. 3-7

to the right of the isotopic mixing line AD. These inclusions may represent distinct nucleosynthetic components. However, a more plausible explanation which is consistent with the Mg and Si data (Clayton et al., 1978), is that they are derived from the isotopic mixing line AD by mass-fractionation and later re-equilibration with oxygen of composition D.

3. Hg Isotopic Characteristics

A sample of the Allende matrix which had been shown to contain Hg isotopic anomalies (Jovanovic and Reed, 1976) was kindly supplied to us by G. Reed. Compared to Mg and O, the Hg isotopic anomaly in this sample is relatively large with either a 17% excess in the neutron rich r-process isotope ^{202}Hg or deficiency in the p-process isotope ^{196}Hg. An anomaly of this magnitude even if diluted by a factor of 100 would be readily detectable in Ba.

RESULTS AND DISCUSSION

1. Normal Samples

The Ba isotopic ratios for the Allende inclusions (except C1 and EK1-4-1) corrected for mass-fractionation are listed in Table 3-2. In Table 3-3 and Figure 3-8 the deviations of these ratios from the terrestrial standard are given in parts per ten thousand. It can be seen that within analytical uncertainty, the Ba isotopic composition in all these samples is identical to the terrestrial normal. The negative Ba results are important because, as has already been discussed, many of these samples contain Mg, O, and Hg anomalies. Assuming that the processes which produced these anomalies are unlikely to exactly reproduce the isotopic abundances of the Ba s- r- and p-process isotopes, then the following conclusions are evident. The production of high Z elements is (1) not associated with ^{26}Al production, and (2) not associated with the anomalous oxygen lying on the isotopic mixing line AD of Figure 3-7. This places constraints on the environment in which oxygen and ^{26}Al were produced. For example, the region in a supernovae explosion in which oxygen and ^{26}Al are likely to be produced, must have restricted neutron fluxes, or a lack of seed nuclei required for heavy element production.

The Allende matrix 54-2 which was shown by Jovanovic and Reed (1976) to contain anomalous Hg has a normal Ba isotopic composition. The lack of comparable Ba anomalies may be due to the geochemical differences between Hg and Ba. Hg is relatively volatile and relative to its chondritic abundance, is depleted in the Allende meteorite by a

Table 3-3. Isotopic composition of barium in Allende inclusions. (normalized to $^{135}Ba/^{138}Ba = 0.09194$)

Sample	137/138 x10^4	136/138 x10^4	134/138 x10^4	132/138 x10^4	130/138 x10^4
Normals					
L3 N16	1565.14±.13[a]	1095.39±.10	337.03±.08	14.15±.03	14.76±.02
L3 N17	1565.21±.07	1095.49±.13	337.15±.08	14.13±.03	14.79±.02
L3 N21	1565.21±.05	1095.40±.05	337.12±.04	14.13±.01	14.76±.01
L3 AVG	1565.19±.05	1095.42±.06	337.10±.06	14.13±.01	14.77±.01
L1 N28[b]	1565.18±.07	1095.42±.10	337.11±.05	14.11±.01	14.75±.01
L1 N30[b]	1565.15±.06	1095.39±.05	337.08±.03	14.12±.01	14.76±.02
L1 N31[b]	1565.12±.07	1095.40±.07	337.12±.04	14.12±.01	14.75±.01
L1 AVG[b]	1565.15±.04	1095.40±.04	337.10±.03	14.12±.01	14.76±.01
Eugster et al. (1969)	1565.30±.20[d]	1095.45±.20	337.40±.10	14.11±.02	14.76±.02
Allende Meteorite					
Total Rock					
TRa	1565.32±.07	1095.37±.06	337.08±.05	14.12±.01	14.76±.01
TRb[b]	1565.11±.07	1095.37±.07	337.10±.05	14.11±.01	14.76±.02
MTX-1[b]	1565.14±.05	1095.34±.07	337.15±.04	14.12±.01	14.76±.01
54-2[b]	1565.17±.07	1095.37±.09	337.08±.04	14.12±.01	14.76±.01
Ca-Al Chondrules					
B28	1565.18±.06	1095.42±.09	337.12±.07	14.13±.02	14.78±.02
A2	1565.20±.05	1095.36±.08	337.06±.07	14.12±.02	14.79±.02
BG10	1565.21±.07	1095.33±.06	337.05±.06	14.11±.03	14.76±.03
WA[b]	1565.27±.16	1095.42±.12	337.03±.14	14.15±.03	14.76±.05
WAf[b]	1565.15±.07	1095.40±.08	337.11±.05	14.12±.04	14.76±.03
BG3-13[b]	1565.11±.07	1095.33±.08	337.10±.05	14.12±.02	14.77±.03
Olivine Chondrules					
B12	1565.22±.04	1095.38±.07	337.02±.05	14.13±.02	14.79±.02
PDA-01	1565.21±.09	1095.29±.09	337.06±.09	14.10±.03	14.79±.03
Pyroxene Chondrules					
A5	1565.20±.07	1095.35±.08	337.06±.04	14.11±.01	14.76±.02
Ca-Al Aggregates					
A8	1565.14±.13	1095.35±.08	337.06±.07	14.12±.02	14.76±.04
BG1	1565.21±.10	1095.44±.06	337.07±.09	14.12±.03	14.76±.04
G31	1565.32±.13	1095.34±.09	337.02±.08	14.14±.04	14.76±.03
B29[b]	1565.06±.08	1095.33±.06	337.07±.04	14.12±.01	14.74±.03
Lunar Samples					
76535[b]	1565.19±.08	1095.35±.06	337.11±.06	14.11±.01	14.77±.02
10072,127[b]	1565.11±.04	1095.36±.05	337.14±.04	14.12±.01	14.76±.01

[a] Errors are 2σ mean

[b] Sample measured on Lunatic 1 mass spectrometer

Table 3-4. Deviations from normal in parts in 10^4 of barium isotopic composition in Allende inclusions

Sample	ε_{137}[a]	ε_{136}	ε_{134}	ε_{132}	ε_{130}
Normals					
L3 N16	-0.3±0.8	-0.1±0.9	-2.1±2.4	+14±21	-7±14
L3 N17	+0.1±0.4	+0.8±1.2	+1.5±2.4	0±21	+13±14
L3 N21	+0.1±0.3	0.0±0.5	+0.6±1.2	0±7	+7±5
L3 AVG	0.0±0.3	0.0±0.5	0.0±1.8	0±7	0±7
L1 N28[b]	+0.2±0.4	+0.2±0.9	+0.3±1.5	-7±7	-3±7
L1 N30[b]	0.0±0.4	-0.1±0.5	-0.6±0.9	0±7	+3±14
L1 N31[b]	-0.2±0.4	0.0±0.6	+0.6±1.2	0±7	-3±7
L1 AVG[b]	0.0±0.4	0.0±0.5	0.0±0.9	0±7	0±7
Eugster et al. (1969)	+1.0±1.3	+0.5±1.8	+8.9±3.0	0±7	0±14
Allende Meteorite Total Rock					
TRa	+0.8±0.5	-0.3±0.6	-0.6±1.5	-6±3	-5±4
TRb[b]	-0.3±0.4	-0.3±0.6	0.0±1.5	-7±7	+3±7
MTX-1[b]	-0.1±0.3	-0.5±0.6	+1.5±1.2	0±7	+4±7
54-2[b]	+0.1±0.4	-0.3±0.8	-0.6±1.2	0±7	+6±7
Ca-Al Chondrules					
B28	-0.1±0.4	+0.2±0.8	+0.6±2.1	0±14	+7±13
A2	+0.1±0.3	-0.4±0.7	-1.2±2.1	-7±14	+13±13
BG10	+0.1±0.4	-0.6±0.5	-1.5±1.8	-14±21	-7±20
WA[b]	+0.8±1.0	+0.2±1.1	-2.1±4.2	+21±21	+3±34
WAf[b]	0.0±0.4	0.0±0.7	0.3±1.5	0±28	+3±20
BG3-13[b]	-0.3±0.4	-0.6±0.7	0.0±1.5	0±14	+10±20
Olivine Chondrules					
B12	+0.2±0.3	-0.2±0.6	-2.4±1.5	0±14	+13±13
PDA-01	+0.1±0.6	-1.0±0.8	-1.2±2.7	-21±21	+13±20
Pyroxene Chondrules					
A5	+0.1±0.4	-0.5±0.7	-1.2±1.2	14±7	-7±13
Ca-Al Aggregates					
A8	-0.3±0.8	+0.5±0.7	-1.2±2.1	-7±14	-7±27
BG1	+0.1±0.6	+0.4±0.5	-0.9±2.7	-7±21	-7±27
B31	+0.8±0.8	-0.5±0.8	-2.4±2.4	+7±28	-7±20
B29[b]	-0.6±0.5	-0.6±0.5	-0.9±1.2	0±7	-10±17
Lunar Samples					
76535[b]	+0.3±0.5	-0.5±0.6	+0.3±1.8	-7±7	+10±4
10072,127[b]	-0.3±0.3	-0.4±0.5	+1.2±1.2	0±7	+3±7

[a] $\varepsilon_i = (({}^{i}Ba/{}^{138}Ba)_{meas}/({}^{i}Ba/{}^{138}Ba)_{normal} - 1) \times 10^4$

[b] Sample measured on Lunatic 1 mass spectrometer

Figure 3-8. Bar graph showing fractional deviations in parts in ten thousand in the isotopic composition of Ba relative to normal for all Allende samples and two lunar samples studied in this work (excluding FUN samples C1 and EK1-4-1). Reference line at 0 is mean of terrestrial values.

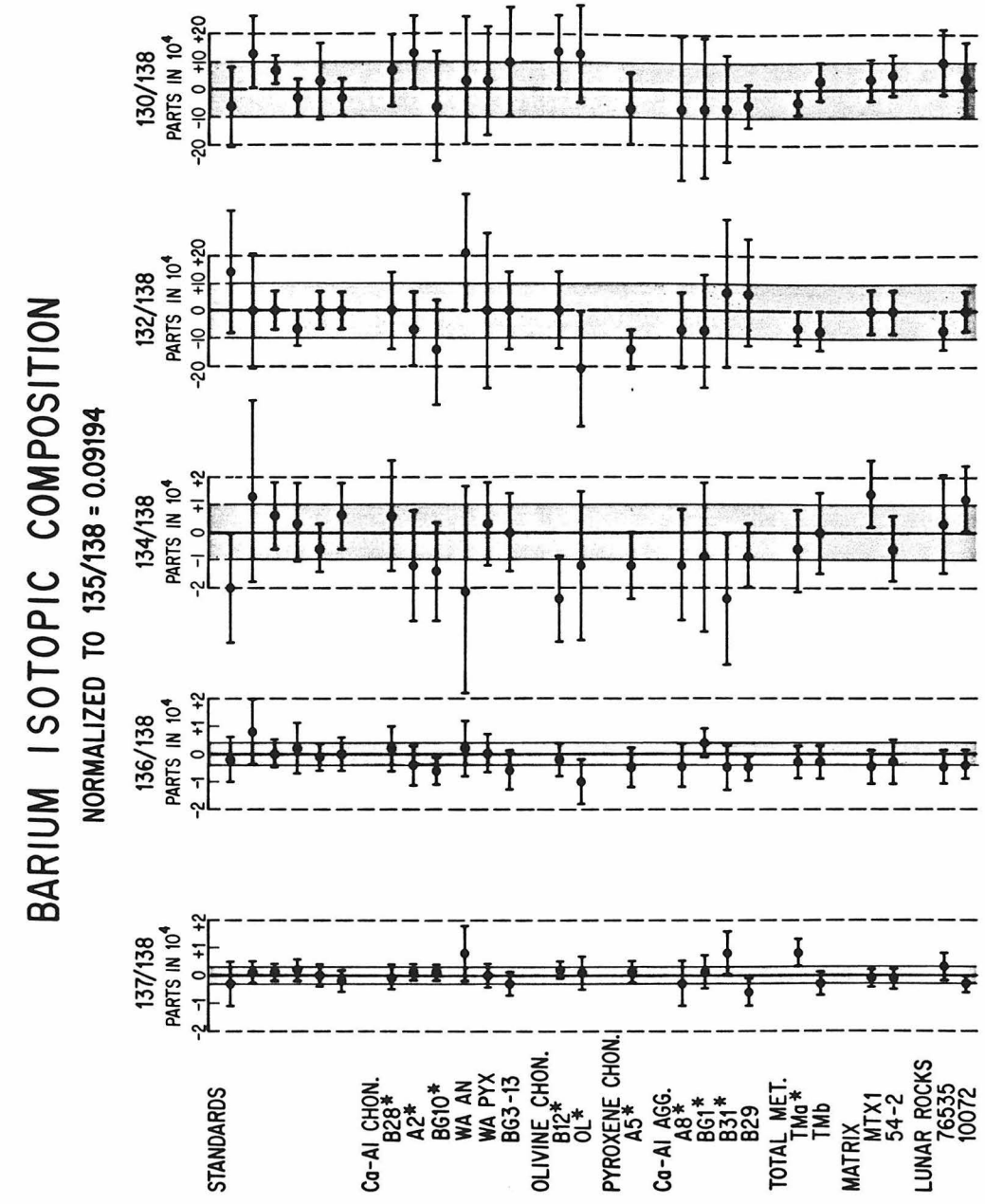
BARIUM ISOTOPIC COMPOSITION
NORMALIZED TO 135/138 = 0.09194
137/138
136/138
134/138
132/138
130/138
PARTS IN 10⁴
STANDARDS
Ca-Al CHON.
B28*
A2*
BG10*
WA AN
WA PYX
BG3-13
OLIVINE CHON.
B12*
OL*
PYROXENE CHON.
A5*
Ca-Al AGG.
A8*
BG1*
B31*
B29
TOTAL MET.
TMa*
TMb
MATRIX
MTX1
54-2
LUNAR ROCKS
76535
10072
* MEASURED ON LIII
ERRORS ARE 2σ MEAN
SHADED AREA IS 2σ MEAN OF STANDARDS
Mc CULLOCH & WASSERBURG 1977

Fig. 3-8

factor of greater than 100, whereas Ba is enriched by a factor of 10 to 20. Therefore, the actual number of anomalous Hg atoms is small, being equivalent to about 10^{12} atoms of ^{202}Hg per gram. The same number of anomalous Ba atoms would only produce a variation of 0.02% in ^{137}Ba for example, which is close to our resolution limit.

Similar arguments also apply to the Xe (for example Lewis et al., 1975) and Cd anomalies (Rosman and DeLaeter, 1976) where there is also only a relatively small number of anomalous atoms.

Another important distinction is that the Hg anomalies were determined by neutron activation techniques. Apart from the relatively low sensitivity of from only 3% to 9% (for Hg), this technique is also susceptible to large interferences. To overcome these problems and confirm the results of Jovanovic and Reed (1976), higher precision mass spectometric measurements of the Hg isotopic composition must be undertaken.

Many of the samples with a normal Ba isotopic composition had previously been analyzed for Sr by Gray et al. (1973). For example, Allende inclusions with low measured $^{87}Sr/^{86}Sr$ ratios are B28 with $^{87}Sr/^{86}Sr = 0.69902$ and A2 with $^{87}Sr/^{86}Sr = 0.69911$. There had been some speculation (Cameron, 1973a and D. Clayton, 1977) that differences in the initial $^{87}Sr/^{86}Sr$ ratios of meteorites, in particular inclusions of the Allende meteorite, were not due to decay of ^{87}Rb ($\tau_{1/2} = 5.0 \times 10^{10}$ years) but were the result of isotopic heterogeneity. Although isotopic heterogeneity not attributable to ^{87}Rb decay was found in two Allende inclusions (C1 and EK1-4-1), it is apparent that the normal Ba isotopic composition requires that most of the $^{87}Sr/^{86}Sr$ variations are a

consequence of ^{87}Rb decay and therefore have time significance.

2. The $^{135}Cs/^{135}Ba$ Chronometer

The presence in the early solar system of the extinct radionuclides ^{207}Pd with $\tau_{1/2} = 6.5 \times 10^6$ years (Kelly and Wasserburg, 1978) and ^{26}Al with $\tau_{1/2} = 7.2 \times 10^5$ years (Lee et al., 1977) suggests that other radionuclides with similar half-lives, in particular ^{135}Cs with $\tau_{1/2} = 2.3 \times 10^6$ years, may also have been present. The nuclide ^{135}Ba is produced mainly by decay of the now extinct nuclide ^{135}Cs. In phases with a high Cs/Ba ratio, enrichments in ^{135}Ba would be expected from ^{135}Cs if it were present in the early solar system. An example of the expected enrichment in ^{135}Ba, in deviations in parts in ten thousand from the normal $^{135}Ba/^{138}Ba$ ratio is shown in Figure 3-9 as a function of time. This time Δ is the interval (in units of 10^6 yr) from the last nucleosynthesis event to the formation of closed isotopic systems (i.e., formation of Allende inclusions). In this example, a terminal spike contributing 10% of the total r-process abundances of cesium and barium, with a $^{135}Cs/^{133}Cs$ production ratio of 0.1 and Cs/Ba = 0.16 in the inclusion is assumed. The standard $^{135}Ba/^{138}Ba$ ratio is defined as that resulting from decay of ^{135}Cs to ^{135}Ba with an average Cs/Ba of 0.08, the solar ratio. For this particular model, enrichments in ^{135}Ba would be detectable in samples which condensed within the free decay interval of $\sim 15 \times 10^6$ years with Cs/Ba > 0.08. This is within the interval of several millions of years required by the presence of ^{26}Al but much shorter than the $\sim 150 \times 10^6$ yr interval indicated by $^{129}I/^{129}Xe$. For models with larger contributions from

Figure 3-9. Deviation of ^{135}Ba in parts per ten thousand as a function of time from a 10% terminal r-process spike for different Cs/Ba ratios. Both enrichments or depletions in ^{135}Ba may be expected depending on whether the sample condensed with a Cs/Ba ratio greater than or less than the solar ratio.

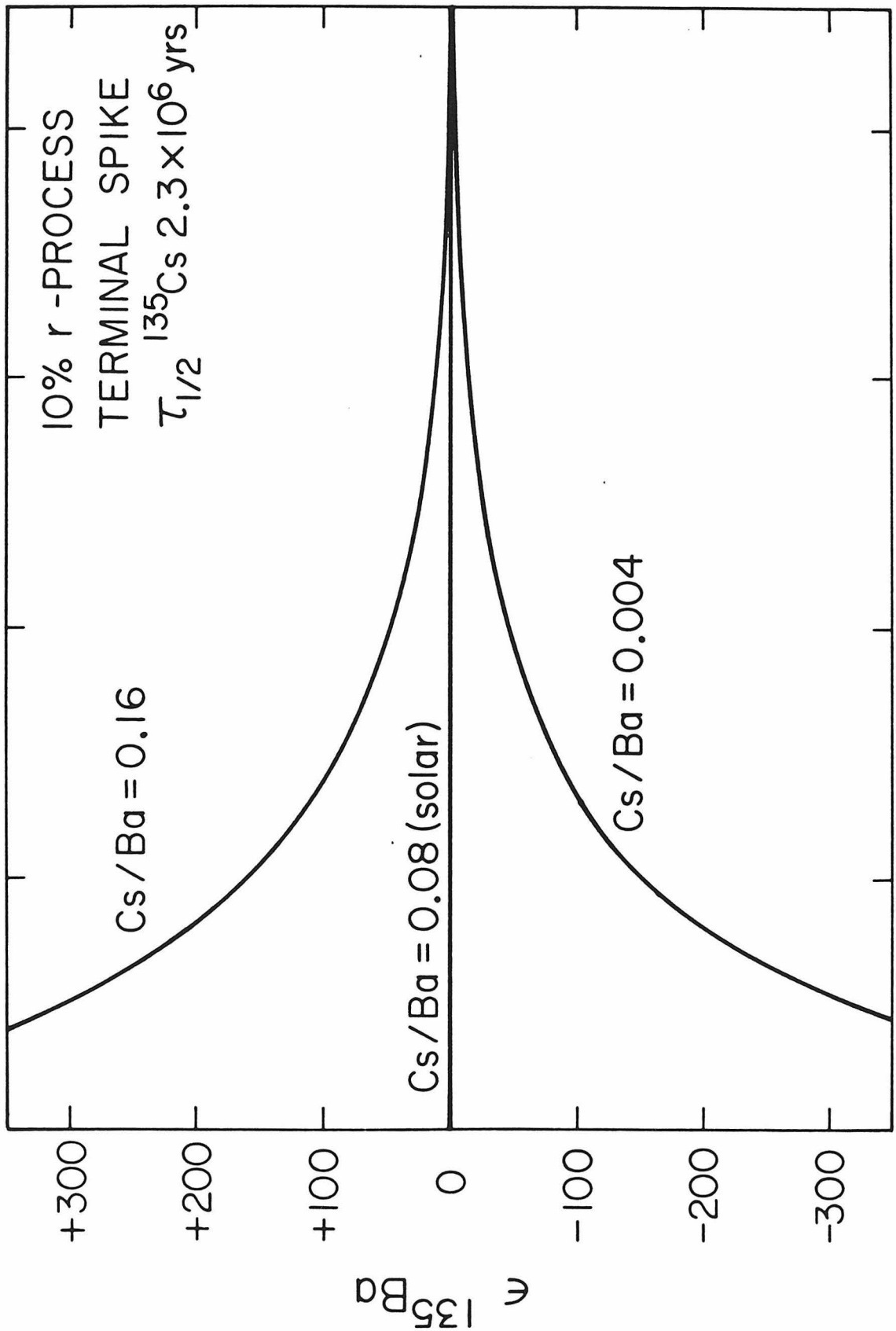
10% r -PROCESS
TERMINAL SPIKE
$\tau_{1/2}$ ^{135}Cs 2.3×10^6 yrs
Cs/Ba = 0.16
Cs/Ba = 0.08 (solar)
Cs/Ba = 0.004
+300
+200
+100
0
-100
-200
-300
4
8
12
16
FREE DECAY TIME Δ×10^6 yrs
ε ^{135}Ba

Fig. 3-9

a terminal spike, the enrichment would be increased proportionally. Conversely, for a continuous uniform synthesis model, the enrichments are reduced by a factor of approximately

$$\frac{\langle ^{135}Cs\rangle}{\langle T\rangle} = 10^{-4}$$

where $\langle ^{135}Cs\rangle$ is the mean lifetime of ^{135}Cs and $\langle T\rangle$ is the mean lifetime of the galaxy (Schramm and Wasserburg, 1970). In this case, even for a condensation time of several million years, no observable enrichment in ^{135}Ba would be expected.

As shown in Table 3-5 and Figure 3-10, all the Allende inclusions analyzed have low Cs/Ba ratios relative to the standard "solar" value of 0.08. They range from 0.0002 to 0.037 with two distinctive groups being apparent. Ca-Al chondrules which are enriched by a factor of 10 to 20 in barium and a high alkali aggregate B31 with a factor of 4 enrichment in cesium, relative to solar values. The remaining samples which consist of olivine, pyroxene chondrules, low alkali Ca-Al aggregates and matrix, have more uniform concentrations with enrichments in barium and depletions in cesium of less than a factor of 2. Thus, for the same model as described previously (10% terminal spike), but with Cs/Ba lower than the solar ratio, depletions of $^{135}Ba/^{138}Ba$ with respect to the standard ratio would be present in objects which were formed within a few million years. This is also shown in Figure 3-9, where ε ^{135}Ba, in this case, represents depletions as a function of free decay interval for Cs/Ba = 0.004. Although the lack of ^{135}Ba depletions in these inclusions is not definitive evidence against the presence of ^{135}Cs, it does not permit a significant terminal spike of high Z elements.

Figure 3-10. Ba versus Cs concentrations for some of the samples analyzed in this study. It can be seen that all the samples have a lower Cs/Ba ratio than the solar value of 0.08. The coarse grained inclusions (e.g., BG10, A8, A2, etc.) have significantly lower Cs/Ba ratios than the fine grained aggregates such as B31.

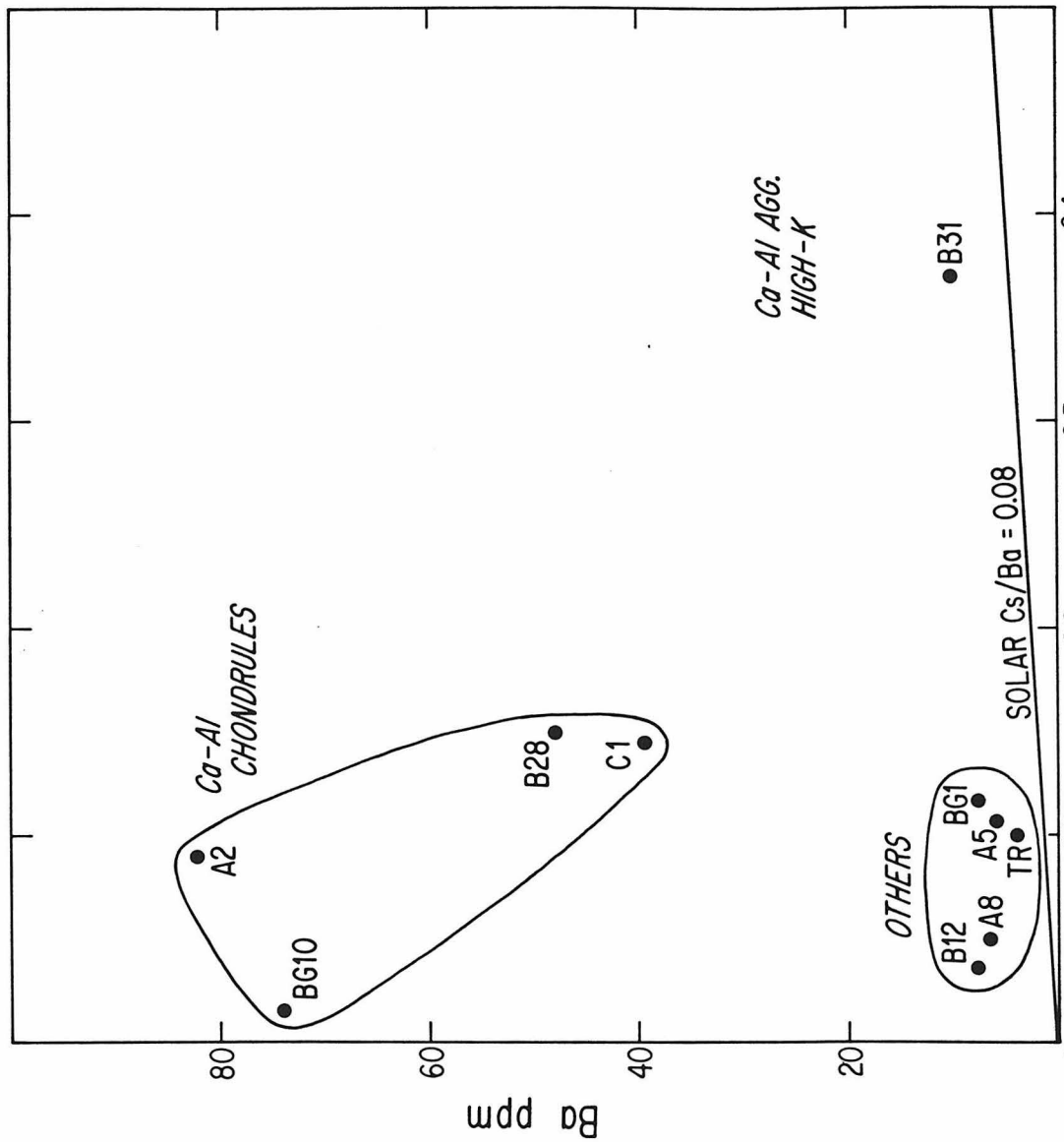
Ba ppm
Cs ppm
0
20
40
60
80
0.1
0.2
0.3
0.4
Ca-Al CHONDRULES
A2
BG10
B28
C1
Ca-Al AGG. HIGH-K
B31
OTHERS
B12
A8
A5
BG1
TR
SOLAR Cs/Ba = 0.08

Fig. 3-10

Table 3-5. Concentrations of barium and cesium in Allende inclusions

Sample	Ba (ppm)	Cs (ppm)	$\frac{Cs}{Ba}$
TR	4.4	0.110	0.025
B28	47.5	0.154	0.0032
A2	80.4	0.093	0.0012
BG10	74.1	0.016	0.0002
C1	39.3	0.145	0.0037
B12	7.9	0.036	0.0046
A5	5.7	0.117	0.021
A8	6.9	0.048	0.007
BG1	7.9	0.118	0.0015
B31	10.2	0.378	0.037

3. Ba, Nd, Sm and Sr Isotopic Anomalies in EK1-4-1 and C1

Of the eighteen Allende inclusions analyzed for Ba, only two were found to contain isotopic anomalies. These are the inclusions C1 and EK1-4-1. As has already been discussed, these two inclusions have fractionated Mg and distinctive O and have so far been shown to contain correlated isotopic anomalies ranging up to mass 154.

a. Barium

Barium was the first element in which high Z isotopic anomalies were found in these inclusions. The Ba results for C1 and EK1-4-1 (McCulloch and Wasserburg, 1978a) are shown in Figures 3-11 and 3-12 normalized to $^{134}Ba/^{138}Ba$. This normalization has the advantage of minimizing the propagation of experimental uncertainties and involves essentially two s-process only isotopes (^{138}Ba has only a relatively small r-process component). For EK1-4-1, the only variations outside of error are positive anomalies at masses 137 and 135. The isotopes ^{135}Ba and ^{137}Ba contain significant r-process components (Figures 3-1 and 3-2) and therefore the excesses observed at these masses in EK1-4-1 strongly suggest an r-process addition. The excesses (*) have a ratio of $^{137}Ba^*/^{135}Ba^* = 1.6$. However, using new values for the Ba cross sections (Musgrove et al., 1976) and allowing for branching (Ward et al., 1976) the calculated solar r-process ratio is $(^{137}Ba/^{135}Ba)_r = 0.69$. This is distinctly different from our observed value and indicates the addition to EK1-4-1 of material with r-process abundances shifted from the average solar value. This problem will be discussed later in conjunction with the Nd, Sm, and Sr data.

Figure 3-11. Bar graph showing fractional deviations in parts in ten thousand in the isotopic composition of Ba in the FUN samples EK1-4-1 and C-1 relative to the terrestrial normal. This figure is similar to Figure 3-8 except that the data are normalized to $^{134}Ba/^{138}Ba$. In the sample EK1-4-1 it can be seen that there are large excesses in the $^{137}Ba/^{138}Ba$ and $^{135}Ba/^{138}Ba$ ratios. These shifts are the same in both the melilite (EK1-4-1 MEL) and predominately fassaite (EK1-4-1 SC) mineral separates. In the other FUN sample C1, there is a small but reproducible deficiency in the $^{135}Ba/^{138}Ba$ ratio.

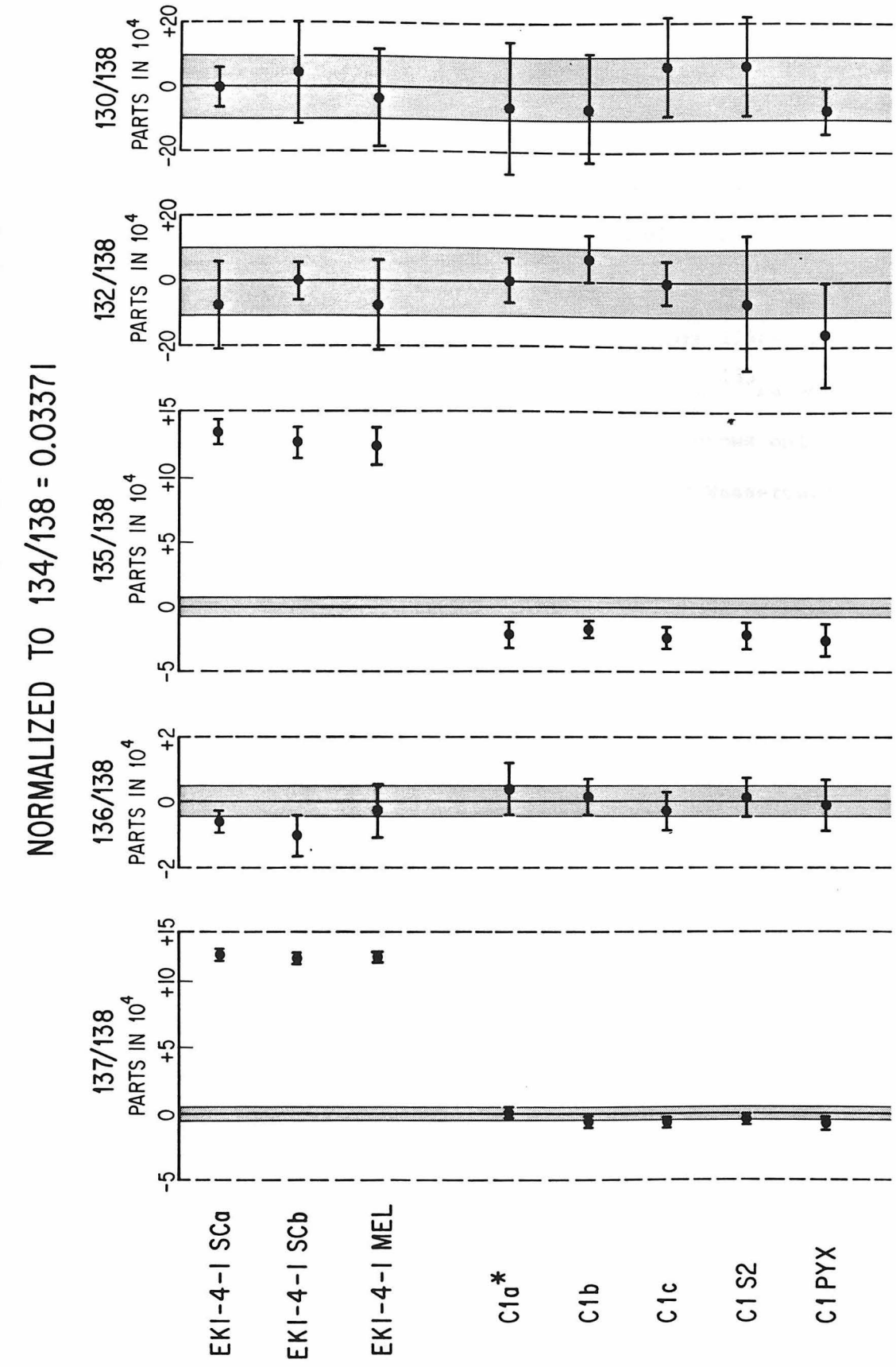
BARIUM ISOTOPIC COMPOSITION
NORMALIZED TO 134/138 = 0.03371
130/138
PARTS IN 10^4
+20
0
-20
132/138
PARTS IN 10^4
+20
0
-20
135/138
PARTS IN 10^4
+15
+10
+5
0
-5
136/138
PARTS IN 10^4
+2
0
-2
137/138
PARTS IN 10^4
+15
+10
+5
0
-5
EKI-4-1 SCa
EKI-4-1 SCb
EKI-4-1 MEL
C1a*
C1b
C1c
C1 S2
C1 PYX
*MEASURED ON L III
ERRORS ARE 2σ MEAN
SHADED AREA IS 2σ MEAN OF STANDARDS

Fig. 3-11

Figure 3-12. Schematic diagram showing the Ba isotopic composition of the FUN inclusions C1 and EK1-4-1. In this and subsequent graphs the two solid circles are the pair of isotopes used for normalization (to remove mass-fractionation effects) and were therefore assumed to have a normal isotopic composition. The nuclear processes which produced the isotopes are listed under the isotope mass. For EK1-4-1, Ba has excesses at ^{135}Ba and ^{137}Ba; consistent with a r-process addition. C1 shows only a small deficiency at ^{135}Ba , (after McCulloch and Wasserburg, 1978a).

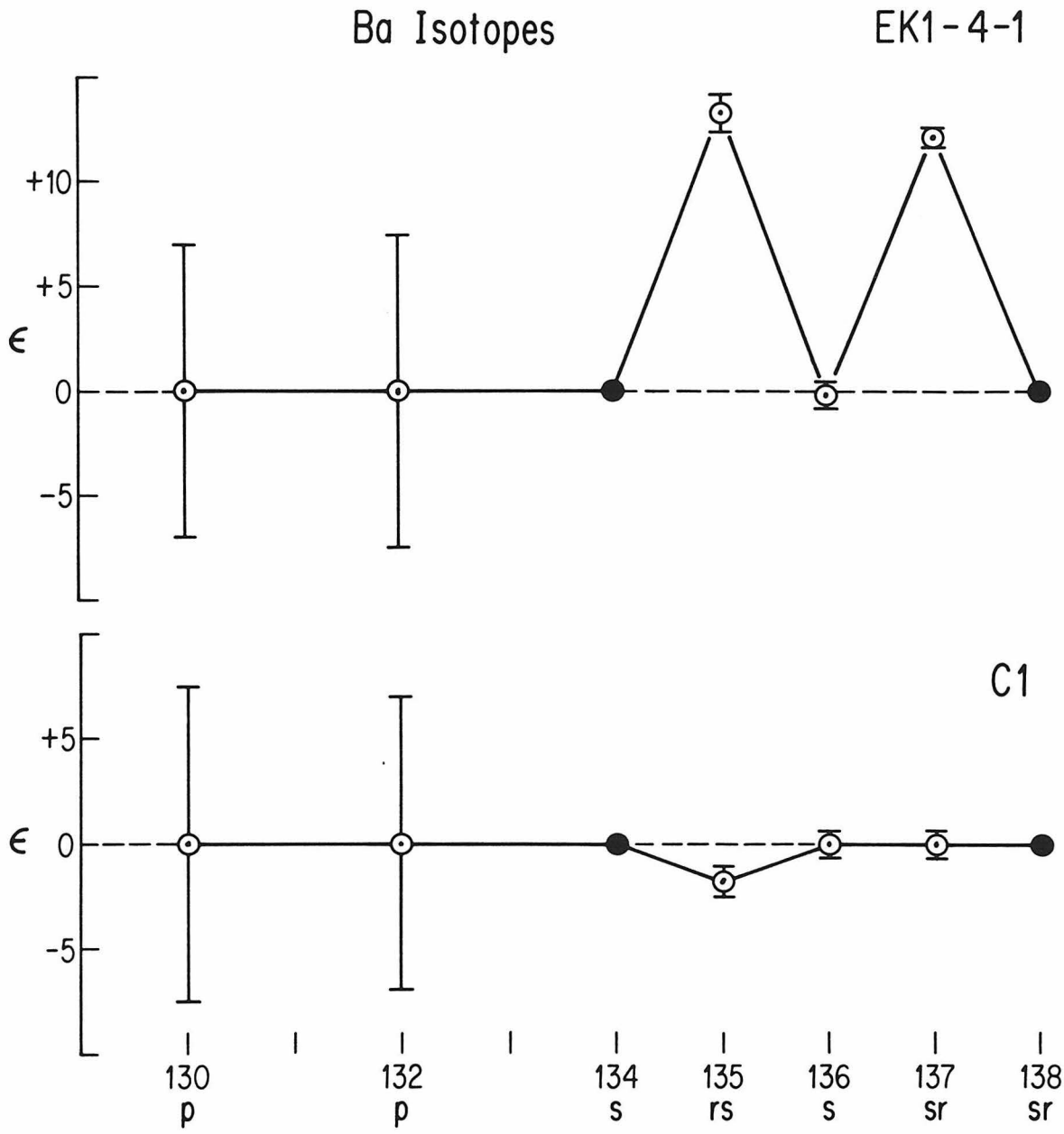
Ba Isotopes
EK1-4-1
+10
+5
ε
0
-5
C1
+5
ε
0
-5
130
p
132
p
134
s
135
rs
136
s
137
sr
138
sr

Fig. 3-12

For the sample C1, the only variation outside of error is the deficiency of ^{135}Ba. The interpretation of an anomaly (and all anomalies discussed in this paper) as a deficiency or an excess is arbitrary. For example, in C1 the anomalies could be interpreted as an excess in all the Ba isotopes apart from ^{135}Ba. The explanation would then require special and in this case highly implausible additions to all the Ba isotopes apart from ^{135}Ba.

In this case we prefer to interpret this anomaly as a deficiency and a possible explanation is that C1 represents the solar system material prior to the addition of material as found in EK1-4-1. If this is the case a deficiency of approximately the same size should also be present in ^{137}Ba. This was not observed. However, no resolvable anomaly would be expected in ^{137}Ba if the deficient r-process material had the same composition as that calculated for the average solar system.

An alternate explanation which has already been considered is that the deficiency in ^{135}Ba is due to the "holdup" at ^{135}Cs. If all the Allende inclusions were isochronous then it would be expected that the deficiency in ^{135}Ba would be proportional to the Cs/Ba ratio. However, in Figure 3-13, where the ε ^{135}Ba versus Cs/Ba ratio is plotted,samples with lower Cs/Ba ratios than C1 do not have any ^{135}Ba effects. Therefore in this model, this would indicate that the inclusion C1 condensed several million years before the other Allende inclusions with normal isotopic compositions. A similar argument may also apply to ^{135}Ba in EK1-4-1, which appears to be deficient compared to that estimated for a solar r-process addition

Figure 3-13. Deviations in ^{135}Ba (parts in 10^4) versus Cs/Ba ratio. It can be seen that the only inclusion with a significant deviation outside of experimental uncertainties is C1. If this deficiency is due to holdup at ^{135}Cs ($\tau_{1/2}$ = 2.3 x 10^6 yr), it indicates that C1 condensed at least several million years prior to the other inclusions. The normal Allende inclusions must have condensed after the free decay of ^{135}Cs which for the model shown in Figure 3-9 corresponds to about 15 x 10^6 yr.

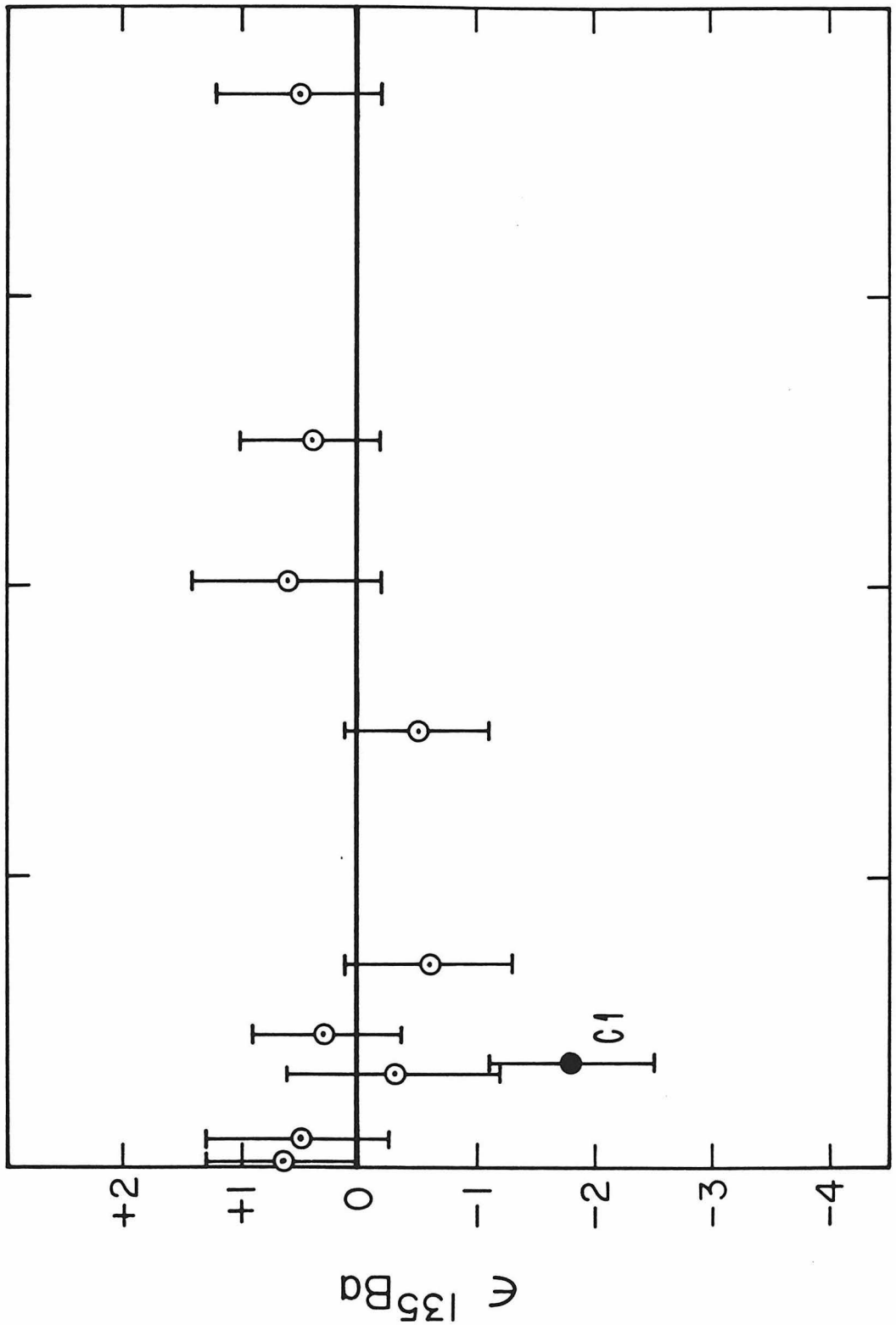

Fig. 3-13

(from the ^{137}Ba excess).

b. Neodymium

The Nd results for C1 and EK1-4-1 (McCulloch and Wasserburg, 1978a) are shown in Figure 3-14 using ^{142}Nd and ^{144}Nd for normalization. Although ^{142}Nd is an s-process only isotope, ^{144}Nd has approximately equal proportions of both r- and s-process components. For this reason the Nd isotopic data for EK1-4-1 do not appear to show any regularities indicative of r-process addition. However, in Figure 3-14 the isotopic pattern for EK1-4-1 is shown using the same normalization, but adding an 18 parts in 10^4 contribution to ^{144}Nd, reflecting the expected r-process addition (see McCulloch and Wasserburg, 1978b). The isotopic pattern for all the Nd isotopes apart from ^{142}Nd shows excesses and is now consistent with an r-process contribution. It is also noted that these isotopic patterns are not consistent with a fission hypothesis, in particular in situ fission, due to a small odd-even effect (McCulloch and Wasserburg, 1978b) which is not present in fission yield curves and due to the same anomaly being present in phases with different Ba/Nd ratios.

For the sample C1 no variations in the Nd isotopic composition (apart from ^{143}Nd due to ^{147}Sm decay) were found. This is not, however, unexpected if the ^{137}Ba depletion in C1 is due to a holdup at ^{135}Cs.

c. Samarium

The Sm results for C1 (McCulloch and Wasserburg, 1978b) and EK1-4-1 (Lugmair et al., 1978 and McCulloch and Wasserburg, 1978b) are

Figure 3-14. Schematic diagram showing the Nd isotopic composition in the inclusions C1 and EK1-4-1 using ^{142}Nd and ^{144}Nd for normalization. Due to the significant r-process component in ^{144}Nd the pattern for EK1-4-1 does not appear to indicate an r-process addition. The appropriate normalization is shown in Figure 3-15. The sample C1 has a normal Nd isotopic composition. Data for ^{143}Nd (triangle) has been corrected for ^{147}Sm decay since 4.5 AE (after McCulloch and Wasserburg, 1978a).

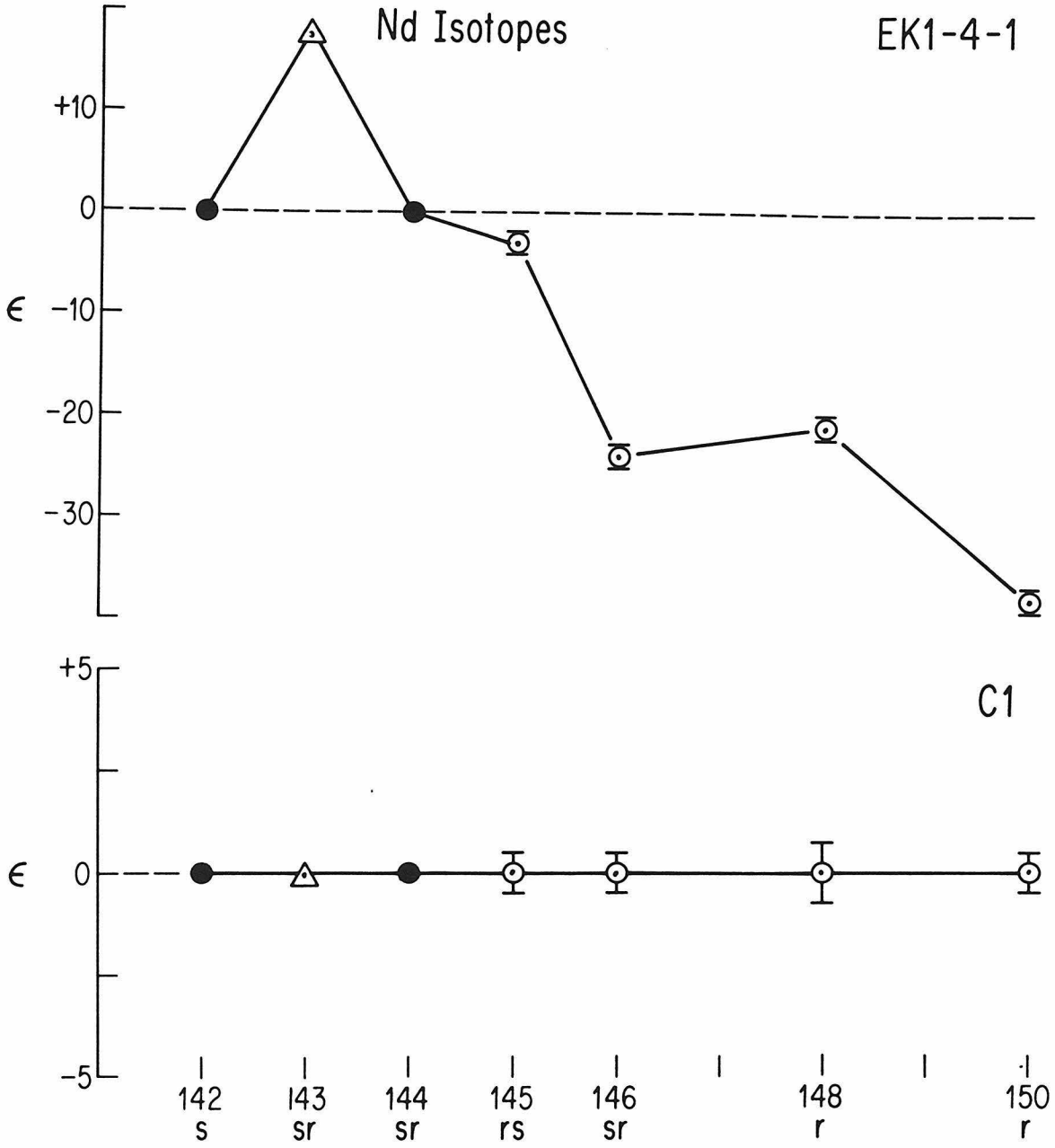
Nd Isotopes
EK1-4-1
+10
0
-10
-20
-30
ε
+5
0
-5
ε
C1
142
s
143
sr
144
sr
145
rs
146
sr
148
r
150
r

Fig. 3-14

Figure 3-15. Nd isotopic composition for EK1-4-1 using ^{142}Nd and ^{144}Nd for normalization but adding 18 parts in 10^4 to ^{144}Nd (see McCulloch and Wasserburg, 1978b) to compensate for the r-process contribution to ^{144}Nd. The Nd isotopic pattern is now consistent with an r-process addition.

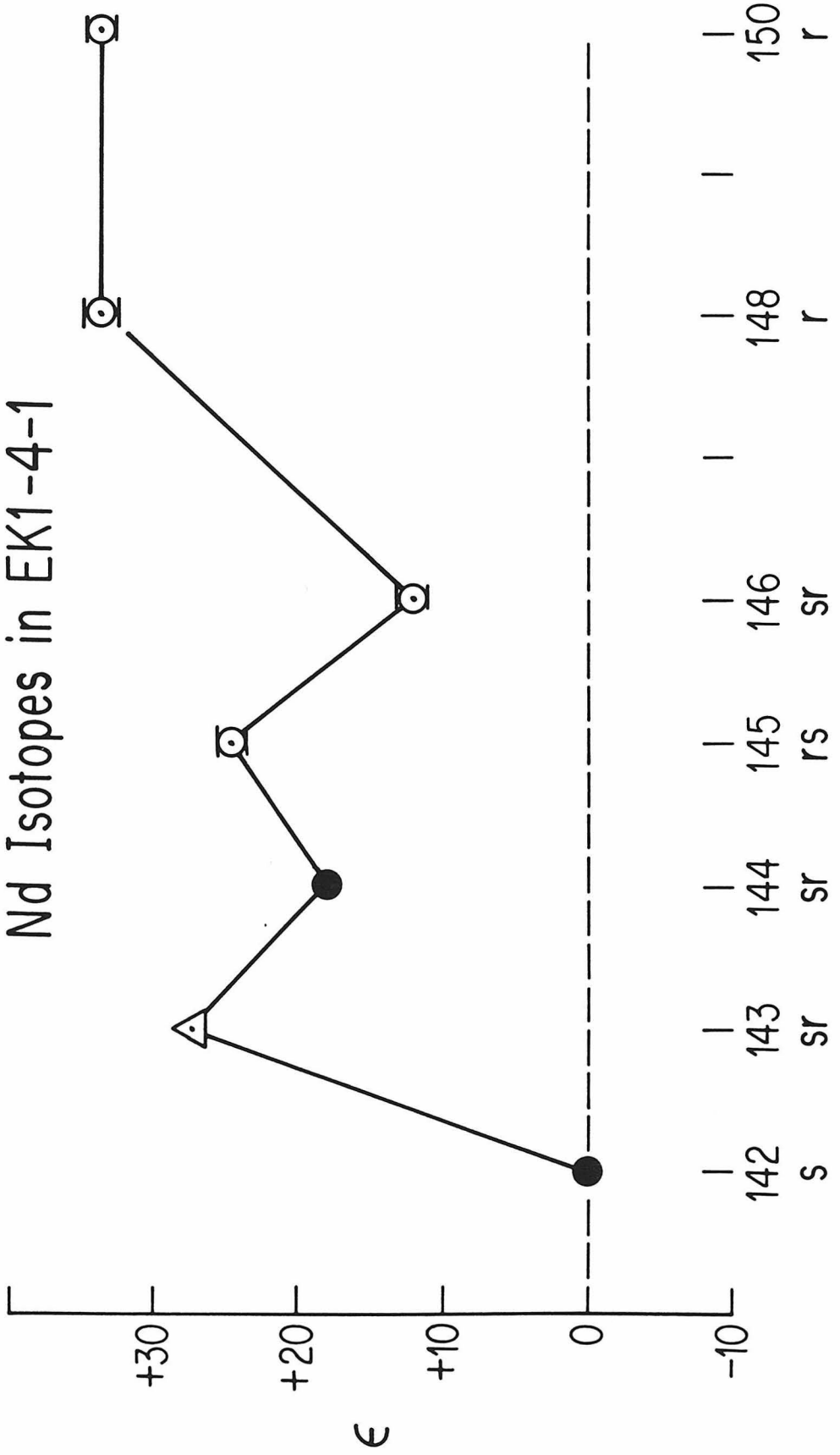
Nd Isotopes in EK1-4-1
+30
+20
+10
0
-10
ε
142
s
143
sr
144
sr
145
rs
146
sr
148
r
150
r

Fig. 3-15

shown in Figure 3-16 using the two s-process only isotopes ^{148}Sm and ^{150}Sm for normalization. For EK1-4-1 there are excesses in all the remaining isotopes indicating both r-process and p-process (to ^{144}Sm) additions. The r-process additions are consistent with the Ba and Nd data but the addition to the p-process isotope ^{144}Sm is somewhat surprising as no corresponding enrichments are found in the Ba p-process isotopes ^{130}Ba and ^{132}Ba. The Sm data for C1 are also somewhat surprising as there is an excess in ^{144}Sm which is about half the amount as found in EK1-4-1. All the other isotopic ratios are normal. These results are still in consonance with the normal Nd isotopic composition in C1 as Nd has no p-process only isotopes. However, there is again a disparity with the Ba results as there are also no observable enrichments in ^{130}Ba and ^{132}Ba for C1. While the uncertainties in measuring the rare Ba isotopes are relatively large, an excess of the same size as present in ^{144}Sm for EK1-4-1 (but perhaps not C1) would certainly have been detectable. A possible explanation of this apparent inconsistency is that although ^{144}Sm, ^{130}Ba, and ^{132}Ba have roughly comparable solar abundances, ^{144}Sm represents a peak in the p-process abundances in this mass region (Cameron, 1973b). This is probably due to its closed neutron shell (N = 82), and it is conceivable that under certain conditions its enhanced stability may have enabled overproduction relative to the solar abundances. It is apparent, however, that more detailed theoretical analysis of the p-process is required.

An additional important feature of only a p-process addition

Figure 3-16. Sm isotopic composition in C1 and EK1-4-1 normalized to the two s-process only isotopes ^{148}Sm and ^{150}Sm. Sample EK1-4-1 shows excesses in all the isotopes (apart from those used for normalization) indicating both r- and p-process additions. An equivalent p-process addition was not found in the Ba p-process isotopes ^{130}Ba and ^{132}Ba which may reflect the greater binding energy of ^{144}Sm due to its magic neutron number N = 82. The sample C1 has only excess in ^{144}Sm indicating that the r- and p-processes are decoupled. (C1 and EK1-4-1 data after McCulloch and Wasserburg, 1978b, and EK1-4-1 data after Lugmair et al., 1978)

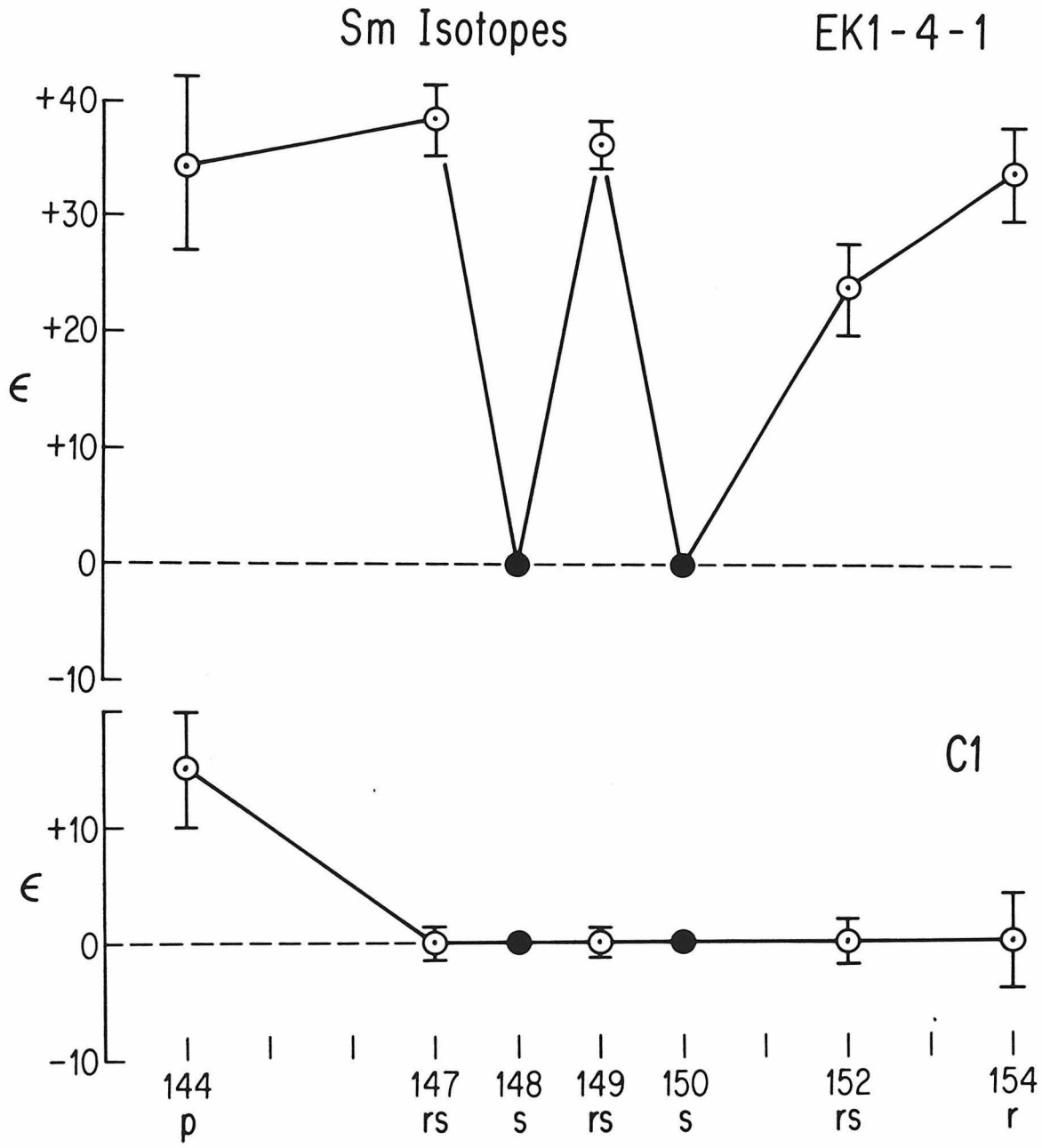
Sm Isotopes
EK1-4-1
+40
+30
+20
ϵ
+10
0
-10
C1
+10
ϵ
0
-10
144
p
147
rs
148
s
149
rs
150
s
152
rs
154
r

Fig. 3-16

to C1 which was pointed out by McCulloch and Wasserburg (1978b), is that it shows that the p-process is not necessarily coupled to the r-process. This obviously has implications on the environments in which these processes occur.

d. Strontium

The Sr results for C1 and EK1-4-1 (Papanastassiou and Wasserburg, 1978) are shown in Figure 3-17 using ^{86}Sr and ^{88}Sr for normalization. Both samples show a deficiency in the p-process isotope ^{84}Sr. However, this is clearly not consistent with the excesses observed in the Ba, Nd, and Sm r-process isotopes of EK1-4-1. Alternate interpretations of the data, allowing for decay of ^{87}Rb ($\tau_{1/2} = 5 \times 10^{10}$ years) to ^{87}Sr, are a deficiency in ^{88}Sr and excesses in ^{86}Sr and ^{87}Sr. These latter interpretations are also not consistent with that expected for r- and s-process components and clearly an investigation of isotopic abundances in EK1-4-1 between Sr and Ba will be required to resolve this inconsistency.

Figure 3-17. Sr isotopic composition in C1 and EK1-4-1, normalized to ^{86}Sr and ^{88}Sr. The patterns show a deficiency in the p-process isotope ^{84}Sr, or may alternatively be interpreted as excesses in ^{86}Sr, ^{87}Sr, and ^{88}Sr (^{87}Sr has been corrected for ^{87}Rb decay). None of these interpretations are consistent with the Ba, Nd, and Sm results (after Papanastassiou and Wasserburg, 1978).

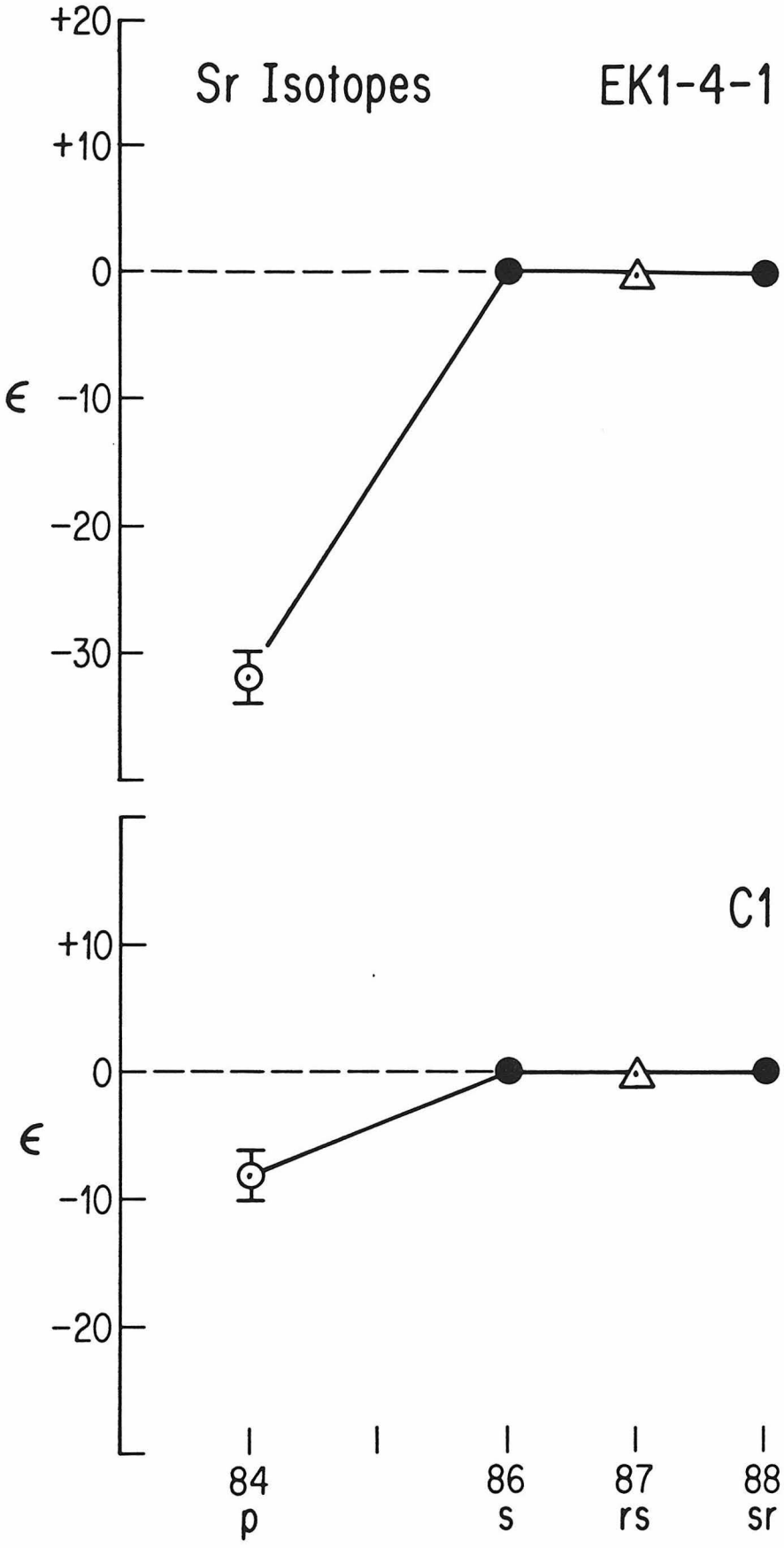
Sr Isotopes
EK1-4-1
+20
+10
0
-10
-20
-30
ε
C1
+10
0
-10
-20
ε
84
p
86
s
87
rs
88
sr

Fig. 3-17

CONCLUSIONS

In Table 3-6 apparent regularities in the isotopic characteristics between EK1-4-1 and C1 are listed. It can be seen that the effects are roughly a factor of two greater in EK1-4-1 than C1. This applies to both the excesses and deficiencies observed in the p-process isotopes ^{144}Sm and ^{84}Sr respectively. A similar relationship is also observed for the normalized $^{26}Mg/^{24}Mg$ ratios. This feature, if not coincidental, is certainly puzzling and an explanation must await more data.

The most obvious regularity is the excesses observed in the Ba, Nd, and Sm r-process isotopes of EK1-4-1. An important question is whether these excesses mimic the average solar r-process pattern or show significant deviations from it? For example, as pointed out by D. Clayton (1979), it would not be expected that a single injection from a neighboring supernova would produce a pattern of anomalies similar to an average of nucleosynthetic events as represented by our solar system abundances.

A comparison of the excesses observed in EK1-4-1 with the average solar system r-process abundances was undertaken by McCulloch and Wasserburg (1978b). The results are shown in Table 3-7 where we have calculated the ratios of excess atoms in EK1-4-1 to solar r-process atoms, normalized to the r-process only isotope ^{154}Sm. This ratio is given by $\varepsilon(A)N(A)/\varepsilon(154)N_r(A)$ where $N_r(A)$ is the calculated cosmic r-process abundance. To obtain $N_r(A)$, the s-process component $N_s(A)$ is subtracted from the total isotopic abundance N(A). Thus

Table 3-6. Regularities in isotopic characteristics between EK1-4-1 and C1

Isotope	EK1-4-1 (deviations from normal in parts in 10^4)	C1
$\varepsilon^{144}Sm$	+34±8	+15±5
$\varepsilon^{84}Sr$	-32±2	-9±2
$\varepsilon^{26}Mg$ (normalized)	-37±4	-16±2

Table 3-7. Nucleosynthetic Components in Ba, Nd, and Sm for EK1-4-1

Nuclide	N(A)[a]	σ(A)[b]	$N_s(A)$[c]	$N_r(A)$[d]	ε(A)[e]	$\frac{\varepsilon(A)x}{N(A)10^{-4}}$[f]	$\frac{\varepsilon(A)N(A)}{\varepsilon(154)N_r(A)}$[g]
^{130}Ba	0.005[m]	2000[k]	0.0	0.0	0.0	0.0	-
^{132}Ba	0.005[m]	650[k]	0.0	0.0	0.0	0.0	-
^{134}Ba	0.116	225[h]	0.116	0.0	0.0	0.0	-
^{135}Ba	0.316	470[i]	0.055	0.261	13.4	4.23×10^{-4}	0.47
^{136}Ba	0.375	70[h]	0.375	0.0	0.0	0.0	-
^{137}Ba	0.543	72.6[i]	0.363	0.180	12.3	6.68×10^{-4}	1.08
^{138}Ba	3.44	5.7[h]	3.30	0.14	0.0	0.0	-
^{142}Nd	0.211	45[j]	0.211	0.0	0.0	0.0	-
^{143}Nd	0.095	332[i]	0.025	0.07	27.8[l]	2.64×10^{-4}	1.1
^{144}Nd	0.186	67[i]	0.116	0.07	18.0	3.35×10^{-4}	1.39
^{145}Nd	0.065	485[i]	0.016	0.049	24.9	1.61×10^{-4}	0.96
^{146}Nd	0.134	105[i]	0.069	0.065	12.0	1.61×10^{-4}	0.72
^{148}Nd	0.045	210[k]	0.0	0.045	33.6	1.50×10^{-4}	0.98
^{150}Nd	0.044	240[k]	0.0	0.044	33.6	1.47×10^{-4}	0.98
^{144}Sm	0.007[m]	120[k]	0.0	0.0	34.4	0.24×10^{-4}	-
^{147}Sm	0.035	1150[k]	0.006	0.029	38.5	1.34×10^{-4}	1.35
^{148}Sm	0.025	260[k]	0.025	0.0	0.0	0.0	-
^{149}Sm	0.031	1620[k]	0.004	0.027	36.5	1.14×10^{-4}	1.23
^{150}Sm	0.017	370[k]	0.017	0.0	0.0	0.0	-
^{152}Sm	0.060	450[k]	0.014	0.046	24.1	1.46×10^{-4}	0.92
^{154}Sm	0.051	380[k]	0.0	0.051	34.3	1.76×10^{-4}	1.0

[a]Cosmic abundance (per Si = 10^6), Cameron (1973). [b]30 KeV cross sections (millibarns). [c]s-process abundance. [d]r-process abundance given by $N_r(A) = (N(A) - N_s(A)$. [e]Deviations from normal in parts in 10^4 from McCulloch and Wasserburg (1978a,b). [f]Excess atoms (see fig. 1). [g]Ratio of excess atoms to cosmic r-process atoms, normalized to ^{154}Sm (see fig. 2). [h]Musgrove, Boldman, and Macklin (1976). [i]Holmes, Woosley, Fowler, and Zimmerman (1976). [j]Conrad (1976). [k]Allen, Gibbons, and Macklin (1971). [l]Corrected for ^{147}Sm decay for an age of 4.56×10^9 yr. [m]p-process only nuclide.

Figure 3-18. Ratios of excess atoms in EK1-4-1 compared to that expected for an average solar r-process addition as a function of atomic number (normalized to $^{154}Sm = 1.0$). It can be seen that in this mass region, the r-process addition observed in EK1-4-1 is very similar to the average solar r-process pattern although there are significant disparities at ^{135}Ba, for example (and also Sr which is not shown); (after McCulloch and Wasserburg, 1978b).

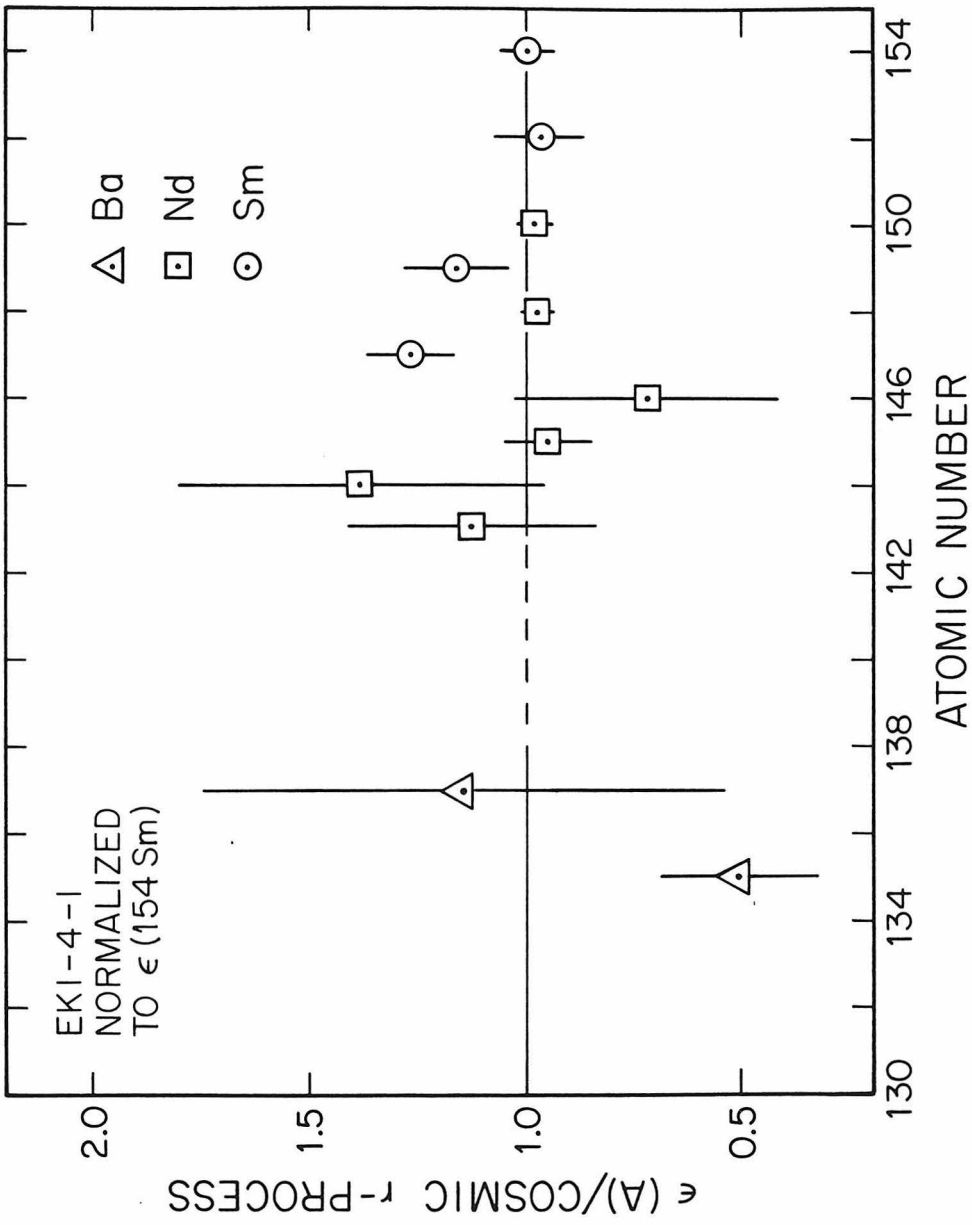
EK1-4-1
NORMALIZED
TO ϵ (154 Sm)
Ba
Nd
Sm
ϵ (A)/COSMIC r-PROCESS
2.0
1.5
1.0
0.5
130
134
138
142
146
150
154
ATOMIC NUMBER

Fig. 3-18

$N_r(A) = N(A) - N_s(A)$. The isotopes ^{154}Sm, ^{150}Nd, and ^{148}Nd are produced only by the r-process. However, several other isotopes also contain a significant s-process component. For these isotopes, $N_s(A)$ was calculated using the local equilibrium approximation, $N_s(A-1)\sigma(A-1) = N_s(A)\sigma(A)$ as modified by the general trend of the $N_s(A)\sigma(A)$ curve and closed neutron shell at ^{138}Ba (see for example Seeger, Fowler, and Clayton, 1965). Improved cross section and abundance data were used (see Table3-7)together with allowance for branching in the s-process chain at ^{134}Cs and ^{151}Sm (Ward, Newman, and Clayton, 1976). The uncertainty in calculating the r-process contribution depends on the accuracy of the calculated s-process and the relative proportions of s and r components. In Figure 3-18 the number of excess atoms in EK1-4-1 relative to cosmic r-process are shown as a function of atomic number and are in general <u>similar</u> to the cosmic r-process distribution. However, significant deviations at ^{149}Sm, ^{147}Sm, and ^{135}Ba show that the exotic material was not <u>identical</u> to the average solar system r-process, or that the additions were made to material which did not have the present average solar system isotopic composition. As has already been discussed, the apparent p-process deficiency in Sr for EK1-4-1 is also inconsistent with a simple model of addition of material with average solar system r-process abundances. It is hoped that this work will provoke further astrophysical and experimental investigations to resolve these problems.

REFERENCES

Allen, B. J., H. H. Gibbons, and R. L. Macklin, Nucleosynthesis and neutron capture cross sections, in Advances in Nuclear Physics, 4, 205-259, 1971.

Burbidge, E. M., G. R. Burbidge, W. A. Fowler, and F. Hoyle, Synthesis of the elements in stars, Rev. Mod. Phys., 29, 547-650, 1957.

Cameron, A. G. W., Are large time differences in meteorite formation real? Nature, 246, 30-32, 1973a.

Cameron, A. G. W., Abundances of the elements in the solar system, Space Sci. Rev., 15, 121-146, 1973b.

Clayton, D. D., On isotopic anomalies in samarium, Earth Planet. Sci. Lett., 42, 7-12, 1979.

Clayton, D. D., Cosmoradiogenic ghosts and the origin of Ca-Al rich inclusions, Earth Planet. Sci. Lett., 35, 398-410, 1977.

Clayton, R. N., L. Grossman, and T. K. Mayeda, A component of primitive nuclear composition in carbonaceous meteorites, Science, 182, 485-488, 1973.

Clayton, R. N., and T. K. Mayeda, Correlated oxygen and magnesium isotope anomalies in Allende inclusions, I: Oxygen, Geophys. Res. Lett., 4, 295-298, 1977.

Clayton, R. N., T. K. Mayeda, and S. Epstein, Isotopic fractionation of Si in Allende inclusions, In Proc. 9th Lunar Science Conf., 1267-1278, 1978.

Clayton, R. N., N. Onuma, L. Grossman, and T. K. Mayeda, Distribution of the presolar component in Allende and other carbonaceous chondrites, Earth Planet Sci. Lett., 34, 209-224, 1977.

Conrad, J., Analysis of the s-process and the nuclear synthesis of the elements, Ph.D. Thesis, Heidelberg, 1976.

DeLaeter, J. R., and R. Date, The isotopic composition of barium, Int. J. Mass Spect. Ion Phys., 12, 455-463, 1973.

Eugster, O., F. Tera, and G. J. Wasserburg, Isotopic analyses of barium in meteorites and in terrestrial samples, J. Geophys. Res., 74, 3897-3908, 1969.

Gray, C. M., D. A. Papanastassiou, and G. J. Wasserburg, The identification of early condensates from the solar nebula, Icarus, 20, 213-239, 1973.

Grossman, L., Condensation in the primitive solar nebula, Geochim. Cosmochim. Acta, 36, 597-619, 1972.

Holmes, J. A., S. E. Woosley, W. A. Fowler, and B. A. Zimmerman, Tables of thermonuclear-reaction-rate data for neutron-induced reactions of heavy nuclei. At. Data Nucl. Data Tables, 18, 305, 1976.

Jovanovic, S., and G. W. Reed, Interrelations among isotopically anomalous mercury fractions from meteorites and possible cosmological inferences, Science, 193, 888-891, 1976.

Kelly, W. R., and G. J. Wasserburg, Evidence for the existence of ^{107}Pd in the early solar system. Geophys. Res. Lett., 5,

1079-1082, 1978.

Lee, T., and D. A. Papanastassiou, Mg isotopic anomalies in the Allende meteorite and correlation with O and Sr effects, Geophys. Res. Lett., 1, 225-228, 1974.

Lee, T., D. A. Papanastassiou, and G. J. Wasserburg, ^{26}Al in the early solar system: fossil or fuel? Astrophys. J. Lett., 211, 107-110, 1977.

Lee, T., D. A. Papanastassiou, and G. J. Wasserburg, Demonstration of ^{26}Mg excess in Allende and evidence for ^{26}Al, Geophys. Res. Lett. 3, 109-112, 1976.

Lewis, R. S., B. Scrinivasan, and E. Anders, Host phase of a strange xenon component in Allende, Science, 190, 1251-1262, 1975.

Lugmair, G. W., K. Marti, and N. B. Scheinin, Incomplete mixing of products from r-, p-, and s-process nucleosynthesis: Sm-Nd systematics in Allende inclusion EK1-4-1. In Lunar and Planetary Science, IX, 672-674, 1978.

McCulloch, M. T., D. A. Papanastassiou, and G. J. Wasserburg, Isotopic analyses of barium in Allende, Meteoritics, 11, 331, 1976.

McCulloch, M. T., and G. J. Wasserburg, Ba and Nd isotopic anomalies in the Allende meteorite. Astrophys. J. Lett., 220, 15-19, 1978a.

McCulloch, M. T., and G. J. Wasserburg, More anomalies from the Allende meteorite: Samarium, Geophys. Res. Lett., 5, 599-602, 1978b.

Musgrove, A. R. de L., J. W. Boldman, and R. L. Macklin, KeV neutron capture cross sections of ^{134}Ba and ^{136}Ba, Nucl. Phys., A256,

173-188, 1976.

Papanastassiou, D. A., and G. J. Wasserburg, Strontium isotopic anomalies in the Allende meteorite, Geophys. Res. Lett., 5, 595-598, 1978.

Reynolds, J. H., and G. Turner, Rare gases in the chondrite Renazzo, J. Geophys. Res., 69, 3263-3281, 1964.

Rosman, K. F. R., and J. R. DeLaeter, Isotopic fractionation in meteoritic cadmium, Nature, 261, 216-218, 1976.

Schramm, D. N., and G. J. Wasserburg, Nucleochronologies and the mean age of the elements, Astrophys. J., 162, 57-69, 1970.

Seeger, P. A., W. A. Fowler, and D. D. Clayton, Nucleosynthesis of heavy elements by neutron capture, Astrophys. J. Suppl., 11, 121-166, 1965.

Umemoto, S., Isotopic composition of barium and cerium in stone meteorites, J. Geophys. Res., 67, 375, 1962.

Ward, R. A., M. J. Newman, and D. D. Clayton, s-process studies: branching and the time scale, Astrophys. J. Suppl., 31, 33-59, 1976.

Wasserburg, G. J., T. Lee, and D. A. Papanastassiou, Correlated O and Mg isotopic anomalies in Allende inclusions: II. Magnesium, Geophys. Res. Lett., 4, 299-302, 1977.

Woosley, S. E., and W. M. Howard, The p-process in supernovae, Astrophys. J. Suppl., 36, 285-304, 1978.

BARIUM AND NEODYMIUM ISOTOPIC ANOMALIES IN THE ALLENDE METEORITE

M. T. McCULLOCH AND G. J. WASSERBURG

The Lunatic Asylum, Division of Geological and Planetary Sciences,* Caltech, Pasadena, CA 91125

Received 1977 October 14; accepted 1977 November 10

ABSTRACT

Isotopic anomalies have been found for Ba and Nd in two inclusions from the Allende meteorite. These inclusions are typical Ca-Al–rich objects associated with early condensates from the solar nebula but have distinctive O and Mg isotopic anomalies of the FUN type. Sample C1 shows a depletion only in ^{135}Ba of 2 parts in 10^4 and normal Nd. Sample EK1-4-1 shows large positive excesses in the unshielded isotopes ^{135}Ba and ^{137}Ba of 13.4 and 12.3 parts in 10^4, respectively. The Nd isotopic composition in EK1-4-1 is highly aberrant in at least five isotopes. Both the Ba and Nd anomalies can be explained by a model of *r*-process addition. These anomalies are found to be uniform between coexisting mineral phases. These observations show the existence of substantial isotopic anomalies in refractory elements in the neighborhood of Xe and extend the range of elements showing isotopic effects to O, Ne, Mg, Ca, Kr, Xe, Ba, and Nd. The observations, in conjunction with the presence of ^{26}Al ($\tau_{1/2} = 7 \times 10^5$ years), are interpreted as the result of a nearby supernova explosion which produced elements over a wide mass range and injected them into the early solar nebula shortly before condensation.

Subject headings: meteors and meteorites — nucleosynthesis — stars: supernovae

I. INTRODUCTION

Ba and Nd isotopic anomalies have been discovered in one inclusion in the Allende meteorite and Ba isotopic anomalies in a second inclusion from the same meteorite. Anomalies in Ca from the same inclusions are reported in a companion *Letter* by Lee, Papanastassiou, and Wasserburg (1978). A new search for isotopic variations in Ba was undertaken because of the existence of isotopic anomalies in O and Mg in Allende inclusions. Ba has seven stable isotopes which are believed to have been made in the *p*-, *s*-, and *r*-processes (Burbidge *et al.* 1957, hereafter B^{2}FH). The relative contributions to each of the isotopes by these processes are quite different. The existence of isotopic anomalies in meteoritic, terrestrial, and solar Xe which are not attributable to the radioactive decay of known nuclides also suggested that nuclear effects might be present in the neighborhood of atomic number $Z = 56$. Previous studies of Ba using high-precision methods were reported by Eugster, Tera, and Wasserburg (1969, hereafter ETW), who found no evidence for nonlinear isotopic shifts to a level of 10^{-4} and a maximum mass fractionation of 2×10^{-4} per mass unit. Measurements of ^{142}Nd/^{144}Nd from an inclusion from Allende have been published by Scheinin, Lugmair, and Marti (1976). These workers have tentatively inferred small excesses in ^{142}Nd which they have attributed to decay of extinct ^{146}Sm. However, the inherent precision of the data was not sufficient to clearly resolve this effect.

Inclusions in which Ba and Nd isotopic effects were found are Ca-Al–rich objects typical of the type considered as high-temperature condensation products in the solar nebula (see Grossman 1972). They contain

* Division Contribution No. 2979 (252).

TABLE 1

BARIUM ISOTOPIC VARIATIONS*

Sample†	Ba(ppm)	ϵ137	ϵ136	ϵ134	ϵ132	ϵ130
		Normalized to $^{135}Ba/^{138}Ba$; Index Isotope ^{138}Ba				
EK1-4-1 SC a‡	20	+7.9±0.4	−9.7±0.6	−17.8±1.2	−28.0±14.0	−34.0±7.0
EK1-4-1 SC b‡		+7.8±0.5	−9.5±0.6	−17.2±1.8	−21.0±7.0	−41.0±14.0
EK1-4-1 MEL	28	+8.2±0.5	−8.7±0.6	−16.0±2.4	−28.0±14.0	−41.0±7.0
C1 a‡§	39	+0.9±0.4	+1.9±0.6	+2.1±1.5	0.0±7.0	−10.0±20.0
C1 b‡		+0.1±0.4	+1.5±0.6	+2.1±0.9	0.0±7.0	+10.0±7.0
C1 c‡		+0.2±0.4	+1.5±0.5	+3.0±1.2	+7.0±7.0	+10.0±7.0
C1 S2	–	−0.1±0.4	+1.5±0.6	+3.0±1.5	+3.0±14.0	+14.0±14.0
C1 PYX	17	+0.4±0.4	+1.8±0.7	+3.9±1.5	0.0±7.0	+7.0±7.0
Normals		0.0±0.4	−0.1±0.5	−0.6±0.9	0.0±7.0	+3.0±7.0
		−0.2±0.4	0.0±0.6	+0.6±1.2	0.0±7.0	+3.0±7.0
Enriched Standards						
(ϵ137=+3.8, ϵ134=+3.6)		+3.5±0.5	+0.3±0.6	+5.0±1.2	--	--
(ϵ137=+7.9, ϵ134=+7.1)		+8.0±0.6	−0.2±0.6	+7.4±1.5	--	--
		ϵ137	ϵ136	ϵ135	ϵ132	ϵ130
		Normalized to $^{134}Ba/^{138}Ba$; Index Isotope ^{138}Ba				
EK1-4-1		+12.3±0.4	−0.8±0.6	+13.4±1.0	−1.0±14.0	+2.0±7.0
C1		−0.6±0.4	+0.6±0.6	−1.8±0.7	−7.0±7.0	−7.0±14

*Errors are $2\sigma_{mean}$. Deviations in parts per ten thousand relative to our grand mean of terrestrial normals: $^{137}Ba/^{138}Ba = 0.156515\pm4$; $^{136}Ba/^{138}Ba = 0.109540\pm4$; $^{134}Ba/^{138}Ba = 0.033710\pm4$; $^{132}Ba/^{138}Ba = 0.001412\pm1$; $^{130}Ba/^{138}Ba = 0.001476\pm1$; $^{135}Ba/^{138}Ba = 0.091940$. †PYX = pyroxene; MEL = melilite; S2, SC = splits of crushed inclusion. ‡Repeat analysis of solution. §Analyzed on L III mass spectrometer.

coarse-grained fassaitic pyroxene, melilite, spinel, and plagioclase. They also contain fine-grained alteration products associated with melilite and plagioclase which are rich in a "sodalite"-like material and believed to result from a late-stage reaction of early condensates with cooler, volatile-rich material in the solar nebula which altered the oxygen isotopic composition of the melilite (Clayton and Mayeda 1977; Wasserburg, Lee, and Papanastassiou 1977, hereafter WLP). These inclusions are known to be distinctive, as they contain magnesium with negative values of δ^{26}Mg and oxygen which does not lie on the usual correlation line between "normal" oxygen (O_N) and extraordinary oxygen (O_E) consisting of nearly pure ^{16}O (Clayton, Grossman, and Mayeda 1973). The Mg in these inclusions shows ^{26}Mg/^{24}Mg ratios shifted from normal values by 2% and 3% per mass unit, favoring the heavier isotopes. These large shifts are almost quantitatively what would be expected by mass fractionation (F) with small but distinct residual negative anomalies in ^{26}Mg which are attributed to unknown nuclear processes (UN). This class of anomalies was designated as FUN anomalies (WLP).

II. RESULTS

Procedures were similar to those described by ETW. Data were taken on the Lunatic I and III mass spectrometers (Wasserburg *et al.* 1969) which give the same self-consistent Ba isotopic ratios within 3 parts in 10^5. An improvement in sensitivity by a factor of 50 and in precision by a factor of 2 was achieved over ETW. Typical ion beams for ^{138}Ba were 2×10^{-11} A when collecting data on masses 134–138. Data for the rare isotopes 130–132 were taken with the ^{138}Ba ion beam at 10^{-10} A. Data are given in Table 1 for isotope k as deviations from the normal ratios in parts in 10^4 with ^{138}Ba as the index isotope:

$$\epsilon k = (R_{k/138}{}^{C}/R_{k/138}{}^{N} - 1) \times 10^4 \qquad (1)$$

where $R_{k/138}{}^{N} = (^{k}\text{Ba}/^{138}\text{Ba})_{\text{normal}}$ and $R_{k/138}{}^{C} = (^{k}\text{Ba}/^{138}\text{Ba})$ measured in the sample and normalized for mass fractionation assuming ^{135}Ba/^{138}Ba to equal the terrestrial value. Standards enriched in ^{137}Ba and ^{134}Ba were measured to establish the sensitivity to which nonlinear anomalies could be detected (see Table 1).

Samples from Allende, including Ca-Al–rich chondrules and aggregates, olivine chondrules, a pyroxene chondrule, and total meteorite, were analyzed for Ba. With the exception of the FUN samples, C1 and EK1-4-1, all other samples yield a Ba isotopic composition identical to terrestrial Ba within limits of error (see Fig. 1). A preliminary report on these data, excluding C1 and EK1-4-1, was published by McCulloch, Papanastassiou, and Wasserburg (1976). A small sample (2×10^{-8} g) of Ba from high-purity anorthite from WA, which shows a 10% excess of ^{26}Mg, and a large sample from the associated pyroxene, were analyzed and found to be normal. The first analysis of Ba from C1a showed possible effects in ^{137}Ba/^{138}Ba, ^{136}Ba/^{138}Ba, and ^{134}Ba/^{138}Ba. An aliquot of the solution was again separated and analyzed, and the anomalies in ^{136}Ba/^{138}Ba and ^{134}Ba/^{138}Ba were reproduced.

The smaller anomaly in $^{137}Ba/^{138}Ba$ was not reproduced. A second split of the bulk inclusion (C1-S2) and a sample of pyroxene from C1 were analyzed and yielded the same shifts in $^{136}Ba/^{138}Ba$ and $^{134}Ba/^{138}Ba$. The nonlinear anomalies, while small, are reproducible by using different spectrometers and different samples.

The only discrepancy is the measurement of $^{137}Ba/^{138}Ba$ for C1a. A sample of EK1-4-1 SC, consisting dominantly of pyroxene, was analyzed and yielded extremely large deviations which exceed the 2 σ_{mean} errors by over a factor of 10. A second mass spectrometer run was performed and isotopic ratios were determined over a wide range in filament temperature. Data were taken for masses 134–138 with the ion beam ranging from 0.5 to 2×10^{-11} A to test for changes in the ratios. The values for those isotopic ratios that could be measured at these emission levels were all identical within error to the means for the high-intensity data of both SC samples. Data for masses 130–135 were taken with the ion beam at 8×10^{-11} A and were also identical with those obtained in the previous run. In addition, a melilite separate from EK1-4-1 was analyzed and yielded an isotopic composition identical to that found for the SC sample. These data demonstrate large nonlinear isotopic anomalies in EK1-4-1 which are the same for different phases with Ba concentrations differing by 40%. For all runs the spectrum was scanned at high sensitivity between masses 120 and 160 and no interfering masses were identified. The only peaks seen were due to LaO and CeO, which were present at a level of 2×10^{-12} A or less and do not interfere with Ba. During data collection the ratios Ba^+/LaO^+ and Ba^+/CeO^+ changed by over a factor of 2 without any changes in the Ba ratios.

Upon finding effects in Ba, we deemed it necessary to establish whether anomalies existed in other higher-Z elements, and a study of Nd was made. The procedures for Nd are similar to those described by DePaolo and Wasserburg (1976). Nd data are presented in Table 2 as deviations (see eq. [1]) from standard normal ratios, with ^{144}Nd as the index isotope and mass fractionation corrections applied by using $^{150}Nd/^{142}Nd$. Sample C1-S2 has a Nd isotopic composition indistinguishable from terrestrial normal. However, sample EK1-4-1 SC has large deviations of Nd isotopic composition from normal which exceed the errors by over a factor of 30. Data were collected for all isotopes with the $^{144}NdO^+$ beam ranging from 1 to 6×10^{-11} A, and isotopic ratios remained constant within experimental errors. The melilite separate from EK1-4-1 was analyzed for Nd and gave an isotopic composition identical to that of SC, except for mass 143, which is affected by ^{147}Sm decay. The Nd concentration in the melilite is lower than that in SC by a factor of 2.4. For the

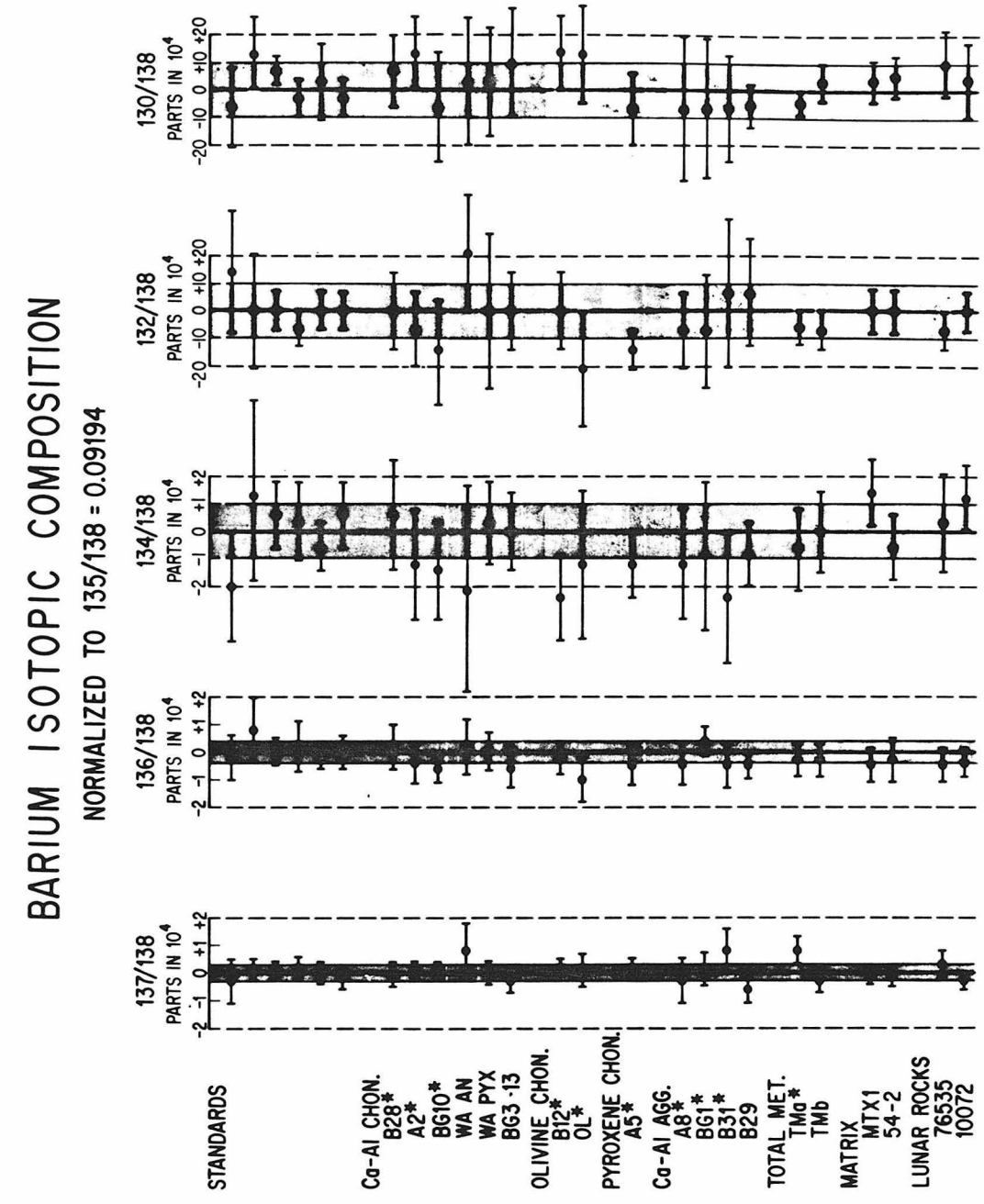

FIG. 1.—Bar graph showing fractional deviations in the isotopic composition of Ba relative to normal for all Allende samples and two lunar samples studied in this work excluding FUN samples C1 and EK1-4-1. Reference line at 0 is mean of terrestrial values.

TABLE 2

NEODYMIUM ISOTOPIC VARIATIONS*

Sample	Nd (ppm)	Sm (ppm)	ϵ142	ϵ143†	ϵ145	ϵ146	ϵ148	ϵ150
				Normalized to $^{150}Nd/^{142}Nd$; Index Isotope ^{144}Nd				
EK1-4-1 SC a	11.7	4.1	−9.6±0.3	+24.1±0.4	+2.7±0.6	−12.4±0.4	−1.5±0.5	−9.6±0.3
EK1-4-1 SC b	11.7	4.1	−9.9±0.3	+23.5±0.4	+2.4±0.4	−12.5±0.4	−1.5±0.9	−9.9±0.3
EK1-4-1 MEL	4.9	1.4	−9.2±0.4	−0.1±0.7	+2.3±0.9	−12.9±0.5	−0.5±1.0	−9.2±0.4
C1 S2	--	--	+0.1±0.3	+0.5±0.4	+0.3±0.6	−0.1±0.5	+1.1±0.9	+0.1±0.3
				Normalized to $^{144}Nd/^{142}Nd$; Index Isotope ^{142}Nd				
EK1-4-1 SC				+28.9±0.4	−2.1±0.6	−22.0±0.6	−20.7±0.9	−38.4±1.0
For f*=20‡				+38.9±0.4	+27.9±0.6	+18.0±0.6	+39.3±0.9	+41.6±1.0

Deviations relative to the grand mean of terrestrial normals: $^{142}Nd/^{144}Nd$ = 1.138266±9; $^{145}Nd/^{144}Nd$ = 0.348968±6; $^{146}Nd/^{144}Nd$ = 0.724109±10; $^{148}Nd/^{144}Nd$ = 0.243079±6; $^{150}Nd/^{144}Nd$ = 0.238581. Standard value of $^{143}Nd/^{144}Nd$ = 0.511836 today for chondritic Sm/Nd. G. Lugmair personal communication. †ϵ143 variations are also due to decay of ^{147}Sm ($\tau_{1/2}$ = 1.06 x 10^{11} years). ‡f = ($^{144}Nd^*/^{144}Nd$) x 10^4.

samples C1 and EK1-4-1 the mass fractionation correction applied to both Ba and Nd was less than ~3‰ per mass unit and within the same range as applied to the terrestrial normal.

III. DISCUSSION

Most samples of the Allende meteorite contain Ba of normal isotopic composition. Some of the samples analyzed for Ba had substantial contributions of O_E (up to 3%) and of excess ^{26}Mg (up to 10%) correlated with ^{27}Al. It follows that no obvious correlation exists between these nuclear effects at low Z and Ba. In contrast, the two inclusions which are distinguished by having FUN anomalies also show distinct nonlinear isotopic anomalies in Ba. Inclusion C1 has anomalies at masses 134 and 136, while inclusion EK1-4-1 shows large marked negative anomalies at 130, 132, 134, and 136, and a positive anomaly at 137. Using normalization to a standard $^{150}Nd/^{142}Nd$ value and ^{144}Nd as the index isotope, we found inclusion C1 to contain normal Nd, while inclusion EK1-4-1 shows marked negative anomalies in Nd at 142, 146, 148, and 150, and a positive anomaly at 145. These observations demonstrate that isotopic anomalies exist in Ba and Nd for several isotopes in some solar-system materials. These isotopic shifts are due to nuclear effects and cannot be attributed to mass fractionation. Normalizations to $^{135}Ba/^{138}Ba$ and $^{150}Nd/^{142}Nd$ were chosen to minimize the propagation of experimental errors and are otherwise arbitrary. The isotopic shifts depend upon the two isotopes (i,j) used for normalization, and the index isotope (m). Generally, the deviation in parts in 10^4 of isotope k is given by $\epsilon_{ij}{}^{km}$. The fractionation per mass unit α is determined from $\alpha_{ij} = (R_{ij}{}^{M}/R_{ij}{}^{0} - 1)/(i - j)$ where M = measured and 0 = standard. For small shifts, the transformation for ϵ to a new index isotope p and a new normalization (u,v) is given by

$$\epsilon_{uv}{}^{kp} = \epsilon_{ij}{}^{km} - \epsilon_{ij}{}^{pm} + (\epsilon_{ij}{}^{vm} - \epsilon_{ij}{}^{um}) \frac{(k - p)}{(u - v)}, \qquad (2)$$

As the cause of the nonlinear anomalies is obscure, it is more useful to choose a normalization which minimizes the number of isotopes at which anomalies occur. If we normalize to $^{134}Ba/^{138}Ba$ to correct for fractionation, we obtain the results shown in the bottom of Table 1. For sample C1, the only variation outside of error is a deficiency at mass 135. For EK1-4-1, the anomalies are positive and lie at masses 137 and 135. This choice of normalization appears to minimize the number of anomalies for both samples and implies an excess in ^{135}Ba and ^{137}Ba in one sample and a deficiency in ^{135}Ba in the other. If we interpret the shifts in EK1-4-1 as due to the addition of ^{135}Ba and ^{137}Ba, this requires that the exotic Ba excesses (*) have $^{137}Ba^*/^{135}Ba^* = 1.6$. We note that ^{135}Ba, ^{137}Ba, and ^{138}Ba are unshielded and may be produced in an r-process. From the estimates of Seeger, Fowler, and Clayton (1965), ($^{137}Ba/$

$^{135}Ba)_r \sim 1.2$, which is comparable to the calculated value. However, this value may be subject to substantial changes, using new values for the Ba cross sections (Stroud 1972) together with a detailed calculation of the branching network (Ward, Newman, and Clayton 1976). If the same number of exotic r-process nuclei are added to ^{138}Ba as are added at ^{137}Ba, this would cause a fractional increase in the ^{138}Ba abundance by 1.00018. This would propagate an error in the discrimination calculation of $\epsilon \sim +1.8$ at mass 130, which is well within errors, and a deficiency of $\epsilon \sim -0.9$ at mass 136, which is just within limits of error. No evidence has been found for variation in the abundance of the p-process isotopes. It does not appear possible to attribute the deficiency at 135 in C1 to the absence of exotic r-process material of the same composition inferred for EK1-4-1 owing to the lack of an effect at 137, although this may be obscured by the errors. Alternatively, the ^{135}Ba deficiency could result from a deficiency in r-process relative to s-process contributions, with r-process production ratios shifted from $^{137}Ba^*/^{135}Ba^* \sim 1.6$. A deficiency in ^{135}Ba could occur if there were a late-stage addition of r-process nuclei and if Ba were condensed before ^{135}Cs ($\tau_{1/2} = 2.3 \times 10^6$ yr) decayed. The deficiency in C1 is particularly important, as it implies that the average solar-system value must be made up by an addition of at least 2 parts in 10^4 of exotic ^{135}Ba. The anomalies in EK1-4-1 are not compatible with in situ fission subsequent to crystallization, as the shifts in Ba and Nd are the same for the total sample and the melilite, although Ba/Nd differ by a factor of 3. Further, the fission hypothesis is not in consonance with the large number of other isotopic anomalies for many elements ranging to low Z.

To expose whether the Nd effects are due to addition of r-process nuclei, ^{142}Nd (shielded) and ^{144}Nd, which must have a large s-process component, are used for normalization. However, the resultant pattern of deviations does not generate positive anomalies for all other isotopes (Table 2). To obtain all positive values, a substantial addition to ^{144}Nd must be assumed ($f^* = 20$ parts in 10^4). To demonstrate general excesses compatible with r-process addition, it will be necessary to obtain data on Sm and other refractory elements in this mass region with two shielded isotopes.

From the data reported here, as well as the wide range of Xe isotopic anomalies, it is reasonable to consider that ^{129}I may also have been added in the same process. Assuming that the negative Ba anomaly in C1 was representative of a deficiency in the whole solar nebula prior to the addition of material as found in EK1-4-1, then as $(^{135}Ba/^{127}I)_\odot \sim 0.3$ (Cameron 1973), we obtain $^{135}Ba^*/^{127}I \sim 0.5 \times 10^{-4}$. The time scale for production and injection of exotic low-Z elements is $\sim 3 \times 10^6$ years from the interpretation by Lee, Papanastassiou, and Wasserburg (1977, hereafter LPW) regarding the in situ decay of ^{26}Al in the solar nebula. If this time scale also applies to the injected exotic high-Z elements, then any associated ^{129}I ($\tau_{1/2} = 1.6 \times 10^7$ years) will not have decayed. Thus, if ^{129}I were

added along with the exotic nuclei identified here and commensurate in amount with the small Ba deficiency, this could account for the observed ratio of $^{129}I/^{127}I \sim 10^{-4}$. Such a model of small last-"minute" injection of *r*-process material is fully compatible with the Xe observations by Reynolds and his co-workers (Reynolds 1960; Podosek 1970). This implies that the observed ^{129}Xe effects are not from ^{129}I produced by earlier galactic nucleosynthesis and that the ^{129}I-^{244}Pu time scale of $\sim 1\text{–}2 \times 10^8$ years is an accident due to the injection of newly made exotic ^{129}I in a ratio of $^{129}I^*/^{127}I \sim 10^{-4}$ (see Schramm and Wasserburg 1970).

Isotopic anomalies have been known for Ne, Kr, and Xe for over 15 years. It now appears that isotopic anomalies are present in solar-system material for O, Ne, Mg, Ca, Kr, Xe, Ba, and Nd. This must be due to incomplete mixing of dust and gas from different sources at the time of formation of early condensates. From the data described here and in the companion *Letter*, it is manifest that the anomalies may extend to much higher atomic number. This may well extend through the transuranics, which could alter the calculation of the time between the termination of nucleosynthesis and the formation of the solar system and could further contribute anomalies by nuclides with $\tau_{1/2} \gtrsim 10^6$ years. The many peculiar isotopic anomalies in Xe are now not isolated but appear to be part of a large family of complex isotopic anomalies extending beyond $Z = 60$. The complex Xe spectra in residual material in Allende and other carbonaceous chondrites by Anders *et al.* (1975), Takahashi *et al.* (1976), and Lewis, Srinivasan, and Anders (1975) have been interpreted as due to superheavy fission and not due to *r*-process addition. This view has been subject to some discussion because of the enrichment in both neutron-poor and neutron-rich isotopes in the strange Xe which these workers discovered. This matter has been studied extensively by the Chicago group and by Frick (1977) and Frick and Reynolds (1977). In light of the existence of anomalies over a wide spread in Z, it now seems more plausible to consider the Xe anomalies to be the result of a very complex mixture of processes which include *r*-process components and various implantation mechanisms rather than superheavy fission.

The ball game seems to be wide open. The most likely generic model which may explain the observations appears to be an onion-shell supernova explosion followed by injection into the solar nebula, as outlined by Cameron and Truran (1977) to account for the O and Mg data. Such a model can produce elements of high Z. A reliable astrophysical model must await the experimental determination of the yields of exotic nuclei in the region of the rare earths where chemical fractionation will not obscure the relative contributions.

We are grateful to H. Nagasawa for the as yet unique sample of EK1-4-1. M. T. M. thanks D. A. Papanastassiou for his generous advice and introduction to high-precision mass spectrometry. D. J. DePaolo provided timely assistance and gave helpful advice. We thank R. Ward for his interest and advice on *p*'s and *q*'s and *s* and *r*. The excitement was communally shared with our calcined colleagues, D. A. Papanastassiou and Typhoon Lee. This work was supported by NSF grant PHY76-83685 and NASA grant NGL 05-002-188.

REFERENCES

Anders, E., Higuchi, H., Gros, J., Takahashi, H., and Morgan, J. W. 1975, *Science*, **190**, 1262.

Burbidge, E. M., Burbidge, G. R., Fowler, W. A., and Hoyle, F. 1957, *Rev. Mod. Phys.*, **29**, 547 (B^2FH).

Cameron, A. G. W. 1973, *Space Sci. Rev.*, **15**, 121.

Cameron, A. G. W., and Truran, J. W. 1977, *Icarus*, **30**, 447.

Clayton, R. N., Grossman, L., and Mayeda, T. K. 1973, *Science*, **182**, 485.

Clayton, R. N., and Mayeda, T. K. 1977, *Geophys. Res. Letters*, **4**, 295.

DePaolo, D. J., and Wasserburg, G. J. 1976, *Geophys. Res. Letters*, **3**, 249.

Eugster, O., Tera, F., and Wasserburg, G. J. 1969, *J. Geophys. Res.*, **74**, 3897 (ETW).

Frick, U. 1977, *Proc. 8th Lunar Sci. Conf.* (Oxford: Pergamon Press), in press.

Frick, U., and Reynolds, J. H. 1977, in *Lunar Science VIII* (Houston: Lunar Science Institute), p. 319.

Grossman, L. 1972, *Geochim. Cosmochim. Acta*, **36**, 597.

Lee, T., Papanastassiou, D. A., and Wasserburg, G. J. 1977, *Ap. J.* (*Letters*), **211**, L107.

———. 1978, *Ap. J.* (*Letters*), **220**, this issue.

Lewis, R. S., Srinivasan, B., and Anders, E. 1975, *Science*, **190**, 1251.

McCulloch, M. T., Papanastassiou, D. A., and Wasserburg, G. J. 1976, *Meteoritics*, **11**, 331.

Podosek, F. A. 1970, *Geochim. Cosmochim. Acta*, **34**, 341.

Reynolds, J. H. 1960, *Phys. Rev. Letters*, **4**, 8.

Scheinin, N. B., Lugmair, G. W., and Marti, K. 1976, *Meteoritics*, **11**, 357.

Schramm, D. N., and Wasserburg, G. J. 1970, *Ap. J.*, **162**, 57.

Seeger, P. A., Fowler, W. A., and Clayton, D. D. 1965, *Ap. J. Suppl.*, **11**, 121.

Stroud, D. B. 1972, *Ap. J.* (*Letters*), **178**, L93.

Takahashi, H., Higuchi, H., Gros, J., Morgan, J. W., and Anders, E. 1976, *Proc. Nat. Acad. Sci.*, **73**, 4253.

Ward, R. A., Newman, M. J., and Clayton, D. D. 1976, *Ap. J. Suppl.*, **31**, 33.

Wasserburg, G. J., Lee, T., and Papanastassiou, D. A. 1977, *Geophys. Res. Letters*, **4**, 299 (WLP).

Wasserburg, G. J., Papanastassiou, D. A., Nenow, E. V., and Bauman, C. A. 1969, *Rev. Sci. Instr.*, **40**, 288.

APPENDIX 7

MORE ANOMALIES FROM THE ALLENDE METEORITE: SAMARIUM

M. T. McCulloch and G. J. Wasserburg
The Lunatic Asylum, Div. of Geological and Planetary Sciences, California Institute of Technology, Pasadena, CA 91125

Abstract. The isotopic composition of Sm has been measured in the Allende inclusions C1 and EK1-4-1. These inclusions were previously shown to have isotopic anomalies for the elements O, Mg, Ca, Ba and Nd. Sample C1 has a normal Sm isotopic composition except for the "p-process" isotope ^{144}Sm, which has an excess of 15±5 parts in 10^4. Sample EK1-4-1 was found to have Sm with a highly aberrant composition, indicating excess at all unshielded isotopes and an excess at ^{144}Sm. These data confirm the previous evidence for an addition of "r-process" isotopes to this material and also indicate an addition to the "p-process" isotope ^{144}Sm. From the observations on C1 it is inferred that the "p-process" addition is decoupled from the "r-process" addition.

Introduction

Sm isotopic anomalies are reported in the two known FUN (Fractionation and Unknown Nuclear effects) inclusions EK1-4-1 and C1 from the Allende meteorite. Extensive data have been reported on these two Ca-Al-rich inclusions (type B) as they are the only known materials with definitive isotopic anomalies for several elements. Anomalies in Sr from the same inclusions are reported in a companion letter by *Papanastassiou and Wasserburg* [1978]. Previous work has shown inclusion C1 to contain anomalous O, Mg, Ca, Ba and Nd [*Clayton and Mayeda,* 1977; *Wasserburg, Lee and Papanastassiou,* 1977; *Lee, Papanastassiou and Wasserburg,* 1978; *McCulloch and Wasserburg,* 1978]. The results obtained on Ba for EK1-4-1 showed that the isotopic effects were compatible with the addition of matter only to the unshielded nuclei ^{135}Ba and ^{137}Ba. The results on Nd were also compatible with the addition of matter to the unshielded nuclei. However, as Nd has only one shielded isotope (^{142}Nd), a definitive interpretation was not possible. For this reason we pointed out [*McCulloch and Wasserburg,* 1978] that to demonstrate general excesses compatible with r-process addition, it will be necessary to obtain data on Sm and other refractory elements in this mass region with two shielded isotopes. In addition, it was pointed out that any reliable astrophysical model must await the experimental determination of the yields of exotic nuclei in the region of the rare earths where chemical fractionation will not obscure the relative contributions. Reports of Sm isotopic effects in EK1-4-1 were subsequently presented by *Lugmair, Marti and Scheinin* [1978] and by ourselves at the Ninth Lunar and Planetary Science Conference. Isotopic anomalies for Sr in EK1-4-1 and C1 were also reported by *Papanastassiou, Huneke, Esat and Wasserburg* [1978].

Results

The experimental procedures used for the separation and measurement of Sm are based on the procedures developed in this laboratory by *Russ, Burnett, Lingenfelter and Wasserburg* [1971]. All samples were analyzed using our standard Sm chemistry apart from EK1-4-1 PYX and C1 PYX(2), which were purified using an additional miniature column to remove Ba. The results are given in Table 1 as deviations from the normal ratios [*Russ et al.*, 1971] in parts in 10^4 after correction for isotopic fractionation by normalizing to $^{147}Sm/^{154}Sm$, and using ^{154}Sm as the index isotope. The results of analyses of a terrestrial sample, a nephelinite from the Oslo Rift, Norway, are shown in Table 1 and are in excellent agreement with the high precision abundances reported by *Russ et al.*, [1971]. For the C1 and EK1-4-1 samples the mass fractionation correction applied to Sm was less than ~3‰ per mass unit and within the same range as applied to the terrestrial sample.

Three analyses of different samples from the inclusion EK1-4-1 are given in Table 1. These samples are a scoop of the crushed inclusion, a pyroxene and melilite mineral separate. All EK1-4-1 samples show large deviations from normal which exceed the uncertainties by over a factor of 10. The deviations for the different samples are identical within error with the exception of $^{144}Sm/^{154}Sm$ deviations for EK1-4-1 SC and EK1-4-1 PYX which are at the limit of 2σ uncertainty. For EK1-4-1 SC peaks at masses 151 and 153 of 10^{-13} amps were present. The relative intensity of these peaks was consistent with Eu which does not interfere with Sm. The larger uncertainties for the melilite analysis are a consequence of a factor of 10 smaller sample size (4 ng Sm). These variations are in agreement with a recent report by *Lugmair et al.* [1978].

From inclusion C1 two different pyroxene separates and a split of the crushed inclusion were analyzed. These analyses all show an enrichment in only $^{144}Sm/^{154}Sm$ of 15±5 parts in 10^4. All other isotopic ratios are identical within error to the terrestrial normal. The only exception is for C1 PYX(1), which shows possible deviation from normal equal to the 4σ uncertainty .for $^{148}Sm/^{154}Sm$ and 3σ uncertainty for $^{150}Sm/^{154}Sm$. This was not present in the higher precision analyses of the other pyroxene separate C1 PYX(2a) or in the analysis of the total inclusion C1S1 and is therefore probably an artifact. A second analysis was carried out on another aliquot of C1 PYX(2a) after repeating the Sm separation on the final column. The values of $^{144}Sm/^{154}Sm$ for repeat analyses of this sample (C1 PYX(2b)) are in good agreement within experimental uncertainty.

As ^{144}Sm is the only anomalous Sm isotope in C1, we investigated the possibility of an isobaric interference. For all runs the mass spectrum was scanned at high sensitivity between masses 130 and 180, and no interfering species were identified. In particular, no $^{142}Nd^+$ or $^{146}Nd^+$ ions were detected and for the analysis of sample C1 PYX(2a), we can place an upper limit to any possible interference to ^{144}Sm from ^{144}Nd of less than 3 parts in 10^4. However, for the other samples of C1 and EK1-4-1, the smaller Sm ion beam intensities only allowed an upper limit of ^{144}Nd interference to ^{144}Sm of less than approximately 10 parts in 10^4. To test whether ^{144}Nd interference could produce an effect of this magnitude, a sample consisting of approximately equal proportions of normal Sm and Nd was loaded on a filament and analyzed. At

Table 1. Samarium Isotopic Variations[a]

Sample[b]	Sm(ppm)	ε144	ε148	ε149	ε150	ε152
		Normalized to $^{147}Sm/^{154}Sm$, Index Isotope ^{154}Sm				
EK1-4-1 SC	4.1	−17.0±5.2	−36.2±2.2	−0.7±1.5	−35.1±2.2	−9.1±1.4
EK1-4-1 PYX	5.3	−5.2±5.9	−38.2±2.6	+0.2±2.1	−33.9±3.1	−9.4±1.7
EK1-4-1 MEL	1.4	−7.4±13.0	−37.0±4.9	+0.2±4.1	−31.4±7.7	−6.5±3.7
C1 S1		+15.5±5.9	−0.4±1.8	−0.2±1.5	−1.2±1.5	−1.7±1.2
C1 PYX (1)	4.9	+11.8±4.0	−4.2±1.8	−0.8±1.8	−3.1±2.2	+0.2±0.6
C1 PYX (2a)	4.4	+17.0±3.0	−0.6±1.0	−0.5±0.7	−1.2±1.2	−0.6±0.5
C1 PYX (2b)		+17.8±3.0	+0.2±1.2	−1.0±1.3	−1.2±1.5	−0.3±0.8
Terr. Sample	20.0	0.0±3.7	−1.0±1.8	−0.3±1.3	−0.3±2.1	+0.6±0.8
		+1.5±3.0	−0.4±0.6	+0.8±1.0	−1.8±2.2	+0.3±0.5
		+0.7±1.5	−0.6±0.8	+0.3±1.3	−0.3±1.5	+0.7±0.7
		Normalized to $^{150}Sm/^{148}Sm$, Index Isotope ^{148}Sm				
		ε144	ε147	ε149	ε152	ε154
EK1-4-1		+34.4±8.4	+38.5±3.3	+36.5±2.1	+24.1±4.0	+34.3±4.2
C1		+15.4±5.0	+0.4±1.6	+1.3±1.0	+2.0±2.1	+2.0±3.9
Terr. Sample		+1.6±4.0	+0.4±1.6	+0.1±1.6	−0.8±3.3	−1.4±4.7

[a]Errors are 2σ mean. Deviations in parts per 10^4 relative to the grand mean of terrestrial normals [*Russ et al.*, 1971]; $^{144}Sm/^{154}Sm = 0.13516\pm1$; $^{148}Sm/^{154}Sm = 0.49419\pm2$; $^{149}Sm/^{154}Sm = 0.60750\pm2$; $^{150}Sm/^{154}Sm = 0.32440\pm2$; $^{152}Sm/^{154}Sm = 1.17537\pm4$; $^{147}Sm/^{154}Sm = 0.65918$.

[b]PYX = pyroxene; MEL = melilite; S1, SC = splits of crushed inclusion; Terr. = Terrestrial.

the Sm running temperature, an apparent excess of ^{144}Sm of 10 parts in 10^4 was measured in this sample with the ratios $Nd/NdO = 10^{-4}$ and $^{144}Sm/^{144}NdO = 0.1$. In the samples C1 and EK1-4-1 the Sm fraction analyzed is essentially free of NdO with the measured ratio $^{144}Sm/^{144}NdO \geqslant 100$. Thus, assuming the same Nd/NdO ratio in C1 and EK1-4-1, the maximum ^{144}Nd interference to ^{144}Sm in C1 and EK1-4-1 is 1 part in 10^6. This is a factor of 10^3 smaller than the observed excesses and we conclude that interference from ^{144}Nd cannot account for the observed ^{144}Sm excesses.

Discussion

To elucidate the effects in Sm it is more appropriate to use the two shielded isotopes ^{150}Sm and ^{148}Sm to correct for fractionation with ^{148}Sm as an index isotope. The weighted average of data renormalized from the raw measured ratios are shown for EK1-4-1, C1 and the terrestrial sample in the bottom of Table 1 and is consistent with data transformed using equation 2 of *McCulloch and Wasserburg* [1978].

For inclusion EK1-4-1, the renormalized data show positive anomalies at the unshielded isotopes ^{154}Sm, ^{152}Sm, ^{149}Sm, ^{147}Sm and at the low abundance shielded isotope ^{144}Sm. The addition of material to the unshielded Sm isotopes is fully consistent with the additions found in the unshielded Ba and Nd isotopes [*McCulloch and Wasserburg*, 1978].

The melilite and pyroxene mineral phases from EK1-4-1 have an identical enrichment although these phases contain different proportions of Sr, Ba, Nd, and Sm. This is not consistent with *in situ* fission subsequent to crystallization but implies that these minerals formed from an isotopically homogeneous liquid or gas phase or were subsequently isotopically reequilibrated. Xe data from EK1-4-1 [*Papanastassiou et al.*, 1978] are also not consistent with an origin of these anomalies by *in situ* fission. The Xe data are consistent with mixtures of ^{244}Pu fission Xe, air Xe, Xe from cosmic-ray-induced reactions on Ba, REE and I, and Xe from ^{129}I decay. There is no evidence for isotopic enrichments from any other sources (e.g., Xe as found in bulk acid-insoluble residues; *Lewis, Srinivasan and Anders*, 1975).

The number of excess atoms in EK1-4-1 can be calculated by assuming that the isotopic effects are due to addition of nuclides to average solar system material with cosmic abundances. This is given by $\epsilon(A)N(A) \times 10^{-4}$ where $\epsilon(A)$ are the measured deviations given in Table 1 and N(A) is the cosmic abundance [*Cameron*, 1973]. These excess atoms are tabulated in Table 2 and plotted in Figure 1. For Ba and Nd the normalizations are as described by *McCulloch and Wasserburg* [1978] with $^{134}Ba/^{138}Ba$ and $^{144}Nd/^{142}Nd$ used for normalization and ^{138}Ba and ^{142}Nd as index isotopes. For Nd the arbitrary assignment of an excess to ^{144}Nd of +20 has been adjusted to +18 to produce a smooth curve between excess atoms of ^{150}Nd and ^{152}Sm. An alternative normalization for Nd using $^{148}Nd/^{150}Nd$ has been proposed by *Clayton* [1978] but this has the disadvantage of assuming a normal cosmic ratio for the $^{148}Nd/^{150}Nd$ excesses. The main feature of the curve in Figure 1 is the pronounced peak between Ba and Nd. Chemical fractionation between the exotic rare earth and Ba nuclei or the addition of unfractionated exotic nuclei to fractionated "solar" material prior to the formation of the inclusion would modify this peak. A small odd-even effect is also apparent in Nd and Sm, with the excess atoms being

greater in the even atomic number nuclei. This effect is not present in fission yield curves [*Meek and Rider,* 1974].

The additions to the unshielded isotopes can be attributed to beta decay from unstable neutron-rich species. Isotopes

Table 2. Nucleosynthetic Components in Ba, Nd and Sm for EK1-4-1

Nuclide	N(A)[a]	σ(A)[b]	N_s(A)[c]	N_r(A)[d]	ϵ(A)[e]	ϵ(A)x[f] N(A)10^{-4}	$\frac{\epsilon(A)N(A)}{\epsilon(154)N_r(A)}$[g]
^{130}Ba	0.005[m]	2000[k]	0.0	0.0	0.0	0.0	--
^{132}Ba	0.005[m]	650[k]	0.0	0.0	0.0	0.0	--
^{134}Ba	0.116	225[h]	0.116	0.0	0.0	0.0	--
^{135}Ba	0.316	470[i]	0.055	0.261	13.4	4.23×10^{-4}	0.47
^{136}Ba	0.375	70[h]	0.375	0.0	0.0	0.0	--
^{137}Ba	0.543	72.6[i]	0.363	0.180	12.3	6.68×10^{-4}	1.08
^{138}Ba	3.44	5.7[h]	3.30	0.14	0.0	0.0	--
^{142}Nd	0.211	45[j]	0.211	0.0	0.0	0.0	--
^{143}Nd	0.095	332[i]	0.025	0.07	27.8[l]	2.64×10^{-4}	1.1
^{144}Nd	0.186	67[i]	0.116	0.07	18.0	3.35×10^{-4}	1.39
^{145}Nd	0.065	485[i]	0.016	0.049	24.9	1.61×10^{-4}	0.96
^{146}Nd	0.134	105[i]	0.069	0.065	12.0	1.61×10^{-4}	0.72
^{148}Nd	0.045	210[k]	0.0	0.045	33.6	1.50×10^{-4}	0.98
^{150}Nd	0.044	240[k]	0.0	0.044	33.6	1.47×10^{-4}	0.98
^{144}Sm	0.007[m]	120[k]	0.0	0.0	34.4	0.24×10^{-4}	--
^{147}Sm	0.035	1150[k]	0.006	0.029	38.5	1.34×10^{-4}	1.35
^{148}Sm	0.025	260[k]	0.025	0.0	0.0	0.0	--
^{149}Sm	0.031	1620[k]	0.004	0.027	36.5	1.14×10^{-4}	1.23
^{150}Sm	0.017	370[k]	0.017	0.0	0.0	0.0	--
^{152}Sm	0.060	450[k]	0.014	0.046	24.1	1.46×10^{-4}	0.92
^{154}Sm	0.051	380[k]	0.0	0.051	34.3	1.76×10^{-4}	1.0

[a]Cosmic abundance (per Si = 10^6), *Cameron* [1973]. [b]30 KeV cross sections (millibarns). [c]s-process abundance. [d]r-process abundance given by $N_r(A) = N(A) - N_s(A)$. [e]Deviations from normal in parts in 10^4 from Table 1 and *McCulloch and Wasserburg* [1978]. [f]Excess atoms (see fig. 1). [g]Ratio of excess atoms to cosmic r-process atoms, normalized to ^{154}Sm (see fig. 2). [h]*Musgrove, Boldman and Macklin* [1976]. [i]*Holmes, Woosley, Fowler and Zimmerman* [1976]. [j]*Conrad,* [1976]. [k]*Allen, Gibbons and Macklin* [1971]. [l]Corrected for ^{147}Sm decay for an age of 4.56×10^9 years. [m]p-process only nuclide.

produced by this general mechanism are often referred to as "r-process." To test whether the excess atoms shown in Figure 1 are produced by an average "cosmic" r-process, we have calculated the ratios of excess atoms in EK1-4-1 to cosmic r-process atoms, normalized to the r-process only isotope ^{154}Sm. This ratio is given by $\epsilon(A)N(A)/\epsilon(154)N_r(A)$ where $N_r(A)$ is the calculated cosmic r-process abundance. To obtain $N_r(A)$, the s-process component $N_s(A)$ is subtracted from the total isotopic abundance N(A). Thus $N_r(A) = N(A) - N_s(A)$. The isotopes ^{154}Sm, ^{150}Nd and ^{148}Nd are produced only by the r-process. However, several other isotopes also contain a significant s-process component. For these isotopes, $N_s(A)$ was calculated using the local equilibrium approximation, $N_s(A-1)\sigma(A-1) = N_s(A)\sigma(A)$ as modified by the general trend of the $N_s(A)\sigma(A)$ curve and closed neutron shell at ^{138}Ba (see for example *Seeger, Fowler and Clayton*, 1965). Improved cross section and abundance data were used (see Table 2) together with allowance for branching in the s-process chain at ^{134}Cs and ^{151}Sm [*Ward, Newman and Clayton,* 1976]. The uncertainty in calculating the r-process contribution depends on the accuracy of the calculated s-process and the relative proportions of s and r components. In figure 2 the number of excess atoms in EK1-4-1 relative to cosmic r-process are shown as a function of atomic number and are in general *similar* to the cosmic r-process distribution. However, significant deviations at ^{149}Sm, ^{147}Sm and ^{135}Ba show that the exotic material was not *identical* to the average solar system r-process, or that the additions were made to material which did not have the present average solar system isotopic composition.

Sample EK1-4-1 also shows an excess in the proton-rich or "p-process" isotope ^{144}Sm. No corresponding enrichment was found in the "p-process" isotopes ^{132}Ba and ^{130}Ba. *Woosley and Howard* [1978] have indicated that the production of these nuclei by photodisintegration reactions operating on r- and s-process seeds is temperature dependent. Using this model, it may be possible to overproduce ^{144}Sm relative to its cosmic abundance without corresponding additions to ^{132}Ba and ^{130}Ba. Sr data from EK1-4-1 [*Papanastassiou et al.*, 1978] show that the p-process isotope ^{84}Sr has a deficiency of -32 ± 2 parts in 10^4 when normalized to $^{86}Sr/^{88}Sr = 0.1194$. This is clearly not compatible with the excess in ^{144}Sm. However, as ^{87}Sr has a contribution from ^{87}Rb($\tau_{1/2} = 5.0 \times 10^{10}$ yr) decay the data for the three remaining Sr isotopes can also be interpreted as an excess in ^{86}Sr (s-process) or a deficiency in ^{88}Sr (s- and r-process). None of these possibilities are in consonance with the

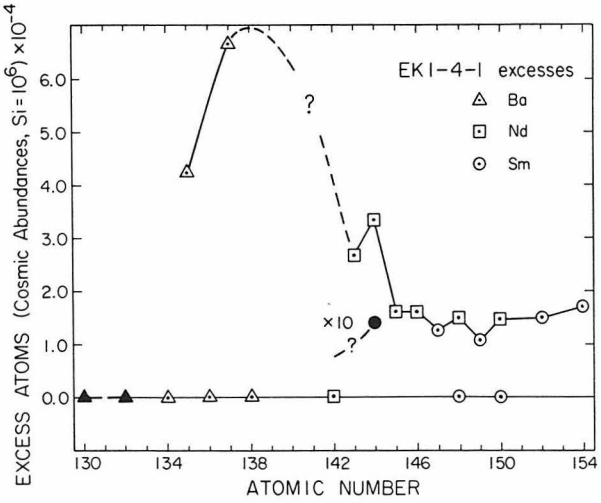

Fig. 1. Excess atoms of Ba, Nd and Sm in EK1-4-1 assuming addition of exotic nuclides to material with cosmic abundances. No excesses are assumed for the shielded nuclides ^{150}Sm, ^{148}Sm, ^{142}Nd and ^{134}Ba and for ^{138}Ba. Solid symbols show "p-process" only isotopes ^{130}Ba, ^{132}Ba and ^{144}Sm.

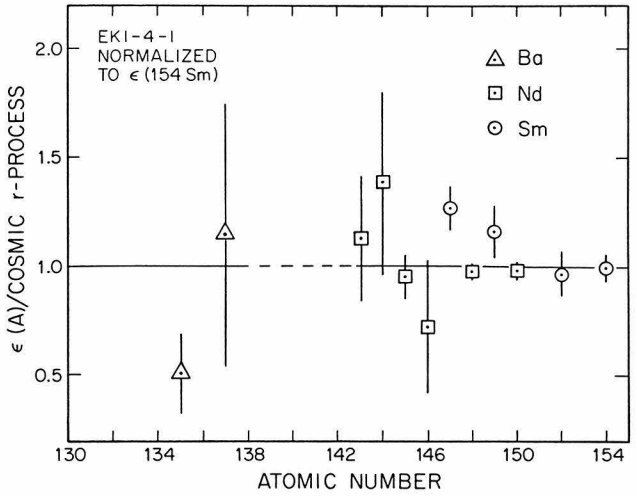

Fig. 2. Ratios of EK1-4-1 excess atoms to an average solar system r-process abundance as a function of atomic number (normalized to $^{154}Sm = 1.0$).

Ba, Nd and Sm results and data on p-process nuclides in EK1-4-1 between Sr and Ba will be required to resolve this apparent inconsistency.

In the other FUN sample, C1, an excess in only the "p-process" isotope ^{144}Sm of 1.0×10^{-5} atoms (per cosmic $Si = 10^6$ atoms) is present. All other isotopic ratios are normal. The presence of only a "p-process" addition to C1 is important as it shows that the "p-process" is not necessarily coupled to the r-process. This is in contrast to EK1-4-1, where both p- and r-process additions are present. The ^{144}Sm "p-process" excess in C1 is approximately a factor of 2 smaller than that in EK1-4-1. No corresponding addition has been detected in the "p-process" isotopes ^{132}Ba and ^{130}Ba in C1 [*McCulloch and Wasserburg*, 1978], although this may be close to the limit of resolution. The normal Nd isotopic composition in C1 [*McCulloch and Wasserburg*, 1978] is in consonance with these results as it has no "p-process" only isotopes. An addition to ^{142}Nd of the same number of atoms as excess $^{144}Sm^*$ in C1 would only produce an effect in $^{142}Nd/^{144}Nd$ of 5 parts in 10^5 which is at the limit of our resolution. ^{142}Nd may also possibly have an indirect p-process contribution from decay by the extinct nuclide ^{146}Sm ($\tau_{1/2} = 1.0 \times 10^8$ yr). *Scheinin, Lugmair and Marti* [1976] and *Lugmair and Marti* [1977] have reported measurements of $^{142}Nd/^{144}Nd$ and from marginal data have inferred small excesses in ^{142}Nd attributed to decay of ^{146}Sm. Our Nd measurements in C1 show no evidence for the presence of ^{146}Sm, although the Sm/Nd ratio in this sample is not substantially fractionated from chondritic. A deficiency in the p-process isotope ^{84}Sr of -9 ± 2 parts in 10^4 is also present in C1, in contrast with the observed excess in ^{144}Sm. This indicates that simple addition of "p-process" material to normal solar system material is not an adequate explanation of the isotopic effects.

From the data reported here, as well as the wide range of Xe isotopic anomalies, it is reasonable to consider that the r-process isotope ^{129}I ($\tau_{1/2} = 1.6 \times 10^7$ yr) may also have been added in the same process. It was shown by *McCulloch and Wasserburg* [1978] that if the negative ^{135}Ba anomaly in C1 was representative of the initial solar system, then the additional $^{135}Ba^*$ required to fill in the negative anomaly would give $^{135}Ba^*/^{127}I \sim 0.5 \times 10^{-4}$. Thus, if the same number of ^{129}I and $^{135}Ba^*$ atoms were added, this would give $^{129}I/^{127}I \sim 10^{-4}$, which is similar to the observed ratio. It is also of interest to note that the addition of approximately the same number of ^{129}I atoms and exotic nuclei tabulated in table 2, would also give $^{129}I/^{127}I \sim 10^{-4}$. This model of small last-"minute" injection of r-process material is consistent with

the time scale of several million years as indicated by the presence of ^{26}Al with $\tau_{1/2} = 0.7 \times 10^6$ years [*Lee, Papanastassiou and Wasserburg,* 1977].

The discussion of Ba, Nd and Sm data for EK1-4-1 and the Sm data for C1 has been based on the premise of addition of exotic materials to material with a normal solar system isotopic composition. However, the presence of negative isotopic anomalies in other elements, ^{135}Ba and ^{48}Ca in C1 and ^{84}Sr and ^{26}Mg in EK1-4-1 and C1, suggests that this may not have been the case and materials which received these additions may have been depleted in some isotopes. This is particularly apparent in Sr [*Papanastassiou et al.*, 1978] which shows negative anomalies in ^{84}Sr/^{88}Sr for both EK1-4-1 and C1, when normalized to ^{86}Sr/^{88}Sr = 0.1194. As suggested by *McCulloch and Wasserburg* [1978], the negative ^{135}Ba anomaly may also imply that C1 represents precursor solar system material before r-process addition. However, the depletions of ^{135}Ba in C1 and the smaller ^{135}Ba excess relative to cosmic r-process in EK1-4-1 could also be due to ^{135}Cs, which is the progenitor for ^{135}Ba. If C1 and EK1-4-1 condensed before the more volatile ^{i35}Cs ($\tau_{1/2} = 2.3 \times 10^6$ yr) decayed to ^{135}Ba, this could account for these discrepancies.

The extent and significance of the correlated isotopic anomalies which have at present only been found in the two Allende FUN inclusions, C1 and EK1-4-1, are still not apparent. An extensive survey of the Ba isotopic composition in a variety of Allende inclusions [*McCulloch and Wasserburg,* 1978] showed that 90% of these inclusions had a normal isotopic composition. Inclusions with a normal Ba isotopic composition included samples which had large ^{26}Mg excesses correlated with Al/Mg ratio, samples with a distinctive oxygen isotopic composition but lying on the mixing line of ^{16}O and normal O [*Clayton, Grossman and Mayeda,* 1973] and a sample with a suggested Hg isotopic anomaly [*Reed and Jovanovic,* 1969]. The Ba isotopic composition in meteorites [*Eugster, Tera and Wasserburg,* 1969; 1969; *de Laeter and Date,* 1973] and lunar samples [*McCulloch and Wasserburg,* 1978] has also been shown to be identical to terrestrial Ba. Thus, in contrast to the widespread O anomalies, only a small proportion of the materials sampled show correlated anomalies for other elements.

Acknowledgements. We thank D. A. Papanastassiou for his constructive criticisms of this manuscript. This work was supported by NASA grant NGL 05-002-188 and NSF grant 76-83685. Contribution 3093(275) Div. of Geological and Planetary Sciences.

References

Allen, B. J., H. H. Gibbons, and R. L. Macklin, Nucleosynthesis and neutron capture cross sections, in *Advances in Nuclear Physics, 4,* M. Barranger and E. Vogt, eds., 205-259, 1971.

Cameron, A. G. W., Abundances of the elements in the solar system, *Space Sci. Rev., 15,* 121-146, 1973.

Clayton, D. D., An interpretation of special and general isotopic anomalies in r-process nuclei, Submitted to *Ap. J. Lett.*, 1978.

Clayton, R. N., L. Grossman, and T. K. Mayeda, A component of primitive nuclear composition in carbonaceous meteorites, *Science, 182,* 485-488, 1973.

Clayton, R. N. and T. K. Mayeda, Correlated oxygen and magnesium

isotope anomalies in Allende inclusions, I: Oxygen, *Geophys. Res. Lett., 4,* 295-298, 1977.

Conrad, J., Analysis of the s-process and the nuclear synthesis of the elements, Ph.D. Thesis, Heidelberg, 1976.

de Laeter, J. R. and R. Date, The isotopic composition of barium, *Int. J. Mass Spect. Ion Phys., 12,* 355-463, 1973.

Eugster, O., F. Tera, and G. J. Wasserburg, Isotopic analyses of barium in meteorites and in terrestrial samples, *J. Geophys. Res., 74,* 3897-3900, 1969.

Holmes, J. A., S. E. Woosley, W. A. Fowler, and B. A. Zimmerman, Tables of thermonuclear-reaction-rate data for neutron-induced reactions of heavy nuclei, *At. Data Nucl. Data Tables, 18,* 305, 1976.

Lee, T., D. A. Papanastassiou, and G. J. Wasserburg, Aluminum-26 in the early solar system: fossil or fuel?, *Ap. J. Lett., 211,* L107-L110, 1977.

Lee, T., D. A. Papanastassiou, and G. J. Wasserburg, Calcium isotopic anomalies in the Allende meteorite, *Ap. J. Lett, 220,* L21-L25, 1978.

Lewis, R. S., B. Srinivasan, and E. Anders, Host phase of a strange xenon component in Allende, *Science, 190,* 1251-1262, 1975.

Lugmair, G. W., and K. Marti, Sm-Nd-Pu timepieces in the Angra dos Reis meteorite, *Earth Planet, Sci. Lett., 35,* 273-284, 1977.

Lugmair, G. W., K. Marti, and N. B. Scheinin, Incomplete mixing of products from r-, p-, and s-process nucleosynthesis: Sm-Nd systematics in Allende inclusion EK1-4-1, in *Lunar and Planetary Science IX,* p. 672-674, 1978.

Meek, M. E., and B. F. Rider, Compilation of fission product yields, *Vallecitos Nuclear Center,* Pleasanton, CA, 1974.

McCulloch, M. T., G. J. Wasserburg, Barium and neodymium isotopic anomalies in the Allende meteorite, *Ap. J. Lett., 220,* L15-L19, 1978.

Musgrove, A. R. de L., J. W. Boldman, and R. L. Macklin, KeV neutron capture cross sections of ^{134}Ba and ^{136}Ba, *Nucl. Phys., A256,* 173-188, 1976.

Papanastassiou, D. A., J. C. Huneke, Tezer M. Esat and G. J. Wasserburg, Pandora's Box of the Nuclides, Abstract in *Lunar and Planetary Science IX,* p. 859-861, 1978.

Papanastassiou, D. A., and G. J. Wasserburg, Strontium isotopic anomalies in the Allende Meteorite, *Geophys Res. Lett., 5,* 1978 (in press this issue).

Reed, G. W., and S. Jovanovic, ^{196}Hg and ^{202}Hg isotopic ratios in chondrites, *J. Inor. Nucl. Chem., 31,* 3783-3788, 1969.

Russ, G. P., III, D. S. Burnett, R. E. Lingenfelter, and G. J. Wasserburg, Neutron capture on ^{149}Sm in lunar samples, *Earth Planet. Sci. Lett., 13,* 53-60, 1971.

Scheinin, N. B., G. W. Lugmair, and K. Marti, Sm-Nd systematics and evidence for extinct ^{146}Sm in an Allende inclusion, *Meteoritics, 11,* 357, 1976.

Seeger, P. A., W. A. Fowler, and D. D. Clayton, Nucleosynthesis of heavy elements by neutron capture, *Ap. J. Suppl., 11,* 121-166, 1965.

Ward, R. A., M. J. Newman, and D. D. Clayton, S-process studies: branching and the time scale, *Ap. J. Suppl.,31,* 33-59, 1976.

Wasserburg, G. J., T. Lee, and D. A. Papanastassiou, Correlated O and Mg isotopic anomalies in the Allende inclusions, II: Magnesium, *Geophys. Res. Lett., 4,* 299-302, 1977.

Woosley, S. E., and W. M. Howard, The p-process in supernovae, *Ap. J. Suppl., 36,* 285-304, 1978.

(Received May 19, 1978;
accepted June 5, 1978.)

APPENDIX 8

CHEMICAL PROCEDURES FOR THE SEPARATION OF Ba, Sr, and REE ELEMENTS

The study of the isotopic composition of a number of different elements from a single sample required the adaption ,combination and development of a number of different chemical separation procedures. This was particularly important in the study of the anomalous inclusions from the Allende meteorite (see appendices 6 and 7) for which there was only an extremely limited quantity of sample (< 20 mg) available. The detailed procedures for the separation of individual elements has already been described by DePaolo (1978) for Sm and Nd, and Eugster, Tera, and Wasserburg (1968) for Ba, and Papanastassiou and Wasserburg (1969) for Sr. Therefore, this description will emphasize the adaption of these techniques for the separation of all of these elements from a single sample.

To separate Sr, Ba, Sm, Nd, and the heavy REE, there are four steps. These are shown in Figure A6-1 and are:

1. Separation of Sr from Ba and REE.

The separation of Sr from Ba and the REE and also the removal of the major elements was achieved by using a "standard" 1cmx17 cm cation exchange column with Dowex 50-8x, 100-200 mesh resin. In the elution scheme shown in Figure A8-2, Sr is separated from Rb and the REE with 2.5N HCl and the REE and Ba are then eluted with 4N HCl. Although Ba and the REE are separated to some extent, Ba and Nd overlap and must be separated by using an additional column.

Figure A8-1. Flow diagram illustrating the steps required for the separation of Sr, Ba, La and Ce, Sm, Nd, and heavy REE using ion exchange procedures. The procedure uses four columns: 2.5 N, 4N HCl, 4N HCl, and lactic acid columns of ph 5.3 and 4.6. The dashed line shows an alternate procedure where the 4N HCl column is bypassed and the Ba and REE fractions are separated by only using the lactic acid column of ph 5.3.

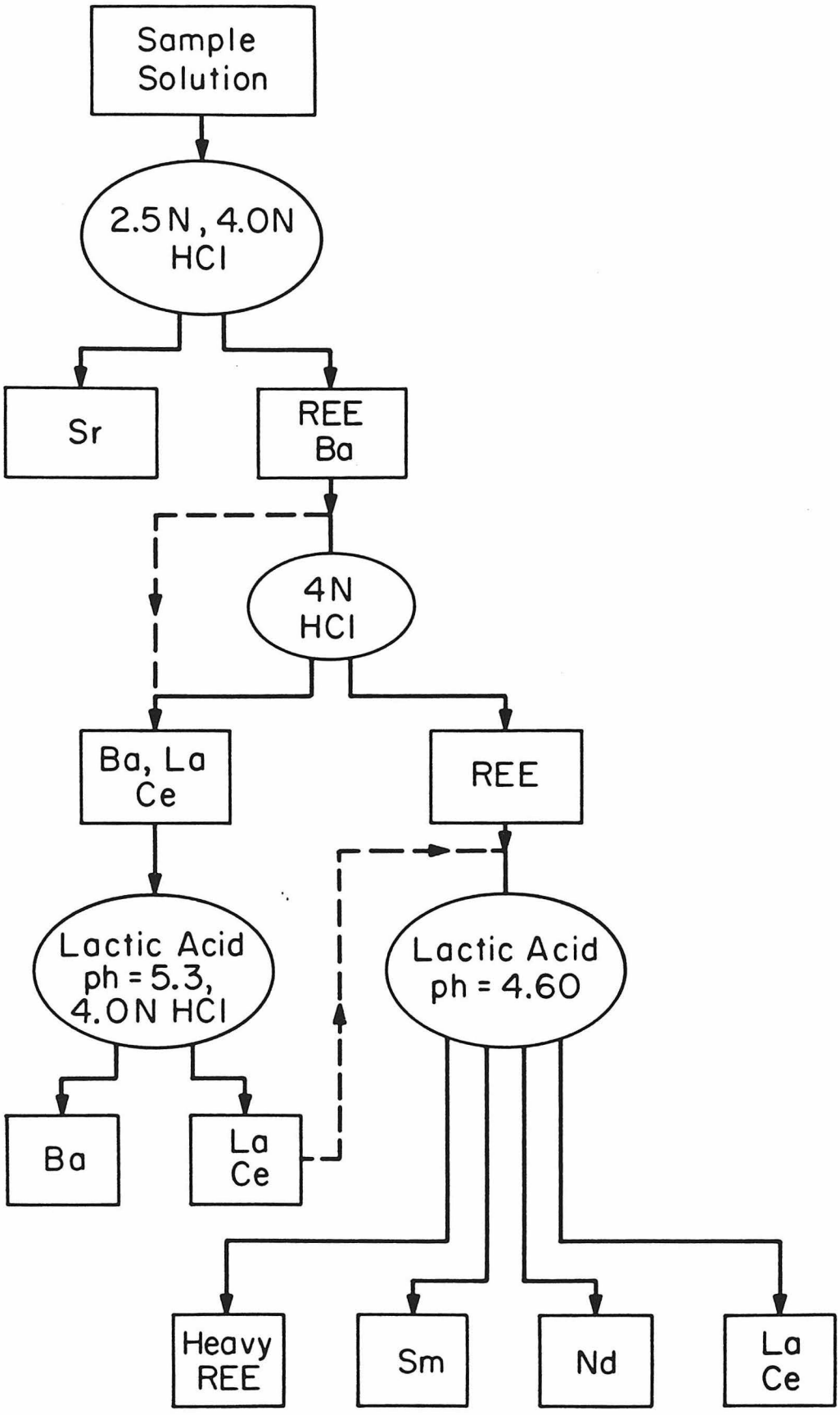
Sample Solution
2.5N, 4.0N HCl
Sr
REE Ba
4N HCl
Ba, La Ce
REE
Lactic Acid ph = 5.3, 4.0N HCl
Lactic Acid ph = 4.60
Ba
La Ce
Heavy REE
Sm
Nd
La Ce

Fig. A8-1

Figure A8-2. Elution scheme for the separation of Sr and Ba and REE using 2.5N HCl and 4.0N HCl eluants. It can be seen that the Sr is separated but the Ba and REE overlap.

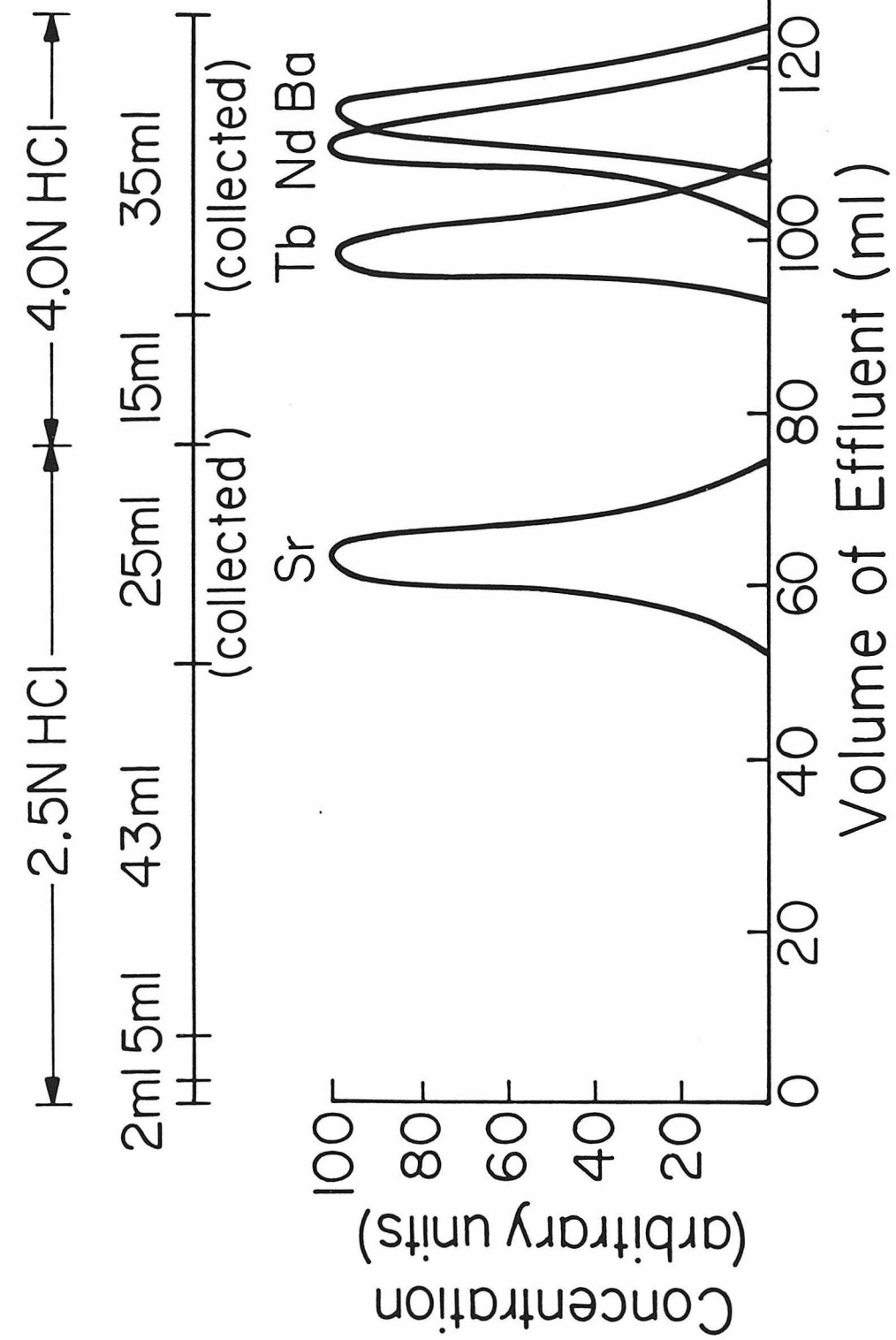
2.5N HCl
4.0N HCl
2ml
5ml
43ml
25ml
15ml
35ml
(collected)
(collected)
Sr
Tb
Nd
Ba
Concentration (arbitrary units)
Volume of Effluent (ml)
0
20
40
60
80
100
120
140

Fig. A8-2

2. Separation of Ba from Nd and heavy REE.

The separation of Ba from Nd was done using the same ion exchange column as in step 1 but by using only a 4N HCl elution. The elution scheme is shown in Figure A8-3 and although there is a reasonable separation of Ba from Nd and the heavy REE, the light REE, Ce, and La overlap into the Ba fraction. The presence of Ce and La in the Ba fraction is not a problem as Ce and La run as oxides in the mass spectrometer and therefore do not interfere with the Ba element (see appendix 6). However, in order to separate Ce and La for future isotopic composition determinations and to eliminate as possibility of interference to Ba another column separation was developed.

3. Separation of Ce and La from Ba.

Ce and La were separated from Ba by using a microcolumn of 2 mm internal diameter and 2 cm length. As shown in Figure A8-4 Ce and La (and any other REE) are eluted in the first fraction with 0.2 M lactic acid of ph = 5.3. Before the Ba is removed, 0.5 ml of H_2O followed by 0.5 ml of 1.5N HCl are added to the column to remove the lactic acid and to prevent the formation of NH_4Cl in the Ba faction. Ba is finally eluted with 4N HCl. This column procedure was developed after the anomalous Allende inclusions had been processed, but in retrospect the use of this column instead of the 4NHCl column (step 2) would be preferable (see Figure A8-1).

4. Separation of Sm and Nd.

An excellent separation of Sm and Nd is achieved by using a 40 cm long, 2mm internal diameter capillary tube with Dowex 50-8x,

Figure A8-3. Elution scheme for the separation of Ba from Nd, Sm, and heavy REE using 4.0N HCl. It can be seen that although the separation of Ba and Nd is adequate, Ce (and La) overlap into the Ba fraction.

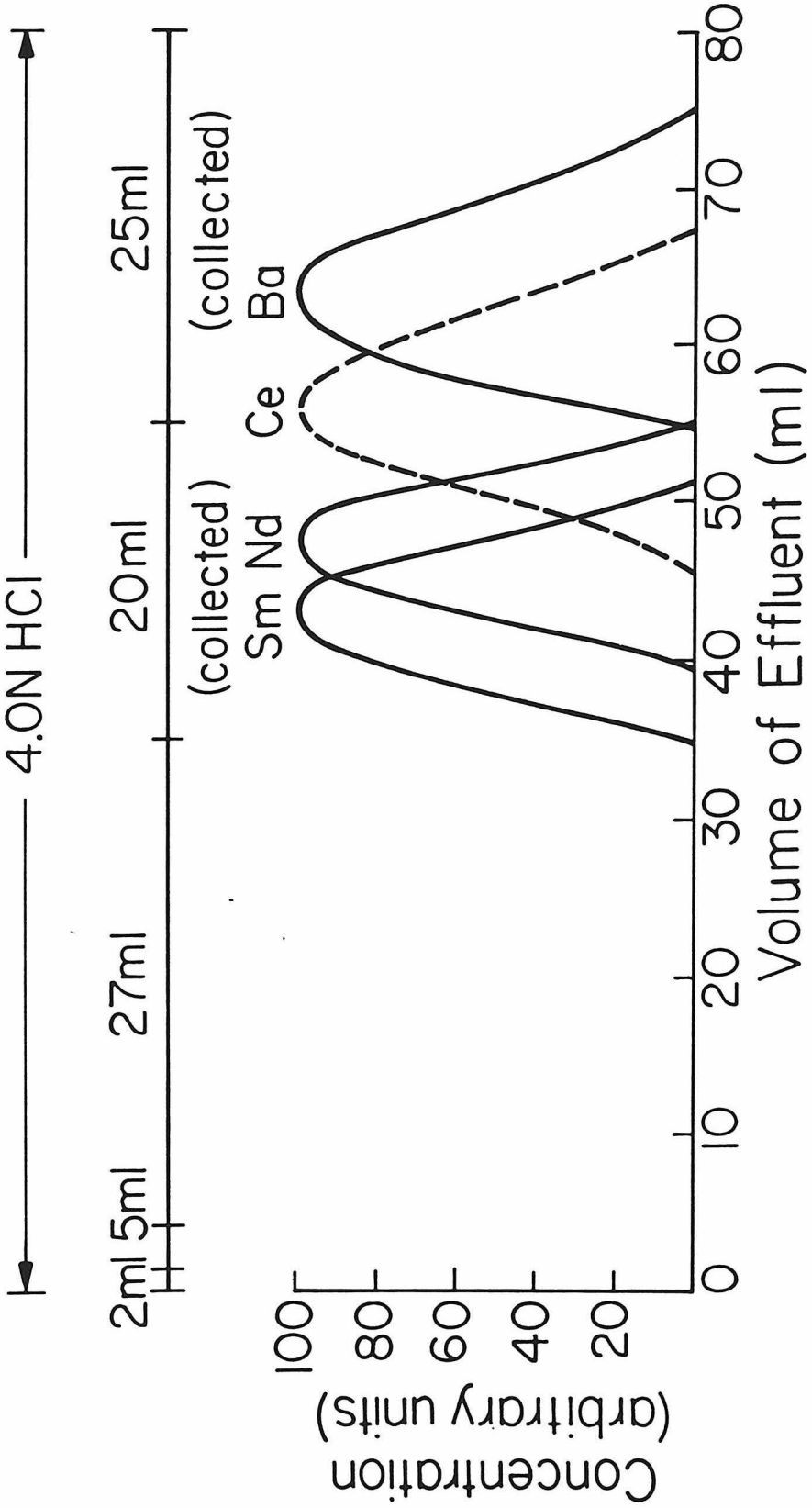
4.0N HCl
2ml
5ml
27ml
20ml
25ml
(collected)
Sm Nd
Ce
(collected)
Ba
Concentration
(arbitrary units)
100
80
60
40
20
0
10
20
30
40
50
60
70
80
Volume of Effluent (ml)

Fig. A8-3

Figure A8-4. Elution scheme for the separation of Ba from La and Ce using 0.2M 2-methylladic acid with a ph = 5.3, followed by 4.0N HCl.

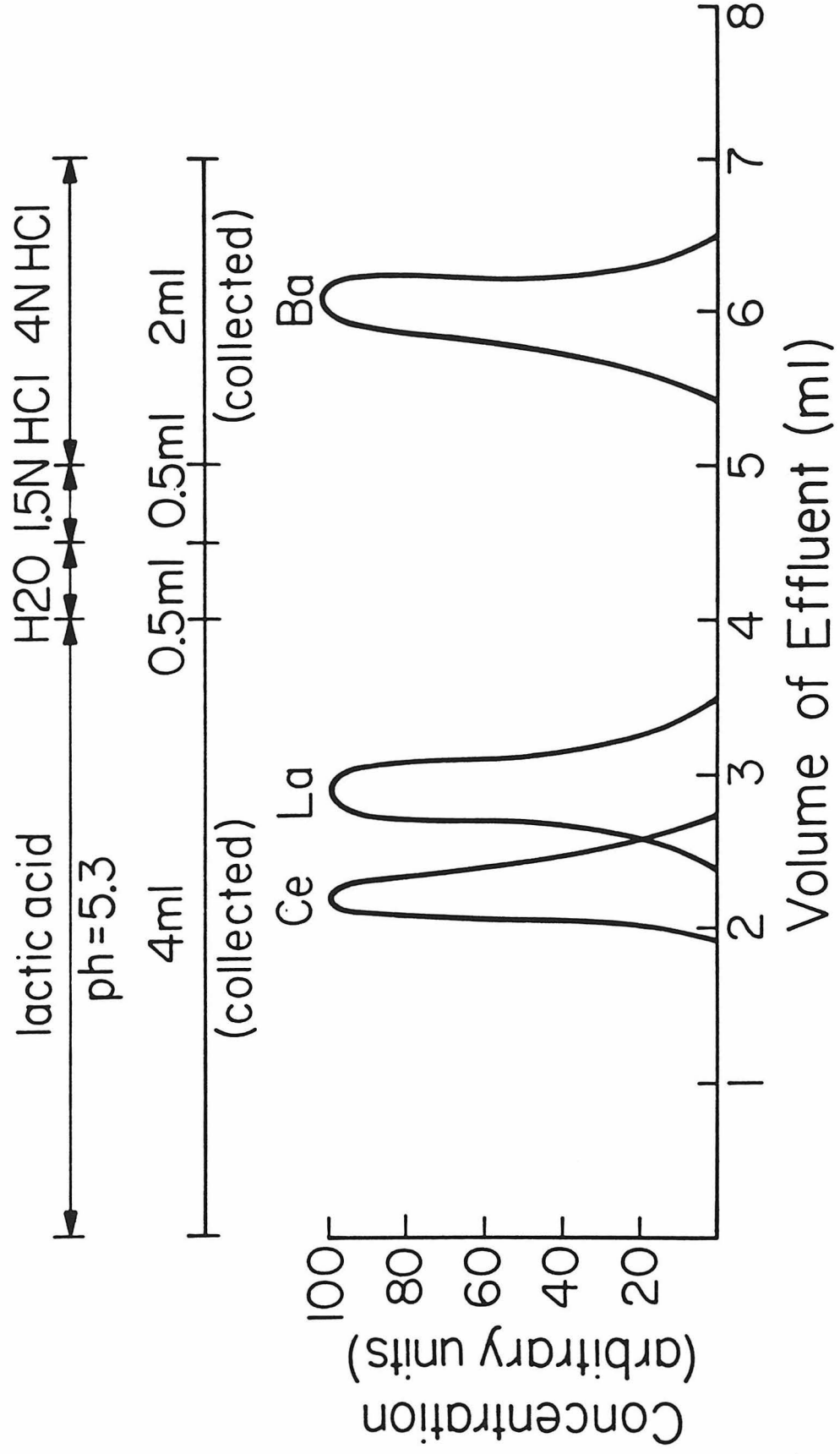
lactic acid
ph=5.3
4ml
(collected)
H2O 1.5N HCl 4N HCl
0.5ml 0.5ml 2ml
(collected)
Ce La
Ba
Concentration
(arbitrary units)
100
80
60
40
20
1
2
3
4
5
6
7
8
Volume of Effluent (ml)

Fig. A8-4

Figure A8-5. Elution scheme for the separation of Sm and Nd using 0.2M 2-methyllactic acid with a ph = 4.60.

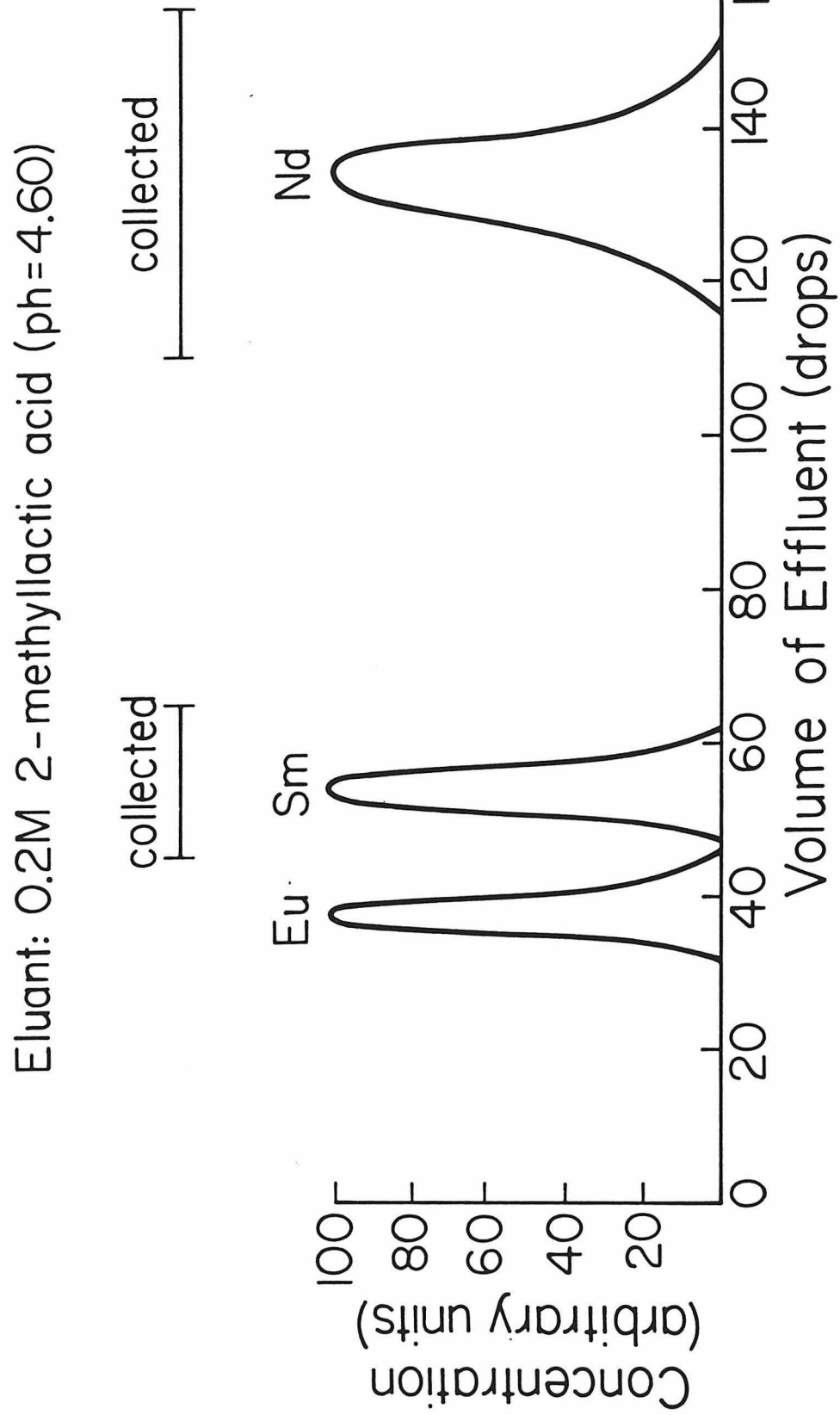
Eluant: 0.2M 2-methyllactic acid (ph=4.60)
collected
collected
Eu
Sm
Nd
Concentration (arbitrary units)
Volume of Effluent (drops)
0
20
40
60
80
100
120
140
160

Fig. A8-5

> 400 mesh resin adjusted to the NH_4^+ form. The REE are eluted with 0.2 M lactic acid of ph = 4.60. The ph is adjusted for the optimum separation of Sm and Nd and to separate for example the heavier REE Gd, a ph of 4.0 would be required.

REFERENCES

De Paolo, D.J., Study of magma sources, mantle structure and the differentiation of the earth from variations of $^{143}Nd/^{144}Nd$ in igneous rocks. PhD Thesis California Institute of Technology, 1978.

Eugster,O., F. Tera, and G.J. Wasserburg, The isotopic composition of gadolinium and neutron capture effects in some meteorites, J. Geophys. Res., 75, 2753-2768, 1970.

Papanastassiou, D.A., and G.J. Wasserburg, Initial strontium isotopic abundances and the resolution of small time differences in the formation of planetary objects, Earth Planet. Sci. Lett., 5, 361-376, 1969.